Exploring the role of GPR65 in driving the pathology of ankylosing spondylitis

Janine Michelle Barrett

A thesis submitted for the degree of DPhil

University of Oxford

Michaelmas Term 2022



Nuffield Department of Orthopaedics, Rheumatology and Musculoskeletal Sciences

St Cross College

Supervisors: Professor Paul Bowness, Dr Hussein Al-Mossawi, Dr Liye Chen, Dr Alastair Lawson

Janine Michelle Barrett
St Cross College, University of Oxford
Thesis submitted for degree of Doctor of Philosophy (DPhil), Michaelmas Term, 2022

Exploring the role of GPR65 in driving the pathology of ankylosing spondylitis

Abstract

Genome wide association studies have identified GPR65 risk loci with many immune-mediated diseases, including ankylosing spondylitis; however, its pathogenic role remains unknown. The inflamed synovial joint has a low pH signature, therefore understanding the role of this lymphocyte-expressed, proton-sensing GPCR in the context of joint inflammation is important.

With no commercial reagents available, I set out to generate monoclonal antibodies specific to human GPR65, with the aim to use them as tools in further studies. Phage display technology paired with novel antigen design, and multiple immunisation strategies proved challenging and largely unsuccessful in my hands. Despite terminal sera titres binding GPR65-expressing HEK cells, antigen-specificity was lost upon screening against primary cells.

In parallel, I have explored receptor expression on PBMC subsets and interrogated the biology of GPR65. Upon stimulation, cellular activation and pro-inflammatory cytokine release was suppressed from cells that express the highest levels GPR65 at pH6.5, compared to those at neutral pH. Due to their receptor expression profile, response to extracellular pH changes and involvement in disease, I focused on mucosal-associated invariant T (MAIT) cells. Significant partial recovery of pH-dependant IFNγ inhibition was observed, at transcriptional and protein levels, when silencing GPR65 in this cell subset; whilst at neutral pH, a pro-inflammatory role

for GPR65 activity was proposed, with an increase of IL-17A production from TCR-stimulated MAIT cells detected.

Total thesis word count: 33,335 words

Declaration

I declare that the work presented in this thesis entitled 'Exploring the role of GPR65 in driving the pathology of ankylosing spondylitis' is entirely my own work, except for where the contributions of my collaborators have been clearly acknowledged. No part of my thesis has been submitted for any degree, or other qualification in this University or elsewhere.

Janine Michelle Barrett
Michaelmas Term 2022
Nuffield Department of Orthopaedics, Rheumatology and Musculoskeletal Sciences,
Botnar Research Centre,
University of Oxford

Acknowledgements

I start by thanking my supervisors Prof. Paul Bowness, Dr. Hussein Al-Mossawi, Dr. Liye Chen and Dr. Alastair Lawson, for their valuable guidance, expert advice, and mentorship throughout this project, as well as the encouragement to reach my potential. I would also like to greatly thank UCB for the opportunity to study and their generous investment into my future, with a particular acknowledgement to Dr. Ash Maroof for his infectious enthusiasm for Immunology, and in part, inspiration for me to undertake a DPhil.

I have been fortunate to have received expertise from within UCB and particularly thank Dr. Tom Edwards, Dr. Lisa Joedicke, Dr. Chris Grice and Dr. Cecile Galmiche for their insightful ideas, stimulating discussions and patience alongside my steep learning curve of all things antibody discovery related. I also thank Dr. Tim Smallie, Catherine Simpson, Adam Hold and James Snowden of UCB, and Dr. Helen Ferry, Dr. Jonathan Webber and Dr. Moustafa Attar from the University of Oxford, who have provided technical support across this project.

A huge thank you to my friends and colleagues within UCB and the Bowness/Chen group, particularly Dr. Suzanne Cole and Dr. Emma Sutton, who have made this such an enjoyable experience and kept me smiling throughout. I am also particularly grateful to have received valuable advice and support from Feng Liu, regarding RNA sequencing analysis.

I am fortunate to be surrounded by great friends and family who have provided me with outlets of distractions and continued moral support. I would like to thank my parents for raising me in a loving environment, supporting me through all I have chosen to do, and demonstrating a work ethic I have aspired to follow. Finally, a big thank you to my husband Chester, for which this thesis would not have existed without your patience, encouragement, and complete belief in me!

Contents

Declaration ..... **iii**

Acknowledgements ..... **iv**

List of Tables ..... **viii**

List of Figures ..... **ix**

List of Abbreviations ..... **xv**

Chapter 1 : Introduction **1**

1.1 Ankylosing Spondylitis *1*

1.1.1 Clinical features 1

1.1.2 Prevalence and diagnosis 2

1.1.3 AS overlap with IBD 5

1.1.4 Genetic associations 6

1.1.5 Immunology of AS 11

1.1.6 Treatments 23

1.2 The proposed function of the proton sensing GPCR, GPR65 ..... *24*

1.2.1 An overview of GPCRs 24

1.2.2 GPR65, a proton sensing GPCR 25

1.2.3 Function of GPR65 30

1.2.4 GPR65 and disease 31

1.3 Application of antibodies in research and development *37*

1.3.1 B cell function within the immune system 37

1.3.2 Antibody structure 38

1.3.3 Antibodies used as tools and therapeutics 44

1.4 Project Aims *47*

Chapter 2 : Materials and Methods **48**

2.1 Antibody discovery *48*

2.1.1 DNA constructs and preparation 48

2.1.2 Cell line culture and transfection 48

2.1.3 Recombinant protein expression and purification 49

2.1.4 Identifying antibodies by phage display 50

2.1.5 Monoclonal antibody discovery through immunisation 53

2.1.6 Antibody discovery through single cell sequencing 55

2.1.7 Enzyme-linked immunoabsorbant assay (ELISA) 56

2.1.8 Antibody purification 56
2.2 Immunology *57*
2.2.1 Buffer and media composition 57
2.2.2 Isolation of peripheral blood mononuclear cells (PBMCs) 57
2.2.3 Magnetic isolation of PBMC subsets 58
2.2.4 Monocyte activation and culture 58
2.2.5 T cell activation and culture 58
2.2.6 Flow cytometry 59
2.2.7 Supernatant protein quantification 62
2.2.8 Gene expression 63
2.2.9 Clustered Regularly Interspaced Short Palindromic Repeats (CRISPR) gene knockout 65
2.2.10 Small interfering RNA (siRNA) gene knockdown 67
2.2.11 RNA sequencing 67
Chapter 3 : Strategies to discover a human GPR65 monoclonal antibody 70
3.1 Introduction *70*
3.2 Aim *71*
3.3 Results *73*
3.3.1 Recombinant protein generation 73
3.3.2 GPR65 phage display campaign to identify antigen-specific antibodies 77
3.3.3 Antibody discovery through antigen-specific B cell isolation 91
3.4 Discussion *106*
Chapter 4 : Investigating the role of acidic pH on immune function 118
4.1 Introduction *118*
4.2 Aim *119*
4.3 Results *120*
4.3.1 Investigating the impact of pH on PBMC subsets 120
4.3.2 MAIT cell-specific effects of an acidic extracellular environment 129
4.3.3 Transcriptional changes were consistent with a suppressive nature of a low pH environment 137
4.4 Discussion *169*
Chapter 5 : Exploring effects of GPR65 function in immune cells 176
5.1 Introduction *176*
5.2 Aim *176*

5.3 Results *178*

5.3.1 GPR65 expression profiling on immune cell subsets 178

5.3.2 Establishing the functional role of GPR65 in primary cells 185

5.3.3 Identification of transcriptional changes within lymphocytes upon the knockdown of GPR65 200

5.4 Discussion *222*

Chapter 6 : Overall Discussion and Future Directions 232

6.1 Main findings *232*

6.2 Overall conclusion *238*

6.3 Future directions *238*

Appendix 240

How COVID has impacted this DPhil *240*

References 241

List of Tables

Table 1 – Composition of media and buffers used within experiments throughout this thesis 57

Table 2 – FACS antibodies used throughout the project 60

Table 3 – Genes investigated by qPCR 64

Table 4 – Composition of CRISPR RNP complexes 65

Table 5 – PCR primer pair for assessing GPR65 knockout 66

Table 6 – Phage-derived GPR65 antibody sequences 85

Table 7 – Bioinformatic output of GPR65-specific B cells, identified using the 10x platform 104

Table 8 – Experimental samples subject to RNA sequencing 205

Table 9 – GPR65 was successfully knocked down in unstimulated cells cultured at pH 7.5 .208

Table 10 – List of upregulated genes in GPR65 silenced cells, observed in both unstimulated CD161^{+} T cells at pH 6.5, and cells stimulated with αCD3 and αCD28 at pH 7.5, compared to non-target siRNA treated cells. 220

List of Figures

Figure 1-1 – ASAS classification criteria for axial and peripheral spondyloarthritis diagnosis..4

Figure 1-2 – A graphical overview of the three proposed hypotheses for the role of HLA-B27 in SpA 9

Figure 1-3 - Model of T helper cell differentiation 13

Figure 1-4 – Proposed snake plot of GPR65 27

Figure 1-5 – A cartoon showing a proposed model of GPR65 signalling.....29

Figure 1-6 - GPR65 mRNA expression in paired PBMC and SFMC from spondyloarthritis patients 33

Figure 1-7 - Schematic diagram of the IgG antibody structure 40

Figure 1-8 - Schematic illustration of the five human antibody classes.....43

Figure 1-9 – Alternative antibody fragments.....46

Figure 2-1– PCR primer pair for assessing GPR65 knockout 66

Figure 3-1 – Overview of antibody discovery efforts to identify a monoclonal GPR65 antibody 72

Figure 3-2 - GFP could be used as a surrogate for GPR65 expression.....74

Figure 3-3 – Analysis of soluble GPR65 recombinant protein 76

Figure 3-4 – Depiction of a novel GPR65 chimeric construct 78

Figure 3-5 - Solubility of GPR65 chimeric proteins 80

Figure 3-6 - Mass spectrometry confirmed chimeric construct biotinylation.....80

Figure 3-7 - Phage display panning overview and strategy 81

Figure 3-8 – Phage panning output titres 83

Figure 3-9 - Antigen-specific monoclonal antibodies generated by phage display were identified 84

Figure 3-10 – Phage-derived antibodies specifically bound ECL1 and ECL2 GPR65 chimeric constructs 86

Figure 3-11 - Phage-derived antibodies raised against chimeric constructs were able to recognise native antigen overexpressed on HEK cells 86

Figure 3-12 – MAIT cells expressed the highest levels of GPR65 mRNA, of the PBMC subsets tested 89

Figure 3-13 – Phage-derived antibodies binding native antigen expressed on PBMCs 89

Figure 3-14 - PBMC gating strategy to identify cellular subsets 90

Figure 3-15 - Rabbit immunisations generated a robust immune response to human GPR65 92

Figure 3-16 - Primary screening data of B cell culture supernatant 94

Figure 3-17 – Isolation of antigen-specific B cells and subsequent PCR confirmation 95

Figure 3-18 - TAP supernatant binding on HEK cells expressing GPR65 97

Figure 3-19 – Rabbit-derived antibodies recognise human GPR65 expressed on HEK cells 99

Figure 3-20 – Rabbit-derived antibodies did not bind GPR65 when endogenously expressed on MAIT cells 101

Figure 3-21 - Flow cytometry sort strategy to isolate antigen-binding B cells for single cell sequencing 103

Figure 3-22 – Experimental design of single cell RNA sequencing of antigen-specific B cells 104

Figure 3-23 – 10x derived antibodies did not bind GPR65 on PBMC subsets 105

Figure 4-1 – T cells cultured in an acidic environment were protected from cell death 121

Figure 4-2 – Flow cytometry gating strategy for the identification of PBMC subsets 123

Figure 4-3 – Acidic pH suppressed LPS-dependent TNFα production from monocytes 125

Figure 4-4 – A low pH environment restricted pro-inflammatory cytokine release by TCR stimulated T cells 128

Figure 4-5 – Acidic pH suppressed Th1-like cytokine production from activated T cells 132

Figure 4-6 – Acidic pH-dependent inhibition of TNFα from MAIT cells was observed in a culture of isolated $CD8^+$ T cells 136

Figure 4-7 – A quality check provided confidence in good quality data attained by single cell RNA sequencing 138

Figure 4-8 –17 distinct clusters were revealed from $CD3^+$, $CD161^+$ sequenced cells 140

Figure 4-9 – Non-target siRNA treated, unstimulated MAIT cells at neutral pH were confirmed to be a homogenous cell population 143

Figure 4-10 – Distinct MAIT subpopulation structure was diminished in an acidic environment 144

Figure 4-11 – TCR stimulation successfully activated $CD3^+$, $CD161^+$ cells 149

Figure 4-12 – Largely shared transcriptional profile between MAIT and γδT cells after stimulation with αCD3 and αCD28 150

Figure 4-13 - MAIT cells expressed both IL-12 and IL-18 receptors 152

Figure 4-14 – Transcriptional changes in lymphocyte populations following IL-12 and IL-18 stimulation at pH 7.5 156

Figure 4-15 – Changes in expression level of genes associated with T cell migration following culture at pH 6.5 162

Figure 4-16 – Low pH had different effects on $CD4^+$ and $CD8^+$ T cell expression of CXCR3 and CXCR4 163

Figure 4-17 – Transcriptional changes in MAIT cells were consistent with the suppression of TCR-driven inflammation in a low pH environment 167

Figure 4-18 – *PDE3B* and *CREM* genes are upregulated in an acidic environment.....168

Figure 5-1 – GPR65 expression in healthy control PBMC subsets.....180

Figure 5-2 – GPR65 expression was equal across genders 181

Figure 5-3 – Commercial anti-GPR65 antibodies show no evidence of specific binding 184

Figure 5-4 – Experimental plan of GPR65 knockout, using CRISPR/Cas9 technology in isolated T cells.....187

Figure 5-5 – GPR65 knock out using CRISPR/Cas9 complexes.....188

Figure 5-6 – Pro-inflammatory cytokine release was increased by T cells treated with GPR65 specific RNP complexes 190

Figure 5-7 – GPR65 was successfully knocked down by siRNA treatment in CD8$^+$ T cells after 24 hours 192

Figure 5-8 – GPR65 expression was efficiently reduced in MAIT cells upon PBMC siRNA knockdown.....195

Figure 5-9 - IFNγ pH-dependent inhibition was attenuated by GPR65 knockdown in CD8$^+$ T cells 199

Figure 5-10 – GPR65 co-expressed with KLRB1 in lymphocytes.....201

Figure 5-11 - Experimental plan of single cell RNA sequencing conditions.....204

Figure 5-12 - MAIT cells were confirmed to express the highest levels of GPR65 mRNA.....207

Figure 5-13 and Table 9 – GPR65 was successfully knocked down in unstimulated cells cultured at pH 7.5.....208

Figure 5-14 - GPR65 siRNA treatment impaired MAIT cell sub clustering 212

Figure 5-15 – Differentially expressed genes of unstimulated GPR65 siRNA and non-target siRNA treated T cell subsets, at pH 7.5 215

Figure 5-16 – GPR65 is suggested to be implicated with CD28 activation in a neutral pH environment 216

Figure 5-17 – Changes in gene expression upon GPR65 silencing in αCD3 and αCD28 stimulated CD161$^+$ T cells 218

Figure 5-18 – GPR65 silencing at pH 6.5 upregulated T cell activation and effector genes, upon TCR stimulation.....220

Figure 5-19 – Relative proton sensing receptor expression levels in CD161$^+$ T cells 221

Figure 6-1 – Model of GPR65 function in TCR stimulated T cells, in neutral and low pH extracellular environments.....237

List of Abbreviations

AD	Atopic dermatitis
AS	Ankylosing spondylitis
ASAS	Assessment of Spondyloarthritis International Society
ASICs	Acid sensing ion channels
APC	Antigen presenting cell
ApoE3	Apolipoprotein E3
axSpA	Axial spondyloarthritis
BASDAI	Bath Ankylosing Spondylitis Disease Activity Index
BFA	Brefeldin A
β_2M	Beta-2-microglobulin
cAMP	Cyclic adenosine monophosphate
CCL	Chemokine ligand
CCR	Chemokine receptor
CD	Cluster of differentiation
cDNA	Complimentary deoxyribonucleic acid
CDR	Complementarity determining region
CHS	Cholesterol hemisuccinate
CREB	cAMP response element-binding protein
CREM	cAMP responsive element modulator
CRISPR	Clustered Regulatory Interspaced Short Palindromic Repeats
CSR	Class-switch recombination
CXCR	CXC chemokine receptor
DDM	Dodecyl-β-D-maltopyranoside
DEG	Differentially expressed genes
DMARDS	Disease modifying anti-rheumatic drugs
DMEM	Dulbecco's Modified Eagle Medium
DMSO	Dimethyl sulphoxide
DNA	Deoxyribonucleic acid
DSB	Disulphide bridges
EAE	Experimental autoimmune encephalomyelitis
ECL	Extracellular loop
EDTA	Ethylenediaminetetraacetic acid

ELISA	Enzyme-linked immunosorbent assay
eQTL	Expression quantitative trait loci
ER	Endoplasmic reticulum
Fab	Antibody-binding fragment
FACS	Fluorescence activated cell sorting
FBS	Foetal bovine serum
Fc	Crystallisable fragment
FDA	Food and Drug Administration
fSEC	Fluorescence-detection size-exclusion chromatography
γδT	gamma delta T (cell)
GAG	Group-specific antigen
GEM	Gel bead-in-emulsion
GFP	Green fluorescence protein
GM-CSF	Granulocyte-macrophage colony-stimulating factor
GPCR	G-protein coupled receptor
GWAS	Genome wide association studies
HA	Hemagglutinin
HEK	Human embryonic kidney (cell)
HLA	Human leukocyte antigen
HPLC	High-performance liquid chromatography
IBD	Inflammatory bowel disease
IFNγ	Interferon gamma
Ig	Immunoglobulin
IL	Interleukin
iNKT	Invariant natural killer T (cell)
JAK	Janus kinase
KIR	Killer-cell immunoglobulin-like receptor
KO	Knockout
LCMS	Liquid chromatography-mass spectrometry
LD	Linkage disequilibrium
LMNG	Lauryl-maltose-neopentylglycol
Log2FC	Log2 fold change
LPS	Lipopolysaccharide

MAF	Minor allele frequency
MAIT	Mucosal associated invariant T (cell)
MHC	Major histocompatibility complex
MS	Multiple sclerosis
NFκB	Nuclear factor kappa B
NICE	National Institute for Health and Care Excellence
NSAIDs	Non-steroidal anti-inflammatory drugs
NK	Natural killer (cell)
OD	Optical density
PBMC	Peripheral blood mononuclear cell
PBS	Phosphate buffered solution
PC	Principal component
PCR	Polymerase chain reaction
PD	Parkinson's disease
PEG	Polyethylene glycol
PKA	Protein kinase A
PsA	Psoriatic arthritis
PTM	Post translational modification
qPCR	Quantitative polymerase chain reaction
RA	Rheumatoid arthritis
RhoA	Ras homologue family member A
RNA	Ribonucleic acid
RNP	Ribonucleoprotein
RPMI	Roswell Park Memorial Institute 1640
RT	Reverse transcription
scFv	Single-chain variable fragment
scRNAseq	Single cell RNA sequencing
SDS-PAGE	Sodium dodecyl sulphate–polyacrylamide gel electrophoresis
SFMC	Synovial fluid mononuclear cells
siRNA	Small interfering RNA
SMAs	Styrene-maleic acid copolymers
SNP	Single nucleotide polymorphism
SpA	Spondyloarthritis

STAT	Signal transducer and activator of transcription
TAM	Tumour associated macrophage
TAP	Transcriptionally active polymerase chain reaction product
TCR	T cell receptor
TF	Transcription factor
TLR	Toll like receptor
TNFα	Tumour necrosis factor alpha
Treg	Regulatory T cell
TRPV	Transient receptor potential channel vanilloid subfamily
UMAP	Uniform manifold approximation and projection
UMI	Unique molecular identifier
UPR	Unfolded protein response
VHH	Variable domain of camelid heavy chain antibody
VLP	Virus-like particle
WT	Wild type

Chapter 1 : Introduction

1.1 Ankylosing Spondylitis

1.1.1 Clinical features

Spondyloarthritis (SpA) encompasses a group of related, but phenotypically distinct inflammatory rheumatic diseases, made up of ankylosing spondylitis (AS), psoriatic arthritis (PsA) and reactive arthritis[1]. The family share several clinical features, including inflammation of the peripheral joints and enthesis.

As the prototype SpA and most common of the diseases, AS presents chronic inflammation primarily in the spine and sacroiliac joints, progressing to new bone formation, and in some cases, eventual fusion of the spine (termed 'bamboo spine'); accompanied by back pain, stiffness and functional impairment. The primary pathological site for AS is the enthesis (the site of attachment of tendon or ligament to bone), where chronic inflammation, bone destruction and new bone formation is observed[2].

Peripheral involvement is often seen, presenting in the form of dactylitis and arthritis, with other extra-articular features also being observed throughout many organs of the body, such as uveitis (eyes), psoriasis (skin) and inflammatory bowel disease (IBD)[3]. Interestingly, these co-morbidities have been shown to differ between ethnicities; affecting only 0.4% Asian patients, compared to 5-10% European Caucasians also presenting with IBD[4].

Like many chronic diseases, AS affects more than just the direct health of patients, with reduced quality of life an additional complication[5]. Self-reported outcomes highlight the pain and fatigue of living with the disease, which impaired patients' daily activities and interfered with work; all leading to nearly a quarter of patients developing mental health conditions.

Burdens also transpire into society in the form of persistent leave or withdrawals from the workplace, and needless to say, substantial healthcare costs.

1.1.2 Prevalence and diagnosis

The prevalence of AS is thought to be the highest in Europe, North America and Asia, between 0.15-0.5%; but a definitive figure is difficult to establish due to delays in diagnosis and under recognition of the disease[6]. The prevalence of ankylosing spondylitis mirrors the occurrence of human leucocyte antigen (HLA) allele B27 (HLA-B27) in a given population (discussed in 1.1.4.1). Disease frequency is different between ethnic groups[7,8] and although the prevalence of AS is lower than in whites, blacks have been reported to have more severe disease[9].

Historically, gender disparities have been reported in AS, with the disease believed to be more prevalent in males[6]. Females often initially present pain in areas less considered typical of AS, such as the foot. This clinical presentation has been, and to some extents still are misdiagnosed as fibromyalgia[10]. Through advances in the understanding of disease, as well as developments in imaging, it is now believed prevalence in gender is relatively equal[11], instead with males perhaps presenting a more severe radiographic disease, coupled with elevated inflammation[12].

Although symptoms typically begin in early adulthood, AS is under recognised and is described as taking up to 7 years for a formal diagnosis, despite improved awareness and imaging capabilities[13,14]. Initial disease presentation is a gradual build-up of non-specific lower back pain and stiffness, which is worse in the morning and improves as the day continues upon activity. However, as persistent back pain can be a result of many causes, inflammatory disease is not always primary care providers first thoughts. Although C-reactive protein, a

biomarker of inflammation, levels are raised in some patients, there is a lack of sensitivity and specificity for AS.

Since the late nineteenth century, ankylosing spondylitis has been described as a distinct disease, with many improvements and modifications to diagnosis ever since[15]. The most traditional form of AS could be diagnosed using the established 1984 modified New York criteria[16], however patients without radiographic evidence were being missed. Therefore, the currently accepted classification was established in 2009 and determined by the Assessment of Spondyloarthritis International Society (ASAS)[17], as shown in Figure 1-1. Taking into consideration genetics, clinical presentation, and radiographic signatures, AS patients are termed and classified upon their predominantly axial (axSpA) or peripheral manifestations. The more common axial disease is further categorised into radiographic and non-radiographic axSpA patients; with non-radiographic largely showing spinal inflammation on MRI, but not showing changes upon conventional x-ray[18].

There are a variety of measures in place after diagnosis to measure disease activity and effectiveness of treatments, including a questionnaire (Bath Ankylosing Spondylitis Disease Activity Index, BASDAI), where patients can score symptoms such as pain, stiffness, and fatigue.

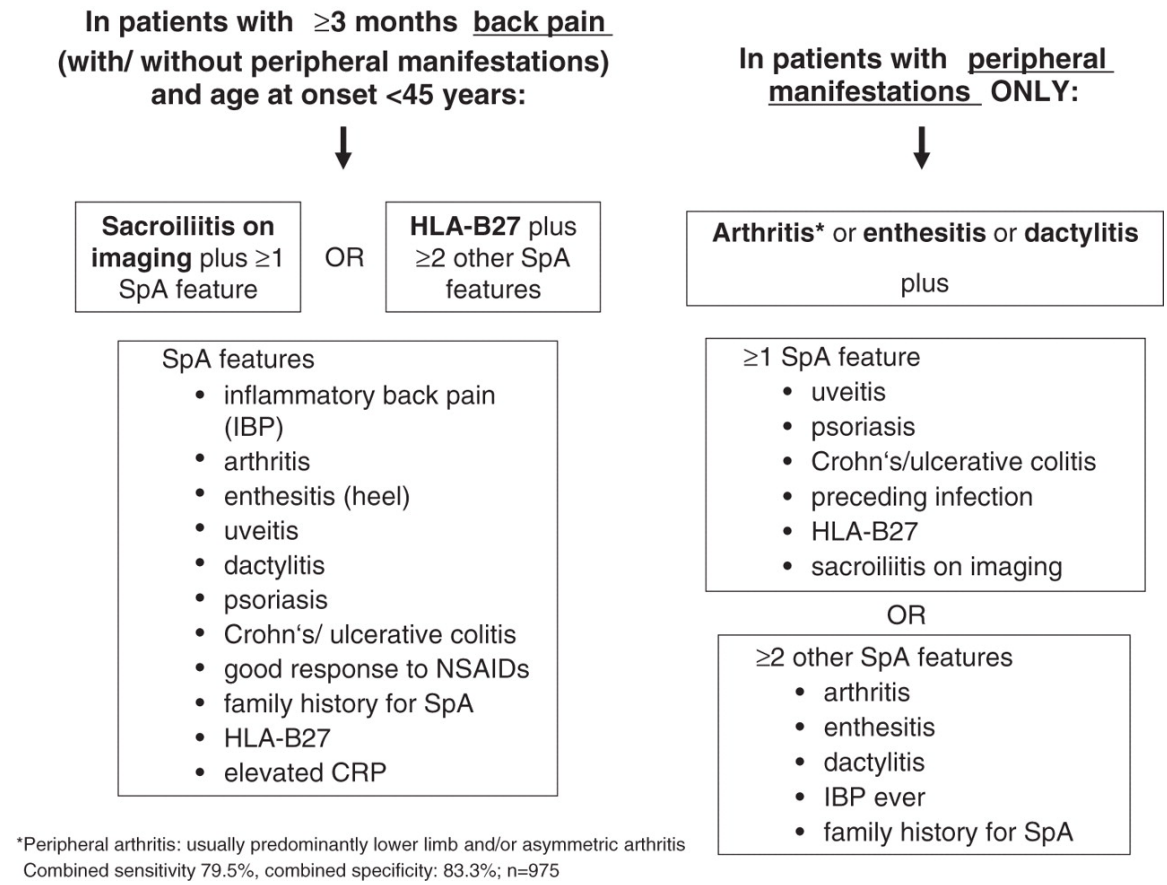


Figure 1-1 – ASAS classification criteria for axial and peripheral spondyloarthritis diagnosis

Taken from Rudwaleit and colleagues[19].

1.1.3 AS overlap with IBD

Ankylosing spondylitis is a largely inherited disease[20], with a potential environmental trigger. A relationship between joint disease and the gut is recognised, where the immune response appears to be primed and tolerance is lost within the gut, spreading to the joints (along the so called 'joint-gut axis'). A prime example is in the form of gram-negative bacterial infections (e.g, non-typhoidal *Salmonella* spp) of the gastrointestinal tract causing reactive arthritis, only days after initial bowel symptom changes[21].

A feature of AS is the clinical overlap with inflammatory bowel disease. It has been shown that patients are around six-times more likely to contract the most common forms, ulcerative colitis, or Crohn's disease, particularly in the initial few years post diagnosis[22]. It is also thought up to 60% of AS patients display clinically silent micro/macroscopic gut inflammation, correlating with worse joint disease activity[23–25]. Conversely, IBD patients most frequent extra-intestinal manifestation is SpA[26].

A hypothesis for microbial dysbiosis contributing to SpA was supported through studies into animal models of AS[27,28]. In particular, when HLA-B27 transgenic rats were raised in germ-free environments, they did not observe peripheral joint or intestinal inflammation, compared to when the same rats were raised in conventional conditions, or upon reintroduction of commensal gut flora[28]. Additionally, there is evidence of a dysregulated gut microbial composition in IBD patients[29,30]. Through microbial sequencing, a discrete microbial signature has been reported within AS patients, with an abundance of Ruminococcaceae, Bacteroidaceae and Clostridaceae, influenced by disease activity[31,32]. Although distinct microbiomes have been reported between AS and IBD patients, there were shared pathogenic genera that could support common triggers of the two diseases[33].

1.1.4 Genetic associations

1.1.4.1 HLA-B27

Ankylosing spondylitis' association with HLA-B27 was first described nearly 50 years ago and is still the strongest known association of any HLA to human disease[34,35]. It is thought the geographic variation in AS is due to the global prevalence of HLA-B27 in different populations, with the Haida community having the highest prevalence of 50%[36]. Despite there being over 150 known subtypes of HLA-B27, only a handful have been reported to significantly increase the risk of disease: B*27:02, B*27:03, B*27:04, B*27:05, B*27:07[37]. The opposite is also suggested, with alternative subtypes believed to be protective (B*27:06 common in the southeast Asian population, and B*27:09, seen almost exclusively in the Sardinian population[38]). Although 84% of AS patients are positive for HLA-B27, most individuals who are HLA-B27 positive do not develop the disease, suggesting the polygenic nature of development[39,40].

As a member of the class I major histocompatibility complex (MHC), the main role of HLA-B27 is to form heterodimers with β_2 microglobulin (β_2M) and display peptides (from either self or non-self antigens) to cytotoxic $CD8^+$ T cells, particularly important in viral infections. However, the precise molecular mechanism by which the association of HLA-B27 causes disease remains unclear. The three most favoured hypotheses are briefly described below, and summarised in Figure 1-2.

<u>The 'arthritogenic peptide' hypothesis</u>

It is proposed that natural ligands or specific peptides for HLA-B27 are target antigens of HLA-B27 restricted $CD8^+$ T cells, promoting an inflammatory response and driving disease pathogenesis[41]. As a form of molecular mimicry, this scenario suggests a peptide derived from

a bacterial infection could resemble a self-peptide. However, this hypothesis has been challenged as there are no specific peptides identified to date, and the development of SpA-like disease was reported in the transgenic HLA-B27 transgenic rat model for AS, upon depletion of $CD8^+$ T cells[42].

The HLA-B27 homodimer formation hypothesis

HLA-B27 can form β_2M-free, disulphide-bonded homodimers[43] and HLA-B27 free heavy chains on the cell surface[44], with aberrant forms shown to be highly expressed on the cells of AS patients[45,46]. The binding of aberrantly folded HLA-B27 to specific killer immunoglobulin-like receptors (KIRs) and leucocyte immunoglobulin-like receptors have been shown to promote inflammation in AS patient $CD4^+$ T cells and natural killer (NK) cells, through their enhanced survival and increased production of proinflammatory cytokines[47,48]. Further support has been shown by the inhibition of the interaction of KIRs and the HLA-B27 homodimer, reducing pro-inflammatory cytokine production[49]. However, it has been suggested that aberrant forms of HLA-B27 are produced from both the protective and causative alleles, questioning this theory of AS pathoetiology[50].

The unfolded protein response hypothesis

Compared to other MHC molecules, misfolding of the HLA-B27 tertiary structure in the endoplasmic reticulum (ER) has been reported[51]. Its accumulation leads to ER stress, which initiates the unfolded protein response (UPR). Along with suppression of protein translation, the transcription factor C/EBP homogous protein is activated resulting in pro-inflammatory cytokine release[52]. This hypothesis was further supported by UPR activation upon HLA-B27 misfolding in transgenic rats[53]. Moreover, in humans there is conflicting evidence of HLA-B27 misfolding driving inflammation through the activation of the UPR in AS patient macrophages,

supporting a complex mechanism of pathogenesis[54,55]. The interest in this theory remains, but it is still unproven, with gut biopsies of AS patients not showing clinical evidence of upregulated UPR gene transcription[56].

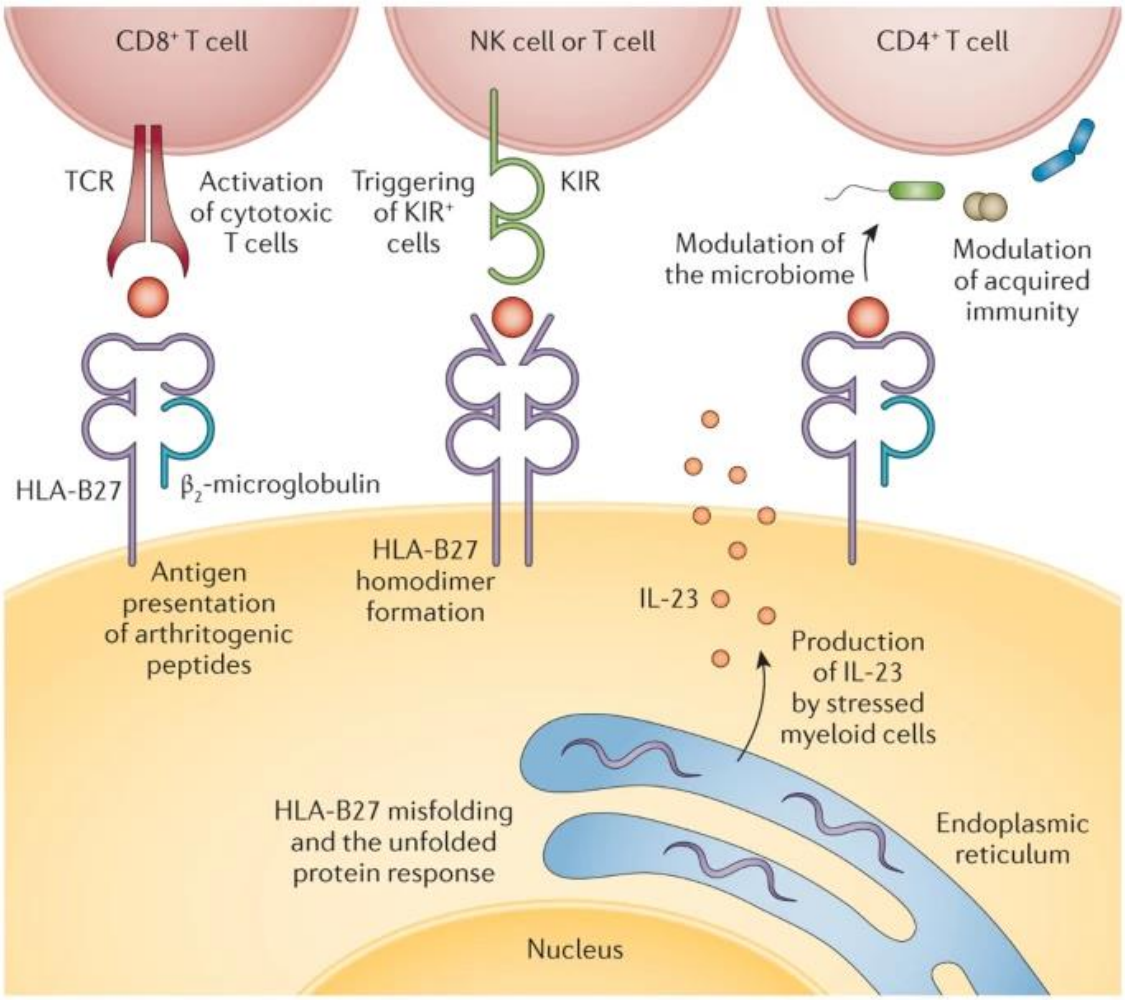


Figure 1-2 – A graphical overview of the three proposed hypotheses for the role of HLA-B27 in SpA

Taken from Sieper and colleagues[57].

1.1.4.2 Genetic associations with AS

HLA-B27 is thought to contribute to only a third of total heritability for AS, with many other contributing genes having been associated by genome wide association studies (GWAS). The International Genetics of Ankylosing Spondylitis surveyed ~10,500 AS patients and ~15,000 healthy controls, made up mostly of a European cohort, with a 10% East Asian cohort; Cortes and colleagues identified 25 loci that met genome wide significance ($P < 5x10^{-8}$) for the disease[58]. More recent GWAS studies not only confirm loci of previously known single nucleotide polymorphisms (SNPs) but have discovered many more, now suggesting there are over 110 genes associated with AS[59]. Risk loci identified can be grouped into categories depending on their function; involvement in T cell immune regulation (*IL12B, IL23R, TYK2, IL6R, RUNX3, IL7R, TBX21, EOMES*), peptide preparation for HLA class 1 presentation (*ERAP1, ERAP2, UBE2E3*) and G-protein coupled receptors (*GPR25*, *GPR35, GPR37, GPR65*).

Second to HLA-B27, the endoplasmic reticulum aminopeptidase, *ERAP1* has the next strongest genetic association with AS. Due to its importance in antigen presentation, the link to disease has been widely studied, establishing *ERAP1* being restricted to HLA-$B27^+$ AS patients. Abnormal function of *ERAP1* prevents optimal trimming of peptides in the ER and leads to MHC class I peptide-complex misfolding, resulting in the presentation of free heavy chain on the cell surface[60], previously discussed for driving the pathogenesis of AS (1.1.4.1). A second family member, *ERAP2*, is also identified as a risk gene for AS.

Many important polymorphisms within the IL-17/IL-23 axis (*IL23R, IL12B TYK2, IL6R, STAT3*) have been highlighted for ankylosing spondylitis[58,61], supporting the influence of this pathway in disease contribution. Binding of the IL-23 receptor activates the janus-kinase/signal transducer and activator of transcription proteins (JAK/STAT) signalling pathway and

regulates the differentiation of Th1 and Th17 cells, resulting in changes to proinflammatory cytokine release.

Finally, GWAS can help us to understand the common risk loci shared among other inflammatory diseases. Most notably for AS, there are ~30 shared loci with IBD[59,62], further supporting the concept of gut involvement contributing to AS pathogenesis.

1.1.5 Immunology of AS

The immune system, consisting of multiple organs, cell types and proteins, is a vital network to protect the host from invading pathogens and remove damaged or dying cells from the body[63]. If an invader breaches the physical barriers, such as the skin, and mucosal membranes (within the digestive, respiratory and reproductive tracts) the first line of the hosts defence is the innate immune system; with the aim to immediately prevent foreign pathogens spreading throughout the body, in a non-specific manner. Upon migration to the site of inflammation and recognition of a pathogen, monocytes, neutrophils, and dendritic cells engulf and kill the microorganisms, in a process known as phagocytosis[64]. In contrast, natural killer cells respond through a so called 'missing self' response and destroy target cells through the assessment of aberrant or reduced MHC class I molecules expressed on the cell surface[65].

Meanwhile, the adaptive immune system, also known as 'acquired immunity', consists of complex cellular signalling to prevent an infection through antibody, or cell-mediated responses, by B or T lymphocytes, respectively. Both cells are derived from haematopoietic stem cells in the bone marrow, with their clonal expansion (the amplification of lymphocytes specific to a matching invading pathogen) being a hallmark of this system[66] .

The term antigen classifies anything that is recognised by the adaptive immune system (primarily T and B cells), whereby an immune response is generated. However, there is a fine balance of ensuring protection from dangerous 'non self' pathogens, whilst maintaining tolerance to 'self' molecules. A characteristic of spondyloarthritis is the aberrant activation of immune cells, with evidence of both autoinflammatory and autoimmune components in AS[67,68].

1.1.5.1 T cells in AS

Upon their development in the thymus, where a series of selection processes are performed, naïve T cells migrate to the periphery displaying functional T cell receptors (TCR) that lack high self reactivity. Two primary cell types, cells either expressing CD4 or CD8 glycoprotein ($CD4^+$ and $CD8^+$ T cells, respectively) make up the majority of αβ T lymphocytes, each with slightly different functions; $CD4^+$ T cells are MHC class II restricted and are preprogramed for helper functions, such as the release of various cytokines to influence alternative pivotal immune responses, whilst $CD8^+$ T cells are MHC class I restricted and preprogramed for cytotoxic functions, through their production of granzyme and perforin. Both cells recognise antigenic peptides presented via MHC on antigen presenting cells ((APCs) e.g dendritic cells, macrophages, and B cells) through their TCR; it is this recognition which encourages co-stimulatory receptors to localise with the TCR, forming an immunological synapse[69]. Together with a range of stimulatory and inhibitory signalling molecules, T cell activation and differentiation is regulated.

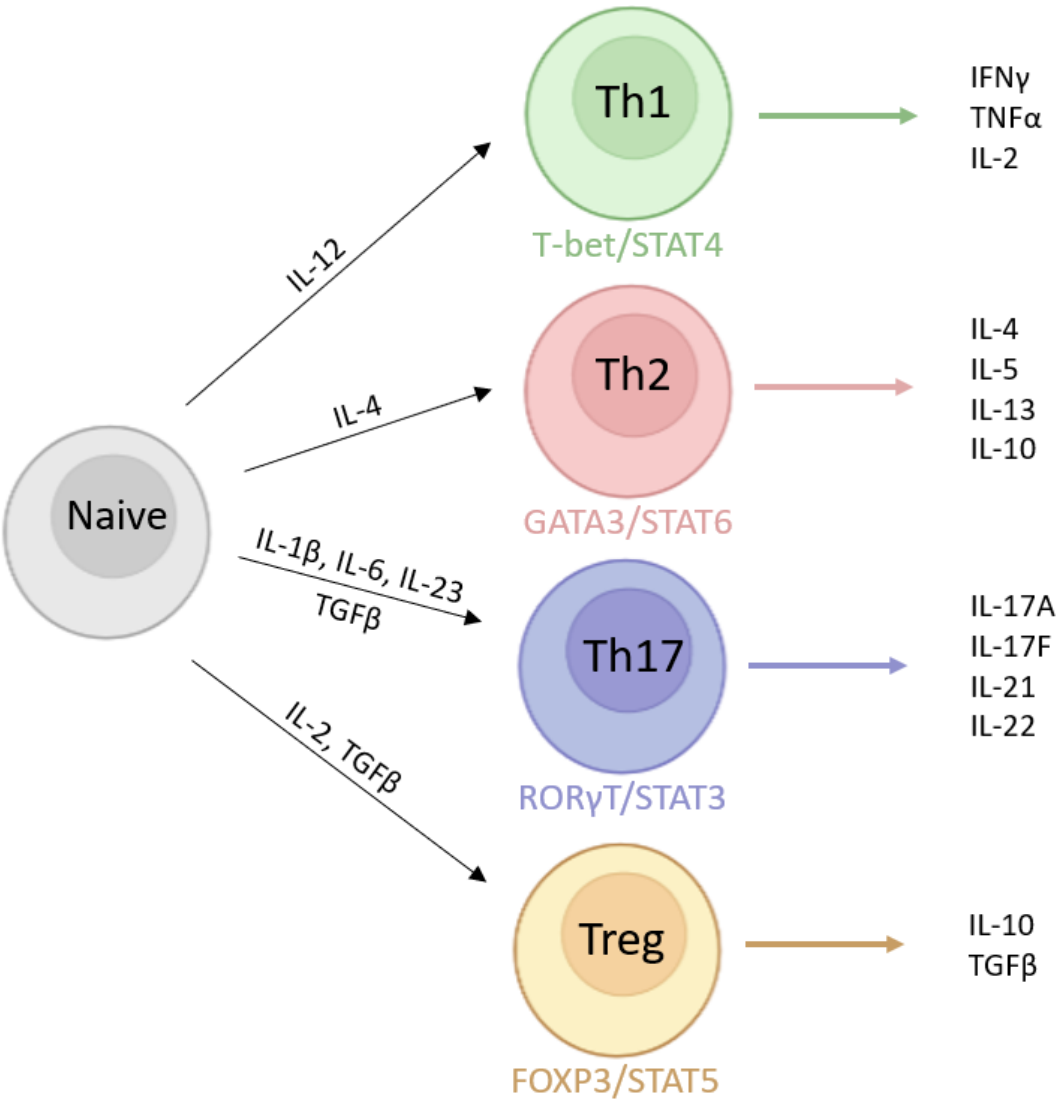


Figure 1-3 - Model of T helper cell differentiation

Naïve $CD4^+$ T cells differentiate into distinct lineages upon their activation and under the influence of cytokines in their environment. Th1 cells require the transcription factor (TF), T-bet and produce IFNγ. Th2 cells produce IL-4 and IL-13 and require the TF GATA-3. Th17 cells produce the signature cytokine IL-17A and require the TF RORγt. Regulatory T cells (Treg) express the TF FOXP3 and broadly suppress inflammation. Adapted from[70,71].

Depending on the microenvironment present when $CD4^+$ T cells are activated, they can differentiate into distinct lineages. Transcription factors (TF) are the master regulators of this transition, leading to specific effector functions (details can be found within Figure 1-3). When only Th1 and Th2 cells were known, it was believed cells were terminally differentiated. However, since the discovery of alternative T cell subsets, it is now understood that there is more complexity in the system considering their stability. For example, Lee and colleagues reported the polarisation of a Th17 cell to a Th1 cell when in the presence of IL-12[72]; particularly relevant as SpA synovial fluid contains high concentrations of IL-12[73]. Moreover, in disease this nature of cell plasticity often presents as intermediate cells with distinct epigenetic signatures[74]; as it has been shown the synovial fluid mononuclear cells (SFMC) from inflamed joints expressed both RORγT and T-bet, coupled with the same cell co-producing Th1-like cytokines interferon-gamma (IFNγ) or granulocyte-macrophage colony-stimulating factor (GM-CSF) along with interleukin (IL)-17A[73,75].

Regulatory T cell (Treg) enrichment in disease associated sites of the gut and joints, versus the blood, of AS patients theorises their recruitment to the inflammatory site[76,77]. However, there are reports of synovial Tregs in arthritic joints displaying an altered state, suggesting plasticity from environmental cues. Factors released from inflamed, local fibroblast-like synoviocytes (such as IL-6) have the potential to polarise Tregs into more Th1-like, and Th17-like cells[78,79]. Supporting evidence shows the intermediate cells as potent IL-17A producers and can release cytotoxic proteins, whilst retaining their ability to inhibit monocyte derived-tumour necrosis factor alpha (TNFα) production, through their expression of LAG3[80,81]. Further investigation is required to determine if this dual activity from Tregs directly affects disease progression. But there is confirmation that the suppressive nature of Tregs is

preserved within the joints and guts of AS patients, with restricted T effector cell activity and their continued production of anti-inflammatory IL-10[76,82].

Successful outcomes of using anti-TNFα therapies in the clinic provide validation for Th1 cell involvement in AS (elaborated in 1.1.6). However, there is debate as to whether IFNγ has a specific role in SpA. Conflicting evidence of Th1 proportions in AS verses healthy controls are reported, with Limon-Camacho and colleagues reporting a significant increase of Th1 cells in patient peripheral blood[83]. Yet, despite similar patient demographics and comparative disease severity, another study suggests a reduction of Th1 cells in the blood[12]. Although IFNγ is slightly elevated in AS sera, compared to health, the Th1 response overall is regarded as being less important when considering alternative inflammatory responses from Th17 activation[84]. The identification of genes and pathways associated with Th17/23 biology through GWAS, suggest Th17 cells to be vital within AS pathology, supported by multiple immunological studies implicating Th17/23 responses in SpA and related diseases, such as IBD.

1.1.5.1.1 Th17 cells

The key effector function of Th17 cells is believed to be immunity against extracellular bacteria and fungal infections, as patients lacking Th17 cells presented with reoccurring infections[85,86]. These effector functions are mediated through the release of the family of IL-17 cytokines, as well as their production of IL-22, and affect T cell priming and stimulation of alternative cell types. Upon the discovery of IL-23 by Opperman et al, this cytokine was identified to expand Th17 cells, leading to the subsequent production of IL-17[87–89] , creating the concept of the Th17/23 axis.

With six family members named IL-17A (often referred to as IL-17) through to IL-17F, the highest homology is reported between IL-17A and IL-17F, and these can exist as heterodimer, or independent homodimers, with varying degrees of potency[90]. IL-17 acts on target cells, such as epithelial cells and synoviocytes, primarily resulting in the release of various cytokines, including pro-inflammatory TNFα and IL-1β[91]. But IL-17 has also been shown to induce chemokine expression on IL-17-receptor bearing cells, for instance the upregulation of CCL2, in turn encouraging the migration of monocytes[92], as well as the regulation of antimicrobial peptides (e.g S100 proteins)[93].

IL-17 has long been associated with ankylosing spondylitis. First, the most trusted and well-established model for AS is the HLA-B27 transgenic rat model, which displays clinical features seen in humans (for example, enthesitis and spondylitis), and is understood to be driven through IL-17 biology[94]. Moreover, the substantial genetic associations confirmed an important role for this cytokine in disease, in the discovery of HLA-B27 and multiple Th17/23 related pathways. The interaction of aberrant HLA-B27 with KIR3DL2 expressed on a subset of Th17 cells, identified within synovial fluid, can promote Th17 survival and secrete high levels of IL-17A[47,95]. Th17/23 related pathways impacting disease are further supported by; an increase of Th17 cells in AS blood compared to health[96,97], the presence of IL-17A producing cells at the facet joint[77] and elevated IL-17A and IL-23 protein in the sera, which positively correlated with BASDAI[98,99]. Despite this wealth of evidence however, it remains unclear whether this pathway is the initiator of pathogenic processes.

As previously alluded to, an important characteristic of Th17 cells is their considerable plasticity and polyfunctional ability for co-expressing IL-17 with a multitude of alternative cytokines, ultimately then displaying differing strengths of the inflammatory response. In

disease, synergies of IL-17A with other pro-inflammatory factors can prove damaging, such as its combination with TNFα, which can induce pro-inflammatory mediators from synoviocytes in the joint and contribute to local damage[100]. Alternatively, it has been reported that IL-17A and IL-1β synergistically increases IL-6 and IL-8 production by keratinocytes, and kick starts mechanisms that could augment skin inflammation observed in psoriasis, a co-manifestation of AS[101].

The Th17/23 axis is notably not restricted to the joint, with evidence of its involvement in the gut, reinforcing the interest into the joint-gut axis. Whilst maintaining the ability to drive inflammatory responses, in the gut this pathway has also been reported to be protective[102]. Here, instability of the differentiation of Th17 is common, with cells transitioning to Tregs during the resolution of inflammation in the intestinal lamina propria[103]. An abundance of IL-23 has been described in the inflamed mucosa of AS patients, but through its triggering of a substantial IL-17 response, it may prove protective via its tissue restoration activity[104].

1.1.5.1.2 $CD8^+$ T cells

GWAS identified associated factors of $CD8^+$ T cell biology, such as *TBX21, EOMES* and *RUNX3*, implying their importance in AS. The presence of disease in the HLA-B27 transgenic rat model of AS, in the absence of functional $CD8^+$ T cells, argues against a key role of these cells in driving disease[42]. Yet, through their expression of proinflammatory cytokines, especially TNFα, IFNγ and IL-17A, as well as cytotoxic factors such as granzyme and perforin, they are likely to play a role in the inflammation observed.

In SpA, $CD8^+$ T cells are reduced in the blood, whilst an enrichment is observed in synovial fluid, where these cells display an inflammatory, 'memory' phenotype and evidence of their local expansion[105,106]. Expression of gut-related trafficking molecules on synovial $CD8^+$ T cells

suggest their migration from the gut to the joint, with further immune cell recruitment encouraged via their expression of CXCR3 and could explain the cellular proportion differences reported in the periphery[107,108]. Interestingly, in AS patients, $CD8^+$ T cells within the joint are more cytotoxic than their counterparts in the blood, so likely contribute to joint destruction[105].

1.1.5.2 Innate-like T cells in AS

The cytokine repertoire and transcriptional profile of Th17 or IL-17-producing $CD8^+$ T cells is also present in other cells, namely the innate-like lymphocytes, so they too have been studied to identify their contribution to AS pathology. A mouse study of IL-23 overexpression in a SpA model showed the induction of enthesitis in the absence of conventional Th17 cells, instead dependent on $CD4^-$, $CD8^-$ T cells, suggesting a role for IL-23 responsive innate-like T cells in AS[109].

By definition of their TCR expression, a small number of T lymphocytes are able to respond to infection in synchrony with the innate immune response. These so called innate-like T cells have been shown to be developmentally preprogramed and have altered TCR responses, removing their need for clonal expansion and differentiation in the periphery, and possessing the ability to becoming successfully stimulated by cytokine triggers[110].

1.1.5.2.1 Mucosal-associated invariant T (MAIT) cells

First described within the CD4- and CD8- T cell subset, mucosal-associated invariant T (MAIT) cells were identified to express an invariant TCR, Vα7.2-Jα33, and are associated with a limited set of Vβ chains[111,112]. Predominantly understood to be $CD8^+$, MAIT cells represent up to 10% of T cells in the blood, and preferentially localise in peripheral tissues, particularly abundant in the liver, and to a lesser degree at mucosal barrier sites[113].

MAIT cells have a restricted TCR repertoire, with a specificity for the MHC class I-like molecule, MR1. Their selection in the thymus is MR1-dependent and is followed by extra-thymic maturation, regulated by multiple factors[114]. Through the discovery of vitamin B metabolites as MAIT cell antigens[115], their biology over the past decade has been interrogated. As first line responders to microbial infections, MAIT cells are capable of rapidly expressing large amounts of cytokines, especially IFNγ, TNFα and IL-17A. Although a homogenous population in a resting state, they display functional plasticity similar to $CD4^+$ T cells and can be skewed towards a pro-inflammatory state. MAIT cell expression of CD161 is universal, and so its expression acts as a surrogate for their identification. This C-type lectin receptor was originally a marker of NK cells and is expressed on many other inflammatory cell types (Th17 cells, γδT cells), for which they all share a distinct phenotype, and are associated with IL-17 biology[116,117].

Proportional changes in MAIT cells within the blood of AS patients yield discordant results, likely explained through differences in the selection criteria of patients, severity of disease, whether they are treatment naïve, and differences in the way of identifying MAIT cells. Largely, reports of a loss of MAIT cells in disease have been identified using the combination of surrogate markers, Vα7.2 and CD161, however both are understood to downregulate upon activation[118–121]. In contrast, very little change, or even increases of MAIT cells in the blood compared to controls have been suggested when MAIT cells were distinguished using the more specific MR1 tetramer[122,123].

Despite these variances, the most consistent finding is the increase of $IL\text{-}17A^+$ MAIT cells in the periphery, producing IL-17A levels similarly expressed by Th17 cells in the blood, and perhaps associated with $HLA\text{-}B27^+$ male patients specifically[119,123,124]. In health, MAIT cells in

the blood are primarily associated with their production of Th1-related cytokines, with only a few expressing RORγt and subsequent ability to produce IL-17[125], suggesting an expansion and maturation of these cells in AS. Additionally, the activation status of MAIT cells has been reported to positively correlate with disease[118].

An abundance of MAIT cells is observed in AS synovial fluid and these cells show even higher IL-17 production, as well as the expression of granzyme B, compared to their counter parts in the blood; curiously, this is in accordance with a reduced IFNγ and TNFα profile[119]. This proinflammatory state is suggestive of local activation; high levels of IL-7 are reported in the diseased joint, with evidence of upregulated IL-7R on AS patient MAIT cells, driving their capacity to produce IL-17, resulting in tissue destruction[119]. Furthermore, increased expression of *IL23R* is shown in AS MAIT cells, compared to healthy controls and speaks to elevated IL-17 production[124], reflecting the support of their involvement in AS through genetic associations.

1.1.5.2.2 Gamma-delta (γδ) T cells

Gamma-delta (γδ) T cells represent another form of unconventional T cell and express a γδ TCR rather than the abundant αβ TCR. These cells are not limited to peptide recognition through MHC presentation, instead responding to non-peptidic molecules[126]. Like MAIT cells, these alternative innate-like T cells follow unique extra-thymic pathways for maturation, including their ability to be activated rapidly, in a TCR-independent manner[127].

Made up of two major subsets, the Vδ2 subset is the most prominent in the periphery of adults, with high levels of IL-23R and CD161 expressed on their surface, compared to a minority of Vδ1 cells, which primarily reside in the thymus and peripheral tissues[128]. Although

Vδ2 cells most reflect the biology of MAIT cells, they do not exhibit type 17 effector function to the same extent, at least in the blood[129].

Compared to MAIT cells, there is less work published to support γδT cell direct involvement in disease, with the connection hypothesised through their prominent production of IL-17. In AS patients there are elevated numbers of γδT cells in the blood, expressing high levels of IL-23R and possessing a skewed IL-17 profile, with co-expression of GM-CSF[75,130]; upon stimulation through their TCR, IL-17 was highly produced, whilst no changes were observed to IFNγ expression, compared to healthy controls. Interestingly, γδT cells have been shown to be tissue resident cells in the normal spinal entheseal tissue. In SpA patients, these innate-like cells extracted from the synovial fluid were reported to have elevated RORγt expression levels and were enriched for IL-23R$^+$ and IL-17$^+$ cells, with cytokine signatures like that of Th17 cells[131,132].

Animal models can help with our understanding of disease pathogenesis, and the IL-23 responsive tissue-resident Vγ6$^+$ RORγt$^+$ γδT cells are somewhat believed to aid the development of SpA in a rodent model of disease[133]. As this subtype has been shown to promote bone growth through IL-17 biology[134], it could link IL-23-induced inflammation to bone growth in the enthesis, a hallmark of AS.

1.1.5.3 NK cells in AS

The assessment of NK cells in AS has reproducibly shown a skewing of the CD56^{dim}, CD16$^+$ NK cell subset, which has been correlated with disease via BASDAI[135–137]. These cells are thought of as cytolytic, expressing KIR receptors, and those expressing KIR3DL2 (a receptor for aberrant HLA-B27) in particular have been reported to be increased in AS patients[48], with the interaction proposed to inhibit NK production of IFNγ[138]. However, there is some controversy

around whether the NK cells themselves are pro- or anti-inflammatory in their nature within disease, with reports of both reduced cytotoxic activity and IL-22-dependent gut regeneration[137,139], versus the upregulation of pathologically activated pathways[140].

Additionally, a rare invariant natural killer T cell (iNKT) display properties of both NK cells and T cells. These cells are activated upon presentation of antigen by CD1d, an MHC class I like molecule and are reported to be increased in both the peripheral blood and inflamed joint of SpA patients, with a disease specific signature, and were transcriptionally like their innate counterparts (γδT cells/innate lymphoid cell 3) secreting IL-17A[124,132,141].

1.1.5.4 Monocytes and macrophages in AS

IL-23 is a key factor in SpA, with polymorphisms in the *IL23R* associated with disease, increased serum concentrations of IL-23 found in patients and IL-23 exposure alone able to induce a model of spondylitis[99,109]. As macrophages and their precursors, monocytes, secrete IL-23, these cells have been associated with disease pathogenesis.

In spondyloarthritis patients, an imbalance of the three monocyte subsets has been reported, with an increase in classical monocytes ($CD14^+$, $CD16^-$) observed[142]. These cells exhibited a more proinflammatory phenotype and were found to correlate with disease[143–145]; as did the pro-inflammatory $CD163^+$ macrophages. AS monocytes from the periphery had upregulated toll-like receptor 4 (TLR4) and were primed to produce TNFα upon bacterial exposure, as well as express higher levels of IL-23, compared to healthy controls[146,147]; particularly important as levels of circulating bacterial derived lipopolysaccharide (LPS, a TLR4 ligand) in the periphery are increased due to a disturbed gut barrier in disease[148].

Within the context of the joint, $CD14^+$ myeloid cells at the enthesis have been deemed a primary source of IL-23, along with a predominance of $CD163^+$ macrophages in AS synovial tissue having been associated with activation of the UPR[149,150].

So, through the release of IL-23 from these myeloid cells, IL-23R expressing cells become activated, signal through the JAK/STAT pathway and lead to the ultimate activation, expansion, and maintenance of cells capable of producing AS-associated, inflammatory IL-17 (Th17 cells, γδT cells and MAIT cells).

1.1.6 Treatments

Without a cure, therapeutics aim to relieve the symptoms for patients and modify disease progression. Those diagnosed with axSpA are initially treated with a combination of non-steroidal anti-inflammatory drugs (NSAIDs) and specialist physiotherapy/exercise. Unlike other rheumatoid diseases, synthetic disease modifying anti-rheumatic drugs (DMARDs), such as methotrexate, do not play a role in treatment of axSpA[151]. Alternative targeted-DMARDs (such as JAK inhibitors) are given to those who do not tolerate NSAIDs.

In the UK patients who fail to respond to 4 weeks' worth of 2 different NSAIDs, and who present a BASDAI ≥ 4, are considered for biologic-DMARDs. The first to be trialled was anti-TNFα therapy, of which there are currently five marketed drugs recommended by NICE, each with slightly different antibody properties[152–156]. These agents have revolutionised the management of AS, with many patients achieving reduced ASAS scores; however, around 30% of patients still fail to show any response, supporting the role of other factors also driving disease.

Through a greater understanding of the pathogenesis of disease, IL-17 inhibition has reported successful outcomes in the treatment of AS[157–160], with improvements of co-manifestations also observed. Considering its role in the maintenance of IL-17 production, IL-23 inhibition was expected to respond similarly to the anti-IL-17s, however biologics targeting either the p40 or p19 subunits of IL-23 are not currently licenced for AS, due to a lack of efficacy[161,162].

Alternative cytokines associated with AS pathology include IL-6 and GM-CSF, however antibody-mediated neutralisation of them both failed to be effective in treating AS patients[163,164]. Despite these failed attempts signalling through the JAK/STAT pathway, small molecule JAK inhibitors in axSpA are successful treatments of disease and support the benefit of blocking multiple cytokines[165,166].

Overall, results in the clinic provide validation of TNFα and IL-17A contributing to disease. But despite these therapeutic advances there remains poor responders to these last-line biologic therapies, suggesting that a key pathogenic driver in ankylosing spondylitis is yet to be elucidated.

1.2 The proposed function of the proton sensing GPCR, GPR65

1.2.1 An overview of GPCRs

G protein-coupled receptors (GPCRs) are highly conserved cell surface receptors which transduce extracellular signals into physiological effects and represent the largest family of proteins encoded by the human genome. Due to the diversity and size of the family, receptors are grouped into classes based upon their amino acid sequence similarities and proposed function; Class A (rhodopsin; the largest of the families), Class B (secretin and adhesion), Class C (glutamate) and Class F (frizzled)[167]. Involved in many key processes such as neurotransmission, hormone release and blood pressure regulation, to only name a few,

GPCR dysfunction contributes to many human diseases, reflected in being a target of ~35% of Food and Drug Administration (FDA) approved therapeutics[168]. Despite years of study into GPCRs, there are still > 100 receptors with natural ligands yet to be identified, of which a proportion would likely emerge to be functionally important and have therapeutic potential for undertreated diseases[169].

A shared characteristic of GPCRs is the seven-transmembrane domain of α-helices and an extracellular N-terminus, and intracellular C-terminus. Activation in response to stimuli alters the structural conformation and exposes an intracellular site enabling the coupling of heterotrimeric G proteins, formed by Gα, Gβ and Gγ subunits[170]. Classified into four major families (G_s, $G_{i/o}$, $G_{q/11}$ and $G_{12/13}$), only the Gα subunit is able to signal independently and generate secondary messengers (e.g cyclic adenosine monophosphate (cAMP) and calcium) to induce diverse signalling cascades[171]. Receptors can couple more than one Gα protein, with the opposite also true, that the same Gα protein can bind distinct receptors. For their regulation, prolonged receptor signalling is desensitised through GPCR internalisation, facilitated by multiple pathways[172].

1.2.2 GPR65, a proton sensing GPCR

Discovered in 1996, GPR65 (also referred to as TDAG8, particularly in mouse studies) is a plasma membrane protein representing 337 amino acids, with a molecular mass of 39 kDa[173] (Figure 1-4). It is understood to be one of three proton sensing GPCRs, along with GPR4 and GPR68. The understanding of how pH sensing occurs via these receptors has recently been advanced with the discovery of a centrally buried triad of acidic residues[174], replacing the original theories into protonation of extracellular histidine residues[175–178]. It was previously

proposed that psychosine could act as a ligand for this receptor[176,179] , but has been contested, with the theory no longer widely accepted[177,180].

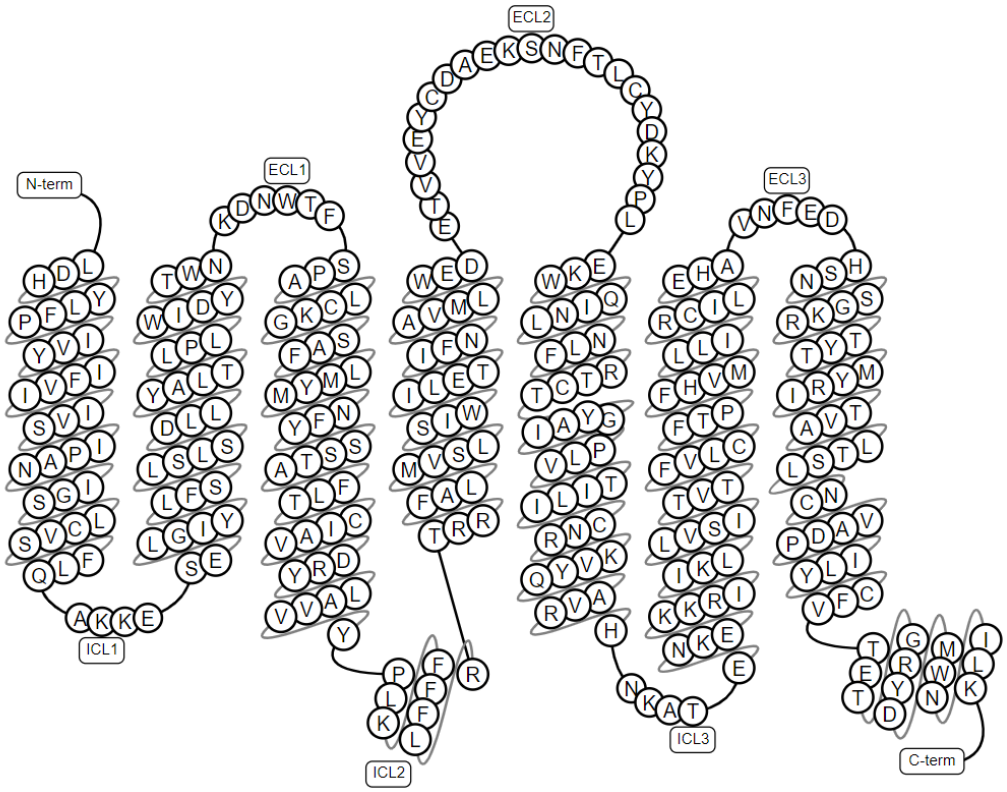


Figure 1-4 – Proposed snake plot of GPR65

GPR65 structure consists of a small N-terminus, 7 transmembrane passes, three extracellular loops (ECL), three intracellular loops (ICL) and a C-terminus. The extracellular loops for this protein are believed to be small in length; ECL1 ~17 aa, ECL2 ~30 aa and ECL3 ~25 aa. N.B. this diagram is to contextualise the loops of the receptor but is not accurate on loop boundaries and has been taken from the GPCR database[181].

GPR65 becomes optimally activated when extracellular pH is between 6.4-6.8. It then predominantly signals through G_s and directly stimulates adenylyl cyclase, promoting catalytic activity and causes an accumulation of cAMP[176]. Through the use of protein kinase A (PKA) inhibitors, GPR65 signalling has been shown to signal through the cAMP-PKA-CREB (cAMP response element-binding protein) pathway for gene transcription regulation[178,182,183]. However, as previously mentioned, GPCRs can bind more than one Gα protein. Additional observations of Ras homolog family member A (RhoA) activation have been reported upon acidic pH sensing from cells expressing GPR65[180,184]. It is understood that $G_{12/13}$ signals through the RhoA pathway[185], therefore suggesting that GPR65 also couples with $G_{12/13}$ (Figure 1-5).

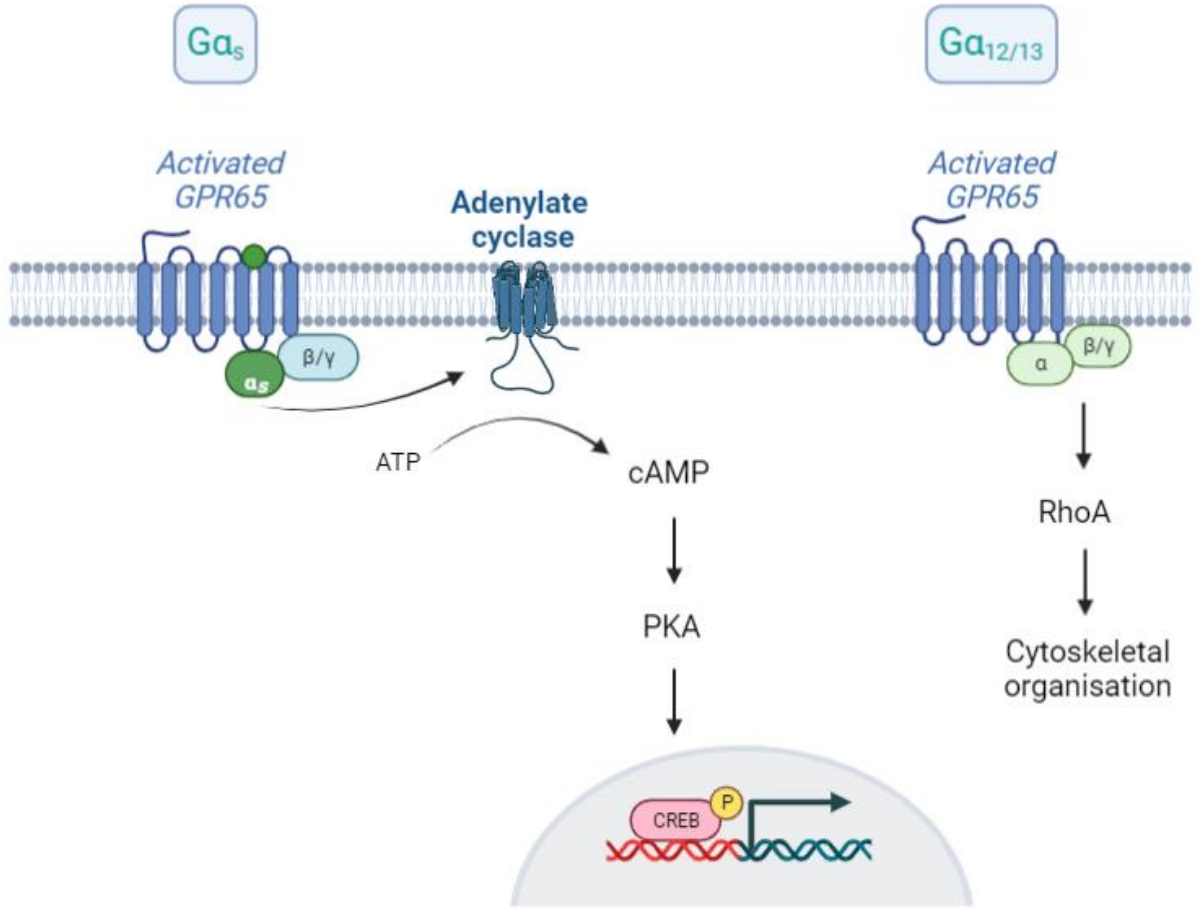


Figure 1-5 – A cartoon showing a proposed model of GPR65 signalling

Stimulation of GPR65 can directly activate adenylate cyclase by $G\alpha_s$, leading to an accumulation of cAMP. cAMP binds PKA, and its active form translocates to the nucleus and activates CREB, resulting in the regulation of genes. Alternatively, GPR65 activation can signal through $G\alpha_{12/13}$ and subsequent RhoA signalling, leading to cytoskeletal organisation affects. Diagram created with BioRender from literature referenced in section 1.2.2.

1.2.3 Function of GPR65

Initially identified as a gene upregulated during T cell activation and apoptosis, GPR65 has since been linked to the regulation of cell survival[173,186,187]. Being predominantly expressed in the spleen, thymus, lymph nodes and peripheral blood leucocytes[186], this receptor is hypothesised to play an important role in the immune system.

As GPR65 can signal through G_s and increase cAMP, CREB subsequently becomes phosphorylated. This post translational modification is understood to inhibit its own binding to the NFκB complex, resulting in the restriction of the inflammatory response[188]; therefore, one would predict GPR65 function to be anti-inflammatory. However, within the literature surrounding GPR65 research, there are conflicting views on its role within the immune system. Evidence for both anti- and pro- inflammatory functions are reported, highlighting the complexity of the biology, but also encouraging further investigation into GPR65 research. A more in-depth review and discussion of GPR65 function can be found in Chapter 5 :

Much like immune function, there are both reports of GPR65 promoting and reducing immune cell migration to sites of inflammation. Opposing profiles often couple with whether GPR65 is suggested to cause or restrict inflammation and may be explained through the receptor having diverse functions in different cell types, or perhaps driven by disease model specific effects[189–191].

Aside from the regulation of cytokine and chemokine responses, alternative GPR65 activity has also been shown to impact cellular metabolism pathways, lysosomal dysregulation and antigen presentation. Single cell studies report effects on fatty acid and cholesterol metabolism, with evidence of the upregulation of polyamine and serine metabolism upon GPR65 knockout, which is ultimately proposed to be important for Th17 differentiation[192].

Moreover, reduced GPR65 activity promoted dendritic cell antigen presentation to $CD4^+$ T cells, promoting T cell activation and differentiation.

1.2.4 GPR65 and disease

Acidic environments have been acknowledged in a variety of processes, organ systems and diseases, and as such GPR65 activity has been implicated with multiple effects in human health and disease. Here I will focus on the immune related biology of the receptor, but there are also reports of GPR65 playing a role in vascular diseases[191,193,194], retinal degeneration[195], depression[196], pain[197] and bone biology[198].

1.2.4.1 Immune mediated diseases

Genetic variants within the *GPR65* locus have illustrated this to be a risk gene for multiple diseases aside from AS, including inflammatory bowel disease[62,199] and multiple sclerosis (MS)[200].

1.2.4.1.1 GPR65 and joint diseases, including SpA

Ribonucleic acid (RNA) sequencing of spondyloarthritis patient-derived synovial T cell populations demonstrate GPR65 expression to be a key marker of inflammatory $CD4^+$ T cells[75] and was found to be overexpressed in distinct cell types in the inflamed joint, compared to paired peripheral blood (Figure 1-6).

The AS associated single nucleotide polymorphism SNP, rs11624293 (GWAS P value = $1.08x10^{-12}$), is in complete linkage disequilibrium (LD) with GPR65 (R^2 = 1.0) and has a minor allele frequency (MAF) of 0.2, implying its presence in 20% of the population. Further, expression quantitative trait loci (eQTL) analysis showed AS-associated genotype-dependent expression of GPR65 in T cells[201] and monocytes after IFNγ stimulation[202].

GPR65 function has also been assessed in mouse models of rheumatoid arthritis due to reports of local acidosis of the inflamed joint[203], despite GPR65 not being reported to be genetically associated with RA. Knockout of GPR65 in the collagen antibody-induced arthritis model reported exacerbated disease scores compared to wild type mice[204], with other groups suggesting GPR65 silencing reduced arthritis induced hyperalgesia[189]; thus implicating a role for this proton sensing receptor in this common disease.

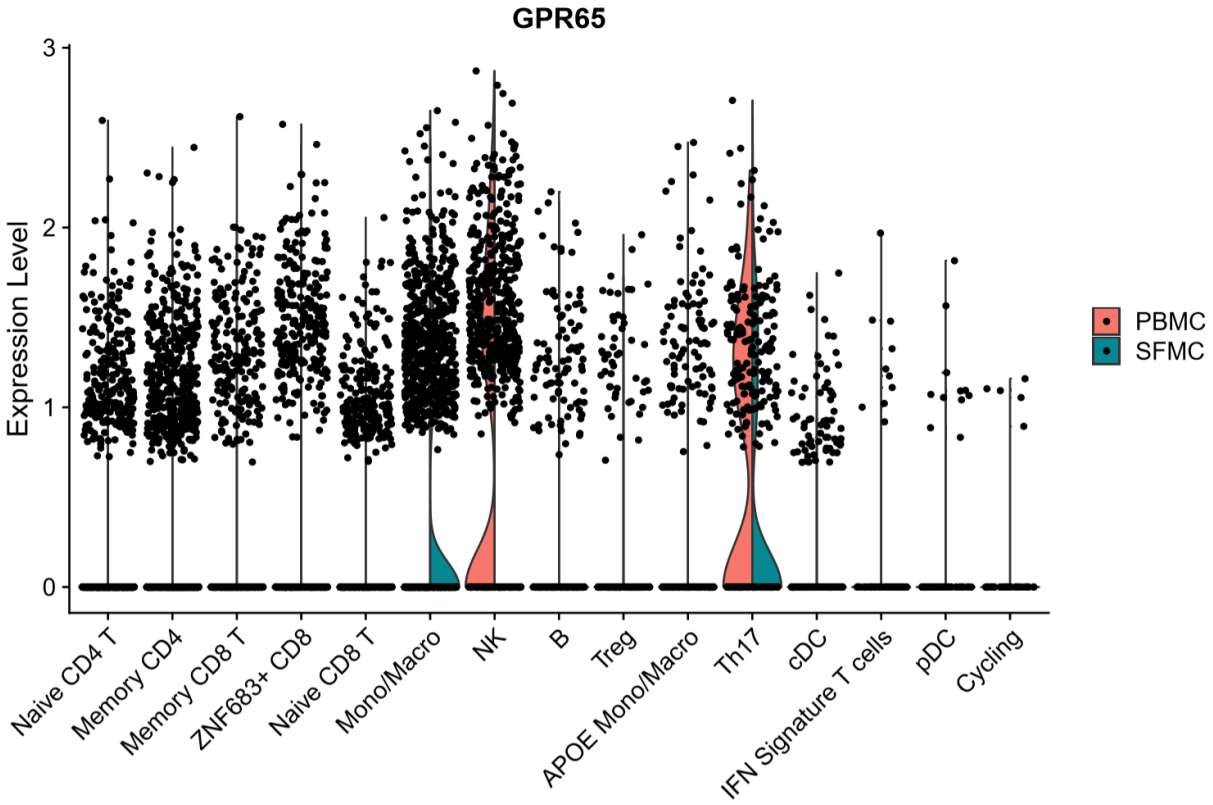


Figure 1-6 - GPR65 mRNA expression in paired PBMC and SFMC from spondyloarthritis patients[a]

Isolated PBMC and SFMC subsets from peripheral blood and paired synovial fluid from spondyloarthritis patients were subject to single-cell RNA sequencing. Violin plots displaying GPR65 expression across the various clusters, split between sample location. Data can be found within the public domain as part of published work[205].

[a] Analysis performed by Hussein Al-Mossawi.

1.2.4.1.2 GPR65 and IBD

Two known SNPs of GPR65 are associated with IBD. The first, rs3742704, represents a missense variant encoding an isoleucine to leucine substitution at amino acid 231 (I231L). With a frequency of 19.67% in the population, cellular function with this mutation is impaired when exposed to acidic environments; reporting reduced cAMP production, reduced IL-17A and IL-22 cytokine production, which are important for gut tissue immunity and regeneration, and impaired autophagy, also known to be important in IBD pathology[206,207]. Overall leading to exacerbated disease in mouse models of colitis and suggestive of a protective role for GPR65 in IBD. As the location of this mutation has been suggested to alter the stability of alpha-helices of the protein, it is likely to disrupt the important structure required for GPR65 activation and signalling, therefore is significant in its effects on health[208].

Secondly, rs8005161, with a MAF of 0.25, is reported to be in LD with rs3742704[209]. Ulcerative colitis patients displayed a higher frequency of the risk allele compared to healthy controls and displayed a more severe clinical phenotype. Additionally, their peripheral monocytes displayed reduced cAMP activity and RhoA activation when exposed to pH 6.5 *ex vivo*[184].

GPR65 expression has been reported to be increased in active IBD patient gut tissue, compared to healthy tissue[210]. However, due to the analysis of messenger (m)RNA directly from the tissue, one cannot be sure whether the increase is due to increased expression of GPR65 on local cells, or whether it is due to the increase of infiltrated leukocytes, which have high endogenous GPR65 expression.

On a side note, the 'gut-joint' axis has already been introduced, but there is also evidence for a bidirectional link between inflammation of the gut and neurodegeneration. The so called 'gut-brain' axis share their genetic association of *GPR65* risk loci, with a Parkinson's Disease

(PD)-associated SNP rs8005172, which is in LD with the IBD-associated rs3742704 (R^2 = 0.14-0.47)[211]. Although the causal variant for PD is yet to be identified, a major risk factor of disease, the *LRRK2* gene has been shown to be tightly linked with *GPR65,* through Bayesian network analysis in IBD patient tissue[212].

1.2.4.1.3 GPR65 and MS

To determine the relevance of GPR65 in MS, single cell studies have identified upregulation of GPR65 expression on pathogenic murine Th1-like cells in the central nervous system, within the experimental autoimmune encephalomyelitis (EAE) model of multiple sclerosis. GPR65 knockout mice were protected from disease, with reduced tissue inflammation observed through the suppression of Th1 and Th17 cells[213]. It is worth noting the work performed by the Regev group was using a conditional GPR65 knockout in $CD4^+$ T cells, in contrast to alternative reports of GPR65 being protective in the EAE model through the regulation of iNKT cells, using complete immune cell silencing[190].

1.2.4.1.4 GPR65 and atopic dermatitis

The immune mediated skin inflammatory disease, atopic dermatitis (AD) has been associated with the GPR65 SNP, rs8005161. The severity of AD has been positively correlated with the pH of diseased skin lesions, which is reported to be in the range of GPR65 activation and is supported by the observation of exacerbated disease in the MC903 model of AD from GPR65 knockout mice[214].

Further validation of this SNP affecting GPR65 function was provided through the increased proinflammatory signature from T cells within an acidic culture, expressing the minor allele. Although the addition of human data was encouraging, GPR65's relevance to disease should be carefully considered as this discovery was conducted by a phenome-wide association study

within the self-diagnosed 23andMe cohort, without GPR65 identification in AD GWAS studies[59].

1.2.4.2 Cancer

Cancer is often thought of as the flip side of inflammation, with shared pathways between tumour biology and the immune response. Through insufficient vascularisation, hypoxic regions are a hallmark of tumour biology, leading to the production of lactate via anaerobic glycolysis, termed the 'Warburg effect'[215,216]. This in turn drives an acidic microenvironment, which has long been known to exert immunosuppressive effects, and so unsurprisingly GPR65 has been shown to have a prominent role in tumour biology.

GPR65 overexpression has been reported on several cancer cell types, including kidney, colon, ovarian, breast and skin[217,218]. Through GPR65 silencing, its activity is thought to favour tumour development, and has been correlated with a negative prognosis for patients[178,219]. Potential mechanisms for GPR65's pro-oncogenic activity have been suggested through its relationship with Bcl-2 and blocking apoptosis. Alternatively, through its association with PD-L1 upregulation, allowing cells to evade the host immune response[220,221]. In contrast, opposing evidence supports GPR65 being a tumour suppressor, with reduced GPR65 expression upon assessment of multiple haematological malignancies, compared to healthy controls, and receptor dependent inhibition of c-Myc oncogene expression in lymphoma cells, when in acidic environment[222,223].

Furthermore, cancer cells are not the only expressors of GPR65 reported in the tumour. Macrophages are one of the most abundant immune cells present[224], and their expression of GPR65 has been considered a key player in driving the impairment of the anti-tumour immune response, upon recognition of the acidic microenvironment[225,226].

GPR65 is therefore thought to be oncogenic, with both pro- and anti-inflammatory effects in cancer, dependent on cell type and biological context. Largely, when GPR65 is expressed on 'solid' cancer cells, it likely encourages their growth and promotes tumour survival, but when activated on local immune cells, it responds in an anti-inflammatory nature suppressing the ability for the immune system to fight the tumour.

1.2.4.3 GPR65 as a drug target

Given the broad nature by which GPR65 is associated with inflammation in a wealth of diseases, specific targeting of this proton sensing pathway has the potential to provide therapeutic effects. As a GPCR this receptor lends itself to small molecule development, with many drugs developed and approved. However, due to large resource requirements and time taken to generate such an entity, as well as the possibility of off target effects, the discovery of a specific antibody is attractive. But the question remains whether to agonise or antagonise GPR65 function for therapeutic benefit?

1.3 Application of antibodies in research and development

Monoclonal antibodies are specific for an epitope on one antigen and provide advantageous tools to explore target biology, as well as being a highly targeted approach for the treatment of disease. Antibodies as tools or therapeutics are produced *in vitro* but reflect the same molecules generated during a normal immune response. Their structure and production are detailed below.

1.3.1 B cell function within the immune system

Unlike the previously discussed T cells (section 1.1.5.1), B cells can recognise antigen independently of its presentation in the context of MHC, instead through transmembrane immunoglobulin, termed the B cell receptor. This antigen-antibody complex is internalised,

where it gets degraded and returned to the surface as small peptides bound to MHC class II molecules. The nature of this antigen presentation allows B cells to become professional APCs and the display is recognised by local helper T cells. Proteins released upon this T cell stimulation in turn activate the B cells, leading to their proliferation and differentiation into antibody-secreting plasma cells, or memory B cells[227].

The primary aim of the relatively short-lived plasma cells is to secrete large quantities of unique antibodies, which become circulated in the blood and lymph and bind to specific antigens, either flagging them for elimination by the complement system, or leading to target opsonisation and ultimate destruction through phagocytosis. In contrast, memory B cells are long living survivors and retain information of past infection. This feature allows the cells to be called upon in response to re-exposure of a 'signature' antigen and results in a fast and strong elimination[228].

1.3.2 Antibody structure

Antibodies are members of the immunoglobulin (Ig) superfamily, where these soluble proteins are involved in the recognition and binding of cells and acellular entities, driving various functions. There are five distinct classes of Ig naturally produced in humans: IgA, IgD, IgE, IgG and IgM. Naïve B cells tend to express IgD or IgM but undergo a process known as class switch recombination (CSR) upon infection or immunisation, and can switch to express IgA, IgE, IgG, whilst retaining their antigen specificity[229,230]. Antibody class is determined by the heavy chain constant region (C_H), with each isotype encoded by a specific C_H gene[227]. As each class has a unique effector function, the process of CSR provides increased diversity within the immune response.

Although effector function can be determined by the antibody isotype, the variable region determines antigen specificity. The amino-terminal of an antibody contains both heavy and light chain regions (V_H and V_L, respectively) encoded for by several gene segments[227]. Both the V_L and V_H domains are encoded by variable (V) and joining (J) gene segments, whilst V_H is also encoded by a third gene segment, the diversity (D) gene segment. These three hyper variable segments are termed the complementarity determining regions (CDR's), and it is within CDR3 where the V(D)J gene segments converge, therefore the site of the greatest combinatorial diversity. It is the recombination of different V(D)J segments which increase the diversity of the antibody repertoire and over comes the diverse antigenic challenges facing antibodies[227]. V(D)J recombination occurs within the bone marrow whilst B cells are developing. Once B cells have been exposed to antigen in the periphery, they migrate to germinal centres where they undergo repeated somatic hypermutation for affinity maturation. Together with clonal selection, these processes bring about further diversification of the antibody variable region[227].

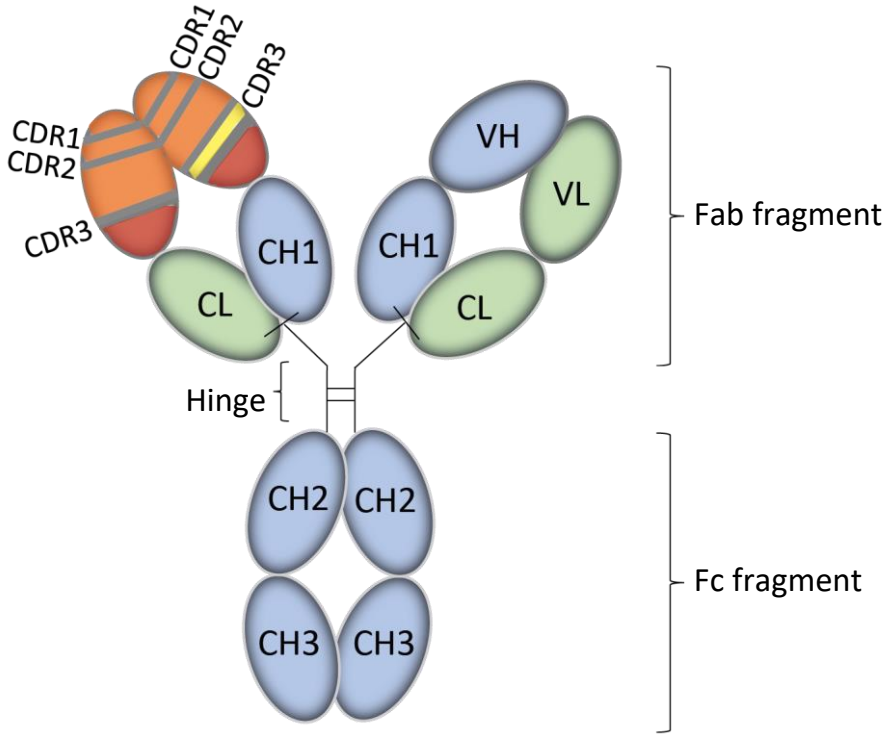


Figure 1-7 - Schematic diagram of the IgG antibody structure

An IgG is comprised of two heavy chains (blue) and two light chains (green). The antibody binding fragment (Fab) is made up of the variable (V) and first constant (C) domain. The variable domain is made up of a combination of variable (orange), diversity (yellow) and joining (red) gene segments, separated by complementarity determining regions (CDR). Each heavy and light chain pair is considered a separate Fab, and so an IgG has two Fab arms. The constant heavy domains (CH2 and CH3) represent the crystallisable fragment (Fc). The hinge region is situated between CH1 and CH2 domains and contains two disulphide bonds between cysteine residues, to hold the two antibody chains together. Adapted from Janeway[227].

IgG is the most abundant isotype in human serum, comprised of two gamma heavy chains and two light chains, which can be either kappa (κ) or lambda (λ), connected by multiple disulphide bridges (DSB) (Figure 1-7). The first of two antibody regions, the antigen binding fragment (Fab) comprises both the variable and constant light domains, along with the variable and CH1 domains of the heavy chain; it is this fragment which binds to specific antigens and activates an immune response[231]. The CH2 and CH3 constant domains of the heavy chain make up the second antibody region, the fragment crystalline (Fc), which is responsible for engaging effector function[232]. A hinge region, situated between CH1 and CH2 domains of the heavy chain, provides essential flexibility within the structure for bivalent antigen binding[233].

There are four human sub-classes of IgG, named IgG1, IgG2, IgG3 and IgG4. Despite sharing the same overall structure, differences in the hinge regions result in varied flexibility and unique effector function[234]. In general, IgG1 and IgG3 recognise protein or peptide antigens and support antibody- and complement-dependent cytotoxicity, IgG2 molecules are restricted to recognising carbohydrate antigens and IgG4 is often involved in anti-inflammatory responses.

Of the other antibody classes, structurally, IgD and IgE resemble the classic Y-shape antibody structure (although IgE lacks a hinge region and has four constant domains), while IgA exists as a dimeric molecule and IgM as a pentameric molecule (Figure 1-8). IgA molecules are present in high concentrations at mucosal surfaces and are referred to as secretory IgA, acting as the first line of defence against pathogens which are ingested or inhaled[233]. IgM is the first antibody produced during an immune response and expressed on the surface of naïve B cells, aiding B cell survival, and forming part of the B cell receptor. On maturation and release into

circulation, IgM molecules link together forming a pentameric structure. In comparison, IgD is either found circulating in the sera or in abundance on the surface of mature follicular B cells[235]. As a transmembrane receptor co-expressed with IgM, its binding leads to B cell activation (introduced in 1.3.1). Finally, although there is little IgE in circulation due to its extremely low half-life, it binds with high affinity to basophils and mast cells resulting in a potent immune response[236].

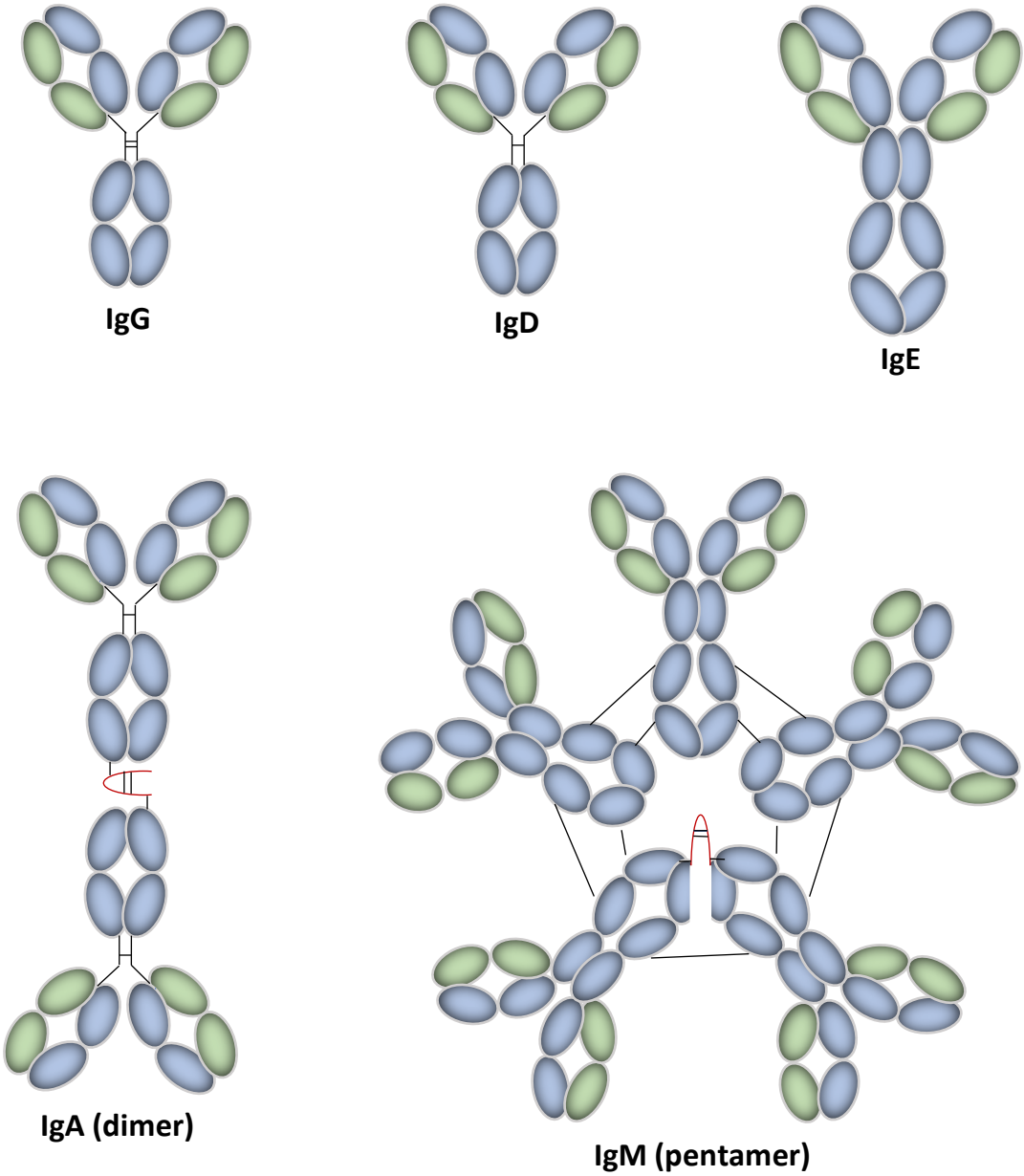


Figure 1-8 - Schematic illustration of the five human antibody classes

IgD is representative of the typical IgG structure, but with only one disulphide bond (DSB). IgE takes on the classic Y-shape of Ig too, but another CH domain replaces the hinge region. IgA is like an IgD structure but can exist as a dimer (as shown), with a J chain (red) linking the two molecules. IgM can exist as a pentameric structure (as shown) and again includes a J chain, and multiple DSB's between each monomeric structure, with each monomeric structure consisting of four CH domains without a hinge. Adapted from Janeway, and Schroeder and Cavacini[227,233].

1.3.3 Antibodies used as tools and therapeutics

Originally antibodies were produced *in vivo* through the immunisation of host animals with the desired target, for the purpose of evoking an immune response. However, antibodies generated via this method tended to only deliver a limited amount of polyclonal antibody (Ig for a specific antigen but identifying different epitopes). However, basic research was enhanced through the discovery of the hybridoma technique in 1975[237]. This novel technology identified the continual production of antigen specific monoclonal antibodies, through the fusion of a single antibody secreting B cell clone to an immortal myeloma cell.

The pharmaceutical industry began exploiting the use of highly selective monoclonal antibodies, possessing strong affinities, for the generation of novel therapeutics over 35 years ago; the first being anti-CD3 approved in 1986, to prevent kidney rejection post transplantation[238]. Since then, developments have overcome many challenges and transformed the success of antibodies as therapeutics, with over 120 monoclonal antibodies approved by either (or both) the FDA and the European Medicines Agency for a variety of diseases, including immune-related diseases and cancer (correct as of November 2022 – The Antibody Society).

Over the years, the evolution of antibody engineering has led to the current ability to produce chimeric, humanised or fully human antibodies, thereby preventing previously observed immunogenicity from treatments using full anti-rodent antibodies[239].

It is common for IgG1 to be selected for therapeutic use due to its long half-life, complement activation and promotion of antibody dependent cellular cytotoxicity, especially for cancer therapies; whilst IgG4 is preferred when effector function is not desired, with this isotype blocking ligand-receptor interactions[240,241]. However, these full-length isotypes have their

disadvantages, such as a lack of penetration of some tissue types *in vivo,* but also when considering their use as tools, observations of non-specific binding due to the Fc fragment *in vitro*.

A range of monovalent, rigid fragments have been defined and are derived from affinity matured, class-switched IgG (Figure 1-9). Fab fragments are generated through the chemical digestion of conventional IgG or IgM antibodies. Whilst single chain variable fragments (scFv) are generated through the manipulation of Fab fragments, removing CH1 and CL1, and combining the heavy and light chain variable regions with a linker.

Alternative monovalent formats make the use of other species unique antibody properties. Within the camelid family (Camel, Llama and Alpaca) a variable heavy chain (VHH) domain can be isolated from a subset of heavy chain only antibodies. If required, this VHH domain can be connected directly to the second heavy chain constant (CH2) region of the Fc, via a hinge. In bovines, a portion of their IgG and IgM antibodies have an ultra-long CDRH3. This structurally unique subset consists of a knob domain (resembling cysteine rich peptides) presented on a beta-ribbon stalk, away from other CDR loops[242], with the isolated knob domain retaining function[243].

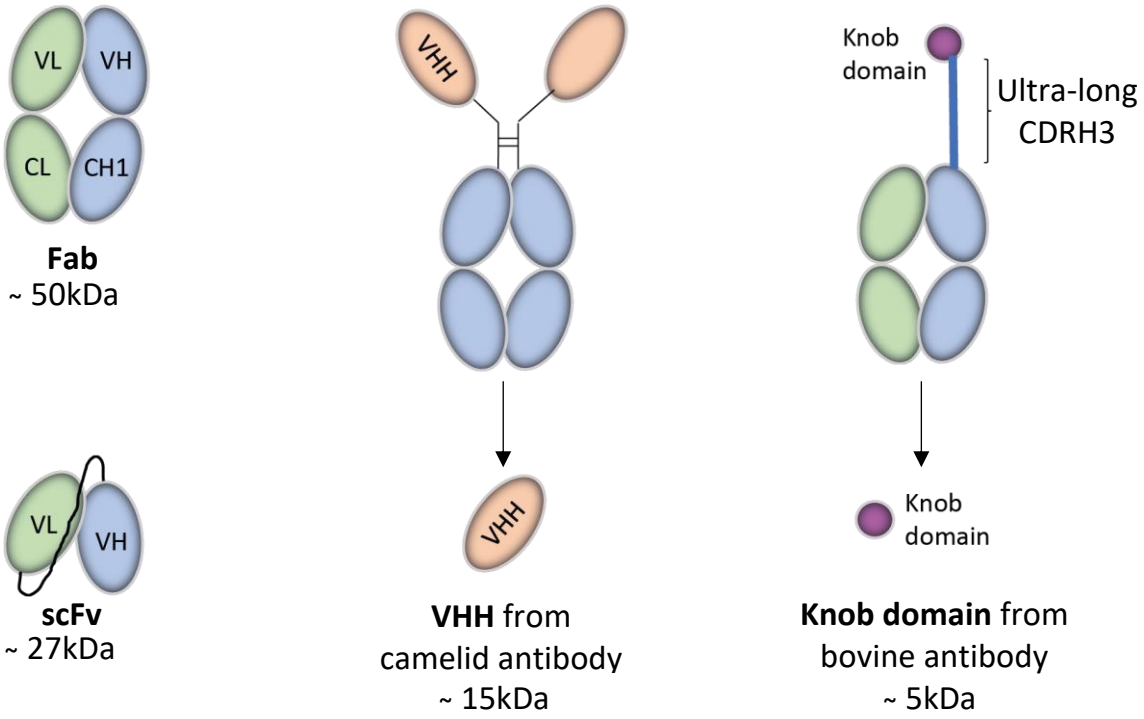


Figure 1-9 – Alternative antibody fragments

Antibody binding fragments (Fab) and single chain variable fragments (scFv) are derived from full-length IgG, through antibody engineering. VHH fragments (orange) and knob domains (purple) are cleaved from their respective full-length antibodies. Comparative assumed molecular weights are also shown; exact molecular weights are contingent on the specific CDR sequence. Adapted from MacPherson *et al*[244].

1.4 Project Aims

While current therapeutic strategies for ankylosing spondylitis include the use of biologics to neutralise specific proinflammatory cytokines, many patients exhibit an inadequate clinical response to current therapies. With significant unmet medical need, further research is required to fully understand the pathogenesis of this disease and understanding the pathogenic role of genetically associated proteins will be key in developing effective therapeutics.

Given inflamed synovial fluid is reported to have a low pH signature[203], investigating how active GPR65 signalling in acidic environments can impact inflammation is of relevance.

Hypothesis

GPR65 exacerbates joint inflammation in patients with ankylosing spondylitis and is a potential therapeutic target.

Therefore, the aims of this thesis were:

I. To develop a tool reagent for exploring GPR65 biology, through multiple antibody discovery strategies
II. To investigate the effects of acidic pH on immune cell function
III. To explore the effects of GPR65 function in immune cells

Chapter 2 : Materials and Methods

2.1 Antibody discovery

2.1.1 DNA constructs and preparation

Constructs were designed, containing DNA of the species specific GPR65 sequence (Uniprot entries Q8IYL9, B0YIR8), along with a N-terminal FLAG tag, a C-terminal 10-histidine tag and labelled with GFP. Custom synthesis and cloning into a mammalian expression vector were performed by ATUM (California, USA). Plasmid DNA for each construct was amplified through Qiagen Plasmid Plus Giga kits and quantified.

2.1.2 Cell line culture and transfection

2.1.2.1 HEK cells

HEK293 cells were cultured in EXPI293 expression media (Life Technologies), and cell concentration and viability were determined using trypan blue (Gibco, Life Technologies). Cells were routinely cultured at 37 °C, in 8% CO_2, in vented Erlenmyer flasks (Corning, Surrey, UK), shaking at 180 rpm and sub-cultured every 3-4 days, at a seeding density of $0.5x10^6$ cells/mL.

Cells were transfected with DNA-lipid complexes comprising DNA and Expifectamine293 (Life Technologies) at a 1µg DNA:$1x10^6$/mL cell ratio and prepared according to manufacturer's protocol. Transfected cells were incubated for 24 hours prior to use.

For cells used within protein purification attempts, cells were pelleted and flash frozen with liquid nitrogen and stored at -80 °C until extraction.

2.1.2.2 Rab9 fibroblasts

Rab9 rabbit fibroblast cells were cultured in RPMI expression media (Gibco, Life Technologies). Cells were routinely cultured at 37 °C, in 5% CO_2, in CellSTACK culture chambers (Corning) and sub-cultured every 3-4 days, at a seeding density of $4x10^4$ cells/cm^2. Cells were harvested using TrypLE (Life Technologies) and resuspended in Earles Balanced Salts (Sigma). Cell concentration and viability were determined using trypan blue.

Rab9 cells were transfected by electroporation. Briefly, $3x10^6$ Rab9 cells and 150µg DNA were shocked with 160 V and further incubated overnight. Cells were harvested, frozen down in fetal bovine serum (FBS, Gibco) + 10% dimethyl sulfoxide (DMSO; VWR) and stored at -80 °C until rabbit immunisation.

2.1.3 Recombinant protein expression and purification

2.1.3.1 Extraction

Cell pellets were thawed and resuspended in lysis buffer, with protease inhibitors. Cells were homogenised prior to being passed through a cell disruption system (Constant Systems) twice, at 12.5 kpsi. After an initial centrifugation (5,500xg for 10 minutes), supernatant was collected and subject to a further ultracentrifugation (55,000 rpm for 1.5 hours) to pellet the proteins. These pellets were then resuspended in Buffer A[b], and further homogenised before being flash frozen and stored at -80 °C, in aliquots.

500µL of each protein sample was thawed, 1mM Iodoacetamide added, along with 25µL detergent[c] (OG, DM, DDM, LMNG) and left to incubate, rolling at room temperature, for 2

[b] Buffer A: dH_20 containing 25mM HEPES, 150mM sodium chloride, 10% glycerol (pH 7.4)

[c] Detergents already pre-prepared: 5mL Buffer A + 5% detergent + 0.5% cholesteryl hemisuccinate was incubated at 42 °C for 10 minutes, and left to incubate on a roller, at 4 °C for 18 hours. This was aliquoted and stored at -20 °C until required.

hours. A final ultracentrifugation (45,000 rpm for 45 minutes) was performed to remove insoluble material and supernatant transferred to 300µL Chromacol vials (ThermoFisher).

2.1.3.2 Fluorescence-detection size-exclusion chromatography (fSEC)

After the high-performance liquid chromatography (HPLC) column and filter were flushed with dH_20 with 25mM HEPES pH 7.4, 150mM sodium chloride and detergent[d], each sample was run through at 0.2µL/min, at 4 °C. HPLC was performed using the Agilent 1200 infinity series (Aligent Technologies).

2.1.3.3 Western blot

2% Sodium Dodecyl Sulfate was added at 1:1 ratio to the samples. Upon mixing with NuPAGE™ LDS sample buffer loading dye (LifeTechnologies), they were run along NuPAGE 4-12% Bis-Tris protein gel lanes (Invitrogen), alongside the SeeBlue® Plus2 prestained standard (Invitrogen) to determine the band sizes. Gels were transferred following iBlot (Invitrogen) and the membrane blocked overnight. A 1:2,000 dilution of anti-FLAG (R&D) was incubated at room temperature for 2 hours, before the ThermoFisher detection kit revealed bands on Quantstudio2000 (ThermoFisher).

2.1.4 Identifying antibodies by phage display

2.1.4.1 Chimeric protein expression and purification

Genes encoding ApoE3 chimeric constructs were synthesised by ATUM, and cloned into BamHI and NcoI restriction sites of a pET14b vector. These constructs were co-transformed with a vector encoding Biotin ligase BirA, into NiCo21 DE3 *E.coli* cells (New England Biolabs). Expression and purification of the constructs were performed, as described by the Swanstrom

[d] Detergent needed to be 10x more concentrated than its samples respective critical micelle concentration.

lab[245]. Protein concentration was determined on a Nanodrop spectrophotometer, using absorption at 280nm (Thermo Scientific). To determine the solubility of each protein, SDS-PAGE was performed. Briefly, NuPAGE™ LDS Sample Buffer 4x (Invitrogen) containing dithiothreitol (Invitrogen), was added to cell lysates, supernatant and cell pellets, before being run along NuPAGE™ 4-12% Bis-Tris Protein Gel (Invitrogen). Instant blue™ (Expedeon) was used to reveal protein bands.

2.1.4.2 Phage panning in solution

Three UCB established phage libraries were used; two naïve human scFv phage libraries were estimated to contain $1.1x10^{11}$ and $5x10^{10}$ clones, whilst a naïve VHH phage library obtained from 10 male llamas, was estimated to contain $7x10^{9}$ clones.

In the first round of panning, ApoE3 GPR65 loop constructs (1.5µM) were pooled and incubated with each library, previously blocked in PBS containing 3% milk. Constructs and associated phage were captured from solution using Sera-Mag™ SpeedBeads Neutravidin-coated (GE Life Sciences). Beads were washed by magnetic capture 5 times with PBS + 0.1% TWEEN (VWR), and bound phage were eluted by 100µg/mL trypsin (Sigma) in Tris buffered saline buffer. Rescued phage from round one was split in two and incubated with either the same pool of antigen, or 1.5µM wild type (WT) ApoE3 construct, to remove binders to the ApoE3 scaffold. Complexes were captured using Dynabeads™ M-280 Streptavidin (Invitrogen), to remove neutravidin binders, followed by selection on chimeric ApoE3 GPR65 proteins. Enriched phage from round two of both human libraries were subject to a final round, and complexes were captured with neutravidin beads. As the VHH library was smaller than the human libraries, only two rounds of panning were carried out. Phage rescue was

performed from individual *E.coli* colonies picked from output phage infected colonies at each round of panning, in all conditions.

2.1.4.3 Phage rescue

Phage rescue was performed using a modification of the standard protocol[246], from individual *E.coli* colonies picked from output phage infected colonies at each round of panning, in all conditions. Cultures were seeded at a starting density of 0.1 OD_{600} in 2xYT medium (made within UCB) with 2% glucose and 100µg/mL carbenicillin and grown at 37 °C, shaking at 220 rpm until the OD_{600} reached between 0.4-0.8. Half of the culture was then infected with 10 multiplicity of infection M13KO7 and incubated at 37 °C for 1 hour, without shaking. The culture was then centrifuged at 4,000 rpm for 10 minutes. The pellets were resuspended in 100mL 2xYT containing 100µg/mL carbenicillin and 50µg/mL kanamycin. These cultures were grown for 18 hours at 30 °C, shaking at 240 rpm. Next, the cultures were centrifuged at 8,000 rpm for 15 minutes and phage particles were purified through incubation with 7mL PEG sodium chloride for 1 hour, on ice.

2.1.4.4 Phage antibody characterisation and optimisation

Monoclonal phage antibodies were screened for binding to the antigen they were raised against, WT ApoE3 and neutravidin, by ELISA. Briefly, biotinylated antigen (chimeric constructs and WT ApoE3) or neutravidin was coated onto ELISA plates at 1µg/mL. Plates were blocked with PBS with 3% milk (Sigma), before 100µL of pre-blocked phage supernatant was applied to the plate. Following a wash step, anti-M13 HRP (Sino Biological) was added at 1:15,000 dilution. Plates were developed with TMB, before being read at 630nm, on Synergy 2 (BioTek).

Phagemid DNA was sequenced (Macrogen), before scFv/VHH regions were extracted, amplified, and reformatted into rabbit Fc fusion vectors, by seamless cloning (GeneArt™ Seamless Cloning and Assembly Enzyme Mix).

Reformatting of phage antibodies were synthesised and cloned into custom vectors by TWIST Bioscience.

2.1.5 Monoclonal antibody discovery through immunisation

2.1.5.1 Rabbit immunisation

Two male New Zealand White rabbits (> 2Kg) were immunised subcutaneously with either $2x10^7$ Rab9 cells expressing either human or rat GPR65. At an adjacent site, a dose of Complete Freund's Adjuvant (Sigma) was given. Booster immunisations were delivered every 14 days. Ear bleeds were taken at the point of the initial dose, then before every booster immunisation. 14 days after the final boost, termination occurred and single cell suspensions of spleen, lymph nodes, bone marrow and peripheral blood mononuclear cells were frozen in 10% DMSO in FBS, at -80 °C.

2.1.5.2 Isolation of GPR65 specific antibodies from mature B cells

2.1.5.2.1 B cell culturing and antigen-specific screening

B cells from spleen, lymph node and peripheral blood mononuclear cells (PBMCs) were cultured in 200µL of B cell culture media (RPMI; Gibco Life Technologies), supplemented with 8.7% FBS, 1.7% HEPES buffer (Gibco, Life Technologies), 1.7% L-glutamine (Gibco, Life Technologies), 0.86% penicillin/streptomycin solution (Gibco, Life Technologies), 0.17% normacin (Invivogen) and 0.09% 2-metcaptoethanol (Gibco, Life Technologies), 3-5% human B cell stimulated supernatant and x-ray-irradiated EL-4 murine thymoma cells (50,000 cells/well) for 8 days, at 37 °C, 5% CO_2. B cell culture supernatant was either incubated with

wild type HEK cells, HEK cells expressing human GPR65 (each at 1,000 cells/well) or ApoE3 constructs labelled with Sol-R beads[e] (2.6ng/mL per well), and AF647 goat anti-rabbit Fc fragment specific (Jackson Immunoresearch) at a 1:3,000 dilution. Supernatant containing antibodies specific for human GPR65 were identified by fluorescence (Mirrorball, TTP LabTech). B cells from the corresponding culture wells were resuspended in 60µL FBS containing 10% DMSO and frozen at -80 °C.

2.1.5.2.2 Fluorescent foci picking

For B cells discovered through the culture process, cells were thawed and prepared as part of individual assay mixes, with GPR65 expressing HEK cells ($2.4x10^5$ cells) and AF647-conjugated secondary antibody, at a 1:600 dilution.

Assay mixes were added to wells of a pre-prepared 6- or 24-well nano well plate (ALS) and incubated at 37 °C for up to 2 hours. Fluorescent halos were identified and cells within individual nano-pens were extracted (CellCelector, ALS, Germany) and placed into reverse-transcription polymerase chain reaction (SuperScript™ IV VILO, ThermoFisher) mix, including 10% NP-40.

2.1.5.2.3 RT-PCR and transcriptionally-active PCR (TAP)

RT-PCR was performed to manufacturers protocol, as follows: 10 minutes at 25 °C, 10 minutes at 50 °C and a final 5 minutes at 85 °C.

Details of TAP methods have been published in patents WO2010/097435 and WO2010/097437, and discussed in a UCB publication[247].

[e] Different Sol-R beads used to tag different proteins. Sol-R R2 labelled WT ApoE3 constructs, Sol-R R4 beads were conjugated with the ApoE3 GPR65 constructs, whilst Sol-R R5 labelled an irrelevant protein.

2.1.5.2.4 Recombinant antibody expression from transiently transfected HEK293 cells

Pairs of heavy and light chain TAP products were transiently transfected into HEK293 cells, using Expifectamine293 (Gibco, Life Technologies). Cells were incubated for 7 days and 30mL supernatant was harvested. IgG presence within the supernatant was determined by an anti-rabbit anti-Fc sandwich ELISA (as described in 2.1.7).

2.1.6 Antibody discovery through single cell sequencing

Immune material (spleen and lymph node) was thawed, filtered and counted using trypan blue. Cells were subject to Fc-block (Miltenyi Biotec) prior to surface staining with anti-IgG-BV421, anti-IgM-FITC (Jackson ImmunoResearch) and incubation with WT ApoE3-APC-Cy7 and GPR65 loop expressing ApoE3-PE (enabled through labelling with Streptavidin tetramers (Biolegend)). Upon resuspension in FACS buffer, cells were sorted (Figure 3-21).

Sample processing for V region sequencing was performed using Chromium Single Cell 5' Library and Gel bead kit (10x genomics, USA), following the manufacturers user guide. Briefly, after FACS sorting, cells were spun down and resuspended in a master mix of RT reagents and injected into a channel (< 8,000 cells per channel). Gel Beads-in-Emulsions (GEMs) were formed within each channel of the chip, in the 10x Chromium instrument and then subject to reverse transcription (53 °C for 45 minutes, followed by 5 minutes at 85 °C) in an 8-well strip. After GEM clean up protocols were performed and a further SPRIselect bead (Beckman Coulter) clean up, cDNA was confirmed through two rounds of PCR, with 14 cycles and 40 cycles respectively, using custom rabbit V_H/V_K primers.

Library construction was prepared as per the manufacturer's user guide (10x Genomics, CG000086_SingleCellVDJReagentKitsUserGuide_RevL-M) prior to samples being sent to

Macrogen (South Korea) for sequencing. Bioinformatic analysis was performed by James Snowdon.

2.1.7 Enzyme-linked immunoabsorbant assay (ELISA)

Expression IgG and ApoE3 based binding ELISAs were performed as follows: Flat bottomed 96-well plates (Maxisorp immunoplate, NUNC ThermoFisher) were coated with 100µL 1µg/mL anti-rabbit Fc fragment (Jackson ImmunoResearch) or 5µg/mL streptavidin (Pierce™), overnight at 4 °C. Plates were washed 3 times in wash buffer, before being blocked for 1 hour with PEG block at room temperature. Plates were washed 3 times, then either neat or diluted samples (and positive controls where necessary) were added and incubated for up to 2 hours. Plates were again washed as before and 100µL 1:2,500 anti-rabbit Fab fragment-HRP (Jackson ImmunoResearch) was added and incubated for 1 hour. After a further six washes, 100µL TMB substrate solution (ThermoFisher) was added and incubated in the dark for up to 30 minutes. Plates were read using the Synergy Neo2 at 630nm.

2.1.8 Antibody purification

30mL supernatants containing antigen-specific antibodies were purified by ProteinA chromatography (ÄKTA pure, GE, USA), using 0.1M sodium citrate pH 3.4 for elution, and 0.1M citric acid pH 2.0 for striping of the column. Following collection of eluted material, buffer exchange was performed into PBS and concentration calculated using the nanodrop. Antibodies were then filtered, and endotoxin levels assessed.

2.2 Immunology

2.2.1 Buffer and media composition

All buffers and media used in the experiments are outlined in Table 1 .

Name	**Composition**
Medias	
R10	RPMI-1640 (Gibco), 10% (FBS), 1% Glutamine (Gibco), 1% Pen/strep (Gibco)
D10 pH 7.5	DMEM (Gibco), 10% FBS, 1% Glutamine, 1% Pen/strep
D10 pH 6.5	DMEM, powder, high glucose, pyruvate (Gibco) (500mL made according to manufacturer's guideline), 10% FBS, 1% Pen/strep, 2.8mM sodium bicarbonate (Sigma)
Buffers	
FACS buffer	PBS, 0.1% FBS, 2mM EDTA (ThermoFisher), 0.01% sodium azide (Sigma)
ELISA wash buffer	PBS, 0.05% TWEEN-20 (Sigma)
PEG block	dH_2O, 1% polyethylene glycol (Sigma), 0.1% TWEEN-20

Table 1 – Composition of media and buffers used within experiments throughout this thesis

Previously optimised concentrations of sodium bicarbonate within media, giving rise to specific media pH values, were provided to me by Associate Professor Maike Glitsch. The assessment of media pH was measured using a portable pH meter (Mettler Toledo).

2.2.2 Isolation of peripheral blood mononuclear cells (PBMCs)

Venous blood was collected from healthy donors, with informed consent, directly into heparin-containing tubes. Samples were diluted 1:1 with PBS and mononuclear cells were separated from whole blood using Leucosep™ tubes. These were centrifuged at 800xg for 15 minutes with no brake, and the PBMC-containing interface was collected using a Pasteur pipette. Cells were washed twice in PBS containing 1mM EDTA (here on in referred to as

PBS+EDTA) for 10 minutes at 200xg, then resuspended in R10. Cells were counted after staining with trypan blue using a haemocytometer under a light microscope.

2.2.3 Magnetic isolation of PBMC subsets

Cellular isolation was performed using kits supplied from Miltenyi Biotec, according to manufacturer's protocols. The following human kits were used; Pan Monocyte Isolation kit, Pan T cell Isolation Kit, and CD8 MicroBeads.

2.2.4 Monocyte activation and culture

$2x10^6$ PBMCs were plated into 96-well U-bottom tissue culture plates (Corning) and LPS (Sigma) was used at final concentration of 20ng/mL, in pH relevant media. For wells without LPS, equal volumes of culture media were used. Plates were cultured at 37 °C, 5% CO_2 for 24 hours.

2.2.5 T cell activation and culture

2.2.5.1 Anti-CD3 and anti-CD28

96-well U-bottom tissue culture plates were coated with 100µL per well 1µg/mL anti-CD3, clone OKT3 (Invitrogen) and incubated at room temperature for at least 4 hours, or overnight at 4 °C. Plates were washed twice with PBS. $2x10^5$ PBMCs were added to each well in 200µL pH relevant media, containing 1µg/mL anti-CD28, clone CD28.2 (Invitrogen). Plates were cultured at 37 °C, 5% CO_2 for up to 72 hours.

2.2.5.2 Recombinant cytokine

$2x10^6$ PBMCs were plated into 96-well U-bottom tissue culture plates and IL-12 (Miltenyi Biotec) and/or IL-18 (R&D) were used at final concentrations of 50ng/mL, in pH relevant

media. For wells without cytokines, equal volumes of culture media were used. Plates were cultured at 37 °C, 5% CO_2 for 24 hours.

2.2.6 Flow cytometry

Monoclonal antibodies used within this thesis are listed in Table 2 for all studies. Data acquisition was obtained using a range of instruments throughout the project; BD Bioscience Canto II, BD Bioscience LSRFortessa X-20 cytometer, Biorad ZE5 Cell Analyser. Fluorescence was compensated using single colour compensation with Ultracomp beads (eBioscience) and data was analysed using FlowJo v9 or newer (BD Life Sciences).

Antibody Target	**Fluorochrome**	**Clone**	**Supplier**	**Dilution**
CD3	R718	UCHT1	BD Bioscience	1:100
CD3	BUV395	UCHT1	BD Bioscience	1:100
CD4	BUV495	SK3	BD Bioscience	1:50
CD4	PE	SK3	Biolegend	1:100
CD4	PerCP-Cy5.5	RPA-T4	eBioscience	1:100
CD8	BUV805	SK1	BD Bioscience	1:100
CD8	PerCP-Cy5.5	RPA-T8	Invitrogen	1:100
CD8	APC	SK1	Biolegend	1:100
CD14	BV605	63D3	Biolegend	1:100
CD14	BV650	M5E2	Biolegend	1:100
CD16	FITC	3G8	Biolegend	1:100
CD16	PerCP-Cy5.5	B73.1	Biolegend	1:50
CD19	APC-Cy7	SJ25-C1	Life Technologies	1:30
CD19	BV605	HIB19	Biolegend	1:100
CD19	PE-Cy7	ST25C1	BD Bioscience	1:100
CD56	BUV395	NCAM16.2	BD Bioscience	1:50
CD56	FITC	5.1H11	Biolegend	1:30
CD56	BV711	HCD56	Biolegend	1:100
CD161	PE	HP-3G10	Biolegend	1:100

CD161	BV421	HP-3G10	Biolegend	1:100
Vα7.2	BV786	3C10	BD Bioscience	1:50
TNFα	BV421	MAb11	Biolegend	1:100
TNFα	AF700	MAb11	Biolegend	1:100
TNFα	FITC	MAb11	Biolegend	1:100
IFNγ	BV711	4S.B3	Biolegend	1:100
IFNγ	BV650	4S.B3	BD Bioscience	1:100
IFNγ	PE-Cy7	4S.B3	Biolegend	1:100
IL-17A	BV605	BL168	Biolegend	1:100
IL-17A	AF488	eBio64DEC17	eBioscience	1:100
IL-17A	BV711	BL168	Biolegend	1:100
IL-17F	PerCP-eFluor710	SHLR17	eBioscience	1:100
GM-CSF	APC	BVD2-21C11	Biolegend	1:100
GM-CSF	PerCP-Cy5.5	BVD2-21C11	Biolegend	1:100
Granzyme B	APC	QA16A02	Biolegend	1:50
Perforin	Pacific Blue	dG9	Biolegend	1:100
anti-GPR65	-	976128	R&D	1:25
anti-GPR65	FITC	Polyclonal	Alomone	1:50
Rabbit IgG isotype	FITC	Polyclonal	Alomone	1:50
Goat anti-mouse IgG	AF647	Polyclonal	Jackson ImmunoResearch	1:1000
Goat anti-rabbit IgG	AF647	Polyclonal	Jackson ImmunoResearch	1:1000

Table 2 – FACS antibodies used throughout the project

2.2.6.1 Surface staining

Up to $2x10^5$ cells/well were stained in FACS buffer, in a total volume of 50µL per well. Cells were incubated for up to 1 hour at 4 °C in the dark with panels of fluorochrome conjugated antibodies. Samples were then washed twice in FACS buffer and resuspended in up to 200µL for acquisition (with/without DAPI (Biolegend) where required).

If primary and secondary antibodies were used, cells were first stained with the primary antibody as described above, washed twice in FACS buffer, and stained with secondary antibody for a further 30 minutes. Instances where Fc block (BD Biosciences) was used, 2.5µg/1x10^6 cells was added for 10 minutes prior to surface antibody incubation.

2.2.6.2 Intracellular cytokine staining (ICS)

Experimental cultures incubated in round bottomed 96-well plates had 100µL supernatant removed and stored at -20 °C for future protein analysis. 100µL media containing 20µg/mL Brefeldin A (BFA, Sigma), along with relevant stimulation, was added for the last four hours of culture. Plates were centrifuged at 400xg for 5 minutes to pellet cells and supernatant was removed. Fixable live/dead (near infrared, Invitrogen) dye was stained for 15 minutes, 4 °C in the dark and washed off. Cells were fixed by re-suspending in 1.6% paraformaldehyde (ThermoFisher) for 5 minutes at room temperature, before washing cells twice with PBS+EDTA. Cells were stained in 1x permeabilisation buffer (eBioscience), in a total volume of 50µL per well, for up to 30 minutes at room temperature and in the dark. Samples were then washed twice and resuspended in up to 200µL PBA+EDTA for acquisition.

2.2.6.3 FACS sorting

Samples for FACS sorting were subject to the same surface staining protocol (described in 2.2.6.1) and resuspended at a density of 1x10^7/mL in either R10 or FACS buffer and filtered into a polystyrene tube with 35µM nylon mesh strainer cap (Stemcell Technologies). Samples were kept on ice, before and after the sort.

Sorting was carried out using the BD Aria III cell sorter (performed by flow cytometry facilitators, referenced to within results sections) and cells sorted into either 1.5mL Eppendorfs or 15mL falcons, containing R10.

2.2.7 Supernatant protein quantification

All supernatant samples were stored at -20 °C prior to analysis.

2.2.7.1 ELISA

IL-17F concentration was measured using the IL-17F (homodimer) human uncoated ELISA kit (ThermoFisher).

A 96-well MAXI-sorb ELISA plate (Nunc, ThermoFisher) was coated with 100µL/well of capture antibody and incubated at 4 °C overnight. Plates were washed three times with 300µL wash buffer and blocked for an hour with 200µL assay diluent at room temperature. Standards were prepared with a top concentration at 2,000pg/mL, and subsequent two-fold serial dilutions, down to 15.63pg/mL. Wells were washed 3 times, before the addition of 60µL standard or sample supernatant, neat or diluted in assay diluent as determined by titration experiments and incubated for 2 hours. After 3 washes, 100µL/well of detection antibody was added for 1 hour. Following this, 3 washes were performed and 75µL Avidin-HRP was added to all wells and left to incubate for 30 minutes. After a further 6 washes, 80µL TMB substrate solution was added and incubated in the dark for up to 30 minutes. To stop the assay, 80µL stop solution (ThermoFisher) was added. Plates were read using the Synergy Neo2 at 450nm.

2.2.7.2 Meso Scale Discovery (MSD) platform

IFNγ, TNFα, IL-1β, IL-6, IL-10, IL-17A and GM-CSF were measured using the U-PLEX MSD platform.

Linked antibodies were prepared for each cytokine; 300µL of a linker was added to 200µL of a biotinylated antibody and incubated for 30 minutes. 200µL stop solution was added before a further 30-minute incubation. A coating solution was made by combining 600µL of each

coupled linker and the addition of stop solution to reach a final volume of 6mL. 50µL/well coating solution was added to a 96-well plate for 1 hour, shaking at room temperature. Standards were prepared with a top concentration as per the manufacturers recommendation, and subsequent four-fold serial dilutions in diluent 43. Wells were washed 3 times, before the addition of 25µL/well standard or sample supernatant, diluted in diluent 43 as determined by titration experiments, followed by a further 25µL/well of diluent 43 to all wells and incubated for 1 hour. After 3 washes, 50µL/well of detection antibody mix (60µL each detection antibody combined and made up 6mL with diluent 3) was added for 1 hour. Following this, 3 washes were performed and 150µL/well 2x read buffer was added. Plates were read using the MSD Microplate Imager 6000 and analysis performed using Discovery Workbench (MSD).

2.2.8 Gene expression

2.2.8.1 RNA extraction

RNA was extracted using the RNeasy Micro kit (Qiagen). Briefly, < $5x10^5$ cells were suspended in 350µL RLT buffer and stored at -20 °C prior to RNA extraction. The defrosted cell lysate was vortexed and 350µL 70% ethanol added. The sample was placed into a RNeasy spin column and spun at 8,000xg for 15 seconds. After the flow through was discarded, columns were washed with 350µL RW1 buffer and spun again before disposing of flow through. 80µL DNaseI incubation mix was added directly to the membrane and left to incubate for 15 minutes, at room temperature. A further 350µL RW1 buffer was added to the column and spun. The spin column was transferred to a new collection tube and 500µL RPE buffer added. After another spin, and subsequent flow through discarded, 500µL 80% ethanol was added and spun at 8,000xg for 2 minutes. To dry the membrane, column lids were opened and spun at 13,000xg

for 5 minutes. Spin columns were finally transferred to 1.5mL collection tubes, 14µL RNase-free water was added directly to the membrane and RNA was eluted from a spin at 13,000xg for 1 minute. RNA sample quality and quantity were measured using Nanodrop 2000 (Thermo Scientific) and stored at -80 °C until further processing.

2.2.8.2 Complementary DNA (cDNA) synthesis

First strand cDNA was synthesised from RNA using the SuperScript™ VILO™ cDNA Syntheses Kit (Invitrogen), using 100ng RNA. Reaction mix tubes were incubated at 25°C for 10 minutes, then for 42°C for 1 hour, and finally 85°C for 5 minutes in a 2720 Thermal Cycler (Applied Biosystems).

2.2.8.3 Quantitative PCR (qPCR)

qPCR reactions were set up to include 10ng of cDNA, with TaqMan Fast Advanced PCR MasterMix (Applied Biosystems) and relevant TaqMan Assay (Table 3). Amplification reactions were run on a QuantStudio™ 7 Flex Real-Time PCR System (Applied Biosystems) and consisted of a 2 minute hold at 50 °C, then 95°C for 20 seconds, followed by 40 cycles of 95°C for 1 second followed by 60°C for 20 seconds. The ΔΔCT method was used to determine the relative expression of the genes, with *ACTB* used as the housekeeping control.

Gene	**Applied Biosystems ID**
ACTB	Hs01060665_g1
GPR4	Hs00270999_s1
GPR65	Hs00269247_s1
GPR68	Hs00268858_s1

Table 3 – Genes investigated by qPCR

2.2.9 Clustered Regulatory Interspaced Short Palindromic Repeats (CRISPR) gene knockout

$1x10^6$ isolated $CD3^+$ T cells were plated into 6-well plates in R10 + 50U/mL IL-2 (R&D). A 1:2 ratio of Dynabeads (Gibco) was added to each well and plates incubated at 37 °C, 5% CO_2 for 48 hours. Cells were separated from stimulation beads using a magnet and pooled together. $1x10^6$ cells were pelleted in 1.5mL Eppendorfs and resuspended in pre-prepared RNP complexes (detailed in Table 4), then transferred to the AMAXA cuvette strip. The nucleofection was performed using the activation primary T cell protocol (V4XP-3032, AMAXA) and cells rescued in pre-warmed R10 + IL-2 + 10U/mL DNaseI (ThermoFisher). A third of each sample was split across wells of a 24-well plate and cultured at 37 °C, 5% CO_2 for 72 hours.

For functional assessment of the cells, they were then stimulated with the addition of 250µL R10, containing a 1:4 ratio of Dynabeads or IL-12 and IL-18 [10ng/mL, final concentration] for a further 72 hours.

Condition	**gRNA:Cas9 ratio**	**gRNA (100pmol/µL)**	**Cas9 (20pmol/µL)**	**Nucleofector solution (µL)**
Unstimulated	Not nucleofected			
Stimulated	Not nucleofected			
Mock AMAXA	-	-	-	20
Non-target control	3:1	2.4	4	13.6
GPR65 (Synthego)	3:1	2.4	4	13.6
GPR65	1:1	0.8	4	15.2
CD28 (positive control)	3:1	2.4	4	13.6

Table 4 – Composition of CRISPR RNP complexes

gRNA was supplied by Synthego.

DNA was extracted from cell pellets using QuickExtract solution (Lucigen) and incubated at 65 °C for 6 minutes, then samples were vortexed for 30 seconds before a second incubation at 98 °C for 2 minutes. After passing DNA through a QIAShredder column (Qiagen), it was centrifuged for 1 minute, at 4 °C and 16,000xg. PCR reactions were set up to include Accuprime Taq DNA Polymerase – High Fidelity Kit (Invitrogen), DNA, water and 10µM forwards and reverse primers (Table 5 and Figure 2-1). Reactions were run on a GeneAmp PCR system 9700 (Applied Biosystems), and consisted of a 30 second hold at 94 °C, followed by 38 cycles of 94 °C for 30 seconds, 58 °C for 30 seconds and 68 °C for 1 minute, then a final 7 minutes at 72°C.

PCR products were mixed with sample buffer loading dye (Invitrogen), and run along a 1% agarose gel, alongside the ladder (Invitrogen) to determine the band sizes. Gels were run at 90 V for 1 hour and bands revealed on a Molecular Imager Gel Doc XR system (Bio-Rad).

Primer	Sequence
GPR65_Forward	ATGCTTGTGGGCTGTTTGTC
GPR65_Reverse	GCTGTGGTCTTCGAAGTTCA

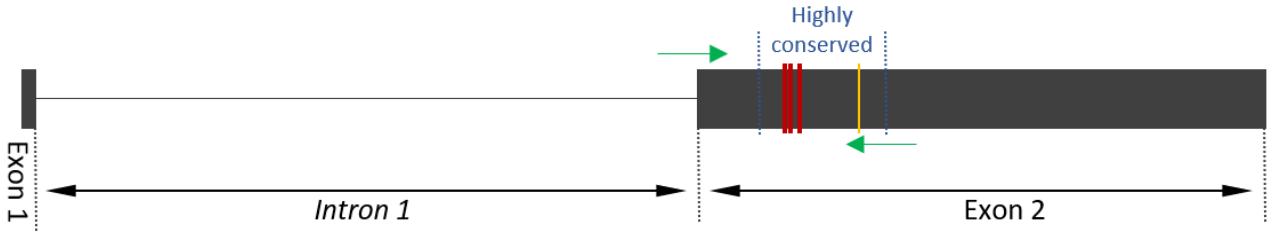


Table 5 and Figure 2-1– PCR primer pair for assessing GPR65 knockout

Using RNA sequences provided by Synthego to calculate the DNA sequence, I used Primer3 (Primer3) to design and generate a forward and reverse primer pair (manufactured by Sigma) for GPR65, to be used in PCR reactions. The schematic represents GPR65 exons and introns, with red sites marking the 3 pooled gRNA sequences within a highly conserved region of exon 2, and the unique primers illustrated by green arrows. The yellow site depicts the SNP rs3742704 discussed in 1.2.4.1.2. Created based on information from the UCSC Genome Browser (UCSC Genome Browser Home).

2.2.10 Small interfering RNA (siRNA) gene knockdown

GPR65 knockdown was performed using the Accell siRNA system (Horizon). Specifically, $3x10^5$ isolated $CD8^+$ T cells, or PBMCs were plated into 96-well U-bottom tissue culture plates, in 100µL Accell siRNA Delivery Media containing either 1µM non-target or GPR65 SMARTpool siRNA. Cells were cultured at 37 °C, 5% CO_2 for up to 72 hours. Effects of knockdown were assessed by qPCR (detailed in 2.2.8).

For functional experiments where cells were pre-treated with siRNA, after the timeframe of knockdown, plates were centrifuged for 5 minutes at 400xg. Cells were then resuspended in 200µL pH relevant media, containing required stimulation, and incubated as described in 2.2.5.

2.2.11 RNA sequencing

2.2.11.1 10x Genomics library generation and sequencing

Sequencing libraries were generated by Dr. Moustafa Attar, using 10x Genomics Single Cell 5' Reagent kits (v2.0 Chemistry), following manufacturers protocol. Cells were loaded onto the Chromium controller (10x Genomics), with one channel representing each of the experimental conditions, containing cells from all three donors.

Library generation and sequencing were performed at the Oxford Genomics Centre (Wellcome Centre for Human Genetics, University of Oxford).

2.2.11.2 Computational/Bioinformatics analysis

2.2.11.2.1 Gene expression quantification, quality control and sample demultiplexing

Sequencing data from 12 samples was aligned separately and quantitated using the 10x Genomic Cell Ranger (V7.0.0) analysis pipeline. For gene expression data, FASTQ files were generated using cellranger mkfastq, reads were aligned to the 10x Genomics human GRCh38

reference genome and quantified using cellranger count. In parallel, donor-identifying hashtags were quantitated with the cellranger multi function. The raw gene expression and hashtag matrices of each sample were then merged and analysed in the Seurat R package (v4.0.5). Merged data was demultiplexed to the three donors using the HTODemux function, while doublets were removed. Quality control was then performed based on expression data. All cells with < 600 or > 5,000 detected genes were removed, as well as cells with < 400 or > 15,000 unique molecular identifiers (UMIs). Cells with > 5% counts mapped to mitochondrial genes were also filtered out.

2.2.11.2.2 Normalisation, data integration and dimensionality reduction

Count data was normalised using the NormalizeData function, based on which 4,000 variable genes were identified. The 3,500 most variable genes were selected across samples as candidates of anchors for data integration using SelectIntegrationFeatures. Ribosome genes, MHC genes and T cell receptor genes were then further excluded, with 3,370 genes remaining. The FindIntegrationAnchors and IntegrateData function were then used to integrate expression metrics from different experiments. ScaleData and RunPCA were performed on the integrated assay to compute 100 principal components (PC). Uniform Manifold Approximation and Projection (UMAP) dimensionality reduction was carried out using the top 30 PC's. Clustering was performed on the Integrated assay at a resolution of 0.8 which yielded a total of 17 clusters, each composed of cells originating from all 12 experimental conditions.

2.2.11.2.3 Differential gene expression analysis

Differential gene expression (DEG) analysis between clusters was performed using the Wilcoxon rank sum test for individual sample analyses through the FindAllMarkers function. Cluster markers were defined as genes with significantly increased expression in one cluster

relative to the average of all other clusters (adjusted $p < 0.05$ based on Bonferroni correction using all genes in the dataset). DEG analysis between experimental conditions was performed using FindMarkers. Genes with a log 2-fold change (log2FC) > 0.5 and false discovery rate set < 0.05 after corrections for multiple comparisons, were defined as significantly differentially expressed, unless specified otherwise in the figure legend. Variable genes identified were plotted using the EnhancedVolcano package[248].

2.2.11.2.4 Pathway enrichment analysis

Pathway analysis for Reactome pathways was performed using XGR software[249].

Chapter 3 : Strategies to discover a human GPR65 monoclonal antibody

3.1 Introduction

Antibodies being used as tool reagents is not a new concept, with many specifically developed to understand target biology and function, or to aid with structural studies. As monoclonal antibodies tend to have high affinity towards a specific epitope of a target antigen, these are favoured in many settings, compared to polyclonal antibodies which contain a heterogeneous mix of serum antibodies with specificity to different epitopes of a given antigen.

An advantage of using antibodies as binding tools is their display of conformational bias and ability to recognise certain conformations of its antigen, with higher affinity than to others[250,251]. They can selectively bind conformations which are naturally sampled by the antigen, and lock them in that state, known as conformational selection[252].

Historically there has been intense interest in the expansive GPCR family, and they still stand as the largest group of therapeutic targets, with most successful approaches through small molecules and peptides[168]. As of 2020, > 270 GPCRs have been identified with having disease links and are considered druggable. Despite decades of work, there are currently still only two antibodies clinically available, speaking to the technical challenges associated with identifying functional antibodies against GPCRs[253].

The structural instability of multiple transmembrane domains in the full-length protein are not favoured immunogenic and antigenic characteristics. It was down to innovative soluble immunogen design of extracellular domains of CGRP-R linked to Fc domains which proved successful in the discovery of erenumab, the first FDA approved antibody against a GPCR[254]. Alternatively, the second, mogamulizumab, was generated through the humanisation of a

chimeric mouse anti-CCR4 antibody, raised by immunising a mouse with a peptide consisting of only 27 amino acids from human CCR4[255,256].

When starting on this project, there were no monoclonal antibodies against GPR65, instead only commercially available polyclonal options, without any published uses described or validated. Taken together with the lack of a known structure, it suggested antibody generation against this target would come with its challenges.

3.2 Aim

The aim of this chapter was to discover a specific monoclonal antibody against human GPR65, to help address the receptors' role in the immune system.

Here, I discuss the antibody campaigns trialled (rabbit immunisation and phage display), using soluble proteins as scaffolds to display extracellular loops of GPR65[245,257] and cell-based approaches (Figure 3-1).

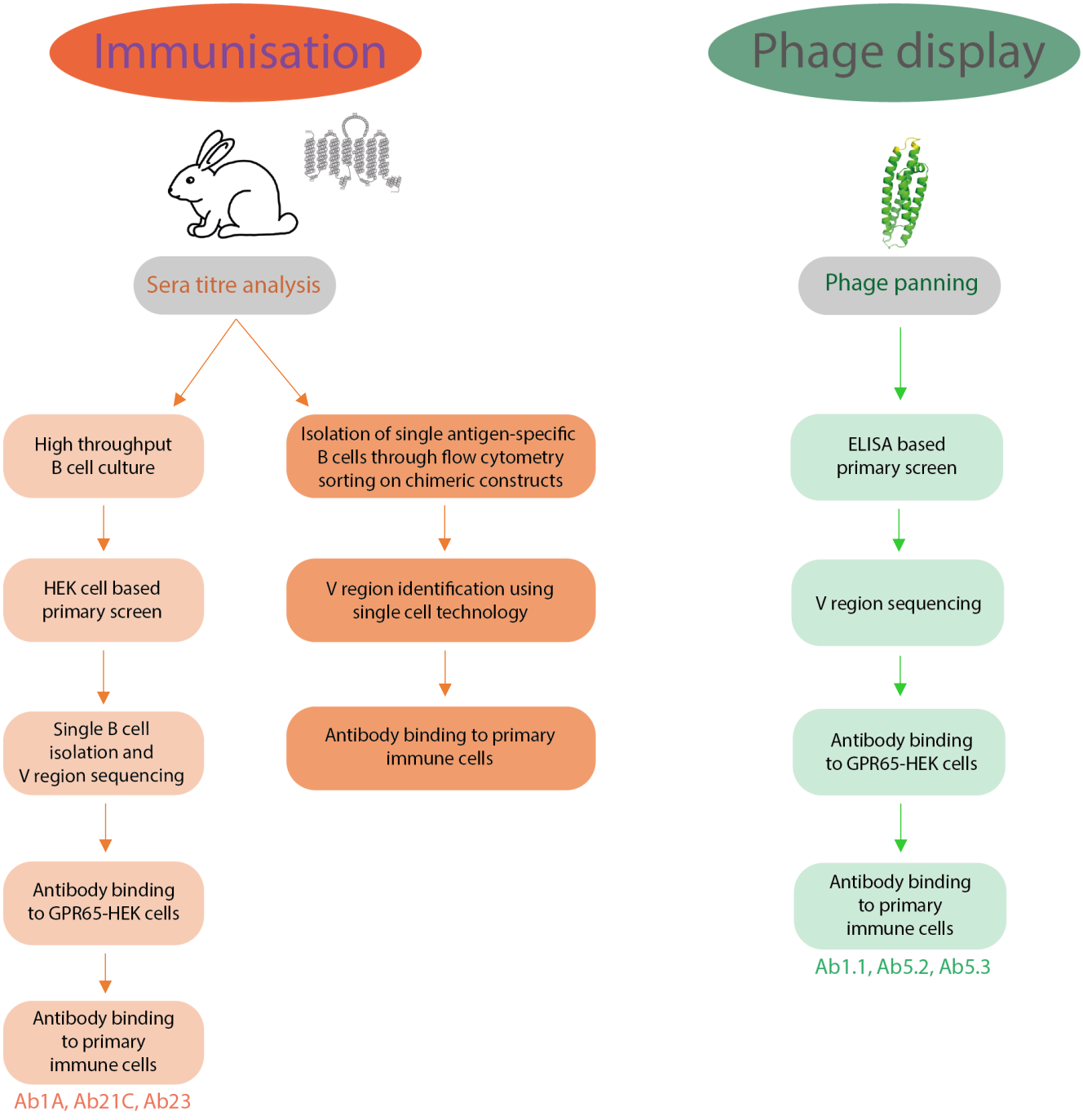


Figure 3-1 – Overview of antibody discovery efforts to identify a monoclonal GPR65 antibody

Antibodies referenced within the chapter are also listed, to depict where they were derived from.

3.3 Results

3.3.1 Recombinant protein generation

To increase my chance of raising antibodies against GPR65, I initially attempted to generate recombinant protein. When designing the construct for expression, it was important to consider the end use of the protein; properties of the construct would differ if the protein was to be used in biological assays, verses its use in structural studies. For this project, full length protein was required to keep its flexibility for expression and function. Starting with the wild type GPR65 sequence, obtained from Uniprot (Data available at GPR65 - Psychosine receptor - Homo sapiens (Human) - GPR65 gene & protein (uniprot.org)), additional features were included to act as surrogate expression markers, and tags required for downstream purification processing (Figure 3-2A). Although the use of 10His could have negatively impacted expression levels, it was used to achieve better recovery and purity, which would eventually be important for immunisation use.

HEK cells, chosen to maintain necessary post translational modifications, were transiently transfected with the purification GPR65 construct (Figure 3-2Ai). Expression of both upstream FLAG and downstream GFP, were used to imply GPR65 cell surface expression. As the GFP signal corresponded to FLAG expression, it was taken with faith that GFP was an appropriate surrogate of GPR65 expression (Figure 3-2B). Cells were shown to be > 90% viable 24 hours post transfection, with > 60% of those expressing GPR65 (via analysis of the GFP surrogate); compared to 48 hours of culture, where cells were less than 70% viable, and > 80% expressing GPR65. The negative peak from those transfected with GPR65, representing ~30% of cells, acted as an internal negative control therefore, providing more confidence in the positive peak signal.

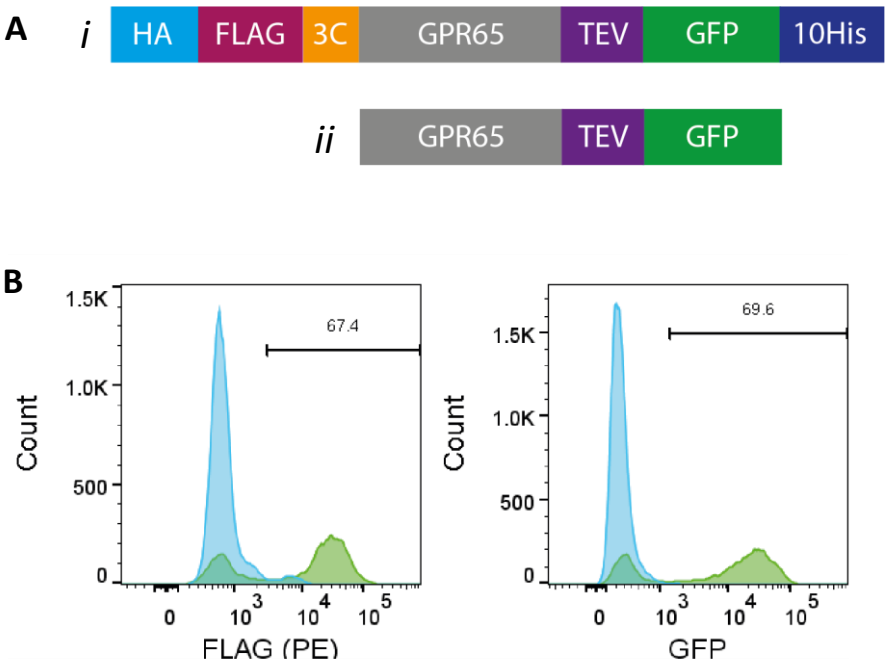


Figure 3-2 - GFP could be used as a surrogate for GPR65 expression

Ai) Purification construct containing hemagglutinin (HA) signal sequence to encourage trafficking to the cell surface, FLAG tag to confirm surface expression, 3C and TEV protease sites to cleave off tags, His tag used within purification stages and GFP to aid with detection of gene expression. Aii) Construct for immunisation and biological assays, where the native leader sequence within each species DNA allowed for cell surface delivery – containing only the fluorescent feature as an additional extra. B) The GPR65 purification construct was transiently transfected into HEK cells and incubated for 24 hours. After gating on live cells, FLAG expression, through a PE-conjugated anti-FLAG antibody, and GFP were analysed by flow cytometry. Wild type HEK cells are depicted in blue, whilst HEK cells transfected with human GPR65 are depicted in green. Percentage of expression is stated within the plots; a positive signal is represented by the green signal, to the right of the blue peak.

To maximise expression, cells were cultured for 48 hours prior to being harvested and frozen for use within the purification process. Alternatively, cells used for immunisation and within assays (DNA in Figure 3-2Aii), were cultured for 24 hours to have as many live cells as possible, with the caveat of lower receptor expression.

Following the harvest of GPR65 expressing HEK cells for purification, cell membranes were disrupted, whilst proteolysis was inhibited, and total protein concentration was measured to be 7.1mg/mL, by bicinchoninic acid analysis. After the addition of iodoacetamide to each homogenate, to prevent protein aggregation from intermolecular disulphide bond formation, four common detergents were tried against equal membrane concentration at pH 7.4, in the presence of cholesterol hemisuccinate (CHS), to stabilise the environment and retain the folded active protein throughout the process.

As well as acting as a surrogate of GPR65 extracellular expression, GFP provided the ability to assess the aggregation state/monodispersity of the protein, by fluorescence-detection size-exclusion chromatography (fSEC). Analysis at neutral pH suggested the two detergents with the mildest properties and lowest critical micelle concentrations, dodecyl-β-D-maltopyranoside (DDM) and lauryl-maltose-neopentylglycol (LMNG), provided the cleanest peak representing the protein of interest (represented by the black arrow in Figure 3-3A).

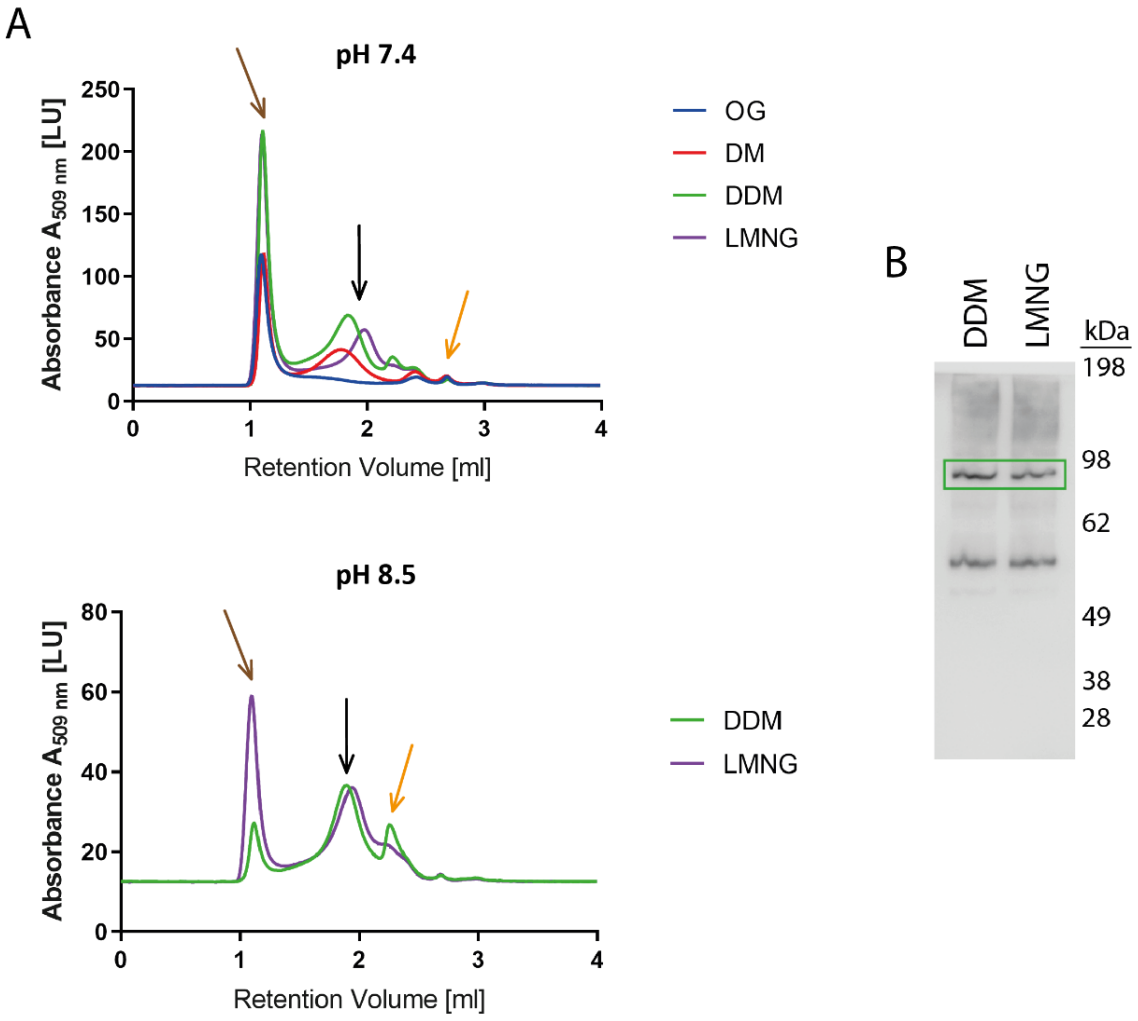


Figure 3-3 – Analysis of soluble GPR65 recombinant protein

Supernatant derived from lysed HEK cell membranes was treated with detergents; octyl- β -glucoside (OG), n-dodecyl-β-D-maltoside (DM), DDM and LMNG for 2.5 hours, at two different pH's. Following ultracentrifugation, the unpurified receptor was analysed by fSEC (A). The brown arrow represents the void peak, the black arrow represents the protein peak of interest, and the orange arrow represents the free GFP peak. B) The same soluble fraction loaded for chromatography was also analysed by western blot, using an anti-FLAG detection antibody. The green box depicts a band at ~75kDa, representing the full-length DNA construct.

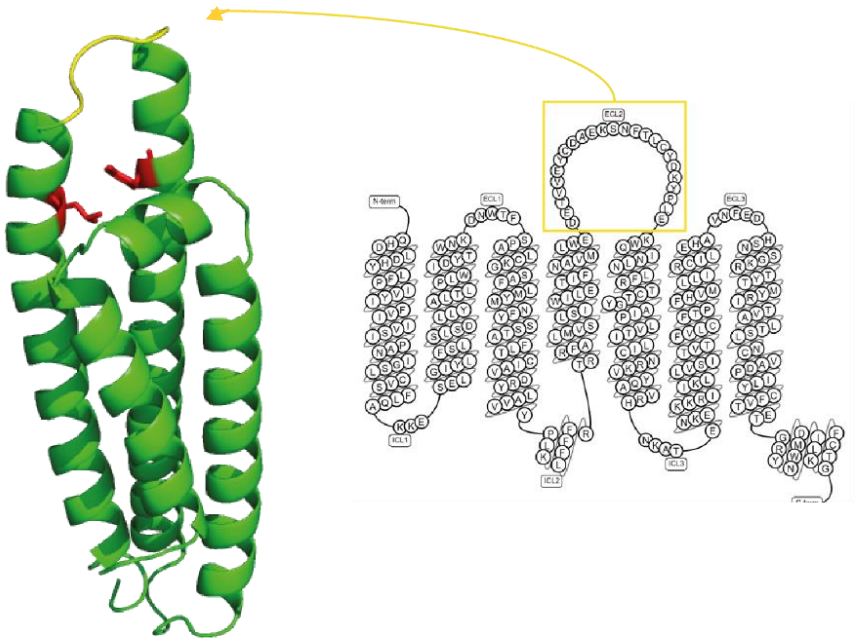
Overall poor levels of GPR65 protein were observed, alongside high void signals. With the aim to improve expression and to prevent even slight GPR65 activation by protons, purification was next carried out in a higher pH environment. At pH 8.5, both detergents tested generated similar protein peaks of interest to each other, with DDM giving the best ratio of folded GPR65 to aggregate (Figure 3-3). However, the levels of protein detected were still very low; so, suggested that pH does not appear to play as much of a role as anticipated here, with protein of interest peaks being similar at both pH conditions tested. When comparing DDM and LMNG, solubilised protein expression was similar for both detergents, further supported by expression of the surrogate FLAG tag (Figure 3-3B).

In the interest of time and the appreciation of requiring optimisation and alternatives to try to achieve better expression/solubilisation results, work here was stopped and effort was put into antibody discovery.

3.3.2 GPR65 phage display campaign to identify antigen-specific antibodies

3.3.2.1 GPR65 loop immunogen design

Phage panning in solution requires the ability to pull out the protein of interest and the corresponding enriched binding antibodies, therefore recombinant protein is often the antigen of choice. Without this option, and the additional challenges of cell-based antigen display, an alternative approach to present extracellular loops (ECL) of human GPR65 was trialled. Utilising the 4-helix bundle structure of soluble human apolipoprotein E3 (ApoE3), each of the three ECL of human GPR65 were directly substituted for the wild type, 5 amino acid ECL of ApoE3 (Figure 3-4).



MGHHHHHHGLNDIFEAQKIEWHEGSENLYFQGQRWELALGRFWDYLRW
VQTLSEQVQEELLSSQVTQELRALMDETMKELKAYKSELEEQLTPVAEETRA
RLSKELQAAQARLGADMEDVCGRLVQYRGEVQAMWEDETVVEYCDAEKS
NFTLCYDKYPLEKWEELRVRLASHLRKLRKRLLRDADDLQKRLAVYQAG

Figure 3-4 – Depiction of a novel GPR65 chimeric construct

Edited structure to symbolise human apolipoprotein E (Uniprot entry P02649, PDB 1BZ4) as a backbone scaffold (green), indicating the loop to be substituted with an extracellular loop (ECL) from human GPR65 (yellow). Red sites represent critical interactions between the two helices which maintain structural integrity of the protein. The corresponding sequence of the construct example (ApoE3 with substituted GPR65 ECL2) is also shown. The His-Avi-TEV site (blue) was included for biotinylation and purification of the protein.

To verify expression of the chimeric proteins, cell lysates before and after induction were analysed. Next, the solubility of the chimeric proteins was assessed by separating the cell lysate (after induction) into a soluble and insoluble fraction through centrifugation (Figure 3-5). Five of the seven proteins were found in the soluble fraction, whilst two (those with multiple substituted amino acids within the α-helix, +4aa and +6aa within Figure 3-5) remained in the insoluble fraction. Only those that were direct swaps of the extracellular loops were purified, via their His tag, and remained soluble (data not shown).

To allow these chimeric proteins to be extracted during phage panning steps, it was important for the proteins to be biotinylated. The inclusion of the Avi-tag within each construct made use of the streptavidin (or neutravidin) biotin strong interaction. Four masses for each purified protein were identified by liquid chromatography-mass spectrometry (LCMS) (Figure 3-6). Each peak was identified upon knowing the molecular weight of each protein and 226 Da representing the addition of biotin, with ~50% biotinylation observed across each of the proteins.

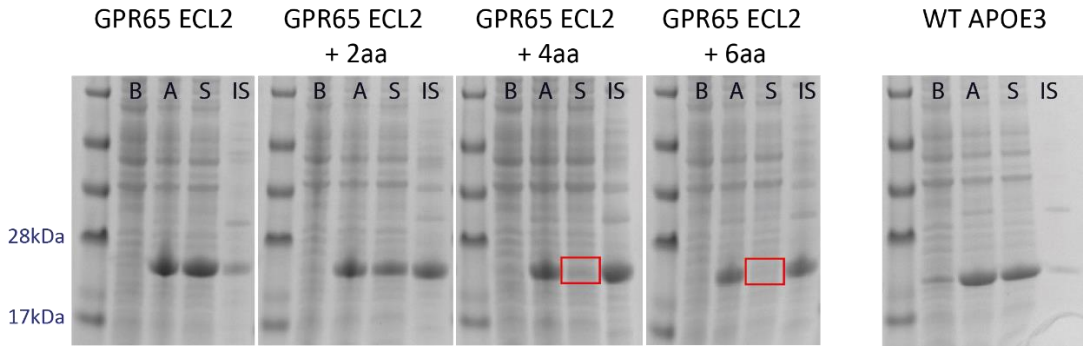


Figure 3-5 - Solubility of GPR65 chimeric proteins

SDS-PAGE gel of cell lysates before (B) and after (A) induction, and soluble (S) and insoluble (IS) fractions of expressed proteins for chimeric constructs with ECL2, representative for both ECL1 and ECL3. The + '*x*'aa represents how many amino acids on each side of the loop, as part of the helix, were also substituted with those from native GPR65. Correct bands are observed between 22-23kDa. Red squares represent a lack of soluble protein.

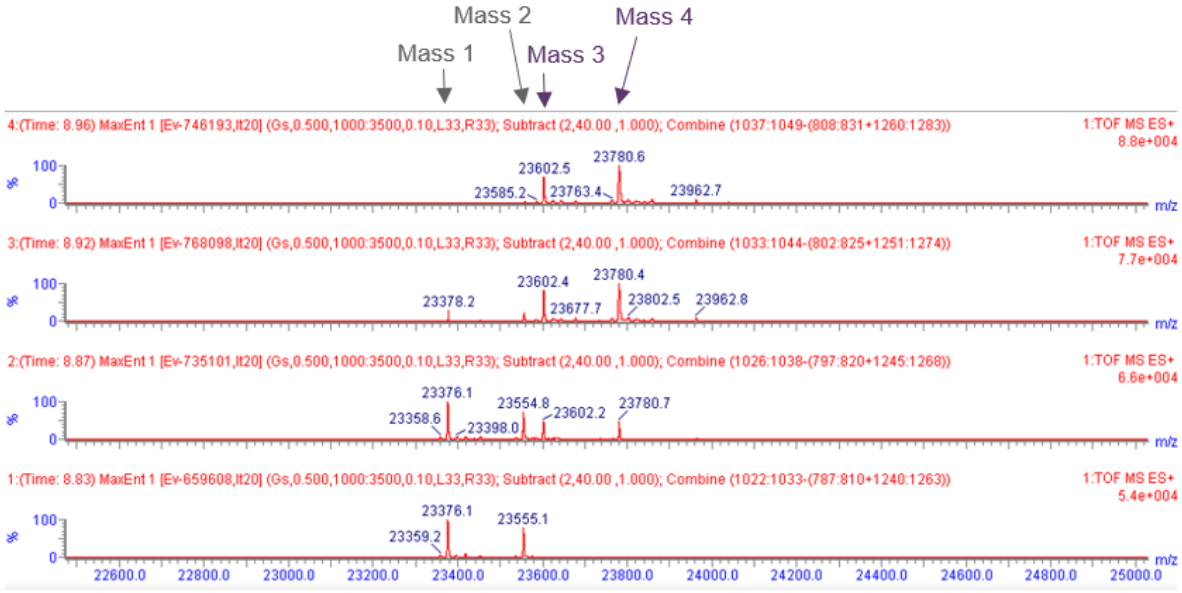


Figure 3-6 - Mass spectrometry confirmed chimeric construct biotinylation[f]

Representative example of purified ApoE3 with GPR65 ECL2. Mass 1 represents the expected protein, with the loss of the starting Methionine; mass 2 represents mass 1 with an addition of 178 Da; mass 3 represents mass 1 which is correctly biotinylated; mass 4 represents mass 3 with the additional 178 Da.

[f] Mass spectrometry performed by Adam Hold.

3.3.2.2 Phage display strategy and enriched antibody identification

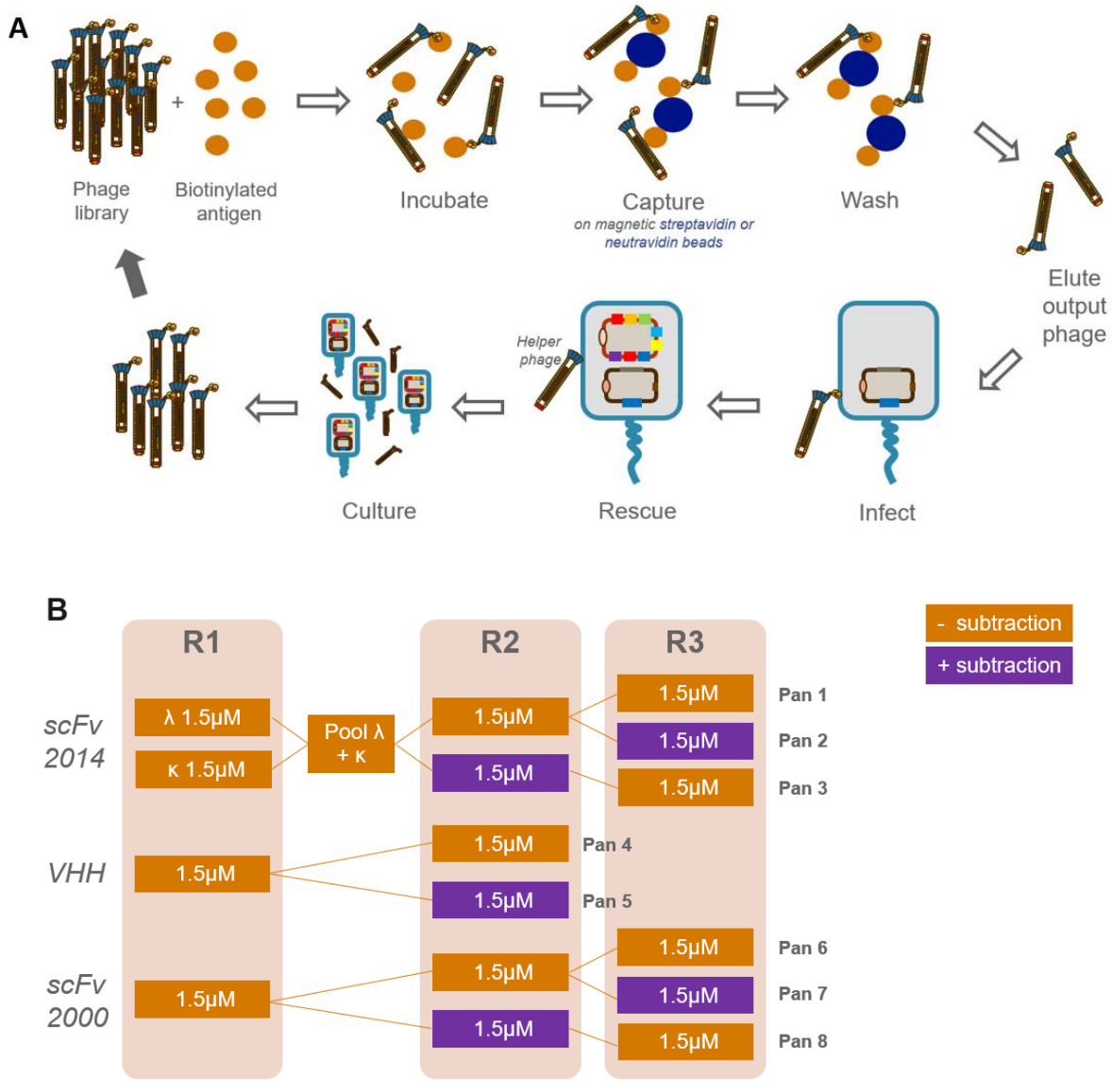


Figure 3-7 - Phage display panning overview and strategy

A) An overview of the phage display process. B) Three constructs representing each extracellular loop of human GPR65 were pooled and acted as antigen throughout all stages of phage panning, for each of the three libraries screened (naïve scFv 2014, naïve scFv 2000 and naïve VHH). The antigen concentration remained the same throughout each round (1.5μM) and rounds 2 and 3 also included a subtraction step against WT ApoE3 (purple boxes), to remove antibodies that bound the backbone. It was unknown whether subtraction of the backbone binders would be best in round two or round three, therefore, both approaches were tried. Eight pans were generated, each representing a different panning strategy.

The novel chimeric proteins with direct loop substitutes were used as biotinylated antigens within a phage display campaign (Figure 3-7). To confirm success and enrichment of phage antibodies throughout each round of panning, output titres were generated (Figure 3-8). Once panning was complete, monoclonal antibodies were rescued and antibody-containing supernatant was screened by ELISA, to identify antigen-specific binders (Figure 3-9).

Following phagemid DNA amplification by PCR, sequencing analysis identified 28 unique antibodies, 26 derived from the human scFv libraries, and 2 from the llama VHH phage library. To screen for antibody activity, extracted VHH and scFv products were subject to seamless cloning and reformatted into scFv-rabbit Fc or VHH-rabbit Fc. Following transformation, cloning success was validated through PCR, and sequencing confirmed that 20 phage antibodies had been successfully cloned into rabbit formats.

Library	Phage round	–/+ subtraction			Output titre	Phage pan
		R1	R2	R3		
VHH	1	-			$5.0x10^{8}$	
scFv 2000	1	-			$2.1x10^{10}$	
scFv 2014 K	1	-			$3.6x10^{8}$	
scFv 2014 λ	1	-			$4.8x10^{8}$	
VHH	2	-	-		$3.3x10^{9}$	**4**
VHH	2	-	+		$3.2x10^{9}$	**5**
scFv 2000	2	-	-		$7.3x10^{8}$	
scFv 2000	2	-	+		$4.4x10^{8}$	
scFv 2014	2	-	-		$8.1x10^{8}$	
scFv 2014	2	-	+		$1.4x10^{9}$	
scFv 2000	3	-	-	-	$2.8x10^{9}$	**6**
scFv 2000	3	-	+	-	$3.8x10^{9}$	**8**
scFv 2000	3	-	-	+	$9.7x10^{8}$	**7**
scFv 2014	3	-	-	-	$1.3x10^{9}$	**1**
scFv 2014	3	-	+	-	$3.7x10^{9}$	**3**
scFv 2014	3	-	-	+	$4.6x10^{9}$	**2**

Figure 3-8 – Phage panning output titres

After each round of panning, phage concentration was determined and recorded as an output titre. Output titre = number of colonies x dilution factor x total volume of cells+phages / volume spread on plate.

A

Pan	Antigen-specific binders	ApoE3 backbone binders	Neutravidin binders
1	32	12	0
2	42	4	0
3	43	4	0
4	3	1	10
5	0	0	5
6	9	24	0
7	13	11	0
8	21	19	0

B

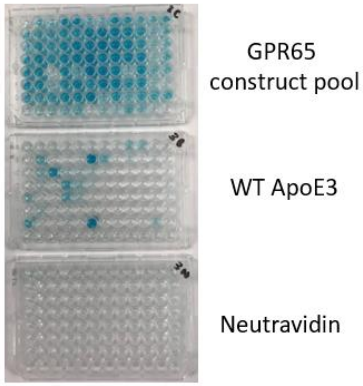


Figure 3-9 - Antigen-specific monoclonal antibodies generated by phage display were identified

Phage antibody-containing supernatant was analysed by ELISA against the pool of chimeric constructs, WT ApoE3 and neutravidin. Those positive only on the construct plate were selected as antigen-specific hits, whilst those which also bound ApoE3 were deemed backbone binders. A) Binding results from each of the different panning conditions. B) Representative ELISA plates for pans 1 and 3 (half a plate each; pan 1 on the left-hand side, pan 3 on the right-hand side).

3.3.2.3 Antibody characterisation

Upon transfection into HEK cells and 7 days in culture, transient supernatant was tested in an ELISA. Of the 17 antibodies successfully expressed, antigen-specific antibodies were confirmed to have been generated, with 7 recognising the ECL1 construct, whilst 10 bound the ECL2 construct (Figure 3-10). For antibodies discovered to be used as tool reagents, it was imperative they had the ability to bind wild type, human GPR65.

Within a primary binding screen on HEK cells expressing GPR65, concentration dependent binding to the receptor was observed for 3 of the phage-derived antibody-containing supernatants, compared to controls (Figure 3-11). The three binders specifically recognised ECL2 and represented the two distinct libraries panned; Ab1.1 coming from the VHH library, and antibodies Ab5.2 and Ab5.3 derived from the scFv library. Intriguingly, Ab5.2 and Ab5.3 shared the same sequence (Table 6) and were picked from two corresponding colonies upon cloning. As they have both continued through screening together, assurance of the binding profile for this antibody was further supported.

Antibody	Type	CDRH3	CDRL3
1.1	VHH	CAQGGTAWGRPFMWG	-
5.2	scFv	CAKVAVRDGMDVWG	CMQALKTPPTFG
5.3	scFv	CAKVAVRDGMDVWG	CMQALKTPPTFG

Table 6 – Phage-derived GPR65 antibody sequences

CDR region sequences of the phage-derived antibodies which bound native GPR65 overexpressed on HEK cells.

	1	2	3	4	5	6	7	8	9	10	11	12
A	0.065	0.036	0.132	0.173	0.039	0.039	0.061	0.036	0.041	0.118	0.054	0.100
B	0.515	0.077	0.187	0.072	1.231	0.042	0.055	0.067	0.043	0.543	1.394	0.115
C	0.562	0.045	0.038	0.048	0.270	0.473	0.045	0.040	0.055	0.548	0.191	0.330
D	0.037	0.436	0.041	0.163	0.036	0.457	0.040	0.036	0.055	0.090	0.538	0.398
E	0.044	0.048	0.044	0.052	0.782	0.041	0.047	0.045	0.043	0.062	0.762	0.042
F	0.040	0.569	0.035	0.677	0.035	0.033	0.041	0.033	0.035	0.637	0.663	0.033
G	0.041	0.467	0.038	0.678	0.033	0.046	0.043	0.047	0.032	0.480	0.626	0.038
H	0.039	0.046	0.035	0.037	0.255	0.034	0.035	0.047	0.036	0.044	0.935	0.051
	ECL1			ECL2			ECL3			All		

Figure 3-10 – Phage-derived antibodies specifically bound ECL1 and ECL2 GPR65 chimeric constructs

20 cloned antibodies were expressed, and antibody-containing supernatant binding was tested by ELISA, against plate bound individual chimeric constructs or as a pool, to determine their specificity. Layouts of antibodies tested were repeated across the plate, per each binding profile (ECL1, ECL2, ECL3 and a pool of all three in 'All'). Binding is highlighted in green. The purple wells represent values from the secondary antibody control, the blue wells were blank, and the red values from an empty HEK cell supernatant, as an additional control.

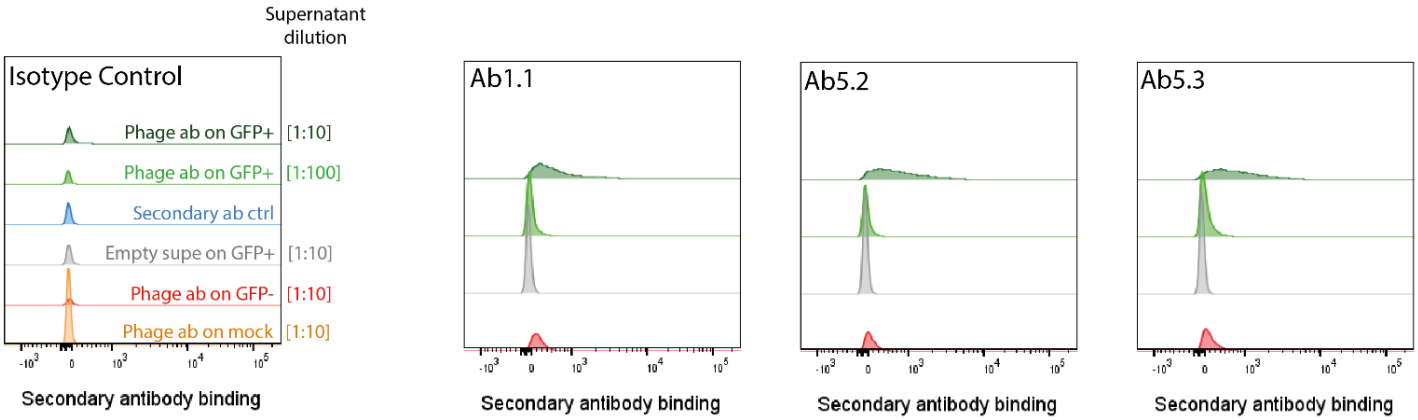
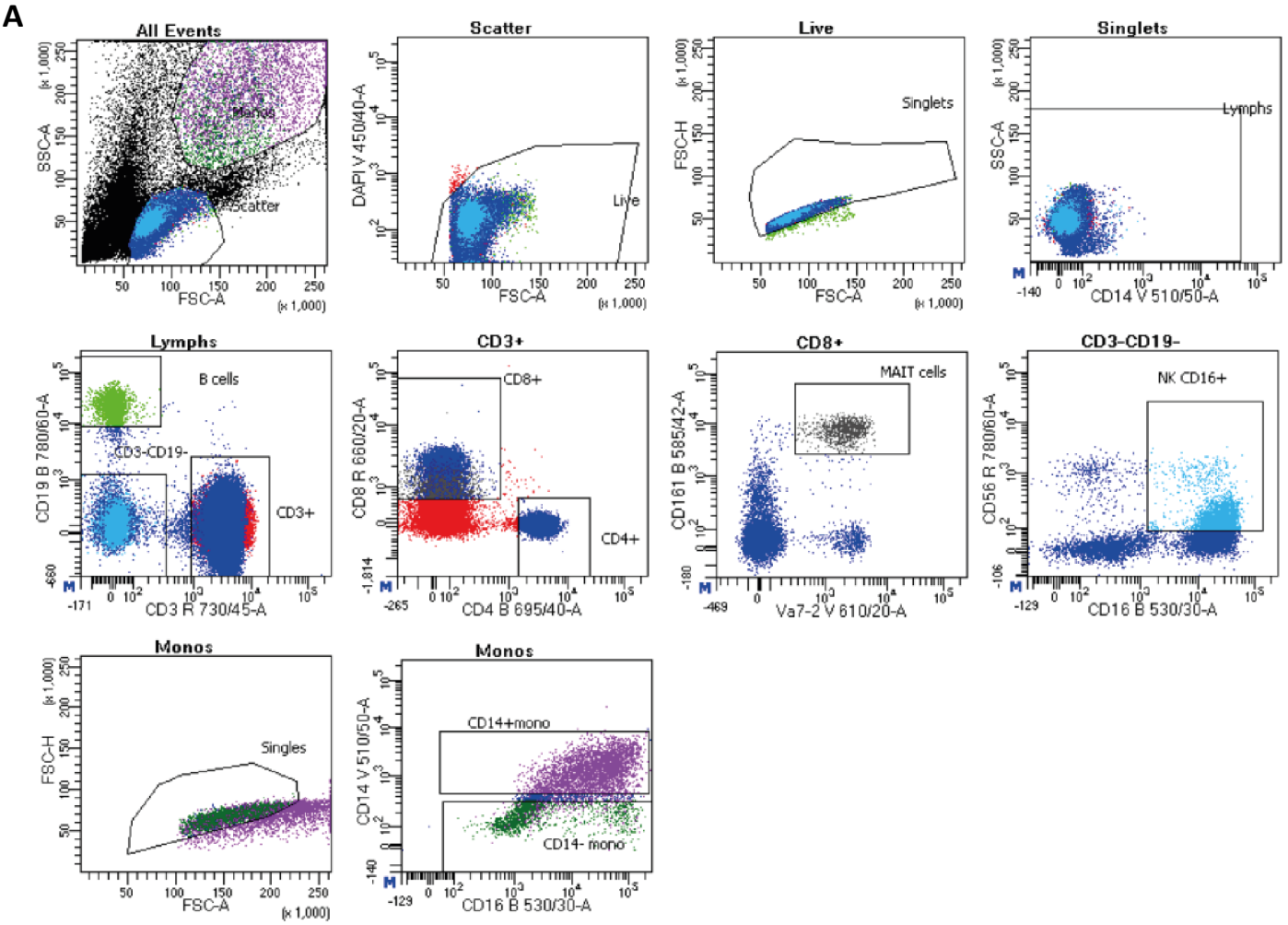


Figure 3-11 - Phage-derived antibodies raised against chimeric constructs were able to recognise native antigen overexpressed on HEK cells

Diluted phage-derived antibody-containing supernatant was incubated with HEK cells ±GPR65, and secondary antibody signals were analysed by flow cytometry to determine binding. GFP^+ cells represent GPR65 expressing cells, whilst GFP^- cells represent the internal negative control of cells not successfully transfected with GPR65 DNA, while mock cells reflect WT HEK cells having undergone the transfection protocol, without the addition of any DNA.

To remove any unwanted signals from artifact that may have been in the supernatant, the three GPR65-specific antibodies were purified by Protein A tips (Phynexus). Binding of these antibodies was assessed against primary immune subsets, to provide further support in recognition of the native receptor.

It is understood from RNA expression analysis, and corresponding qPCR data of the human donors screened (Figure 3-12), that MAIT cells, followed by $CD16^+$ NK cells and non-classical monocytes express the highest levels of GPR65, compared to B cells as the lowest expressors of the receptor. Therefore, it was surprising when all three antibodies, at either concentration (1 or 10µg/mL), did not bind MAIT cells (Figure 3-13). However, for Ab1.1 only, population right shifts, which appeared to titrate out, were observed on $CD16^+$ NK cells, B cells and monocytes, suggesting recognition of the receptor expressed on the surface of these cells.


A
All Events
Monos
Scatter
SSC-A
FSC-A
Scatter
DAPI V 450/40-A
Live
Live
Singlets
FSC-H
Singlets
Lymphs
SSC-A
CD14 V 510/50-A
Lymphs
B cells
CD3-CD19-
CD3+
CD19 B 780/60-A
CD3 R 730/45-A
CD3+
CD8+
CD4+
CD8 R 660/20-A
CD4 B 695/40-A
CD8+
MAIT cells
CD161 B 585/42-A
Va7-2 V 610/20-A
CD3-CD19-
NK CD16+
CD56 R 780/60-A
CD16 B 530/30-A
Monos
Singles
FSC-H
FSC-A
Monos
CD14+mono
CD14- mono
CD14 V 510/50-A
CD16 B 530/30-A

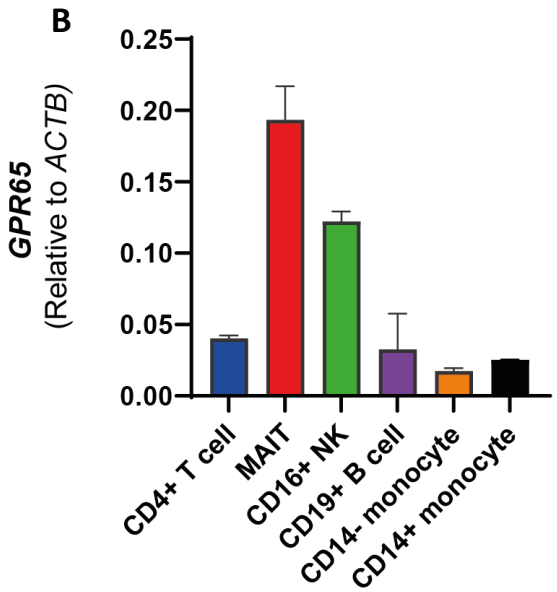

B
GPR65
(Relative to ACTB)
0.25
0.20
0.15
0.10
0.05
0.00
CD4+ T cell
MAIT
CD16+ NK
CD19+ B cell
CD14- monocyte
CD14+ monocyte

Figure 3-12 – MAIT cells expressed the highest levels of GPR65 mRNA, of the PBMC subsets tested

A) PBMCs from two donors were sorted[g] into relevant cell subsets based on their expression of conventional phenotypic markers. RNA was extracted, cDNA synthesised and qPCR performed using the Taqman system. B) *GPR65* expression shown is normalised to the housekeeping gene *ACTB*.

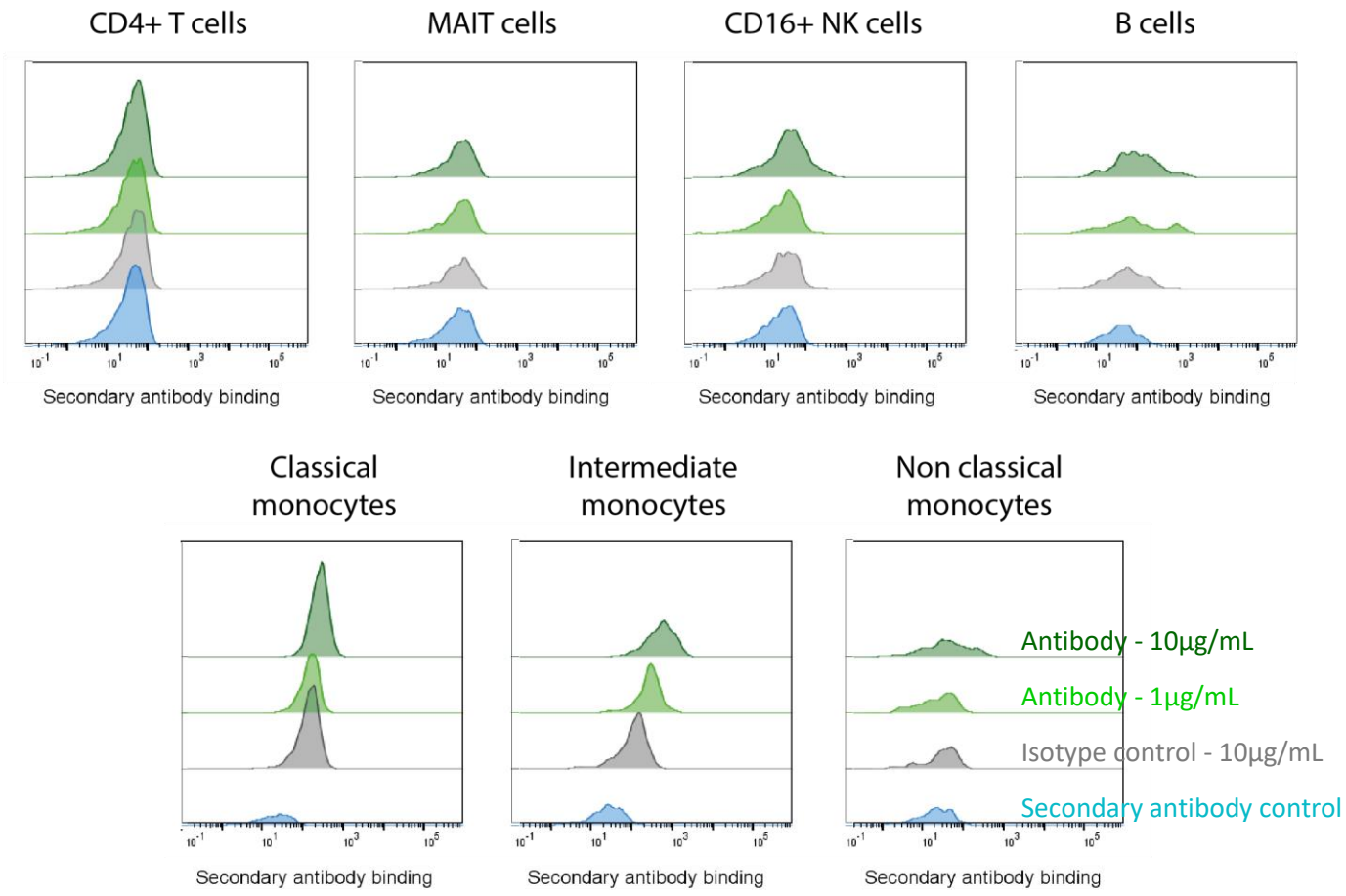


Figure 3-13 – Phage-derived antibodies binding native antigen expressed on PBMCs

PBMCs were isolated from a healthy control (n=1), treated with Fc block for 10 minutes, then phage-derived antibody was incubated with the cells for 1 hour. Live cell subsets were identified according to their phenotype (Figure 3-14) before secondary antibody (anti-rabbit IgG AF647) binding was assessed by flow cytometry. Phage-derived antibody binding is depicted in light or dark green, for 10µg/mL or 1µg/mL respectively, with the secondary antibody control depicted in blue, and the isotype control reflected in grey. Ab1.1 is the example shown.

[g] Sort was performed by Catherine Simpson.

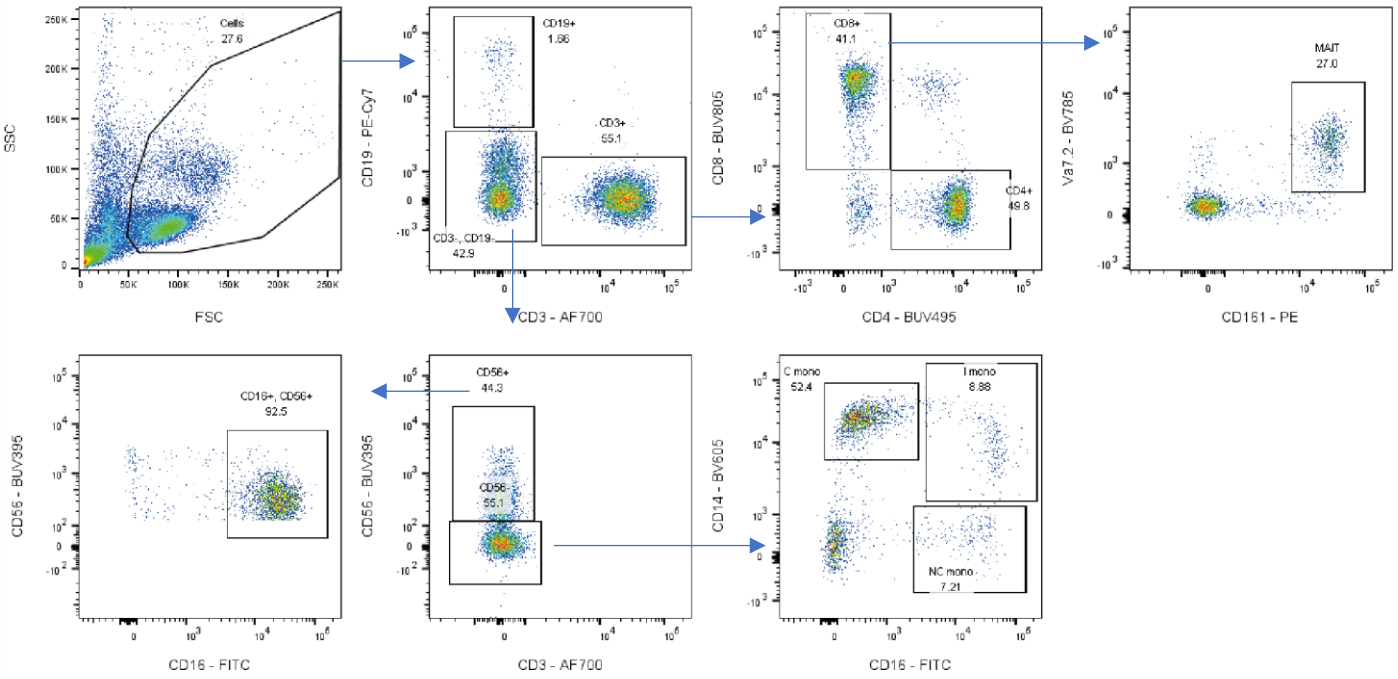


Figure 3-14 - PBMC gating strategy to identify cellular subsets

Firstly, PBMCs were selected based on their forward (FSC) and side scatter (SSC). B cells were identified using CD19 expression and T cells were identified using CD3, and further subset on their expression of CD4 and CD8. MAIT cells were discovered by expression of CD161 and Vα7.2. From the CD3-, CD19- gate, NK cells were identified using CD56 expression, then being further subset using CD16. Finally, monocytes were CD3, CD56 and CD19 negative, and further subset upon their expression of CD14 verses CD16.

3.3.3 Antibody discovery through antigen-specific B cell isolation

The field of monoclonal antibody discovery was established nearly 50 years ago, upon the publication of the hybridoma technique[237]. Although this method is still widely used today, it is relatively inefficient, and many groups have since progressed the technique to improve the process. Here, I make use of the innovative antibody platform routinely used within UCB Pharma[247].

3.3.3.1 B cell culture method of discovery from rabbit immunisations

3.3.3.1.1 Sera titre response

Two New Zealand white rabbits were immunised with Rab9 fibroblasts expressing either human or rat GPR65, each with their own immunisation strategy (Figure 3-15A), to increase chances of identifying a cross reactive antibody. Sera titre analysis showed a lack of a rat response from either rabbit; however, a mild human response was seen in both immunisation strategies (Figure 3-15B and Figure 3-15C), indicating an effective and robust immune response. Each boost of antigen was deemed successful, as the sera titre response was built upon after each bleed; this was despite the 79% sequence homology between human and rabbit extracellular domains.

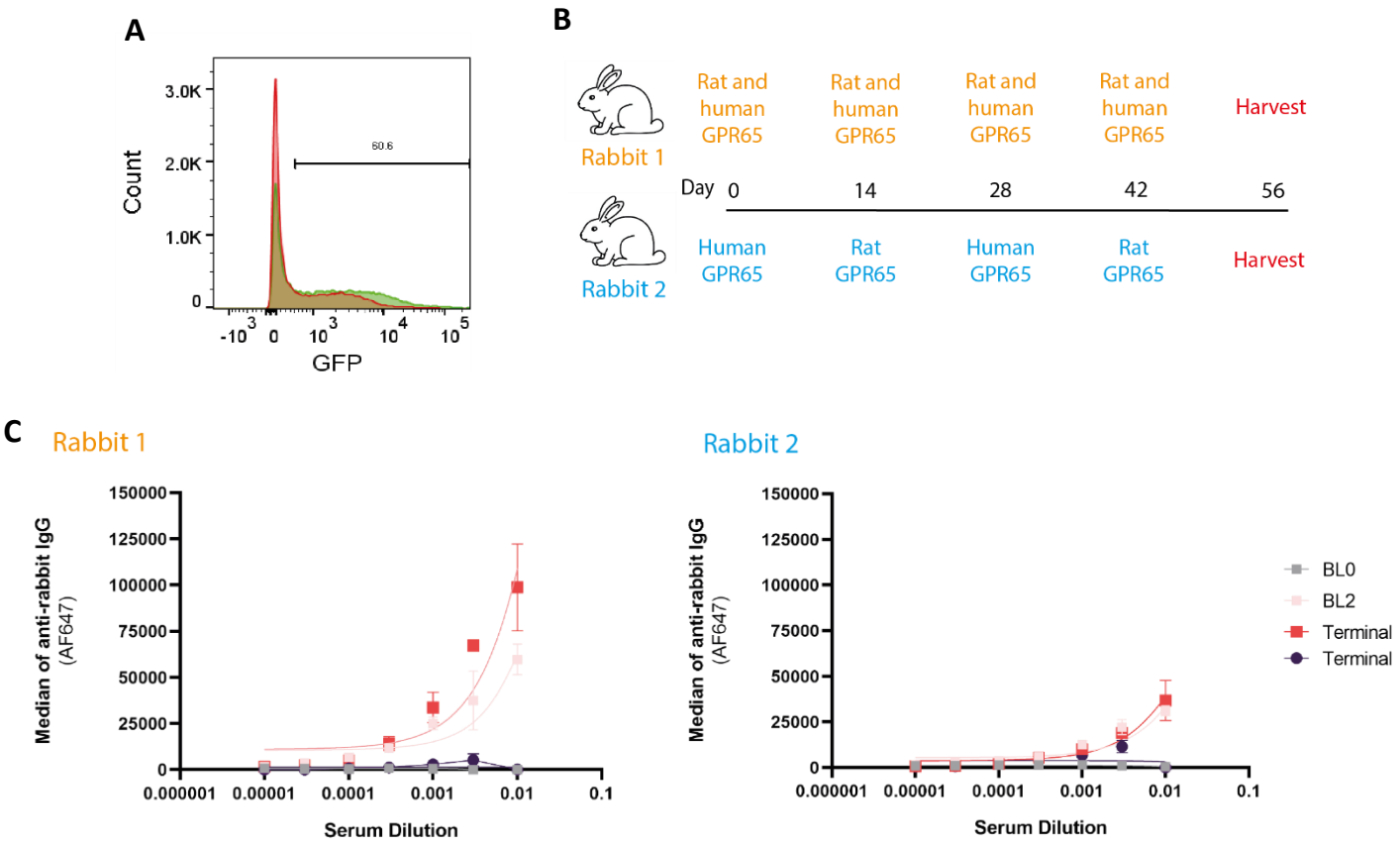


Figure 3-15 - Rabbit immunisations generated a robust immune response to human GPR65

A) GPR65 immunisation constructs representing human and rat receptor were electroporated into Rab9 fibroblasts and incubated overnight. Expression of the target was assessed by flow cytometry, prior to rabbit immunisation. Rat GPR65 expression is depicted in red, whilst human GPR65 expression is depicted in green, the corresponding expression gate can also be seen in the plot. B) Immunisation strategy for both rabbits; rabbit 1 received four doses of mixed human and rat GPR65 expressing cells, whilst rabbit 2 received four shots of cells with alternating species expression of GPR65. Animals were bled at baseline, after boost two and upon harvest of the rabbit, and sera tested for the presence of antigen-specific antibodies. Sera from all timepoints were diluted 1:100 and subsequent ½ log dilutions, down to 1:100,000. C) Diluted sera were incubated with HEK cells expressing human (pink/red) or rat (purple) GPR65, and binders detected by goat anti-rabbit IgG antibody conjugated to AF647. Fluorescence was analysed by flow cytometry, and previously gated on live HEK cells.

3.3.3.1.2 B cell culture and primary screen on HEK cells

B cells from spleen, lymph node and PBMCs were cultured for 7 days, and supernatant was screened against HEK cells expressing GPR65, in a homogenous assay (Figure 3-16). An estimated $5.5x10^7$ B cells were screened as part of the 200 x 96-well plates cultured from rabbit 1. Primary screening, where hits of y > x were filtered out, identified 278 positive wells exceeding a fluorescence threshold of > 35, which represented a hit rate of 1.4%. Criteria selection for foci picking corresponded to a GPR65 signal of > 95 and a difference of > 75, from that of WT HEK cell binding.

Of the 100 plates screened from rabbit 2, an additional 250 wells were positively identified as hits (a hit rate of 2.6%, surprisingly higher than that from rabbit 1 culture, despite having a weaker serum titre). Considering hits from the cultures of the two rabbits, the top 72 hits with the largest difference in binding GPR65-HEK cells over WT-HEK cells were progressed.

Next, the antibody variable regions from antigen-specific B cells were isolated (Figure 3-17). The fluorescent foci method identified and picked 419 single B cells. cDNA was extracted by RT-PCR and three rounds of transcriptionally active PCR (TAP) were performed, generating 375 paired heavy and light chain regions. Variable region pairs were transiently transfected into HEK cells. Analysis by ELISA confirmed the generation of 121 recombinant rabbit IgG antibodies.

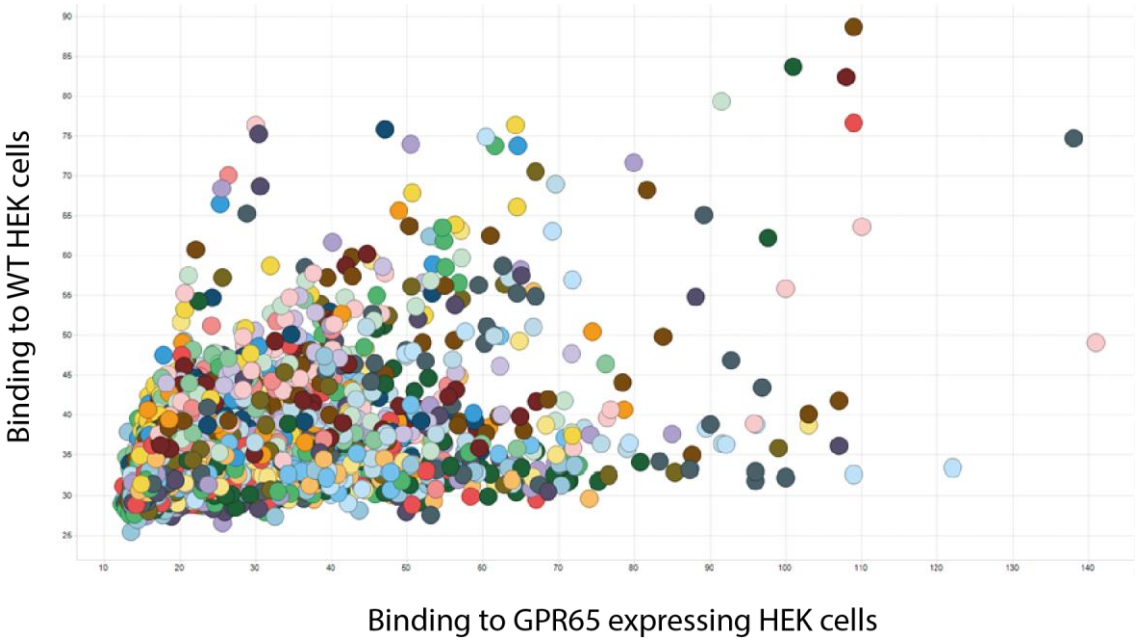


Figure 3-16 - Primary screening data of B cell culture supernatant

B cell culture supernatants were screened against WT HEK cells and human GPR65 expressing HEK cells. Secondary antibody signals, gated on each cell type, was plotted against each other to determine specificity. Each coloured dot represents data from individual assay plates analysed. Rabbit 1 data is shown here and is representative for both rabbit primary culture screens.

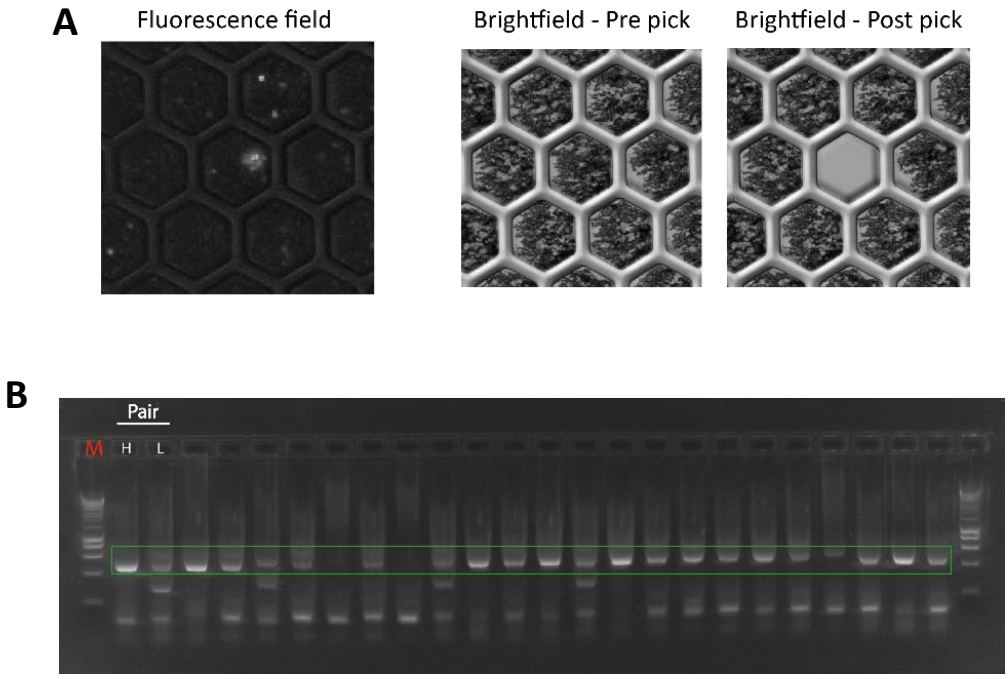


Figure 3-17 – Isolation of antigen-specific B cells and subsequent PCR confirmation

Representative example of picked foci (A), depicting a halo of fluorescence surrounding a B cell secreting antigen-specific IgG. Within the TAP process, a gel is run after the second round of PCR to confirm success (B) before committing to the final PCR step. Paired heavy and light chain V regions were run alongside each other against a marker, with expected fragments observed at ~500bp (as shown by those in the green box).

3.3.3.1.3 Characterisation of GPR65 specific rabbit-derived antibodies

3.3.3.1.3.1 Antibodies screened on HEK cells expressing GPR65

For initial characterisation, the antibodies were screened for their ability to bind native human receptor. TAP antibody-containing supernatants were incubated with HEK cells expressing GPR65, to confirm the antibodies were able to recognise what they were raised against and provide confidence that the correct B cells were isolated and sequenced. Flow cytometry results suggested that ~60% bound GPR65^{+} HEK cells, over that of mock HEK cell binding (HEK cells transfected with an irrelevant membrane protein). To capture low affinity binders, and normalise supernatant to expression, geometric means of binding were plotted against IgG expression. At an OD of 2, anything > 20 binding in flow cytometry was deemed reasonable and provided the marker for where to place the overlaid grey line, which gave 24 hits of interest (Figure 3-18). Taking it one step further, the top 10 antibodies were identified (those above the green line).

Through the process of cloning, transformation and DNA preparation, sequences were identified. After numerous attempts, 7 were unsuccessfully sequenced, whilst the remaining 17 hits gave rise to 37 different V_H and V_L pairings. These pairs were then transiently transfected into HEK cells for monoclonal antibody expression.

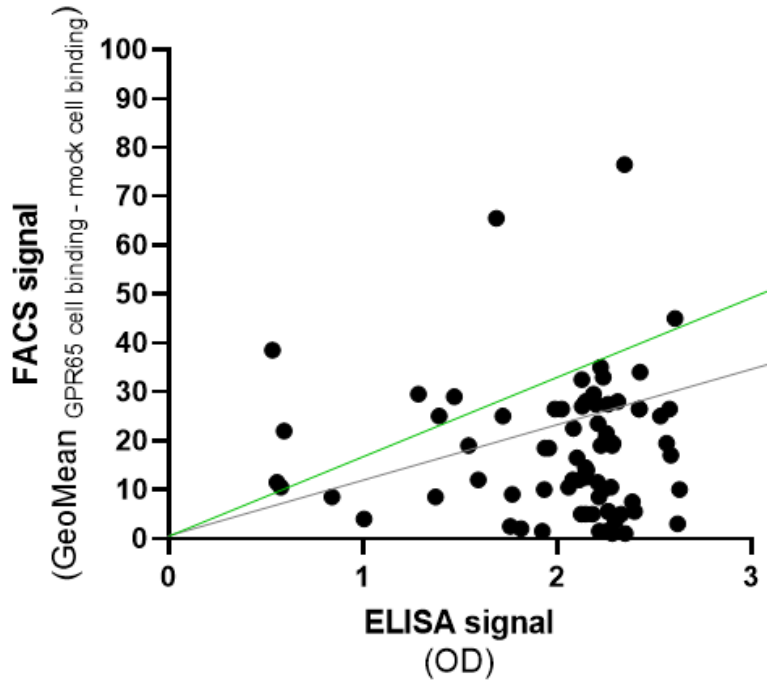


Figure 3-18 - TAP supernatant binding on HEK cells expressing GPR65

TAP supernatant was incubated with HEK cells expressing GPR65 and binding was assessed by flow cytometry. Geometric mean values of a secondary antibody control were subtracted from all signals before mock binding was further subtracted from corresponding GPR65 binding signals. These values were then plotted against their relevant expression from an assembly IgG ELISA. Hits above the grey line were followed up, with highest confidence in those hits above the green line.

Having undergone significant processing, it was important the sequenced monoclonal antibodies were again assessed on their ability to bind to the native receptor. Considering the function of GPR65 and its associated confirmational change, it was also beneficial to factor in the effect of pH upon the antibodies ability to bind GPR65. At neutral pH two antibodies, termed Ab1A and Ab23, specifically recognised a small percentage of GPR65 positive HEK cells (Figure 3-19). Remarkably, not only did the two still bind when incubated at the lower pH (pH 6.5, chosen due to it being the optimal pH for GPR65 activation), antibody Ab21C also bound, again only to a small percentage of GPR65 positive HEK cells, and was perhaps suggestive of recognising an epitope with conformational advantage. It is of note these three hit antibodies were identified within the 'Top 10' hits, whilst all other antibodies assessed did not show any binding, as represented by Ab21B.

A picture was building for these antibodies recognising human GPR65. But to develop our understanding for a potential role in probing GPR65 biology, their cross-reactivity to rat GPR65 and other proton-sensing family members was investigated. Unfortunately, no binding to rat GPR65 was seen, however Ab23 appeared to bind to GPR68, the closest family member to GPR65 (data not shown).

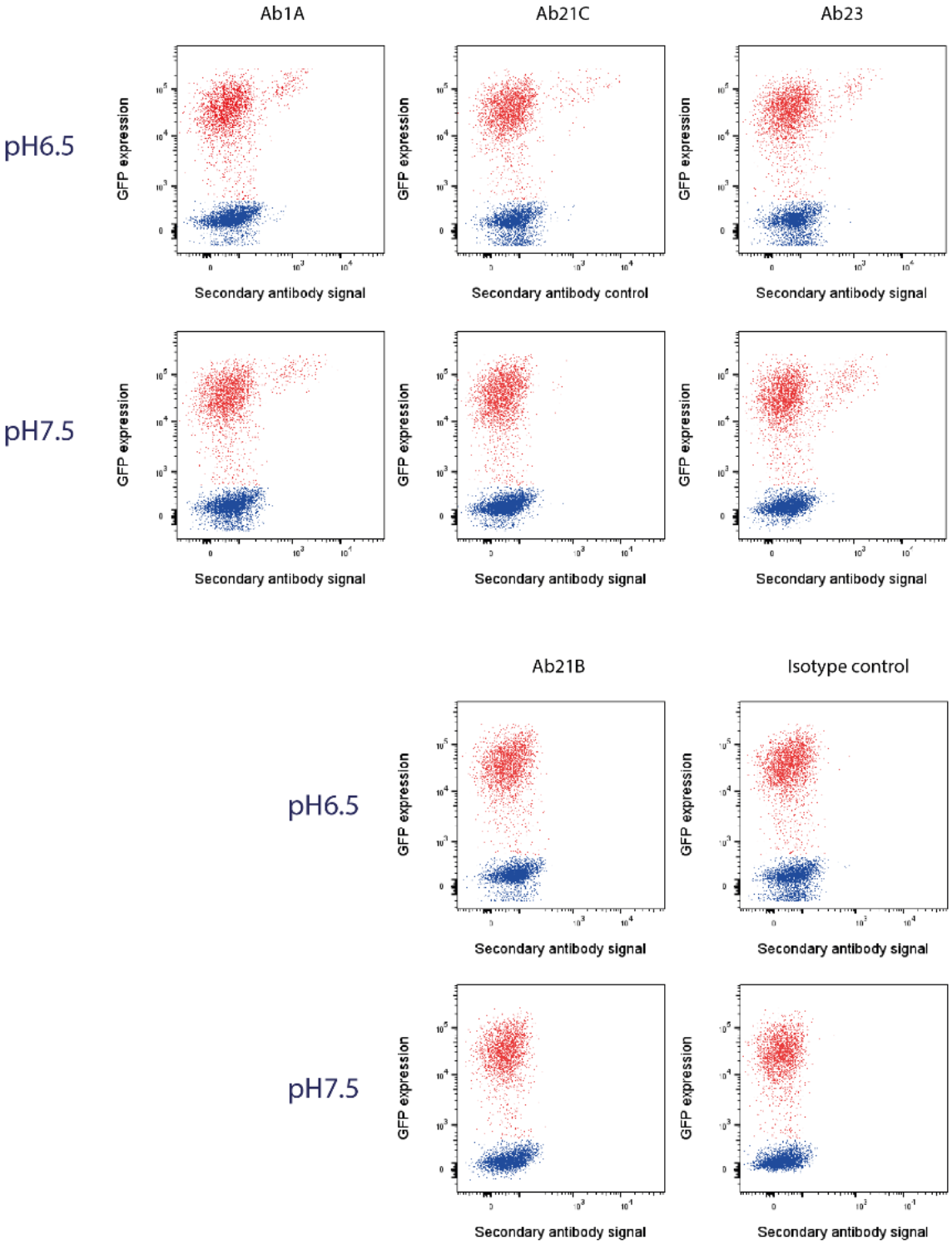


Figure 3-19 – Rabbit-derived antibodies recognise human GPR65 expressed on HEK cells

Antibody-containing supernatant was incubated with HEK cells -/+ GPR65, at either pH 6.5 or pH 7.5, with binders detected by goat anti-rabbit anti-IgG at neutral pH. Fluorescence was analysed by flow cytometry and the cells were previously gated as viable and separated on their expression of GFP (blue = $GPR65^-$ HEK cells, red = $GPR65^+$ HEK cells). Data shown is representative of four experiments.

3.3.3.1.3.2 Antibodies screened on primary immune cells endogenously expressing GPR65

Although HEK cells were ideal for initial high throughput TAP screening, they rely on transient transfection of this complex receptor, and include caveats of doing so. It was worrying only a small subset of GPR65-HEK cells were recognised by the antibodies, rather than an expected full right shift of binding. Therefore, the 37 rabbit-derived antibodies were further assessed for their ability to bind primary cell subsets. As stated in section 3.3.2.3, MAIT cells are thought to express the highest levels of messenger RNA for GPR65, however extracellular binding was not observed to these cells of interest from any of the antibodies tested, including those that bound GPR65 expressed on HEK cells, or to any of the other cell types identified (Figure 3-20).

The antibodies discovered and thought to recognise GPR65 on HEK cells did not translate to primary cell binding. Therefore, it posed the question as to whether the results from the HEK based screens were misleading. Knowledge gained throughout the project allowed for an informed view on what would perhaps have been a useful control for screening. Thus, an additional GPR65 construct was designed with extracellular loops substituted for G_4S sequences, rendering the structure of the protein to be as unchanged as possible, but for the ECLs to be unrecognisable. No binding was observed from any of the antibodies incubated with these control GPR65 mutant HEK cells (data not shown), strongly supporting the original HEK cell data. So, it speaks to the theory that GPR65 overexpression on HEK cells was not mimicking the conformation the receptor has in its most natural form, endogenously expressed on immune cells.

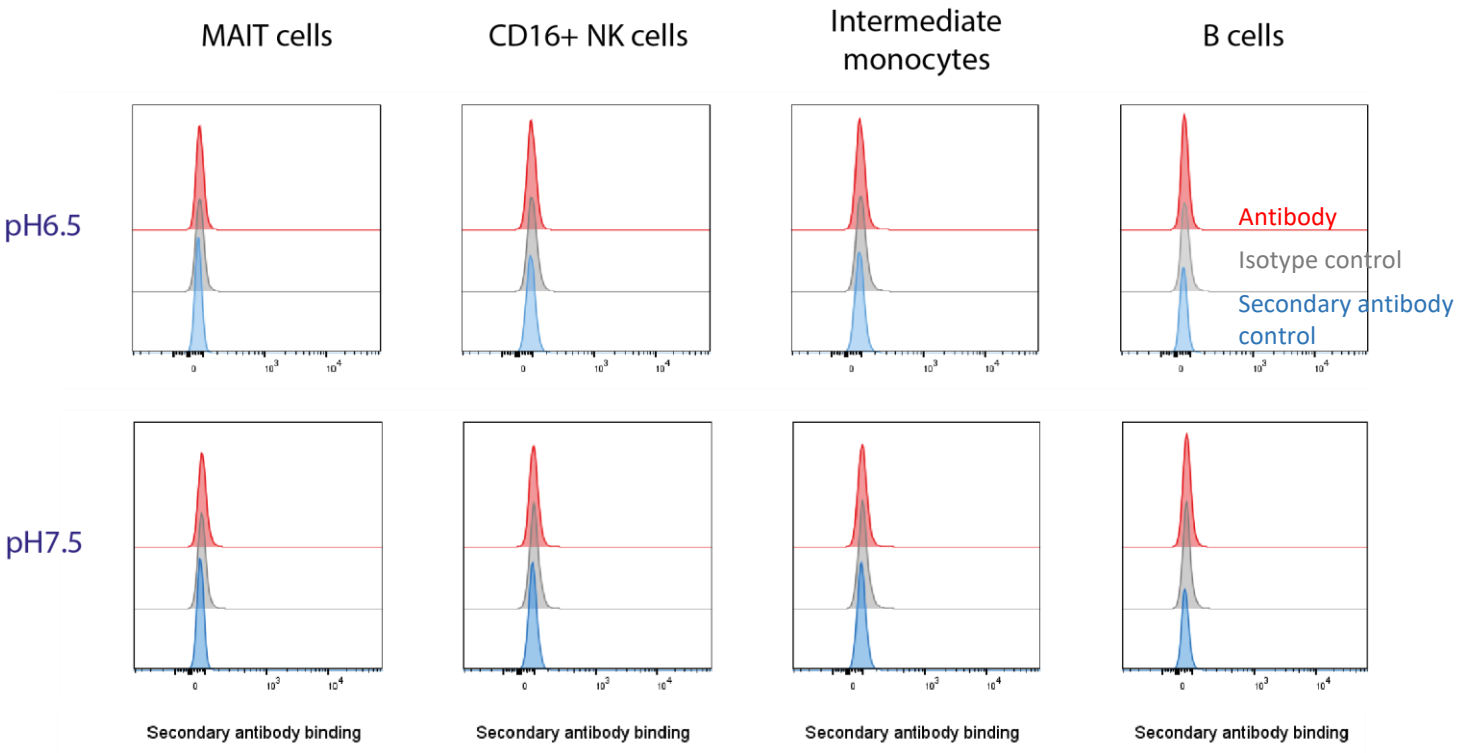


Figure 3-20 – Rabbit-derived antibodies did not bind GPR65 when endogenously expressed on MAIT cells

PBMCs were isolated from healthy controls (n=2), treated with Fc block for 10 minutes, then neat antibody-containing supernatant was incubated with the cells for 1 hour. Live cell subsets were identified according to their phenotype, before goat anti-rabbit IgG binding was assessed by flow cytometry. Rabbit-derived antibody binding is depicted in red, with the secondary antibody control depicted in blue, and the isotype control reflected in grey. Ab23 is the example shown on one donor, and is representative of all the antibodies tested, and both donors.

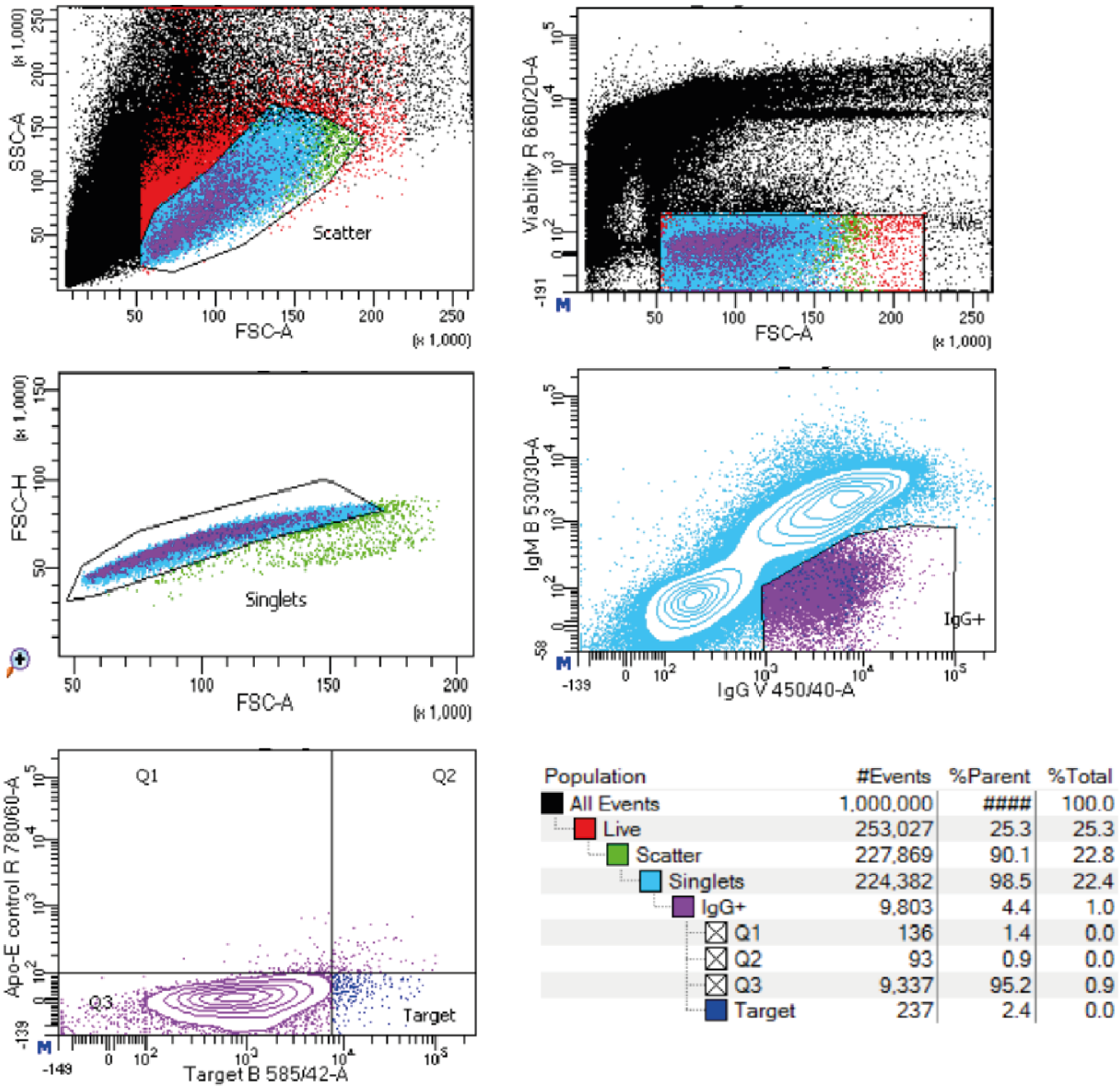
3.3.3.2 Antigen-specific V region identification through single cell technologies

Although the UCB defined B cell culturing platform covers a wide range of the B cell repertoire, due to its very high throughput nature, there is always the risk of missing that all important antigen-specific antibody in downstream molecular biological processes. Developments in alternative technologies have recently enabled antibody discovery through single cell sequencing, capturing all V regions associated with isolated antigen-specific cells.

Here, > 25,000 individual IgG^{pos} B cells from spleens and lymph nodes of both immunised rabbits were analysed (Figure 3-21), using the 10x Genomics workflow of emulsion-based encapsulation, cDNA generation and sequencing (Figure 3-22). Downstream bioinformatic analysis[h] discovered 163 clones, of which 54 were unique heavy and light chain pairings (Table 7); with 98% of those successfully expressed as full-length IgG.

As an initial check, the successfully expressed antibodies were assessed on their ability to recognise the ApoE3 chimeric constructs they were identified as binding. Unexpectedly, only one weak signal was obtained for binding by ELISA (data not shown), therefore it didn't suggest success from this approach. Despite this, final confirmation of their recognition of natural GPR65 expressed on primary cells was undertaken; unsurprisingly, the antibodies did not show convincing binding of any of the PBMC subsets of interest (Figure 3-23). At the time, this technology was being established within UCB, and recovery of the appropriate sequences was probably suboptimal due to technical teething issues. Nevertheless, the approach is immensely powerful and could be used in future to recover very rare antibodies to GPR65.

[h] Performed by James Snowden.



Population	#Events	%Parent	%Total
All Events	1,000,000	####	100.0
Live	253,027	25.3	25.3
Scatter	227,869	90.1	22.8
Singlets	224,382	98.5	22.4
IgG+	9,803	4.4	1.0
Q1	136	1.4	0.0
Q2	93	0.9	0.0
Q3	9,337	95.2	0.9
Target	237	2.4	0.0

Figure 3-21 - Flow cytometry sort strategy to isolate antigen-binding B cells for single cell sequencing

B cells from either the spleen or lymph nodes from rabbit 1 (a representation of both rabbits 1 and 2) were incubated with the three ApoE chimeric constructs presenting the extracellular loops of GPR65, labelled with streptavidin tetramers, for 30 minutes, along with anti-IgM and anti-IgG antibodies. Cells of interest were sorted[i] as live, single cells binding IgG and not IgM, which bound Target B only (pooled chimeric ApoE constructs), and not binding to the WT ApoE control.

[i] Sort performed by Catherine Simpson.

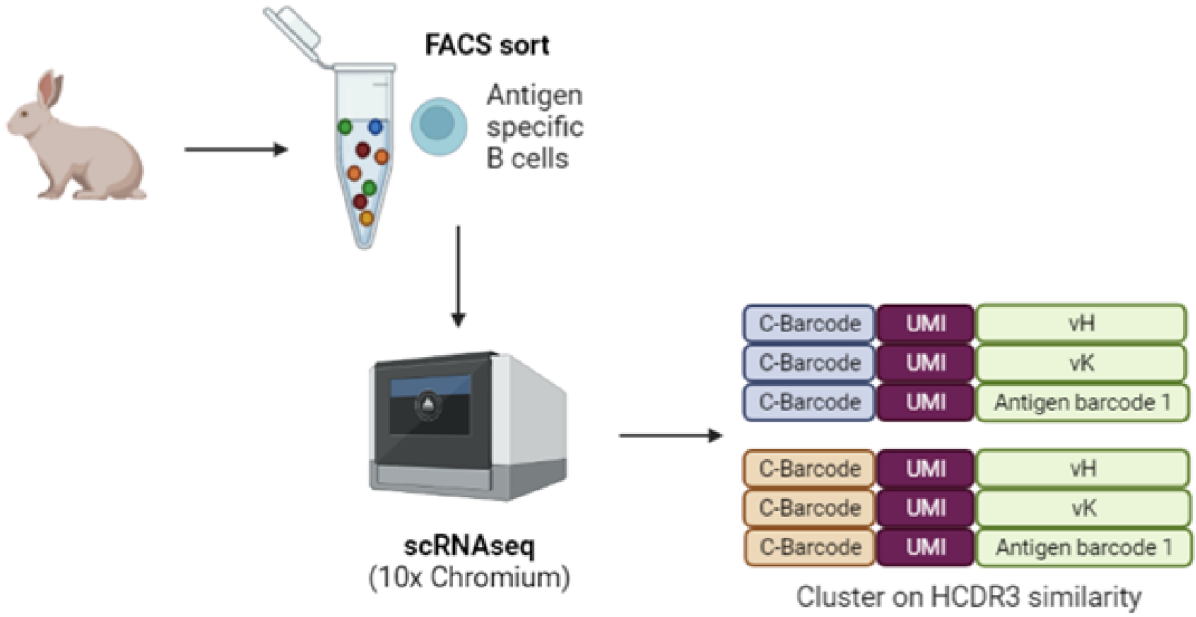


Figure 3-22 – Experimental design of single cell RNA sequencing of antigen-specific B cells

Upon their binding profiles to the ApoE3 constructs, antigen-specific B cells were isolated from lymph nodes and spleen of rabbits immunised with GPR65-Rab9's, by FACS sorting. These cells V-regions were identified using the 10x Genomics workflow and Illumina sequencing, and clustered together based on their similarities within the heavy chain CDR3 region. Diagram created with Biorender.

Sort	V_H	V_L	Paired	Clones	Families
1	864	240	67	58	3
2	3294	557	163	105	15

Table 7 – Bioinformatic output of GPR65-specific B cells, identified using the 10x platform[j]

Using the CDR3 framework, V_H and V_L sequences were identified for single B cells and clustered based on > 80% similarity and size. Alignment of the sequences highlighted either repeats, or unique pairings of antibodies to be expressed.

[j] Bioinformatic analysis of 10x output was performed by James Snowdon.

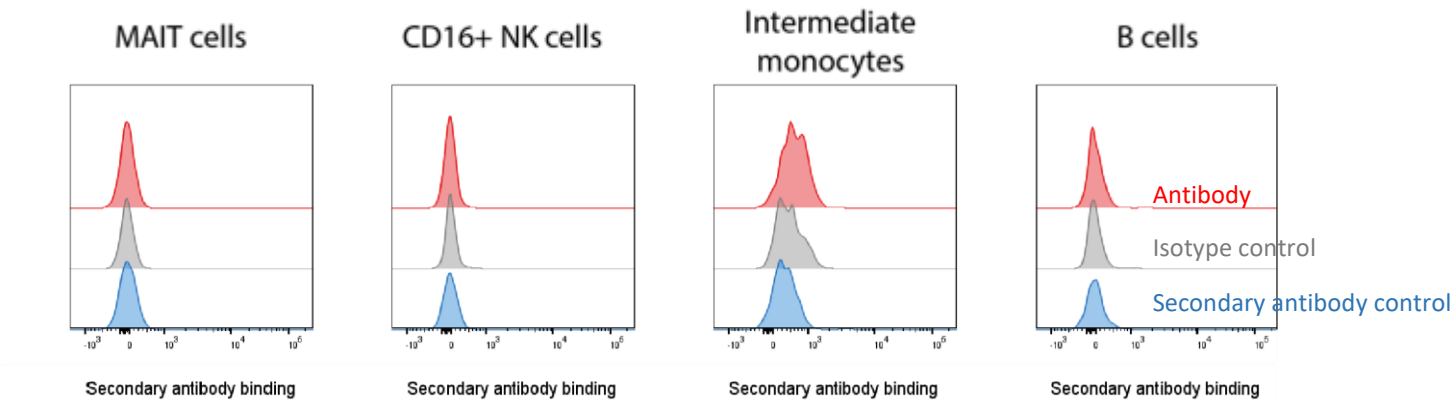


Figure 3-23 – 10x derived antibodies did not bind GPR65 on PBMC subsets

Monoclonal IgG expressed antibodies in supernatant were incubated with Fc-blocked healthy control PBMCs (n=2), and binding detected by goat anti-rabbit IgG antibody. Fluorescence was analysed by flow cytometry, previously gated on live cells, and PBMC subtypes identified by their expression of known phenotypic markers. Antibody binding is depicted in red, with the secondary antibody control depicted in blue, and the isotype control reflected in grey. C6, the antibody that showed weak signal in the ApoE3 ELISA, is the example shown and is representative of the antibodies tested, and binding profiles to both donors.

3.4 Discussion

With the aim to quantify GPR65 at the protein level, and uncover its expression characteristics and true cellular localisation, I set out to discover a GPR65 binding antibody. This proved to be an immensely challenging undertaking, with only one antibody potentially recognising endogenously expressed GPR65 on primary cells.

There is currently no gold standard for antibody generation to any given target, with a broad variety of strategies used in campaigns, to leverage upon each of their advantages and disadvantages. Antibodies derived from antigen-specific B cells are popular starting points for many discovery strategies, as they have already undergone affinity maturation, have a high specificity and provide low immunogenicity, important factors when raised for therapeutic use. Rather, alternative display technologies offer the screening of large libraries covering up to 10^9 V(D)J combinations, compared to the circulating average 10^7 in humans, improving the chance of isolating rare antibodies.

Throughout the antibody discovery process, it is favourable to be in possession of high-quality protein reagents, such as for use in, immunisations, functional assays, and structural biology. However, commercially available recombinant protein did not exist for GPR65 at the time of starting this project, speaking to the difficult nature of identifying membrane protein structures. Advances in both science and technology over the past couple of decades have improved the field, but there remains a vast quantity of structures for this family of receptors yet to be identified[258], including the structure of GPR65. Understanding structure, would not only provide insights into mechanisms of function, but also importantly provide a basis for drug design.

Expression of membrane proteins is notoriously difficult and there have been many expression systems developed, each with their own advantages and disadvantages of use. *E.coli*, yeast and insect expression systems are popular options for recombinant protein expression; particularly is the case for insect cells, as they yield large amounts of high quality protein. However, they lack phosphatidyl serine in their plasma membrane, making them redundant for a membrane protein expression system. Although mammalian expression systems are comparatively expensive and likely to achieve lower yields, it was favourable for this project as they possess the required cellular machinery to correctly translate and process GPCRs post translational modifications (PTM), such as glycosylation, which plays a role in ensuring correctly folded protein gets trafficked to the cell membrane. Although I had optimised temperature, cell density and DNA concentration, in hindsight, it would have been good to also test a high pH condition to see whether a total lack of activation of the receptor would have improved expression efficiency.

As a membrane protein, with an unidentified complex structure, difficulties extracting/solubilising this GPCR from its native lipid membrane environment came as no surprise. Without trial, error and laborious optimisation of buffer properties (ie pH and salt concentration) and conditions, initially the method of purification for this difficult protein was unknown. Starting with the four most used detergents for membrane proteins, DDM was identified as the best of those tested. However, it still did not perform as well as required. These detergents use their amphiphilic nature to partition the lipid bilayer and extract the hydrophobic membrane protein, whilst remaining soluble in solution. However, it is understood even within these processes, they may trap the receptor in an undesirable

conformation or drop required unique lipids for stability and/or activity and reduce lateral pressure important for receptor confirmation[259,260].

The use of styrene-maleic acid copolymers (SMAs) and virus-like particles (VLPs) offer an advantage over these common detergents by keeping the original neighbouring lipids of the cell membrane intact with the protein, offering structural integrity and stability. SMAs generate stable nanodisc particles, but due to their small nature they are not a suitable option for large proteins and are pH sensitive when used at the most ideal styrene-to-maleic acid ratio of 2:1, precipitating at < pH 6[261]. Alternatively, VLPs take advantage of the GAG (group-specific antigen) polyprotein to bud sections of the cell membrane into lipovesicles enriched with the target of interest[262,263]. By maintaining the membrane architecture, GPCRs in this setting would likely be correctly folded and remain functionally active. Preliminary experiments to generate GPR65 VLPs were carried out, with the thought of using them as a potential source of antigen in a phage display campaign. However, there was limited success of detecting surface protein and as lots of other work was ongoing in parallel, there was unfortunately not enough time to optimise and continue investigating this method.

It is worth mentioning, personal communication found GPR65 to be highly unstable in three different detergents tested (DDM, LMNG and Glyco-diosgenin (GDN)); with a suggested Tm between 20-30 °C. In addition to this, two point mutations were introduced following the report of improved expression profiles in GPR65[264]. A 2-fold increase of expression and subsequent improved solubilisation with the favoured DDM/CHS detergent setting was observed, compared to the WT. Moreover, with the aim to lock a structural conformation and prevent receptor instability, the addition of a GPR65 ligand did not improve expression, compared to a DMSO control. These struggles, paired with GPR65 expression behaviours,

speak to a very challenging protein to work with. Given the difficulties with protein expression and presentation, it was decided to use cell expressed GPR65 as an antigen source.

For over 35 years[265] phage display has offered an alternative approach to the identification of discovering rare antibodies against challenging antigens, within a relatively quick period, ~2 months[266,267]. This technology can screen large naïve and/or immune phage display libraries, comprised of variable regions, displayed on the surface of filamentous phage particles, which represent the whole B cell repertoire from which the cDNA was derived. Multiple rounds of immobilised antigen and phage library incubations give rise to an enriched population of target specific antibodies.

For the optimal success of phage antibody discovery, the antigen being presented needs to be as close to its native conformation as possible. Although recombinant protein provides the highest success from display technologies, screening against whole cells expressing the target is an alternative solution, particularly for GPCRs, as native conformation is presented. However, this approach also has its own limitations. Low abundance of membrane protein expressed on cells, coupled with a high background of other proteins displayed on the surface of a cell do not create the best environment for identifying target specific binders, particularly here where small extracellular domains are the site of interest. Moreover, phage particles are notoriously sticky and have been known to be internalised by cell membrane receptors[266], shrinking the library being screened. Thus, a novel take on antigen presentation was used within my phage campaign.

Although a structural model of GPR65 is unknown, due to its seven-transmembrane feature, the extracellular loops will likely exit from and enter back into alpha helices. Interestingly, work carried out in the vaccine field suggested that substituting structures of interest onto

protein scaffolds can elicit an immune response to the antigen[257]. With this concept in mind, constructs were designed with human GPR65 ECL substituted into a soluble 4 α-helix bundle scaffolds, to mimic the membrane protein ECL leaving and entering the helix on each side. Additional constructs were also designed to incorporate several amino acids of the helices that lead into and away from the loop from the GPR65 sequence, to see whether it would provide a closer structure of the loops, to the WT GPR65 protein. While the substituted, loop only, chimeric constructs were well tolerated and provided soluble protein to work with, the lack of solubility of those where amino acids of the backbones were replaced with GPR65 residues, suggested an alteration to the structure of the scaffold, possibly causing the proteins to misfold and aggregate into inclusion bodies. Although further LCMS analysis of the soluble chimeric proteins identified half to be correctly biotinylated, peaks with an additional 178 Da was present were observed; this was believed to be a PTM of the His-tag (α-N-Gluconoylation) incorporated into the protein[268] and considered to be unimportant for using these proteins as antigen.

With caveats known at the planning stage of panning design, some key decisions were made to gain the most success from this novel campaign. The three constructs representing each GPR65 ECL were pooled for screening efficiency (despite the risk for progressing antibodies dominant for one construct), and only 3 rounds of panning were performed to prevent nonspecific binders from overriding. The multiple rounds of screening allowed for subtraction through enrichment, minimising attrition at later stages. Binders to the ApoE3 backbone were removed, encouraging only those recognising the substituted loops of interest to become enriched. Finally, as peptides were acting as the antigen, the concentration of the constructs remained high throughout all the rounds. Despite these considerations, output titres after

each panning round were not suggestive of optimal enrichment; perhaps due to the epitopes being too small. Usually, antigen concentration is dropped after each round to encourage enrichment of binders, hence the maintenance of the high concentration here could offer an alternative explanation.

The phage display campaign was a success, with 17 antibodies discovered to bind what they were panned against. As three phage-derived antibodies bound GPR65 on HEK cells, excitement and confidence were provided for the use of scaffold proteins to display antigen and elicit a response to identify native antigen-specific binders.

Although mRNA expression does not always correlate to protein expression, due to posttranscriptional processing and regulation[269], the total lack of phage-derived antibody binding to MAIT cells came as a surprise. At the time of writing there are no reports of GPR65 protein being expressed on MAIT cells, and the binding seen in the current study, to intermediate monocytes in particular, could be credible. But with such small shifts of binding to GPR65, together with unexpected expression profiles, it was decided this antibody would not be a useful tool moving forwards.

At the beginning of this project, it was important to consider where future directions may head, even so far as the confirmation of GPR65 function in an animal model of disease. The HLA-B27 transgenic rat model is well defined and widely accepted as the most relevant ankylosing spondylitis model[94]. Therefore, it was important to consider and design immunisation strategies, to identify rat cross reactive antibodies.

Upon the immunisation of two rabbits, a moderate response to human GPR65 was observed and plausible for this form of antigen, as well as suggesting that the HEK cells were reasonably expressing GPR65. In the case of rabbit 1, who received 4 shots of human and rat GPR65

expressing cells, a particularly good response was shown, nevertheless an immune response to the rat receptor was not generated by either rabbit. Rab9 fibroblast transfections were highly efficient for both species and provided a suitable host cell displaying the receptor from both species, thereby directing the immune response to the transfected protein. As most of the sequence homology between the three species lies within the transmembrane and intracellular regions of the receptor, the difference in response between the two species was hard to explain. Also, without antibodies to test, it was unknown which of the immunisation strategies were favoured for cross reactive output.

The hit rate from this study was within the expected range of 1-5%. Over 500 antigen-specific hits were identified from the primary B cell supernatant cell-based screen. Due to time and resource, only those with the highest levels of binding GPR65 expressing cells, compared to WT HEK cells, were taken forward to pick GPR65-specific IgG secreting B cells. Although a manual method of foci picking has been published[247], I had the opportunity to pioneer a new technology for automated picking, using microfluidic technologies. As foci picking is usually associated with bead-coupled antigen, I had a further challenge with cell-based screening. Although fluorescence was observed, true antigen 'halos' surrounding individual B cells were difficult to identify, and so anything resembling fluorescence was picked. Therefore, influenced by a learning phase of new technology, recovery of paired variable fragments was lower than expected. Antibody generation using this method is optimal when the antigen is a recombinant soluble protein. Upon isolating the cDNA from antigen-specific IgG producing B cells, heavy and light chain variable regions were recovered through established RT-PCR techniques[247], retaining the natural, cognate pairings of > 100 antibodies. Considering this was a cell-based antibody campaign, particularly against a GPCR membrane receptor,

outcomes here were deemed a success and attrition rates were in line with what would be expected.

The initial binding screen needed to be somewhat high throughput, hence the use of transiently transfected HEK cells, together with flow cytometry read outs. Upon incubation with GPR65-HEK cells, less than half the antibodies appeared to bind and were progressed for sequencing. Confidence in antigen-specificity is gained when strong similarities are identified between the sequences of the CDR3 regions. However, little convergence was observed in the sequences identified and spoke to the high attrition at this stage.

It has been observed that extracellular loops of GPCRs are able to self-agonise and cause activation, through movement and conformation changes[270]. GPCR extracellular loops continually sample[271], reaching a natural established equilibrium. As loop movement often relates to function, it was thought that incubating these antibodies with GPR65-HEK cells at an activatory pH may allow the loops to adopt a different state, which some antibodies may recognise and bind. Considering the incubation of culturing antibodies with GPR65-HEK cells at two pH's, 3 of 121 (2.5% hit rate) were thought to bind the antigen they were raised to recognise. Nonetheless the antibodies did not produce the most convincing binding profiles. Within flow cytometry analysis, if a strong antibody bound its target, a full right shift of the population would be observed. Instead, only a weak peppering of signal was seen, which could suggest there were too few receptors either expressed, or in the optimal conformation for binding therefore, not enough to sample and be picked up by the technique being used.

As previously discussed, the biggest test for these apparent GPR65-specific antibodies came in the form of their ability to bind primary immune cells. Unfortunately, rabbit-derived antibodies were unable to recognise the most natural form of the receptor in an immune

setting, alluding to the disconnect of epitope display between transfected overexpression and the natural display of GPR65.

Next generation sequencing approaches have been reported to identify paired heavy and light chains. Here, I've used single cell RNA sequencing to identify full length, paired V regions within a single B cell, combined with barcodes to deconvolute where the cell in question was derived from. The 10x Chromium workflow has revolutionised the understanding of gene expression profiles in a host of diseases and applications, but its use within antibody discovery is relatively new[272].

The ability for phage-derived loop binders being raised against constructs, recognising native receptor, provided confidence for the use of these chimeras to act as relevant antigen. Hence, these proteins were also used as surrogate loop expressors for screening of rabbit-derived antibody binding. Isolation of antigen-specific B cells by flow cytometry has been optimised over the years[273–275], yet a lot of this work had been restricted to humans, due to established methods for FACS sorting. Unfortunately, there was no way of enriching rabbit B cells, or a general marker to help identify them by flow cytometry. By adapting a workflow reported by Starkie *et al*[276] a pool of single antigen-specific rabbit B cells were identified as live, binding antigen (pooled GPR65 ECL ApoE3 constructs) and expressing IgG; including markers for staining on unwanted IgM^+ cells. In reflection, an additional 'dump gate' could have been included to capture cells with unwanted lymphocyte subset markers, to potentially avoid antigen-capturing cells being falsely pulled through[277].

A complication presented itself in the form of species-specific primers for sequencing during the 10x Chromium workflow. Although validated human and mouse primer sets were commercially available, custom rabbit primers needed to be designed. Indeed, during the

inhouse pioneering of this technology, it was possible that primer design was not well established and may be responsible for the low recovery rate. Despite suggested enrichment and similar epitopes being targeted, upon the presence of 18 families from 230 V-region pairs, the antibodies expressed were unable to bind anything of promise. It was disappointing this approach to antibody discovery was unsuccessful in my hands, most likely due to technical failures. Since performing these experiments, UCB have developed and optimised the methods, as well as using an alternative sequencing supplier; if I were to have more time, I would repeat using this revised workflow, as my confidence in this technology remains.

Despite the discovery of antibodies to the antigen targets from both campaigns, their lack of significant binding to GPR65 expressed on immune cells raised the question of how representative receptor expression was on cell lines. Even with the presence of a natural leader sequence and the surrogate markers suggesting extracellular expression of the protein, I have no way of accurately finding out if my target was expressed on the surface, with subtle epitopes in the correct conformation, and to what level. When considering the use of the strong cytomegalovirus promoter within the vector of the construct, and the concentration of DNA transfected (although initially titrated and optimised based on GFP-surrogate marker expression and viability), it is possible the cells may be overwhelmed for such a complex protein to be displayed in a natural conformation. Further, if the RNA and protein levels are not representative of each other, it likely speaks to something about the biology of receptor we are not currently aware of.

Overall, the data raises questions about whether epitope presentation is different between the overexpressed receptor on cell lines, verses endogenous expression on an immune cell. Some thoughts as to why are:

- Are the binding profiles of the antibodies generated in this study pointing towards temporal epitope occlusion due to differences in conformational sampling of GPR65?
- Is GPR65 part of a bigger complex, and we aren't currently aware of key interacting proteins?
- Do the loops cooperate with each other differently when associated with other nearby membrane proteins that we are currently not aware interact with the receptor?
- Is the size of an antibody's footprint too big to fit onto its epitope in all conformations of the protein?

If the last point is true, the recently identified peptide like bovine knob domains could provide improved success for the targeting of complex GPCRs. Their very small and rigid nature, due to extensive disulphide bonding, provide similar properties to chemical matter, which historically are more successful GPCR targets[244]. These affinity matured peptides, in theory, could access 'hidden' epitope sites, only accessible upon conformational sampling of the receptor, or upon the presence of structural changes in an activatory pH environment.

I knew this aim of my project would be very challenging, with history teaching us that GPCRs are notoriously difficult to raise antibodies to, not only due to a lack of structural knowledge and protein isolation as previously mentioned, but also explained through the limited size of the extracellular loops and their ability to conformationally sample different shapes[278–280]. Developments in genetic immunisation have responded to the need for innovation for complex antibody discovery. The methods offer an attractive alternative as the host expresses, folds and presents a membrane protein within its own native environment and without potential target disruption upon cell handling after transfection[281]. Thus, offering improved quality, quantity, and exposure of the protein of interest to the host immune

system, also giving potential to identify a functional antibody[280]. The two approaches, DNA and mRNA immunisations, also eliminate the need for multiple cell lines per species immunised, removal of the ethically questionable adjuvant delivery required for cell immunisations and reduce background immune responses observed from traditional methods. Whilst DNA immunisations have successfully raised monoclonal antibodies[282], they require a specific tool in the form of a 'gene gun' for delivery, therefore favour the lab environment, reducing efforts in cows and llamas (species expressing unique antibody fragments which may be advantageous). The COVID era has propelled the use of mRNA immunisations, with powerful pre-clinical and clinical data providing confidence that the method mounts an immune response safely[283–286]. When mRNA is encapsulated in a liponanoparticle, draining lymph nodes and local immune cells take up the nucleic acid material and improve on DNA based immunisations, as higher copies of target are produced on more relevant cells[287–289]. It will be interesting to see how this new technology may be advantageously applied to the discovery of antibodies to GPCRs in future.

Despite the many efforts and novel approaches tried, I was not successful in identifying a reliable monoclonal antibody to this notorious target; and so, without a tool reagent, further investigation into the role of GPR65 in immune cell function was achieved by alternative means (detailed in Chapter 5).

Chapter 4 : Investigating the role of acidic pH on immune function

4.1 Introduction

The concentration of extracellular hydrogen ions (pH) varies throughout the body in health, with some bodily fluids and tissues presenting controlled acidic or alkaline environments to maintain their function. For example, gastric acid is < pH 3.5 to aid with digestion[290], whilst circulating blood pH is highly regulated, ranging between pH 7.35-7.45[291]. However, this fine balance can be disrupted and mark a sign of disease, with extracellular space being shown to become acidic at sites of inflammation and within solid tumours[292–294].

Due to the protective nature of the immune system, related cells are equipped to recognise changes to extracellular pH and display multiple types of receptors that are sensitive to acidosis. One mechanism is through ion channels, such as acid sensing ion channels (ASICs) and transient receptor potential channel vanilloid subfamily 1 (TRPV1), whilst the other mechanism is represented by proton sensing GPCRs.

ASICs are proton-gated channels, permeable to Na+, and are primarily expressed in immune cells of the central and peripheral nervous systems. In response to low pH, they have been shown to play a role in pain perception and synaptic plasticity[295,296]. TRPV1 is also expressed on cells of the nervous system and usually studied for its role in pain sensing. It can become activated upon sensing low pH and has been reported to directly affect T cell immune responses[297,298].

Proton sensing GPCRs have all been shown to influence inflammation. An increase of GPR68-dependent IL-8 was observed from pancreatic β-cells at low pH[299], whilst activation of GPR4 expressed on endothelial cells induced the NF-κB pathway and subsequently increased the expression of inflammatory genes[300]. GPR65 has been introduced in section 1.2.2, and it

seemed reasonable to hypothesise that an acidic stimulus plays a role in GPR65 biology, in turn affecting lymphocyte function.

4.2 Aim

The aim of this chapter was to discover the effects of extracellular pH changes, particularly slightly acidic environments, on immune cell function. Here, I discuss the experiments carried out to characterise cytokine release from immune cells and support the findings with transcriptional changes responsible.

4.3 Results

4.3.1 Investigating the impact of pH on PBMC subsets

I broadly started by addressing the question of the functional effects of pH on the immune response using mixed PBMC subsets, to not bias results of cell types hypothesised to recognise changes in extracellular pH.

4.3.1.1 Optimisation of the bicarbonate-based culture system

As stated in section 1.2.2, GPR65 is optimally activated around pH 6.5. Therefore, I decided to test 3 different pH culture conditions; pH 6.5 for receptor activation, pH 7.5 representing neutral conditions and pH 8.5 to act as a negative control, as it was thought a non-stimulatory environment.

I first established that D10 incubated at 37 °C and 5% CO_2 had a pH of 7.5. I then began to alter culture pH using hydrochloric acid for acidic affects, and sodium hydroxide for alkaline changes. However, the stability of pH over time was not sustained in the presence of cells, particularly post-stimulation. Therefore, culture conditions were optimised, utilising the CO_2 buffering system and specific concentrations of sodium bicarbonate.

T cells stimulated with αCD3 and αCD28 in a low pH environment exhibited improved viability from 72 hours, compared with those at neutral pH (Figure 4-1). Moreover, PBMCs cultured in a pH 8.5 environment were not viable after 24 hours, so this condition was dropped, continuing only to compare effects of low and neutral pH on immune cell function, for the rest of the thesis.

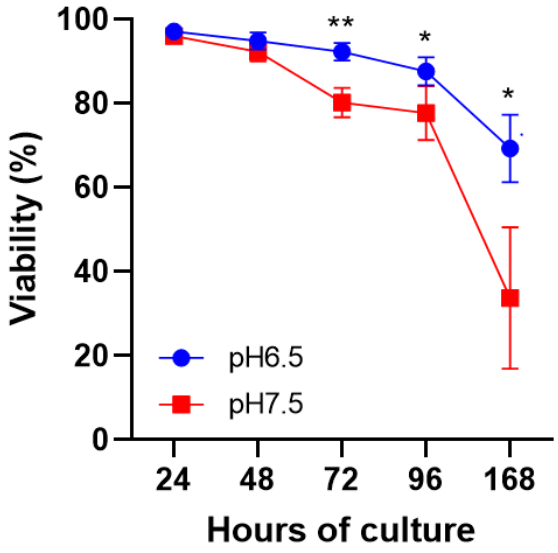


Figure 4-1 – T cells cultured in an acidic environment were protected from cell death

PBMCs were stimulated with αCD3 and αCD28 [1µg/mL] in two pH cultures, for up to 1 week (n=3). A time course of viability was assessed by DAPI stain and analysed by flow cytometry. T cells were identified by their expression of CD3, with those cultured at a low pH are depicted in blue, whilst those at pH 7.5 are in red. Statistical significance was performed using a paired Student's t-test between culture conditions. *p≤0.05, **p≤0.01.

4.3.1.2 LPS stimulation

To gain insight on how low pH affects monocyte function, including bystander effects of their activation on other PBMC cell subsets, PBMCs were stimulated with lipopolysaccharide (LPS) for 24 hours, at pH 6.5 and pH 7.5 culture conditions, and cytokine production was determined. Brefeldin A (BFA) was used in the final 4 hours of culture to prevent cytokine proteins from being transported and promoting their accumulation in the endoplasmic reticulum. Upon gating on live cells, relevant cell populations were identified using established phenotypic markers; $CD14^{+}$ for monocytes, $CD3^{+}CD4^{+}$ for $CD4^{+}$ T cells, $CD3^{+}CD8^{+}CD161^{lo}$ for $CD8^{+}$ T cells (captured both $CD161^{-}$ and $CD161^{+}$ cells), $CD3^{+}CD8^{+}CD161^{++}$ for MAIT cells and $CD56^{+}$ for NK cells (Figure 4-2). A key marker to identify MAIT cells is the TCRαV7.2 (Vα7.2) receptor, however as it becomes downregulated upon activation, I did not use it as an identifier throughout this chapter. The green boxed plot within Figure 4-2 was from an unstimulated control, to confirm that my surrogate identification captured this cell type. Also, due to the size restrictions of the fluorescence activated cell sorting (FACS) panel, B cells were not assessed here. Intracellular cytokine expression was then assessed for each cell type.

A significant increase of the pro-inflammatory cytokine IL-1β was detected from culture supernatant when cells were incubated in an acidic environment. However, conflicting trends for the suppression of TNFα from monocytes was observed when cultured at pH 6.5 (Figure 4-3A). Restriction of inflammation was further confirmed for TNFα at the protein level, along with an increase of IL-6 at pH 6.5, compared to neutral pH (Figure 4-3B).

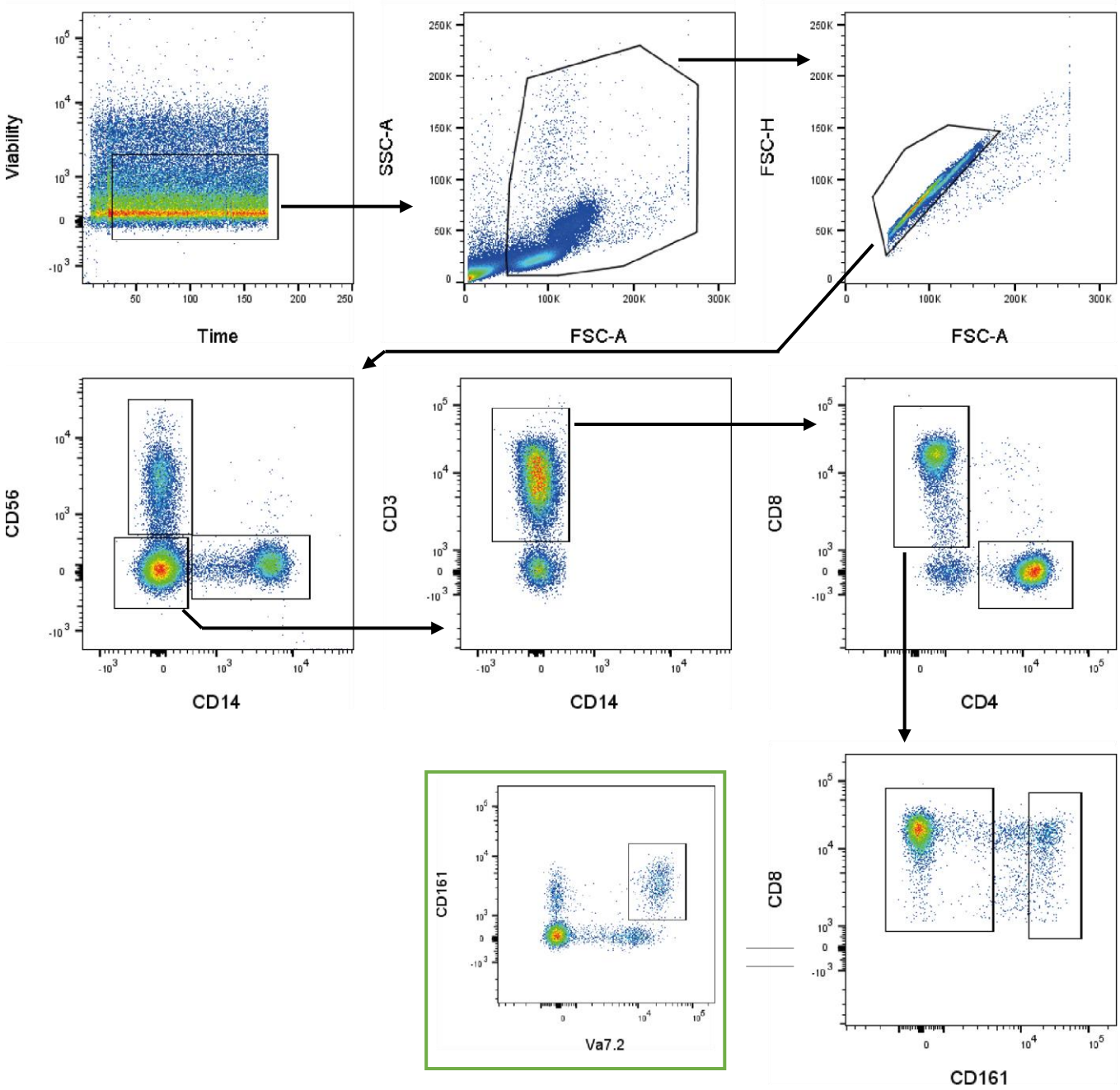


Figure 4-2 – Flow cytometry gating strategy for the identification of PBMC subsets

Flow cytometry gating for cultured PBMCs (example shown is PBMCs stimulated with LPS for 24 hours). Cells were stained with surface markers for at least 30 minutes at 4 °C and included a fixable live/dead viability dye step, as per manufacturers protocol. After gating on live cells verses time, lymphocytes (SSC-A vs, FSC-A), single cells (FSC-H vs, FSC-A) and cellular subsets were gated upon expression of established extracellular markers; monocytes ($CD56^-$ vs, $CD14^+$), NK cells ($CD56^+$ vs, $CD14^-$), T cells ($CD3^+$ vs, $CD14^-$), $CD4^+$ and $CD8^+$ T cells, MAIT cells ($CD8^+$ vs, $CD161^{++}$) and $CD8^+$, $CD161^{lo}$ ($CD8^+$ vs, $CD161^-$ and $CD161^+$). The plot within the green box represents an unstimulated control and shows a more stringent MAIT cell identification using expression of Vα7.2.

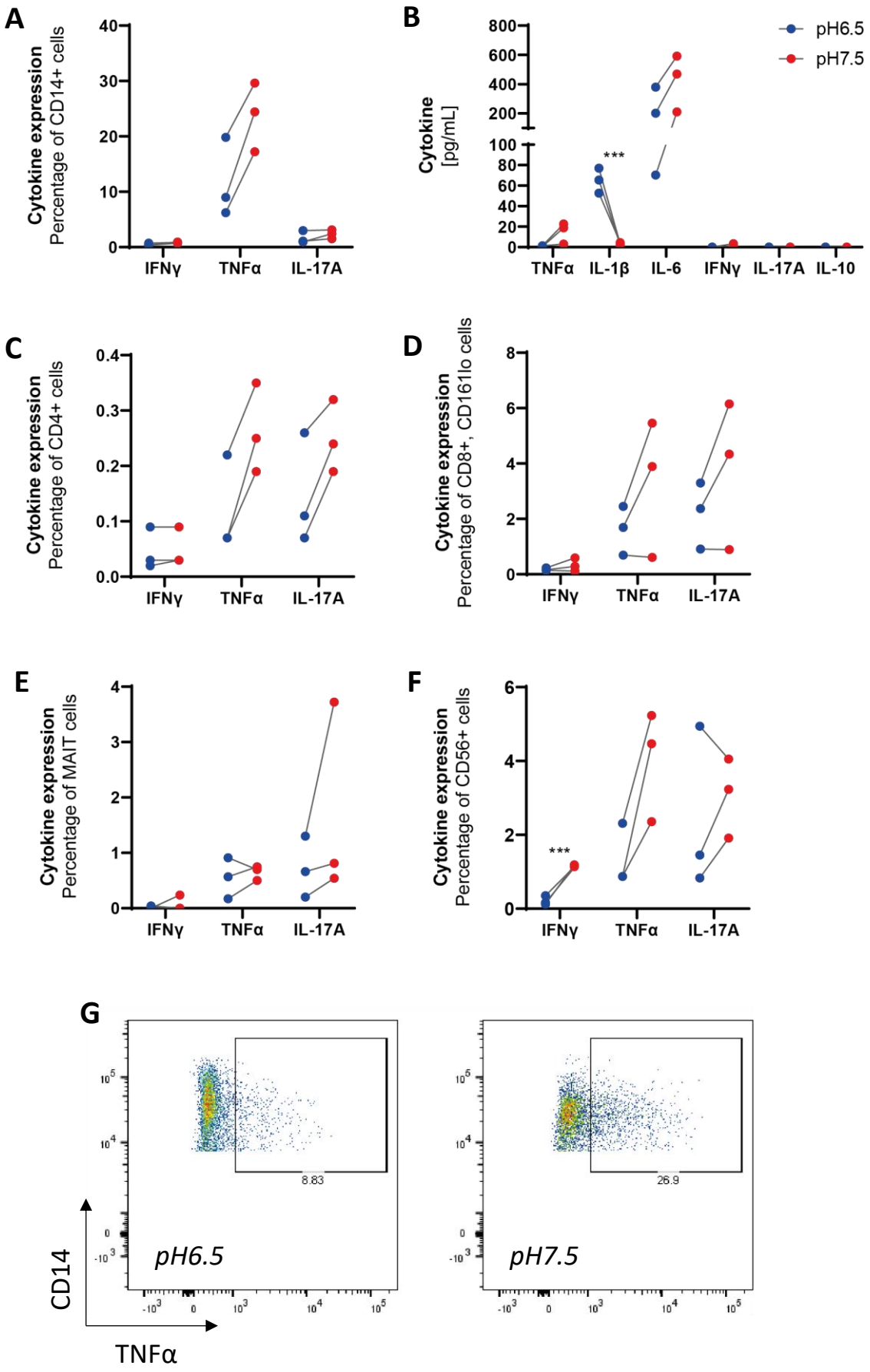

A
Cytokine expression
Percentage of CD14+ cells
IFNγ
TNFα
IL-17A
B
Cytokine
[pg/mL]
pH6.5
pH7.5
***
TNFα
IL-1β
IL-6
IFNγ
IL-17A
IL-10
C
Cytokine expression
Percentage of CD4+ cells
D
Cytokine expression
Percentage of CD8+, CD161lo cells
E
Cytokine expression
Percentage of MAIT cells
F
Cytokine expression
Percentage of CD56+ cells
G
8.83
26.9
pH6.5
pH7.5
CD14
TNFα

Figure 4-3 – Acidic pH suppressed LPS-dependent TNFα production from monocytes

PBMCs were isolated and stimulated with LPS [20ng/mL] for 24 hours (n=3). Expression of intracellular cytokines was determined in monocytes (A), $CD4^+$ T cells (C), $CD8^+$ T cells (D), MAIT cells (E) and NK cells (F), with representative flow cytometry plots from monocytes expressing TNFα (G). Corresponding protein levels were quantified by MSD (B). Cells cultured at a low pH are depicted in blue, whilst those at pH 7.5 are in red. Data represents the mean of three technical replicates, for each of the three biological replicates. Statistical significance was performed using a paired Student's t-test between culture conditions. ***$p \leq 0.001$.

Although monocytes are not believed to produce IL-17A, this cytokine read out was included to see if off-target changes to alternative cell types were present. Interestingly, suppressive effects of acidic pH were also observed for multiple clinically validated cytokines in alternative cell types within the same assay, such as a decrease of IL-17A from $CD4^+$ T cells and a significant reduction in IFNγ from NK cells (Figure 4-3C and F, respectively).

4.3.1.3 T cell stimulation

Combined anti-CD3 and anti-CD28 stimulation for 72 hours provided the preliminary assessment of the effects of pH on T cell activity. BFA was again added to the culture for the final 4 hours to determine intracellular cytokine expression. It is of note, due to the timing of this assay and lack of a low-binding plate, I was unable to assess the effects of monocytes here.

Analysis of T cell function supported the suppressive nature of acidic pH. Most strikingly a significant reduction in all pro-inflammatory cytokines analysed was observed from MAIT cells (Figure 4-4C). However, when comparing to other cell populations, only IFNγ production was sensitive to low pH conditions (Figure 4-4A, B and D). Complementary protein analysis supported suppression of TNFα at low pH (Figure 4-4F), with a significant result from $CD4^+$ T cells, and a trend for $CD8^+$ T cells observed.

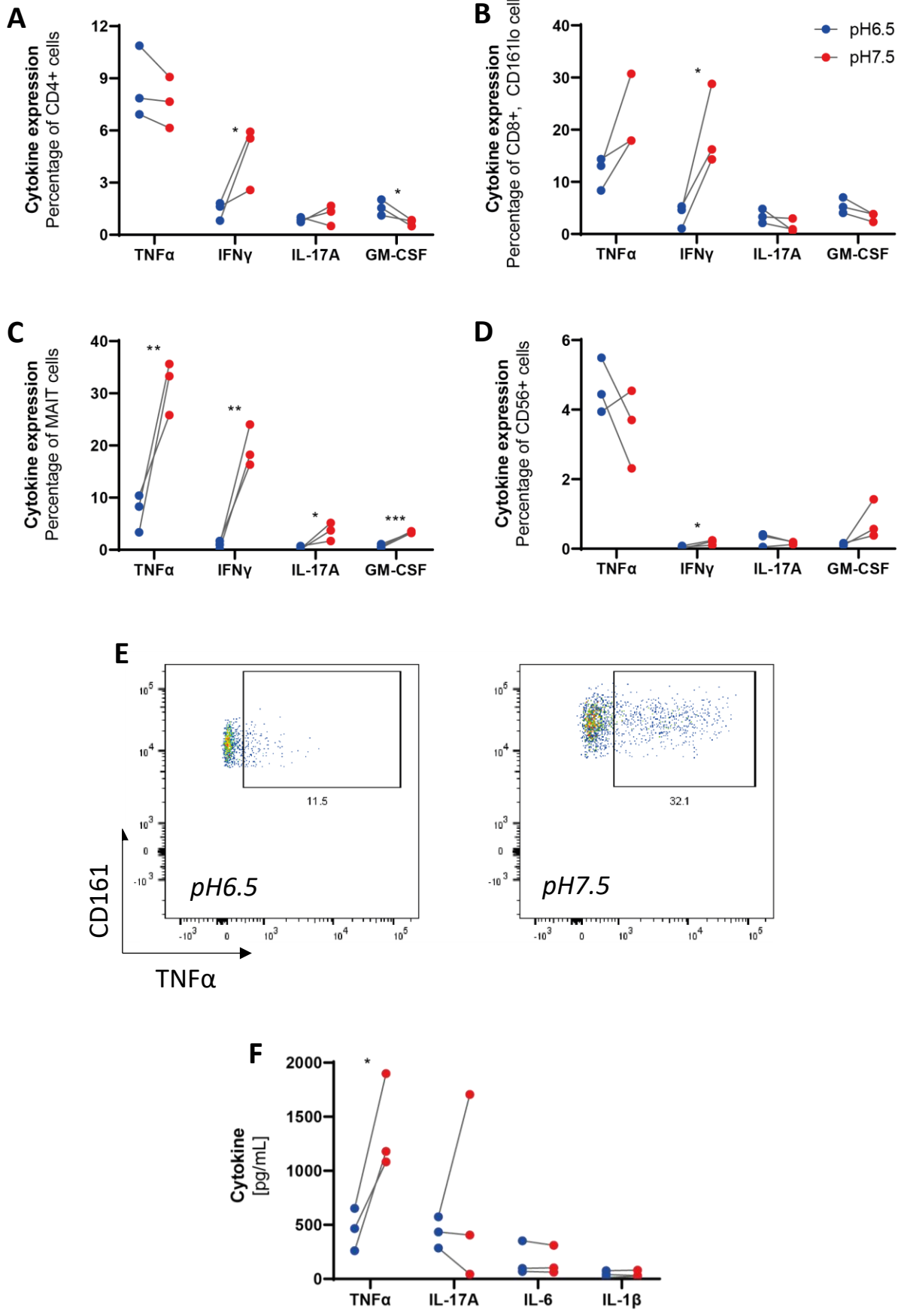

A
Cytokine expression
Percentage of CD4+ cells
TNFα
IFNγ
IL-17A
GM-CSF
B
Cytokine expression
Percentage of CD8+, CD161lo cells
pH6.5
pH7.5
C
Cytokine expression
Percentage of MAIT cells
D
Cytokine expression
Percentage of CD56+ cells
E
CD161
TNFα
pH6.5
pH7.5
11.5
32.1
F
Cytokine
[pg/mL]
IL-6
IL-1β

Figure 4-4 – A low pH environment restricted pro-inflammatory cytokine release by TCR stimulated T cells

PBMCs were isolated and stimulated with αCD3 and αCD28 [1µg/mL] for 72 hours (n=3). Expression of intracellular cytokines was determined in $CD4^+$ T cells (A), $CD8^+$ T cells (B), MAIT cells (C) and NK cells (D), with representative flow cytometry plots from MAIT cells expressing TNFα (E). Corresponding protein levels were quantified by MSD (F). Cells cultured at a low pH are depicted in blue, whilst those at pH 7.5 are in red. Data represents the mean of three technical replicates, for each of the three biological replicates. Statistical significance was performed using a paired Student's t-test between culture conditions. *p≤0.05, **p≤0.01, ***p≤0.001.

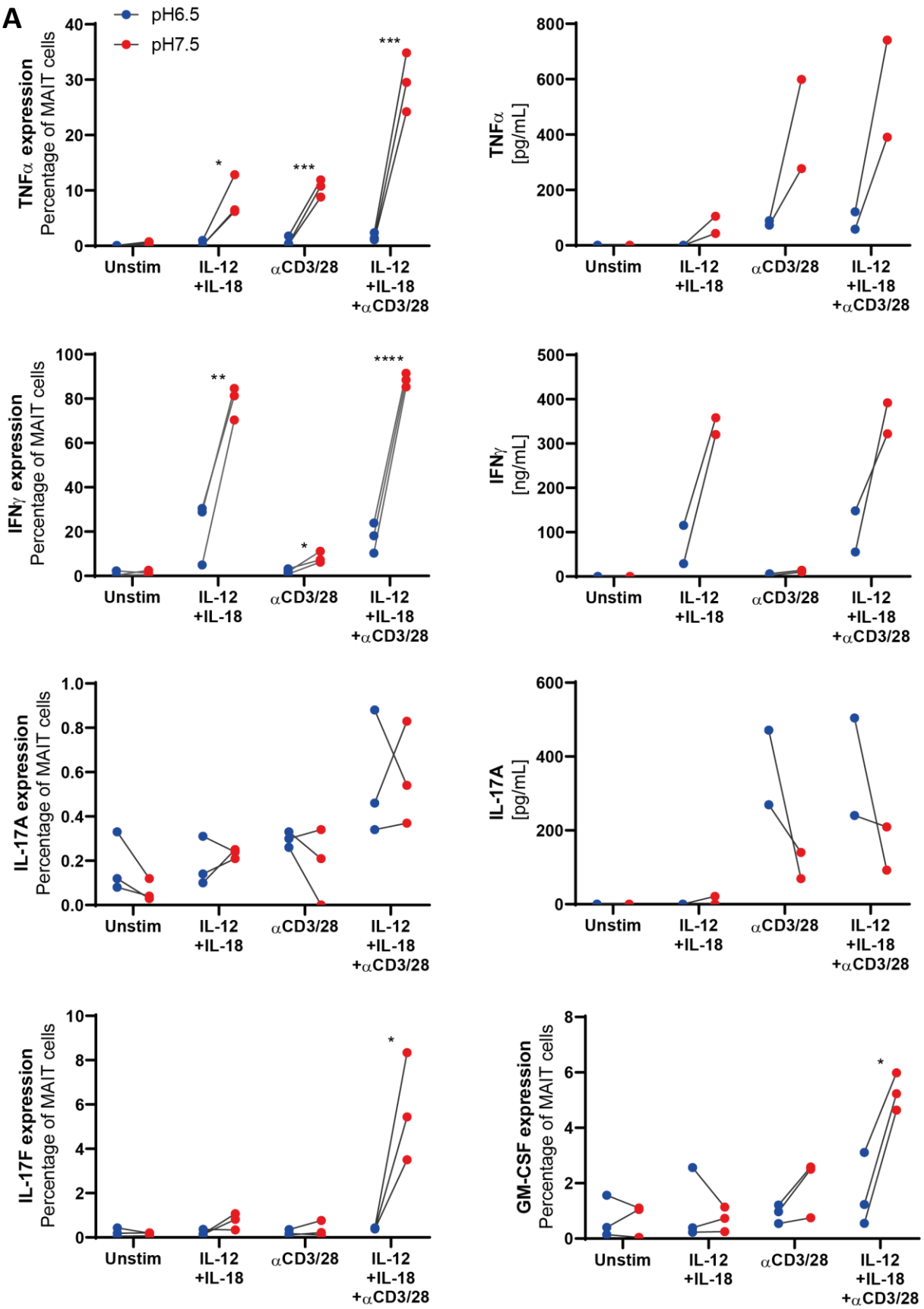
Interestingly, effects of pH on GM-CSF were discovered to be different across the cell types. The innate-like cells (MAIT and NK cells) suggested a reduction of cytokine release, whilst conventional $CD4^+$ and $CD8^+$ T cells showed the opposite, with an increase of GM-CSF produced in an acidic pH environment (Figure 4-4).

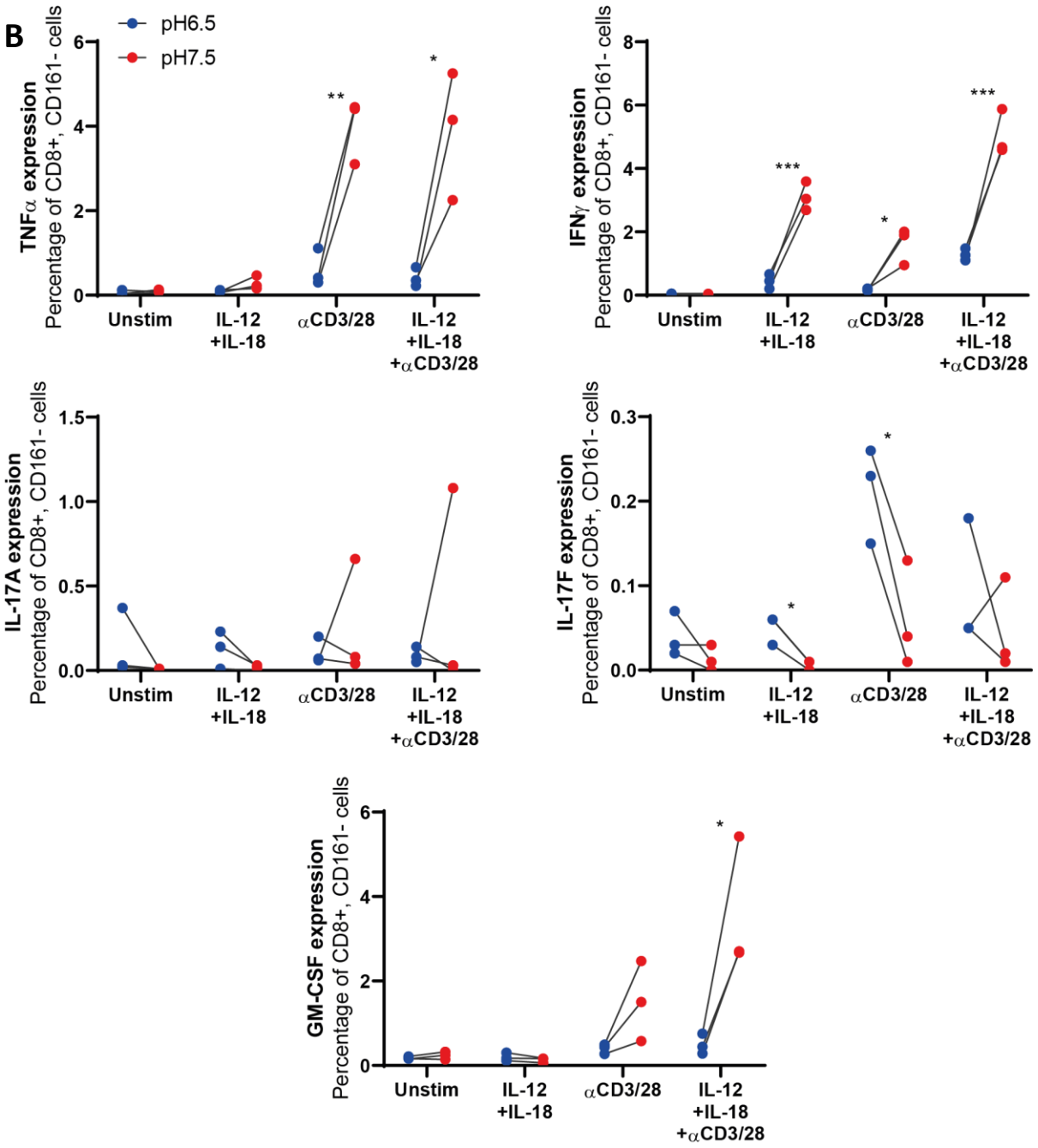
4.3.2 MAIT cell-specific effects of an acidic extracellular environment

Significant suppression of MAIT cell cytokine expression upon TCR stimulation supported the hypothesis that these cells would be able to recognise extracellular pH changes, potentially due to their high levels of GPR65 expression (Figure 5-1). Although expressors of the T cell receptor and therefore responsive to αCD3 and αCD28 stimulation, MAIT cells can also be activated through alternative methods, such as the cytokines IL-12 and IL-18[114,301,302]. To expand upon low pH effects on MAIT cells, I wanted to establish MAIT-specific stimulation conditions.

4.3.2.1 MAIT cell activity within a mixed cell culture system

After a preliminary assessment of multiple methods of stimulation including cytokines, TCR and *E.coli* (data not included), I decided upon the use of TCR (αCD3/28) and cytokine (IL-12 and IL-18) stimulation alone, or in combination, to continue my investigations.


A
pH6.5
pH7.5
TNFα expression
Percentage of MAIT cells
TNFα
[pg/mL]
IFNγ expression
Percentage of MAIT cells
IFNγ
[ng/mL]
IL-17A expression
Percentage of MAIT cells
IL-17A
[pg/mL]
IL-17F expression
Percentage of MAIT cells
GM-CSF expression
Percentage of MAIT cells
Unstim
IL-12
+IL-18
αCD3/28
IL-12
+IL-18
+αCD3/28


B
pH6.5
pH7.5
TNFα expression
Percentage of CD8+, CD161- cells
IFNγ expression
IL-17A expression
IL-17F expression
GM-CSF expression
Unstim
IL-12 +IL-18
αCD3/28
IL-12 +IL-18 +αCD3/28

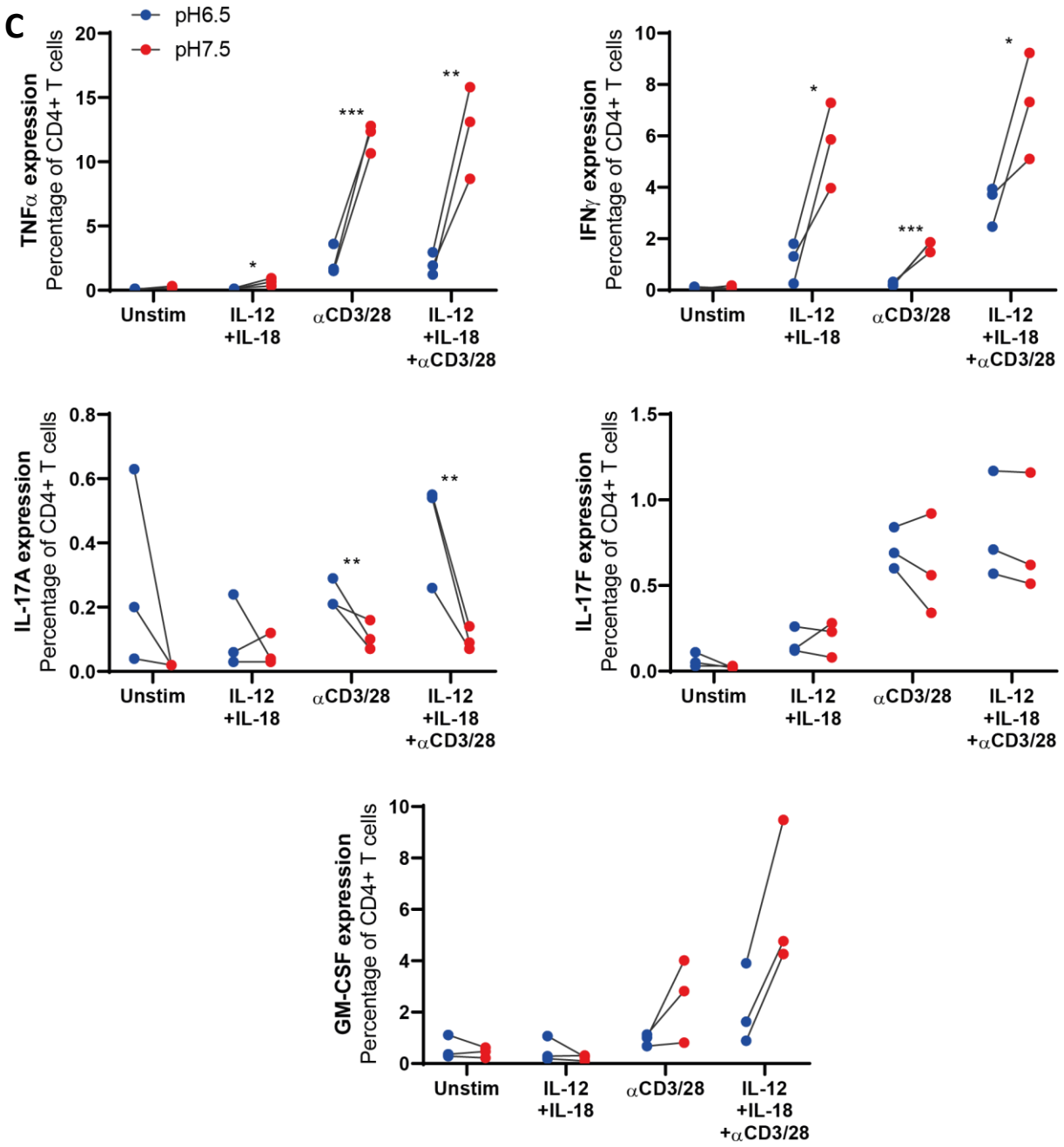


Figure 4-5 – Acidic pH suppressed Th1-like cytokine production from activated T cells

PBMCs were isolated and stimulated for 24 hours (n=3). Expression of intracellular cytokines was determined in MAIT cells (A), $CD8^+$, $CD161^{lo}$ T cells (B), and $CD4^+$ T cells (C), of which paired supernatant protein levels were quantified by MSD for some cytokines (n=2). Cells cultured at a low pH are depicted in blue, whilst those at pH 7.5 are in red. Data represents the mean of three technical replicates, for each of the three biological replicates. Statistical significance was performed using a paired Student's t-test between culture conditions. *p≤0.05, **p≤0.01, ***p≤0.001, ****p≤0.0001.

When assessing effects on MAIT cells, a low pH culture significantly suppressed TNFα and IFNγ (Figure 4-5A), regardless of stimulation type, whilst reduced IL-17F was most striking upon the combination stimulation of TCR and cytokines; these effects were further supported through dampened corresponding protein secretion. Conflicting results of how an acidic environment affects IL-17A was observed using flow cytometry readouts. However, supernatant protein quantification suggested a trend of increased cytokine release at pH 6.5, when activated through the TCR receptor.

Additional analysis of other cell subsets present in the experiment further supported the prominent suppression of Th1-like cytokines from TCR stimulated T cells in an acidic extracellular environment (Figure 4-5B and C). However, IL-17 biology differed between $CD4^+$ and $CD8^+$ T cell phenotypes. Acidic pH-dependent increase of IL-17F appeared to be specific to $CD8^+$, $CD161^{lo}$ T cells, with elevated IL-17A production most striking upon TCR stimulated $CD4^+$ T cells (Figure 4-5C).

Whilst reduced expression of GM-CSF was observed from all cell types at pH 6.5 stimulated with αCD3 and αCD28 (Figure 4-5), it is of note the opposite was seen from $CD4^+$ T cells, shown in Figure 4-4. This could be due to kinetics of cytokine release, as here the results were assessed after 24 hours, whilst the previous data set was read out after 72 hours.

4.3.2.2 $CD8^+$ T cells in isolation

In preliminary experiments I observed that culture of purified MAIT cells impaired their function (confirming the findings of Slichter and colleagues[303]), so I rarely study them in isolation. However, I wanted to see whether the suppressive effects of low pH on MAIT cell activity was independent of cell-cell interactions.

As expected, cytokine release was lower for all proteins assessed from isolated MAIT cell cultures (10-20% TNFα release from MAIT cells cultured at pH 7.5), compared to when cells were in a mixed culture (25-35% TNFα release from MAIT cells cultured at pH 7.5). With the combination of TCR and cytokine stimulation proving to most strongly activate the MAIT cells, pro-inflammatory cytokine release was still restricted in a lower pH setting (Figure 4-6A), including both Th1 and Th17 related cytokines.

When comparing the difference in response between CD161 hi or lo expressing $CD8^+$ T cells, support for low pH-dependent suppression of TNFα and IL-17F was observed (Figure 4-6B), whilst pH effects on IL-17A were not seen here. Upon assessing the effects of pH on IFNγ production from $CD8^+$, $CD161^+$ T cells, the level of expression was lower than expected (and previously seen in my assays) and I questioned the reliability of the results obtained; so, didn't take this data into consideration. Yet, cross-cell interaction was thought to be important for GM-CSF production from $CD8^+$ T cells, as it was not detected by the methods used.

Overall, the suppressive nature of low pH on inflammation was still observed by these cells in isolation, suggesting direct pH sensing by MAIT cells.

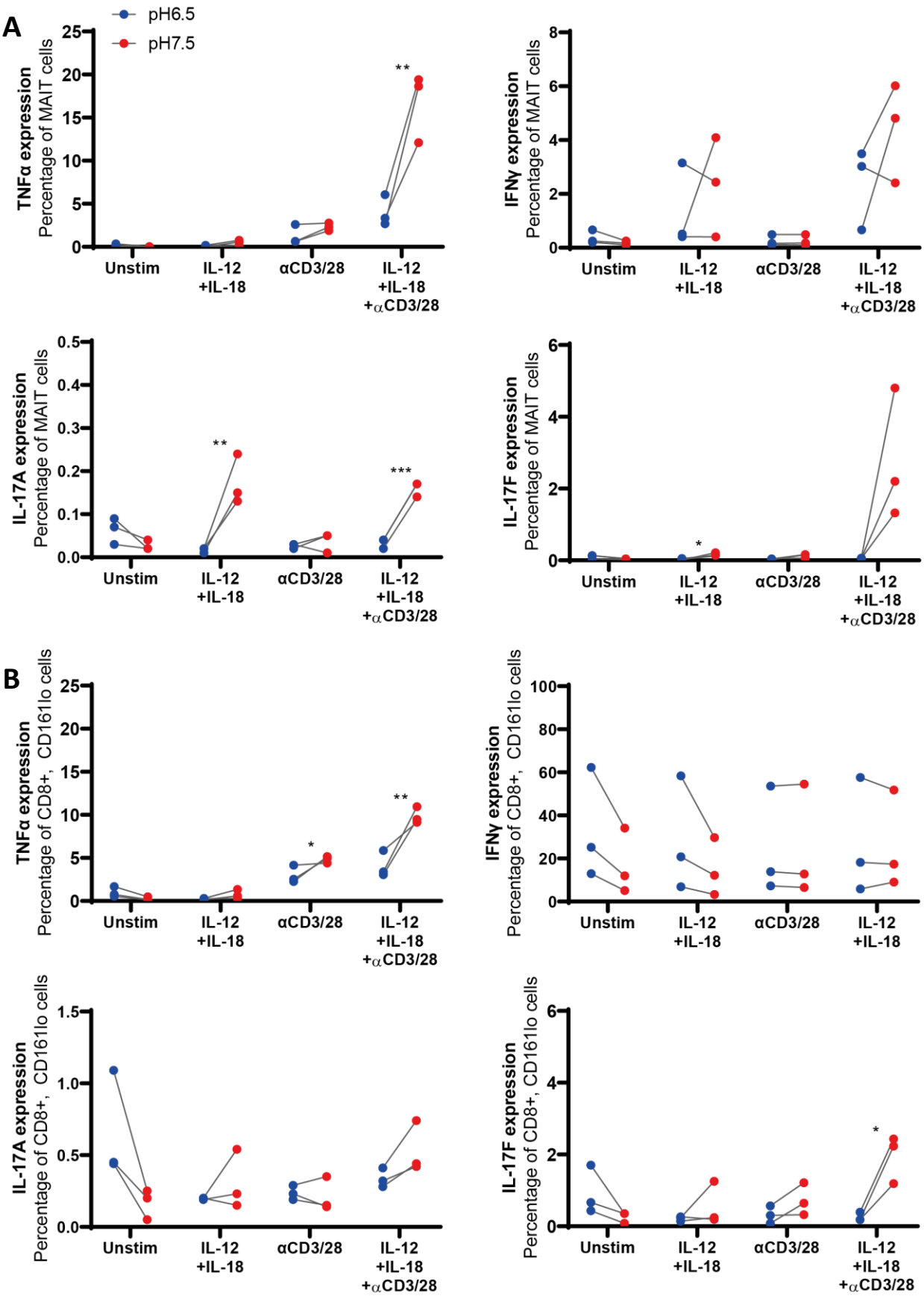

A
pH6.5
pH7.5
TNFα expression
Percentage of MAIT cells
IFNγ expression
Percentage of MAIT cells
IL-17A expression
Percentage of MAIT cells
IL-17F expression
Percentage of MAIT cells
B
TNFα expression
Percentage of CD8+, CD161lo cells
IFNγ expression
Percentage of CD8+, CD161lo cells
IL-17A expression
Percentage of CD8+, CD161lo cells
IL-17F expression
Percentage of CD8+, CD161lo cells
Unstim
IL-12 +IL-18
αCD3/28
IL-12 +IL-18 +αCD3/28

Figure 4-6 – Acidic pH-dependent inhibition of TNFα from MAIT cells was observed in a culture of isolated $CD8^+$ T cells

$CD8^+$ T cells were positively isolated from PBMCs and stimulated for 24 hours (n=3). Expression of intracellular cytokines was determined in MAIT cells (A) and $CD8^+$, $CD161^{lo}$ T cells (B). Cells cultured at a low pH are depicted in blue, whilst those at pH 7.5 are in red. Statistical significance was performed using a paired Student's t-test between culture conditions. *p≤0.05, **p≤0.01, ***p≤0.001.

4.3.3 Transcriptional changes were consistent with a suppressive nature of a low pH environment

I have so far presented established inflammatory protein changes upon a low pH environment in multiple immune cell populations. As part of an alternative question to understand the genes responsible for GPR65 effects in $CD161^+$ T cells (discussed in Chapter 5) I was able to further address the question of transcriptional changes responsible for the suppression of inflammation observed in a low pH environment.

Details of the experimental conditions can be found in Figure 5-11A. Briefly, $CD3^+$, $CD161^+$ T cells, enriched for GPR65 expressing cells, were subject to either GPR65 or non-target control siRNA treatment for 24 hours, then left unstimulated or stimulated with cytokines IL-12 and IL-18, or αCD3 and αCD28 at both pH 6.5 and pH 7.5. After 20 hours, live cells were sorted for single cell RNA sequencing (scRNAseq).

Approximately, 20,000 cells per experimental condition were loaded into one channel of a Chromium chip for 10x 5' single-cell gene expression processing. The cell number yielded, varied between 6,533 and 11,179 per sample, and a mean read depth of 50,000 achieved in nearly all conditions (Figure 4-7A and B). Once output libraries from sequencing were converted into a gene expression matrix, this was then analysed using the Seurat R package. Quality control analysis suggested the sequencing data was of good quality, upon assessment of feature counts and mitochondrial metrics (Figure 4-7C[k]).

[k] QC analysis in R performed by Feng Liu.

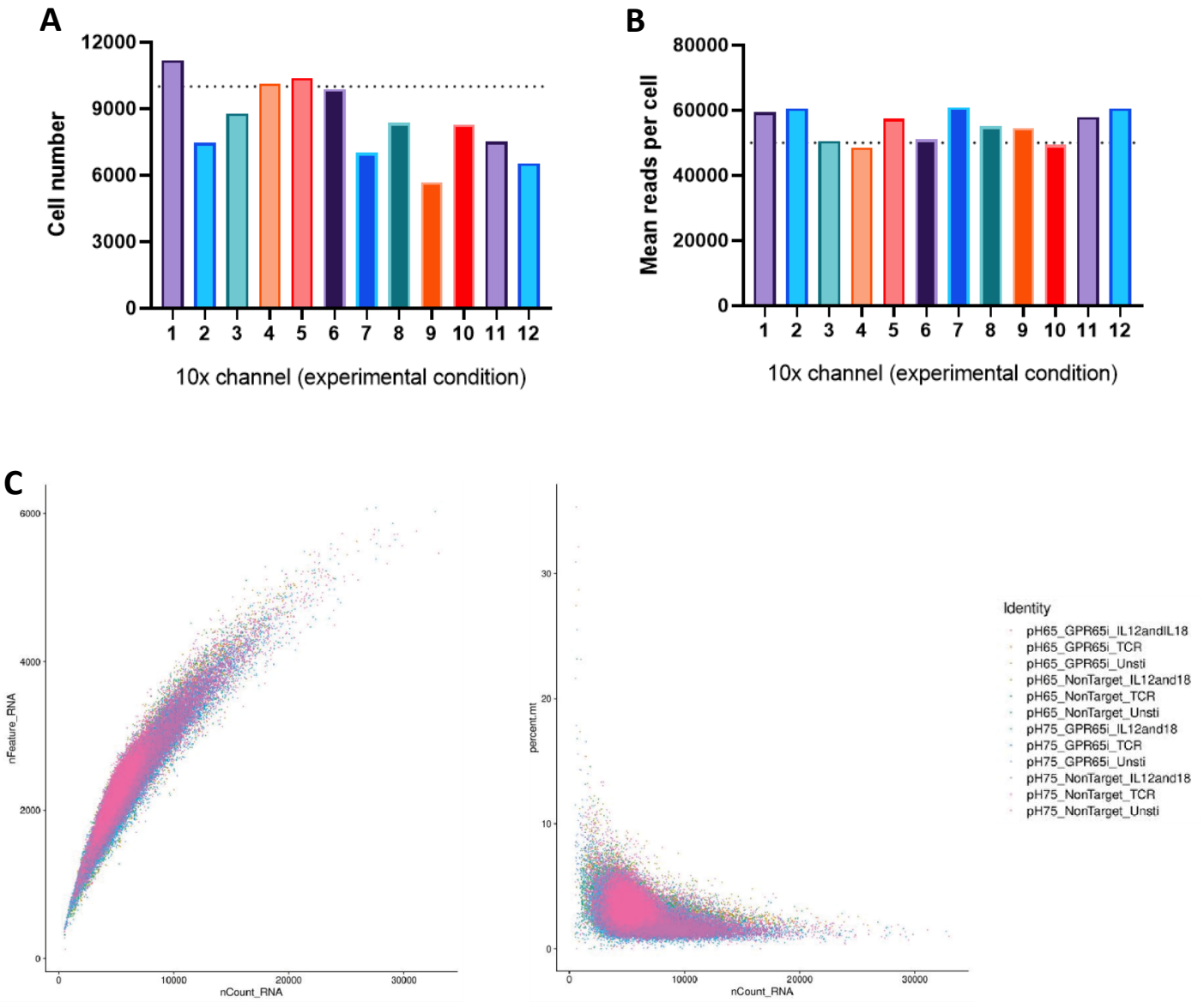
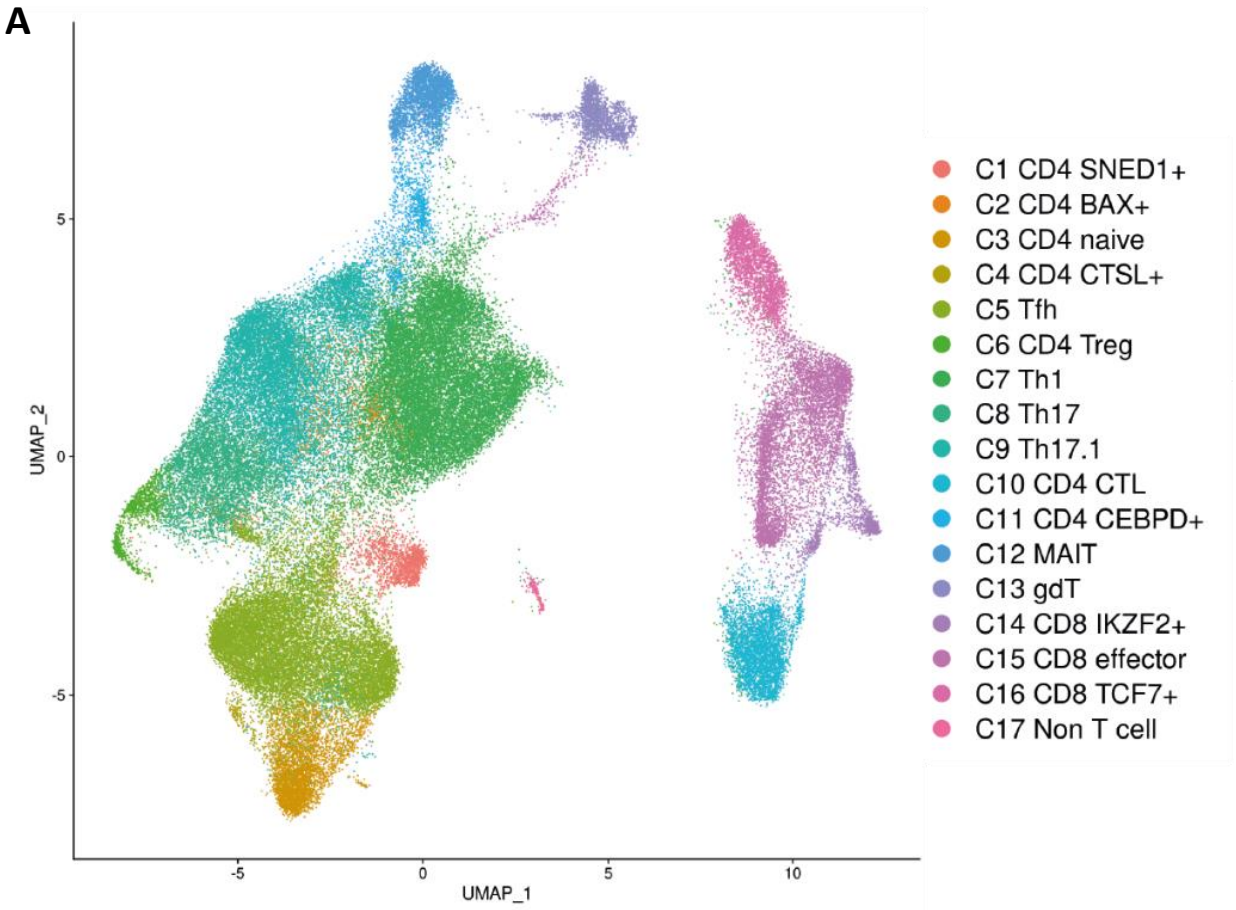


Figure 4-7 – A quality check provided confidence in good quality data attained by single cell RNA sequencing

(A) Cell number successfully sequenced per experimental condition, with corresponding mean read depth (B), the dotted line represents the number being aimed for. (C) Quality control feature plots[I] comparing the number of reads (nCount_RNA) with both the number of genes (nFeature_RNA) and the percentage of mitochondrial reads (percent.mt). All 12 conditions are plotted on the same graph, with them overlapping and suggest no outliers.

[I] QC analysis performed by Feng Liu.


A
UMAP_2
UMAP_1
5
0
-5
-5
0
5
10
C1 CD4 SNED1+
C2 CD4 BAX+
C3 CD4 naive
C4 CD4 CTSL+
C5 Tfh
C6 CD4 Treg
C7 Th1
C8 Th17
C9 Th17.1
C10 CD4 CTL
C11 CD4 CEBPD+
C12 MAIT
C13 gdT
C14 CD8 IKZF2+
C15 CD8 effector
C16 CD8 TCF7+
C17 Non T cell

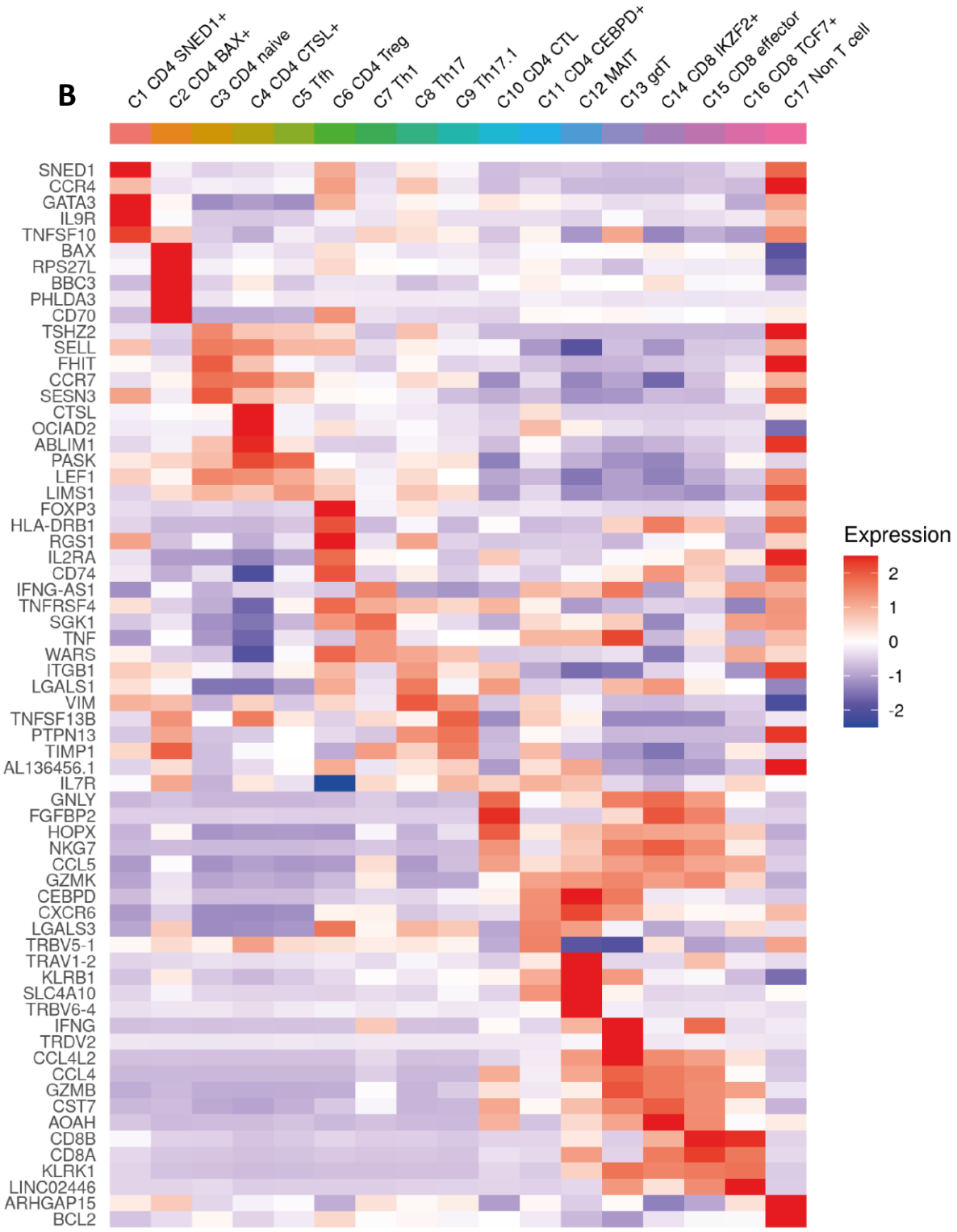


Figure 4-8 –17 distinct clusters were revealed from CD3$^+$, CD161$^+$ sequenced cells

(A) Seurat generated Uniform Manifold Approximation and Projection (UMAP) of 86,070 cells colour-coded for the indicated cell type. Clusters are numbered according to the number of cells represented; 1 having the most, to 17 with the least. (B) Heatmap showing row-scaled, average, log-transformed normalised expression of up to the top 5 significant marker genes for each cluster.

In total, 86,070 cells from the three donors and 12 experimental conditions were analysed post-filtering (details within section 2.2.11.2.2)[m]. As the high dimensional gene matrix generated is hard to interpret, this was reduced into a 2D representation. Using the Uniform Manifold Approximation and Projection (UMAP) algorithm, I generated a plot with 17 distinct cellular clusters, where each point represented a cell, and positioning of the points represented the relationship between clusters, as well as within each cluster (Figure 4-8A).

Key cluster specific genes were identified through the FindAllMarkers function, based on the average log 2-fold change (avg log2FC) of normalised RNA gene expression. The Wilcoxon Rank Sum test highlighted significant (adjusted P value < 0.05) differentially expressed genes, with a list generated for each cluster, ordered by avg log2FC. To distinguish which cell subsets each cluster signified, relative expression of established cluster identifying gene markers was assessed, as well as analysis of up to the top 5 genes average expression for each cluster (Figure 4-8B).

[m] Feng Liu performed the conversion of the sequencing data output, generation of the R compatible gene expression matrix and quality control assessments. I then performed all downstream analysis, from the generation of the UMAP onwards.

4.3.3.1 Upon stimulation in acidic conditions MAIT cells lost their ability to cluster

All $CD8^+$ T cells were shown to be evenly distributed between the three donors (data not shown). I initially focussed on MAIT cells since my functional experiments had shown significant effects of low pH on MAIT function (section 4.3.1.3). Represented by cluster 12, this cell type made up 3.3% of the whole cell population (2,866 cells) and as expected, unstimulated MAIT cells were confirmed to be a homogenous population (Figure 4-9).

Having selected the MAIT cell cluster specifically, upon running the UMAP algorithm on combined non-target siRNA stimulated cells at neutral pH, three subclusters were generated (Figure 4-10A); with the smallest of the clusters, cluster 2, more abundant in the TCR condition, thus believed to be driven by TCR stimulation (Figure 4-10B). Interestingly, when executing the same FindClusters code on non-target siRNA stimulated cells at low pH, the MAIT cell clusters were diminished, with only one homogenous population of cells present (Figure 4-10C), which suggested striking changes to the transcriptome.

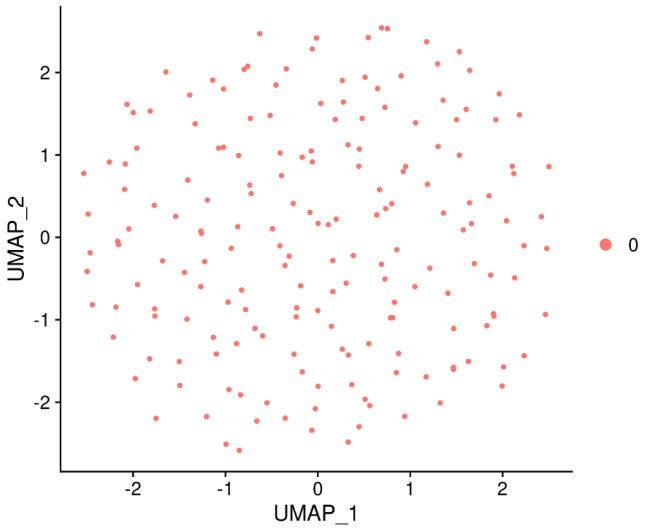


Figure 4-9 – Non-target siRNA treated, unstimulated MAIT cells at neutral pH were confirmed to be a homogenous cell population

UMAP of non-target siRNA treated, unstimulated MAIT cells at neutral pH.

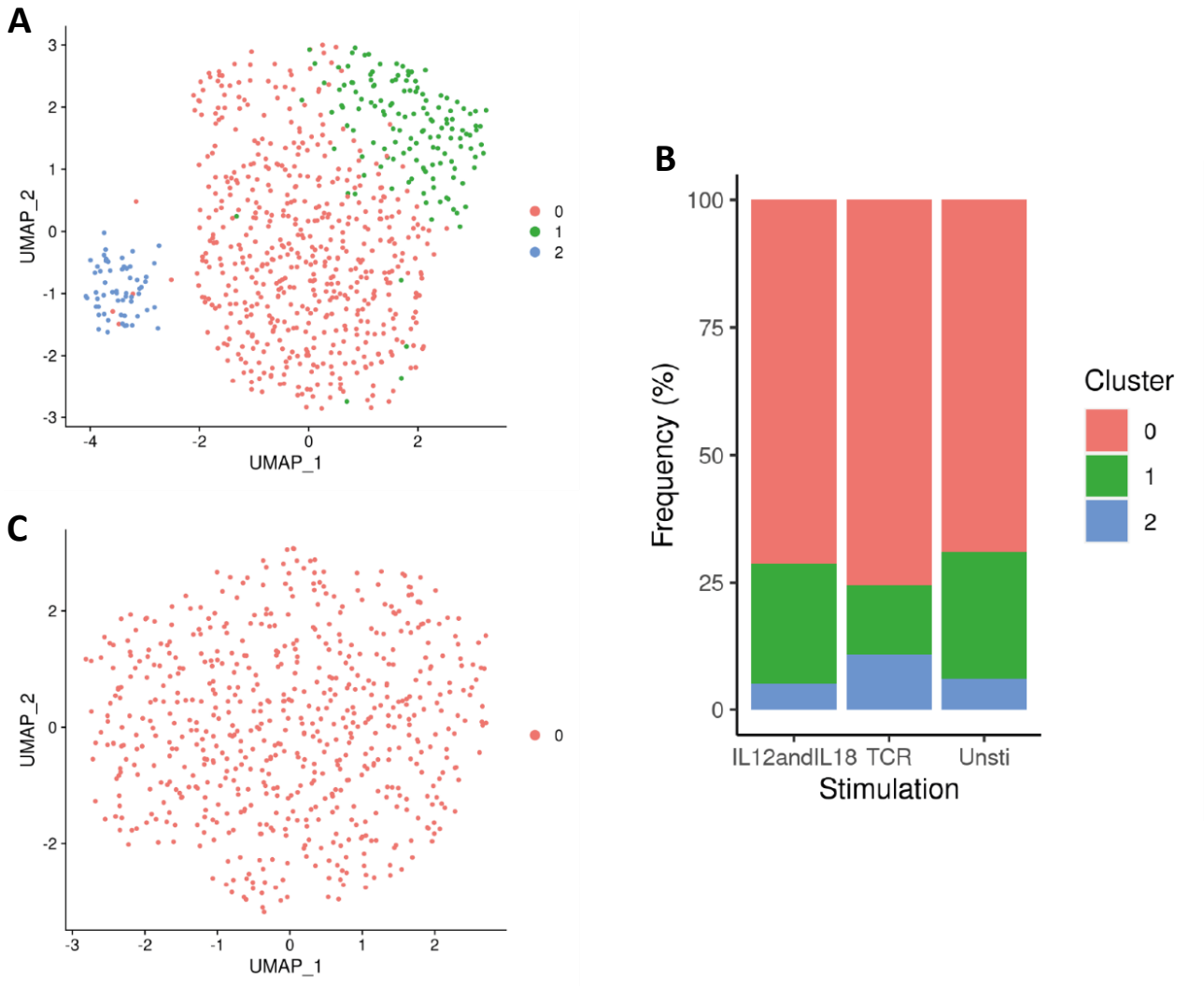


Figure 4-10 – Distinct MAIT subpopulation structure was diminished in an acidic environment

(A) UMAP of non-target siRNA treated MAIT cells, consisting of all three stimulation conditions, at neutral pH. (B) Proportion of cells in each cluster from the three stimulation conditions. (C) UMAP of non-target siRNA treated MAIT cells, consisting of all three stimulation conditions, at pH 6.5.

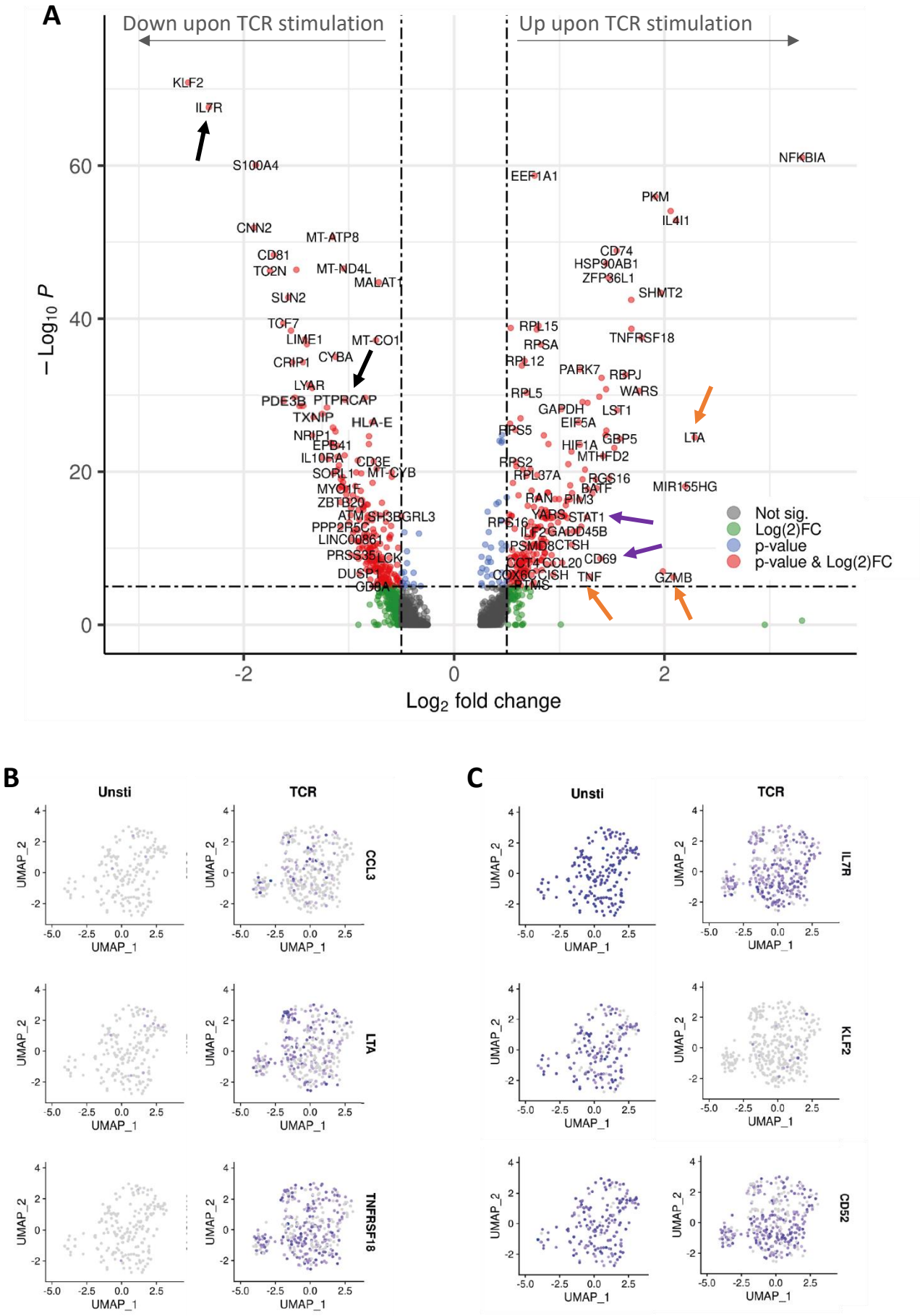
4.3.3.2 Multiple T cell populations were successfully activated by stimulation at neutral pH

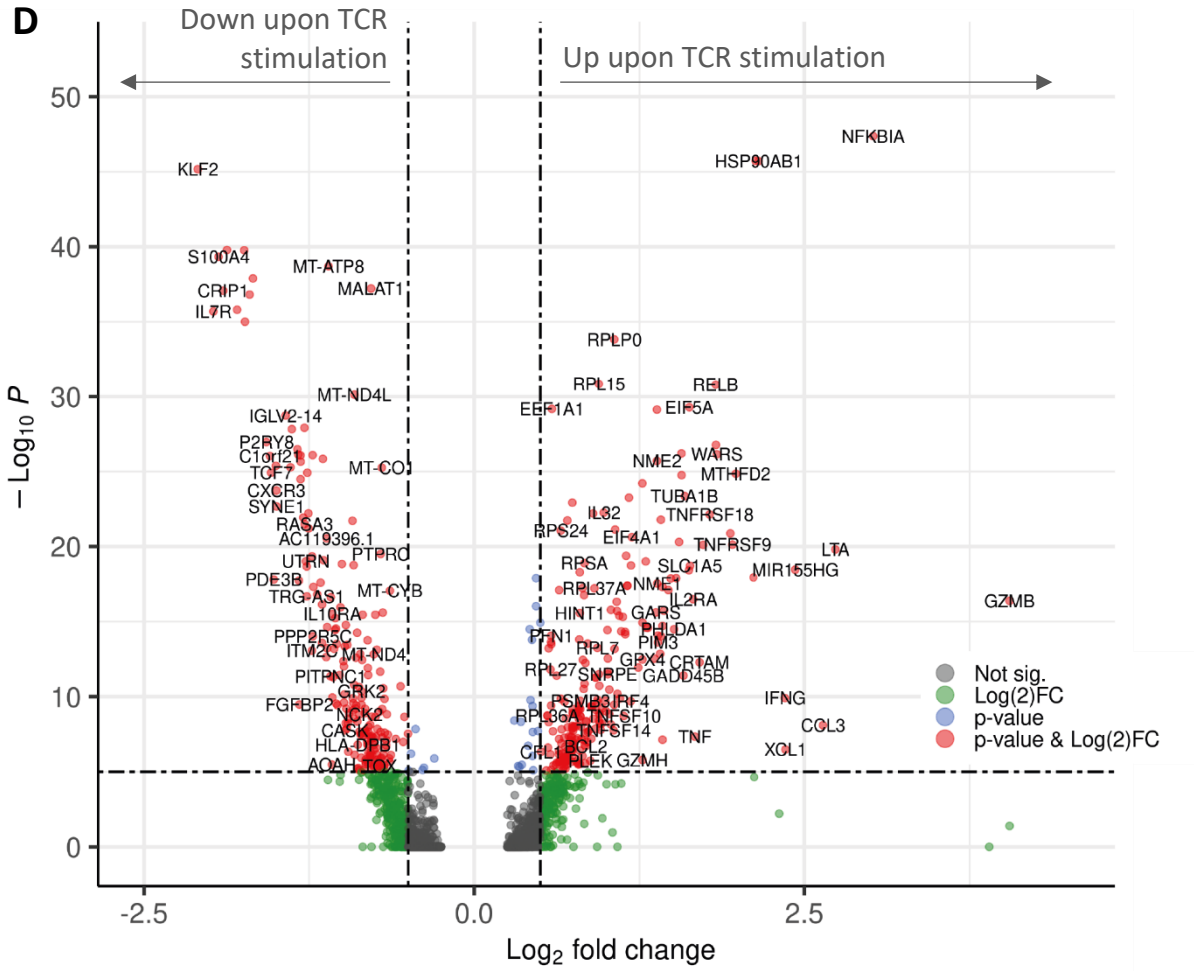
Before addressing the role of acidic pH on immune cell function, it was first important to understand the effects of stimulation in neutral conditions. As mentioned, MAIT cells were of interest due to their GPR65 expression profile and functional response to low pH. But to address whether results obtained were MAIT cell specific, I expanded my transcriptional investigations to include assessment of pH on γδT cells (Cluster 13 - represented 2,036 cells, 2.4% of whole population), Th17 cells (Clusters 8 and 9 - represented 19,265 cells, 22.4% of whole population) and conventional $CD8^+$ T cells (Clusters 14, 15, and 16 - represented 10,921 cells, 12.7% of whole population).

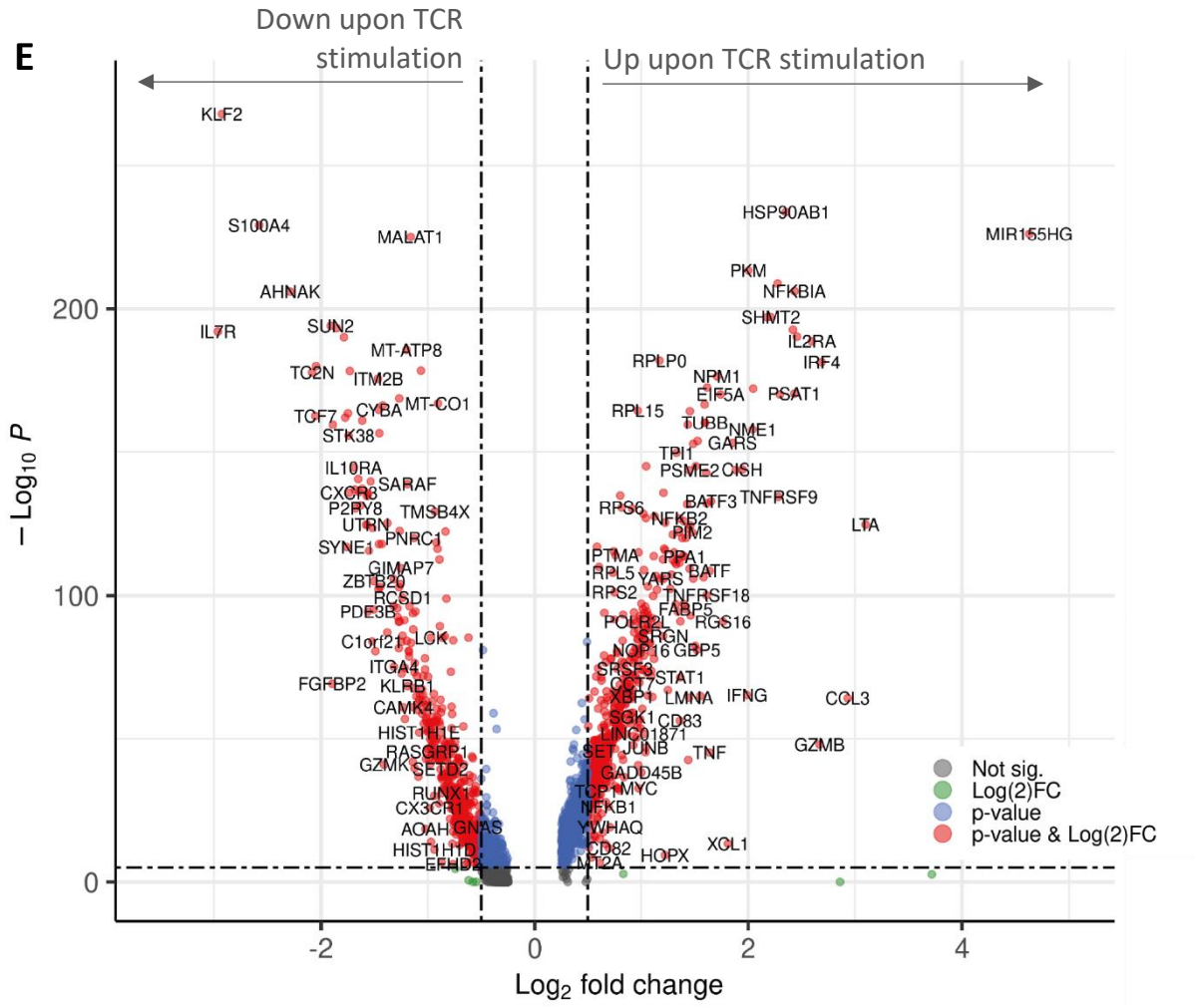
4.3.3.2.1 TCR stimulation

Upon MAIT cell activation with αCD3 and αCD28, I found transcriptional changes in 2,312 genes, compared to unstimulated cells: at a false discovery rate-adjusted p-value < 0.05 and minimum log2FC of ±0.5. This was highly suggestive of successful TCR-mediated activation. Upon stimulation, an increase of activation markers such as *CD69* and *STAT1* (Figure 4-11A (purple arrows)) was observed. As well as upregulation of functional pro-inflammatory genes (*TNF, GZMB, LTA*) (Figure 4-11A (orange arrows) and B). On the other hand, a downregulation of genes consistent with a resting transcriptional profile[304] (*IL7R, CD52, PTPRCAP)* was witnessed (Figure 4-11A (black arrows) and C).

It has been reported MAIT and γδT cells share transcriptional profiles[129,305], so I next decided to assess the crossover of genes affected by TCR stimulation in these two clusters. A largely shared gene set was detected (Figure 4-12), but the differentially expressed genes (DEG) did not appear to be innate-like T cell specific, as all cells within the assay exhibited similar effects and responded as expected to this activation method (Figure 4-11D, E and F).


A
Down upon TCR stimulation
Up upon TCR stimulation
KLF2
IL7R
S100A4
CNN2
MT-ATP8
CD81
TC2N
MT-ND4L
MALAT1
SUN2
TCF7
LIME1
MT-CO1
CYBA
CRIP1
LYAR
PDE3B
PTPRCAP
TXNIP
HLA-E
NRIP1
EPB41
IL10RA
CD3E
SORL1
MT-CYB
MYO1F
ZBTB20
ATM
SH3BGRL3
PPP2R5C
LINC00861
PRSS35
LCK
DUSP1
CD8A
NFKBIA
EEF1A1
PKM
IL4I1
CD74
HSP90AB1
ZFP36L1
SHMT2
RPL15
RPSA
TNFRSF18
RPL12
PARK7
RBPJ
RPL5
WARS
GAPDH
LST1
EIF5A
RPS5
LTA
GBP5
HIF1A
MTHFD2
RPS2
RPL37A
RGS16
BATF
MIR155HG
RAN
PIM3
YARS
STAT1
RPS16
ILF2
GADD45B
PSMB8
CTSH
CCT4
COL20
CD69
COX6C
CISH
TNF
GZMB
PTMS
Not sig.
Log(2)FC
p-value
p-value & Log(2)FC
– Log10 P
Log2 fold change
B
Unsti
TCR
CCL3
LTA
TNFRSF18
C
Unsti
TCR
IL7R
KLF2
CD52
UMAP_1
UMAP_2


D
Down upon TCR stimulation
Up upon TCR stimulation
KLF2
S100A4
MT-ATP8
CRIP1
MALAT1
IL7R
MT-ND4L
IGLV2-14
P2RY8
C1orf21
TCF7
MT-CO1
CXCR3
SYNE1
RASA3
AC119396.1
UTRN
PTPRC
PDE3B
TRG-AS1
MT-CYB
IL10RA
PPP2R5C
ITM2C
MT-ND4
PITPNC1
GRK2
FGFBP2
NCK2
CASK
HLA-DPB1
AOAH-TOX
NFKBIA
HSP90AB1
RPLP0
RPL15
RELB
EEF1A1
EIF5A
NME2
WARS
MTHFD2
TUBA1B
IL32
TNFRSF18
RPS24
EIF4A1
TNFRSF9
LTA
RPSA
SLC1A5
MIR155HG
RPL37A
NME1
IL2RA
GZMB
HINT1
GARS
PFN1
PHLDA1
RPL7
PIM3
GPX4
CRTAM
RPL27
SNRPE
GADD45B
PSMB3
IRF4
IFNG
RPL36A
TNFSF10
CCL3
TNFSF14
TNF
CRL1
BCL2
XCL1
PLEK
GZMH
Not sig.
Log(2)FC
p-value
p-value & Log(2)FC
50
40
30
20
10
0
-2.5
0.0
2.5
– Log10 P
Log2 fold change


E
Down upon TCR stimulation
Up upon TCR stimulation
KLF2
S100A4
MALAT1
AHNAK
IL7R
SUN2
MT-ATP8
TC2N
ITM2B
MT-CO1
TCF7
CYBA
STK38
IL10RA
SARAF
CXCR3
P2RY8
TMSB4X
UTRN
PNRC1
SYNE1
GIMAP7
ZBTB20
RCSD1
PDE3B
C1orf21
LCK
ITGA4
FGFBP2
KLRB1
CAMK4
HIST1H1E
RASGRP1
GZMK
SETD2
RUNX1
CX3CR1
AOAH
GNAS
HIST1H1D
EFHD2
HSP90AB1
MIR155HG
PKM
NFKBIA
SHMT2
IL2RA
IRF4
RPLP0
NPM1
EIF5A
PSAT1
RPL15
TUBB
NME1
GARS
TPI1
PSME2
CISH
RPS6
BATF3
TNFRSF9
NFKB2
PIM2
LTA
PTMA
PPA1
RPL5
YARS
BATF
RPS2
TNFRSF18
FABP5
POLR2L
RGS16
SRGN
NOP16
GBP5
SRSF3
CCT7
STAT1
XBP1
LMNA
IFNG
CCL3
SGK1
CD83
LINC01871
SET
JUNB
TNF
GZMB
GADD45B
TCP1
MYC
NFKB1
YWHAQ
CD82
HOPX
XCL1
MT2A
Not sig.
Log(2)FC
p-value
p-value & Log(2)FC
200
100
0
-2
0
2
4
– Log10 P
Log2 fold change

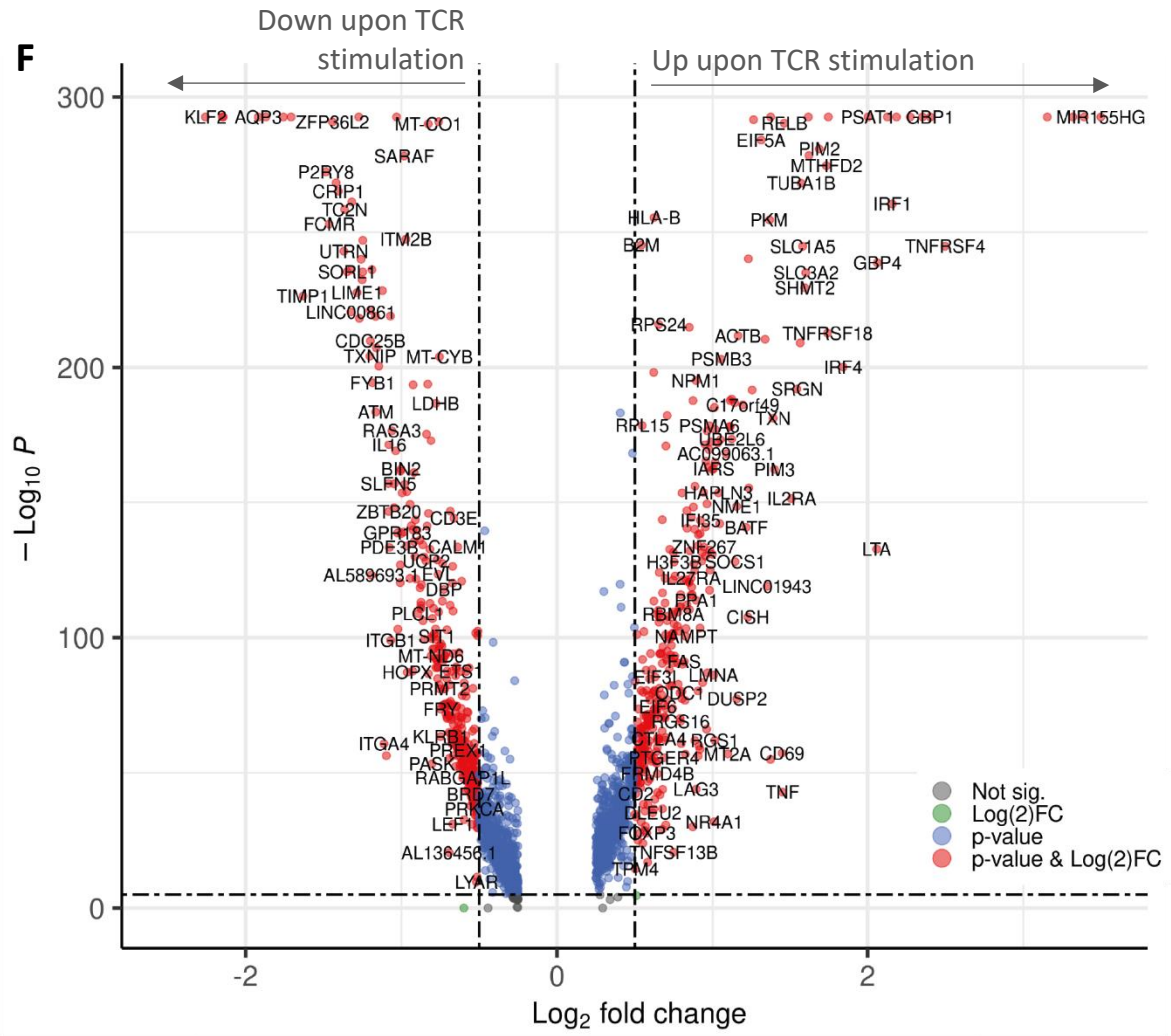


Figure 4-11 – TCR stimulation successfully activated CD3⁺, CD161⁺ cells

Volcano plots indicating genes upregulated and downregulated in MAIT cells (A), γδT cells (D), CD8⁺ T cells (E) and Th17 cells (F), upon TCR stimulation at neutral pH. Coloured arrows depict genes referenced in the text. MAIT cell UMAPs coloured by the increased (B) and decreased (C) expression of key markers, in unstimulated and TCR stimulated conditions.

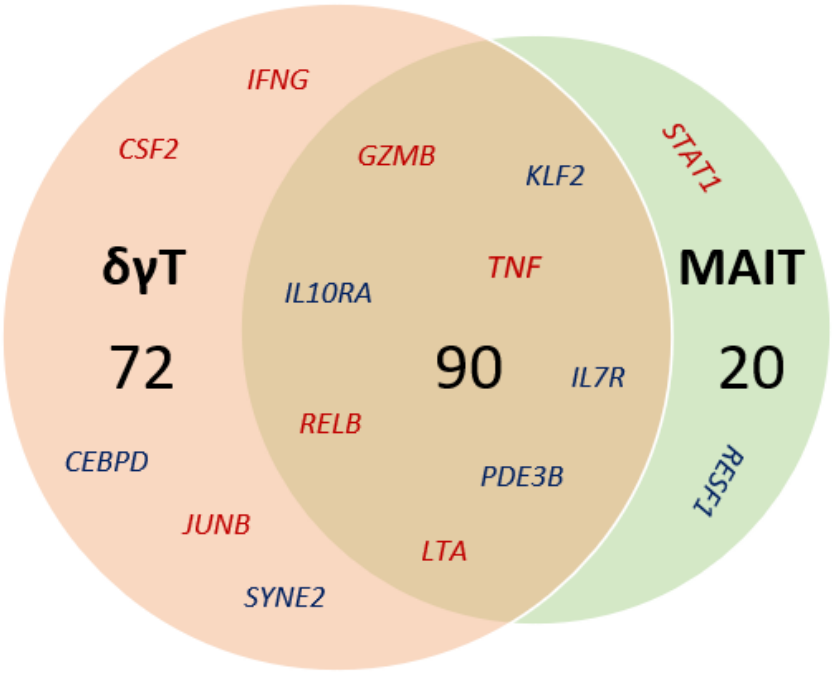


Figure 4-12 – Largely shared transcriptional profile between MAIT and γδT cells after stimulation with αCD3 and αCD28

Venn diagram of overlapping differentially expressed genes between MAIT and γδT cells upon TCR stimulation. Genes that were upregulated are depicted in red, with those downregulated in blue.

4.3.3.2.2 Cytokine stimulation

Following cytokine stimulation, 822 DEGs were observed in MAIT cells. Although there were signs of an activated phenotype upon stimulation, with an upregulation of *STAT1* and *NFKB1*[306] and downregulation of *KLF2* and *CD52*, the response was weak (Figure 4-14A (purple and black arrows) to D). Despite confirming expression of both cytokine receptors expressed by MAIT cells (Figure 4-13), a lack of key IL-12 and IL-18 specific transcriptional response characteristics, including upregulation of *IFNG*[304], supported concerns of an unsuccessful stimulation (Figure 4-14C). By contrast, an increase of fold change > 6 for *IFNG* expression in γδT cells upon cytokine stimulation was observed (Figure 4-14E, orange arrow).

When assessing cytokine-dependent transcriptional changes from conventional T cells, early signs of activation were suggested with upregulation of *STAT1* and *CD74*, but again without an increase of functional genes and with very few genes suppressed (Figure 4-14F and G, purple arrows). Therefore, I lacked confidence in the reliability of the data output from the cytokine stimulated conditions.

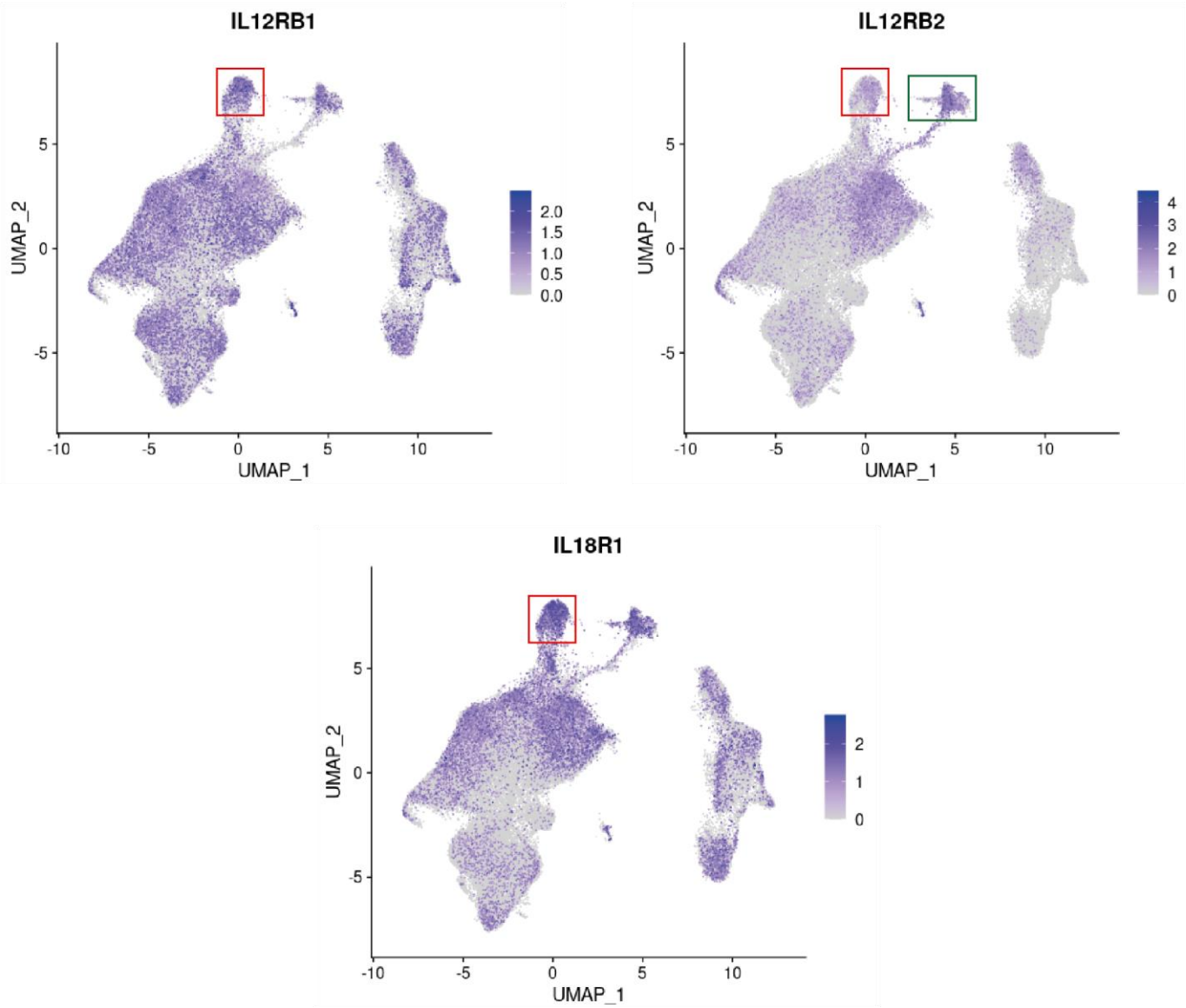
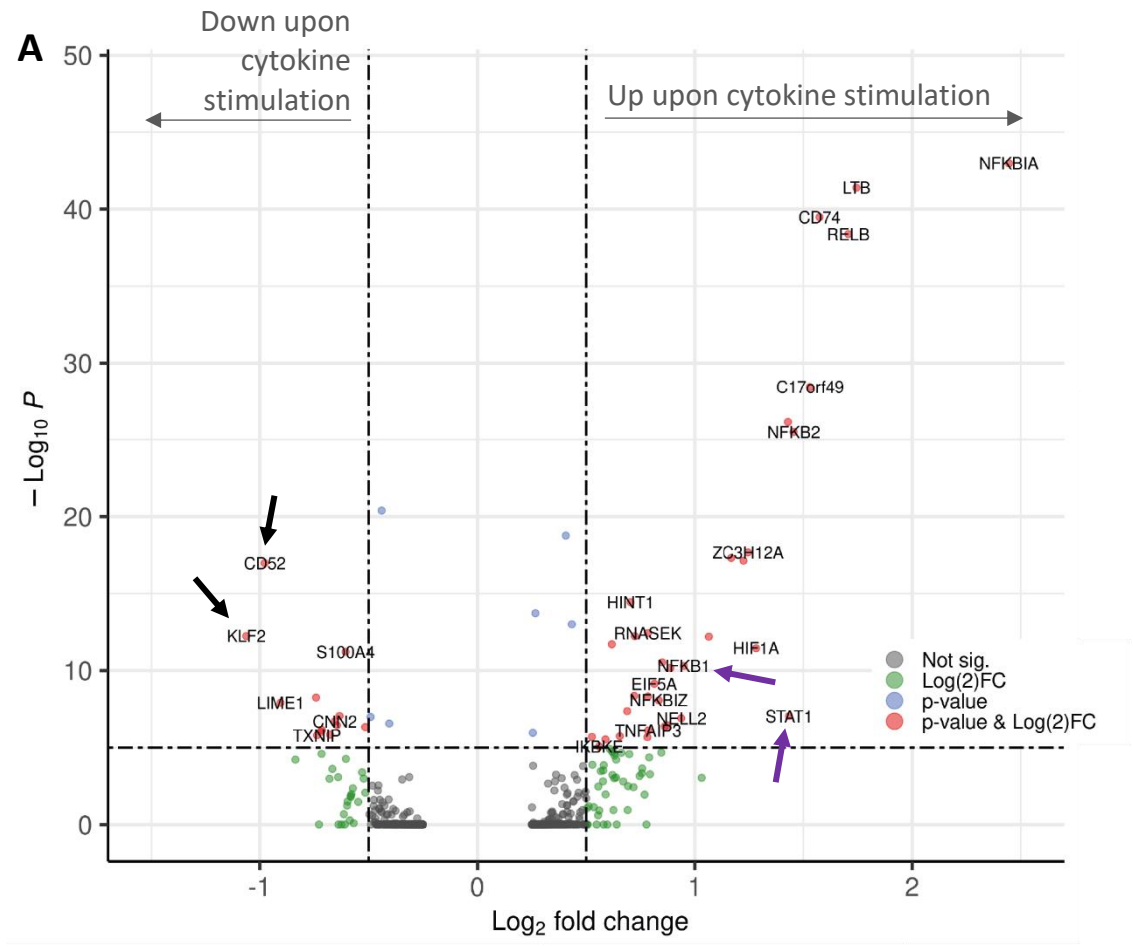
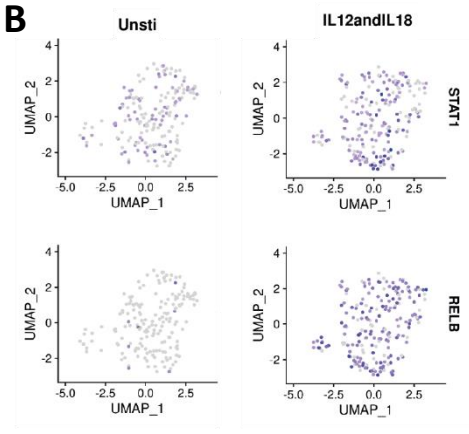
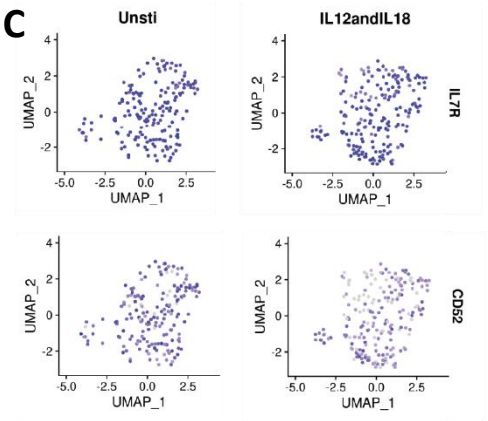


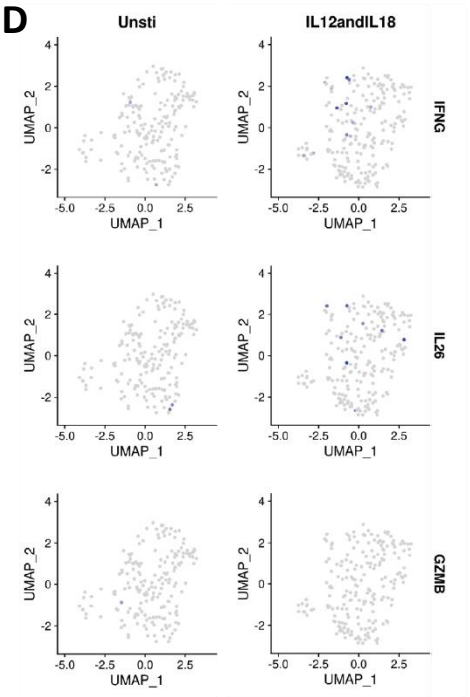
Figure 4-13 - MAIT cells expressed both IL-12 and IL-18 receptors

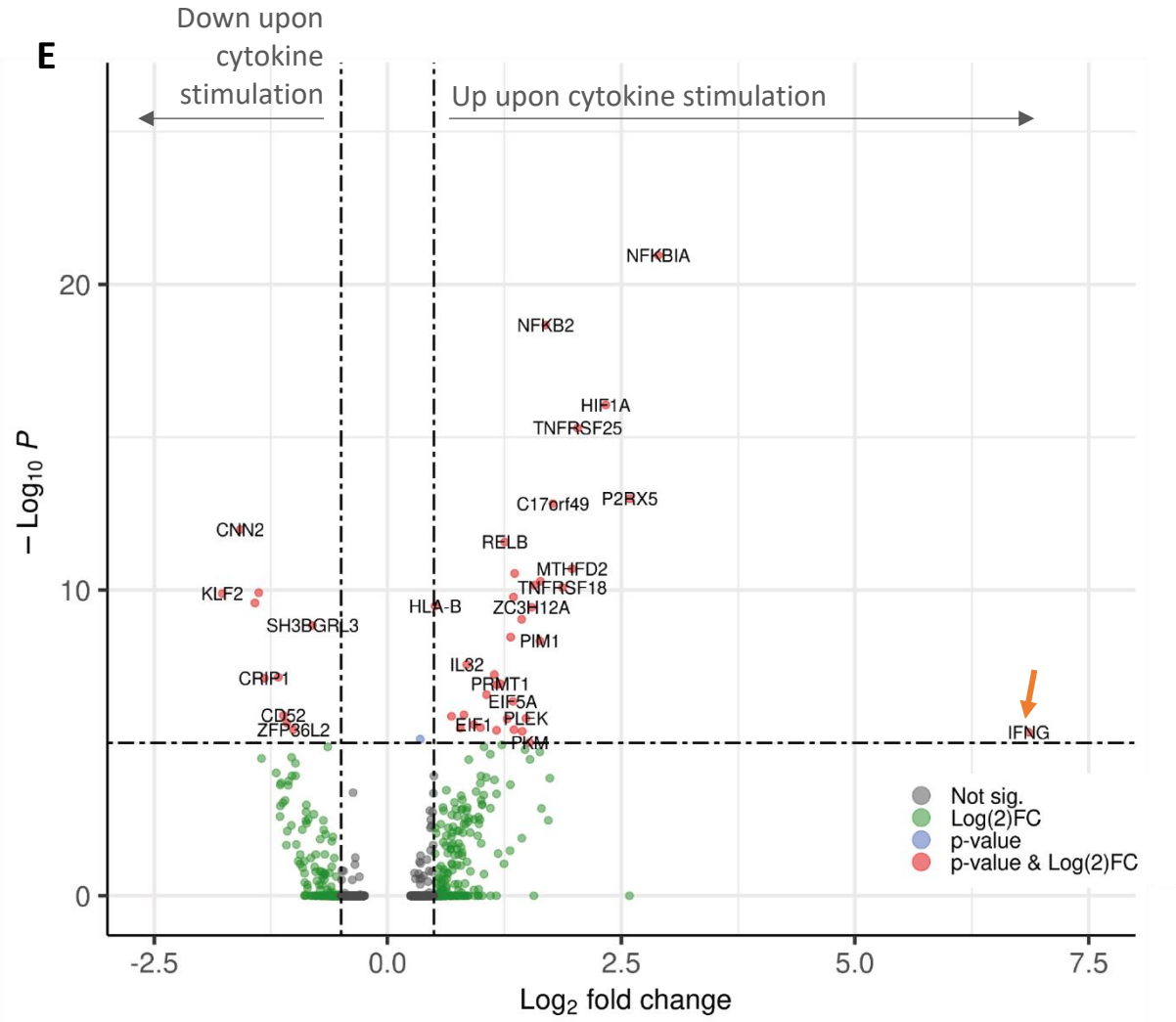
UMAPs of the relative expression of IL-12 (*IL12RB1* and *IL12RB2*) and IL-18 (*IL18R1*) receptors from all the $CD3^+$, $CD161^+$ cells sequenced, with the MAIT cell cluster highlighted by the red box. The green box depicts γδT cells.


A
Down upon cytokine stimulation
Up upon cytokine stimulation
NFKBIA
LTB
CD74
RELB
C17orf49
NFKB2
ZC3H12A
HINT1
RNASEK
HIF1A
NFKB1
EIF5A
NFKBIZ
NFLL2
TNFAIP3
IKBKE
STAT1
CD52
KLF2
S100A4
LIME1
CNN2
TXNIP
Not sig.
Log(2)FC
p-value
p-value & Log(2)FC
−Log10 P
Log2 fold change

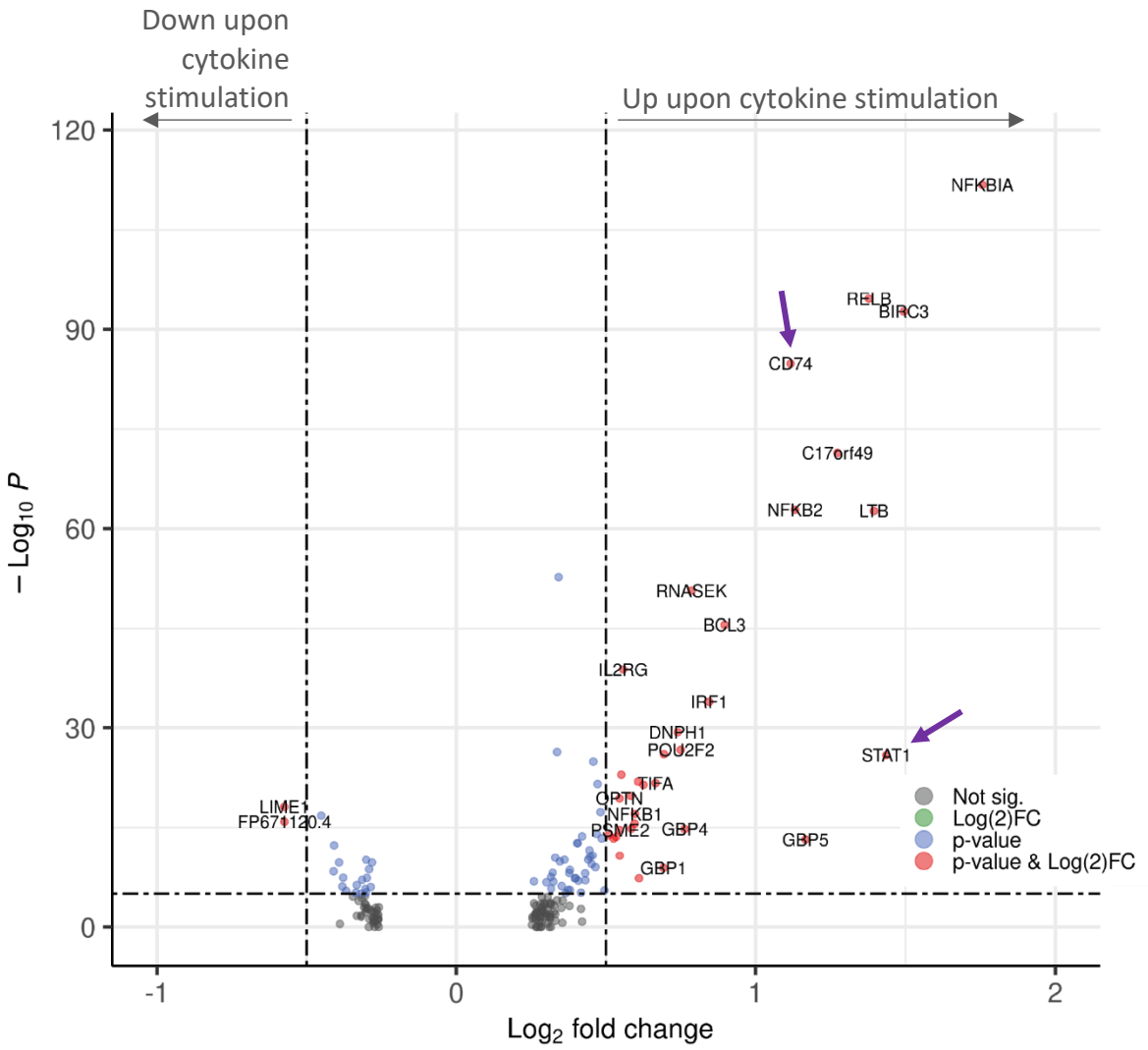

B
Unsti
IL12andIL18
STAT1
RELB
UMAP_1
UMAP_2


C
Unsti
IL12andIL18
IL7R
CD52
UMAP_1
UMAP_2


D
Unsti
IL12andIL18
IFNG
IL26
GZMB
UMAP_1
UMAP_2


E
Down upon cytokine stimulation
Up upon cytokine stimulation
NFKBIA
NFKB2
HIF1A
TNFRSF25
C17orf49
P2RX5
CNN2
RELB
MTHFD2
TNFRSF18
KLF2
HLA-B
ZC3H12A
SH3BGRL3
PIM1
IL32
CRIP1
PRMT1
EIF5A
CD52
ZFP36L2
EIF1
PLEK
PKM
IFNG
Not sig.
Log(2)FC
p-value
p-value & Log(2)FC
20
10
0
-2.5
0.0
2.5
5.0
7.5
– Log10 P
Log2 fold change

G


Down upon cytokine stimulation
Up upon cytokine stimulation
120
90
60
30
0
− Log10 P
-1
0
1
2
Log2 fold change
NFKBIA
RELB
BIRC3
CD74
C17orf49
NFKB2
LTB
RNASEK
BCL3
IL2RG
IRF1
DNPH1
POU2F2
STAT1
TIFA
OPTN
NFKB1
PSME2
GBP4
GBP5
GBP1
LIME1
FP671120.4
Not sig.
Log(2)FC
p-value
p-value & Log(2)FC

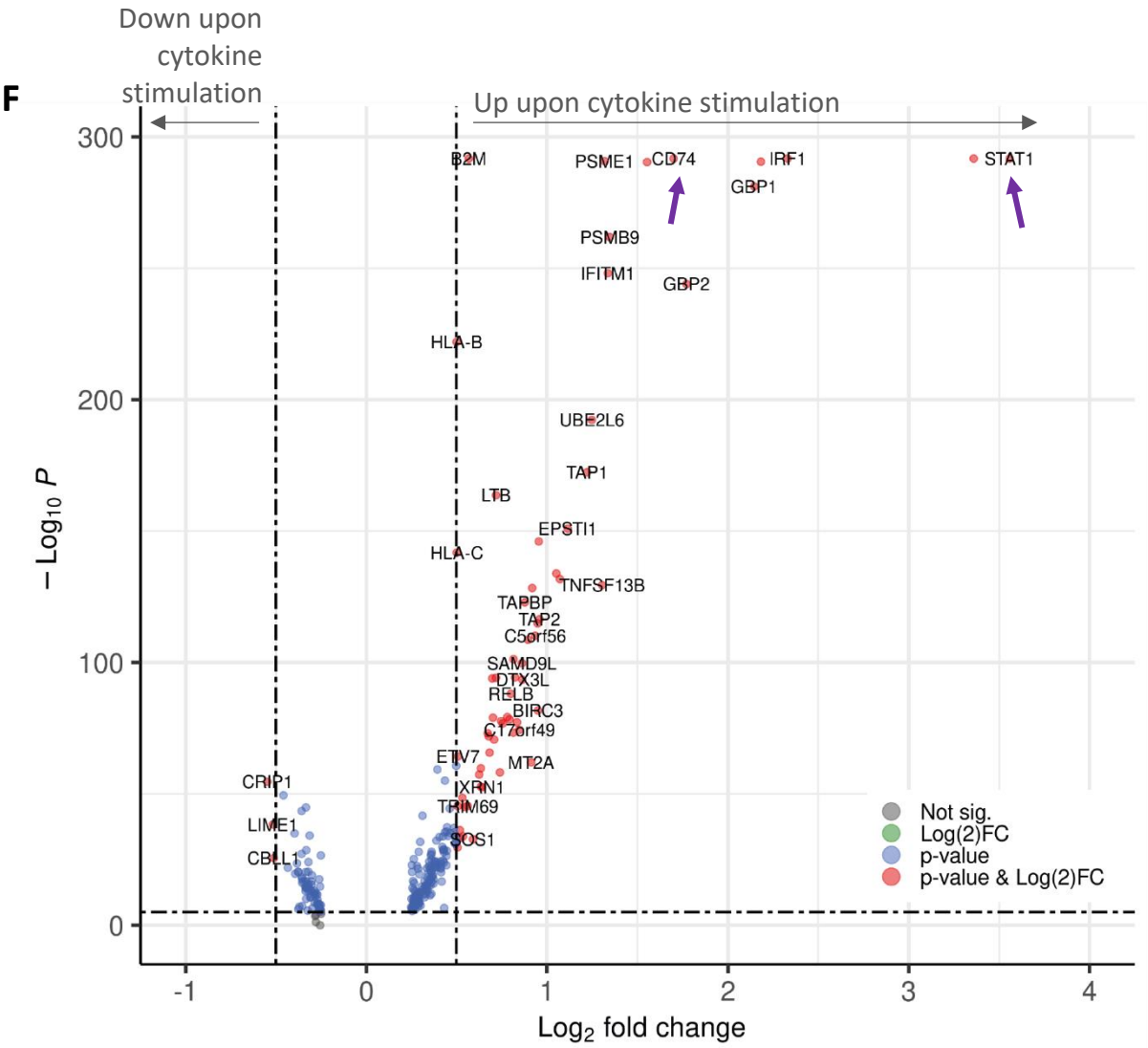


Figure 4-14 – Transcriptional changes in lymphocyte populations following IL-12 and IL-18 stimulation at pH 7.5

Volcano plots indicating genes upregulated and downregulated in MAIT cells (A), γδT cells (E), $CD8^+$ T cells (F) and Th17 cells (G), upon IL-12 and IL-18 stimulation at neutral pH. Coloured arrows depict genes referenced in the text. MAIT cell UMAPs coloured by the increased (B) and decreased (C) expression of most significant markers, as well as expression of key cytokine activation dependent genes (D), in unstimulated and stimulated conditions.

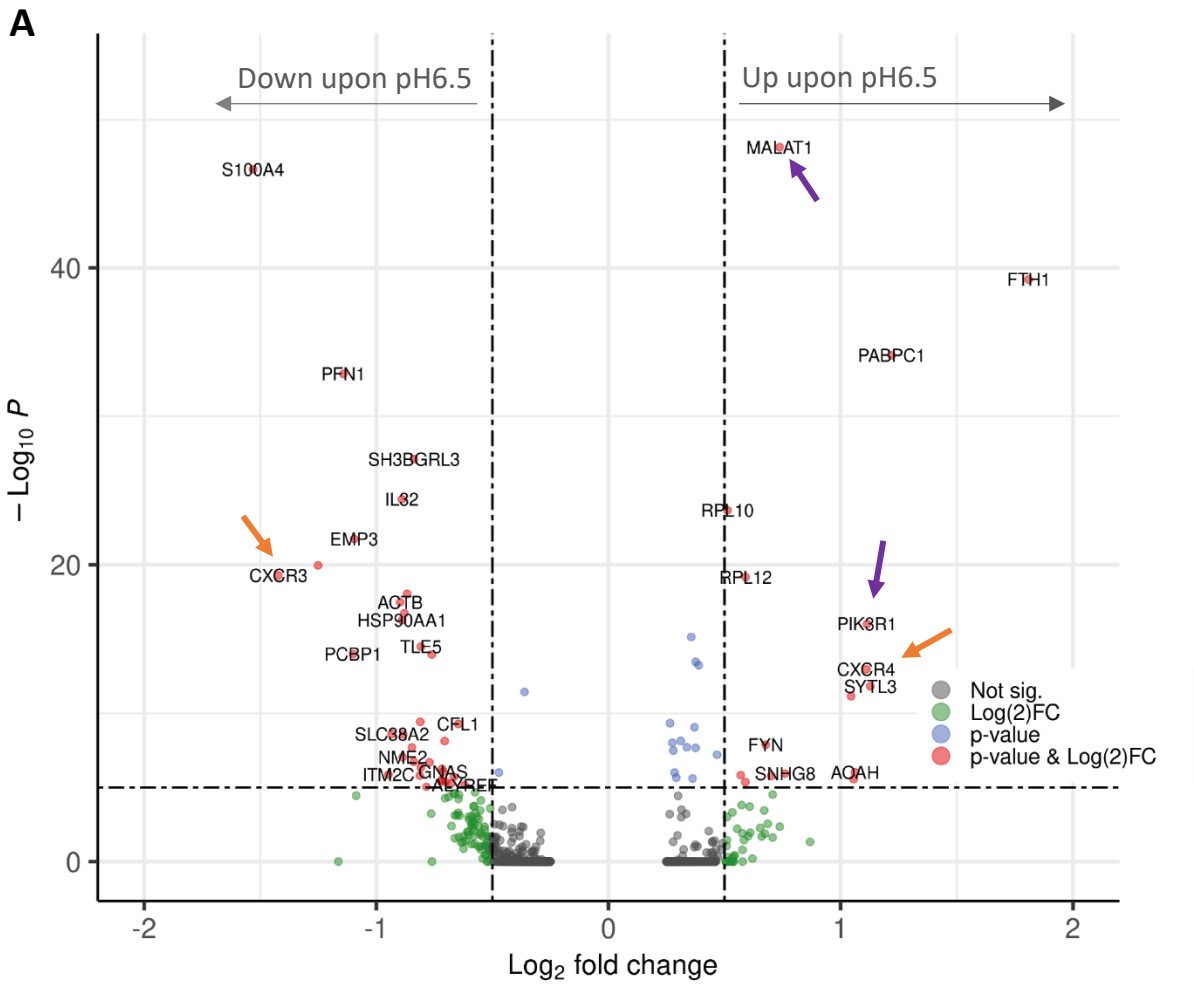
4.3.3.3 A low pH environment downregulated activatory and inflammatory gene markers

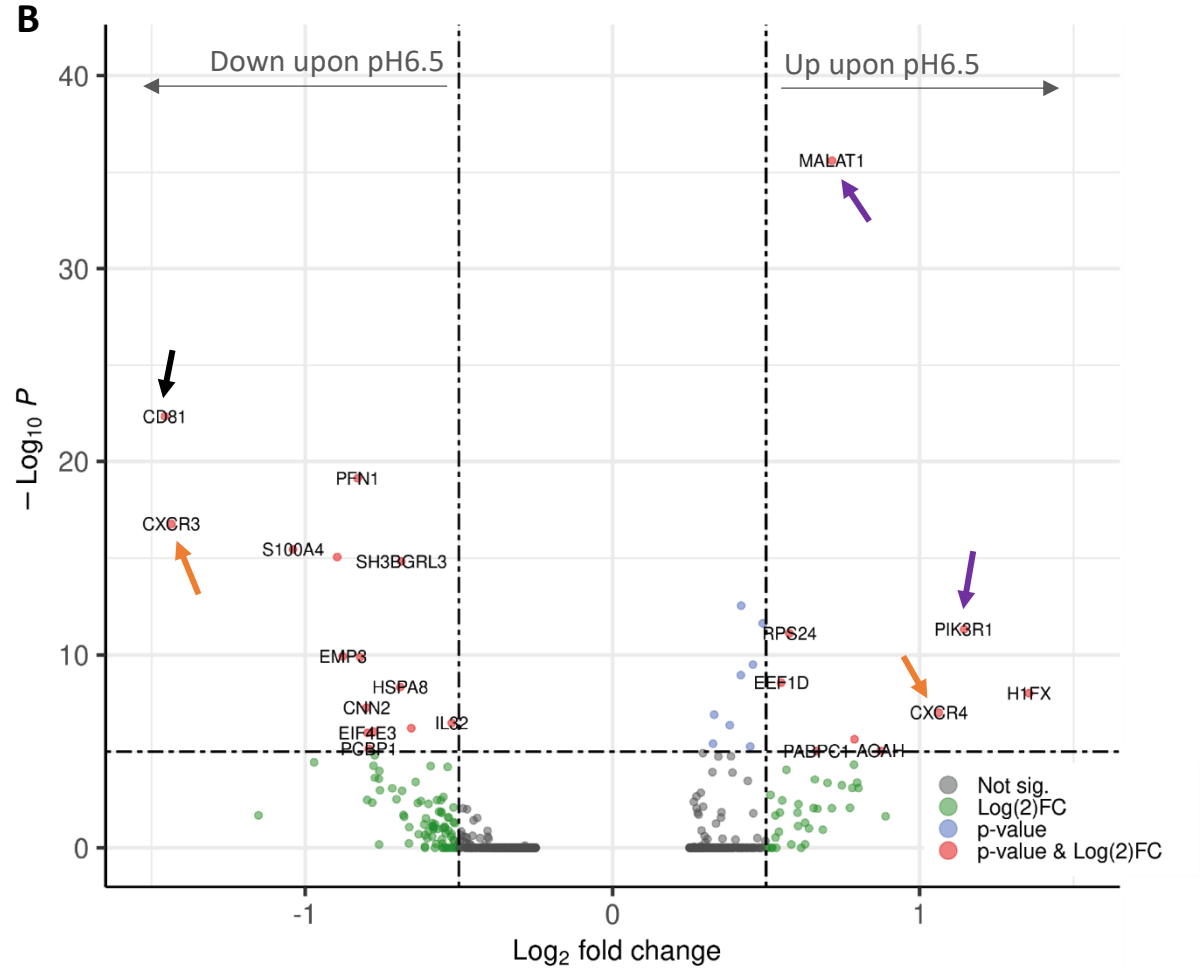
To address whether characteristics of the cells of interest were altered by a low pH environment specifically, I first begun assessing the effects of extracellular pH on unstimulated cells. Overall, very few genes were differentially expressed between the two cultures, with the most DEG recorded for the Th17 cluster (639 genes in total, but not all achieving significance thresholds set). A downregulation of the co-stimulatory receptor *CD81* was observed at a low pH for all four of the cell types analysed (Figure 4-15 (black arrow)); with increased expression of the T cell protective gene, *MALAT1* (Figure 4-15 (purple arrow)). It is of note, the innate-like T cells showed an upregulation of *PIK3R1,* upon culture at pH 6.5 (Figure 4-15A and B (purple arrow)). Fundamental genes involved with cell trafficking were significantly altered from cells cultured in acidic conditions; while *CXCR3* decreased in a low pH environment, *CXCR4* was upregulated (Figure 4-15A and B (orange arrows)). As CXCR3 has been implicated in inflammatory disease[307], I next wanted to see if the gene observations translated to protein changes. Validation of low pH effects on migration were observed from $CD8^+$ T cells, with the trend altered until at least 5 days (Figure 4-16), whilst fewer effects were observed for $CD4^+$ T cells.

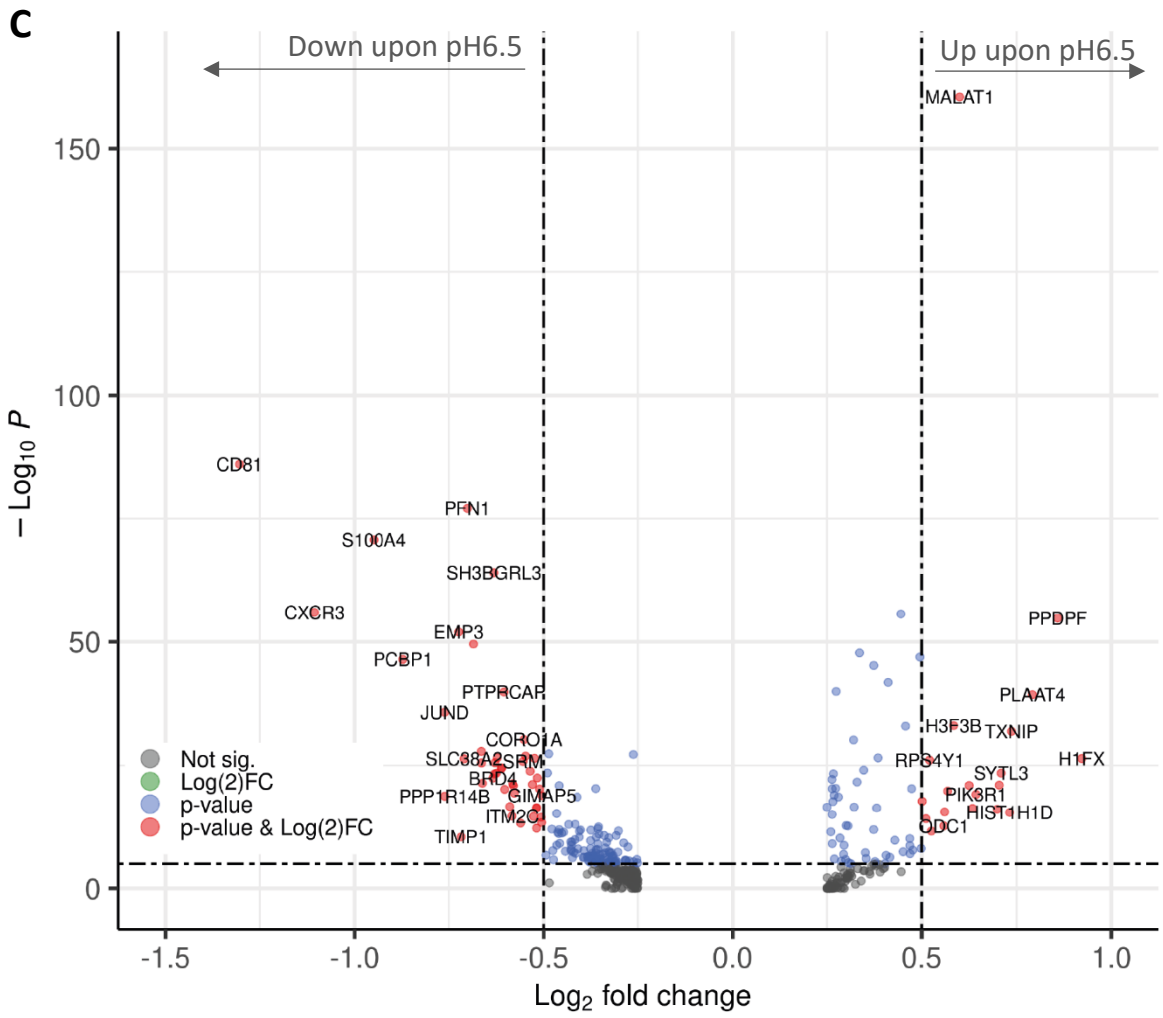
Having previously described the transcriptional profile observed upon TCR stimulation in section 4.3.3.2.1, I could next assess the pH-dependent changes between cells cultured at neutral and low pH. When stimulating non-target siRNA treated MAIT cells with αCD3 and αCD28 and culturing at pH 6.5, upregulation of genes described in resting and naïve T cells were observed (*IL7R, KLF2, MALAT1*). On the other hand, downregulation of activatory (*CD69, NFKBIA, SHMT2, PKM, RELB*), inflammatory (*TNF, LTA, LTB*) and tissue repair (*CCL3, VEGF*) markers was seen[308] (Figure 4-17A).

Although here I was not considering the role of GPR65 specifically (to be discussed in Chapter 5) downstream signalling of the receptor uses the cAMP pathway. Interestingly, in all cell types assessed, two cAMP related genes were shown to be upregulated at pH 6.5, *PDE3B* and *CREM* (Figure 4-18).

In summary my results show that culture of MAIT cells at pH 6.5 inhibits expression of genes associated with T cell activation and function, supporting in vitro protein results previously reported within this chapter. Similar genes changes were also seen in the other lymphocyte populations assessed (Figure 4-17B-D).


A
Down upon pH6.5
Up upon pH6.5
S100A4
MALAT1
FTH1
PABPC1
PFN1
SH3BGRL3
IL32
EMP3
CXCR3
RPL10
RPL12
ACTB
HSP90AA1
PCBP1
TLE5
PIK3R1
CXCR4
SYTL3
CFL1
SLC38A2
NME2
ITM2C
GNAS
ALYREF
FYN
SNHG8
AOAH
Not sig.
Log(2)FC
p-value
p-value & Log(2)FC
40
20
0
-2
-1
0
1
2
− Log10 P
Log2 fold change


B
Down upon pH6.5
Up upon pH6.5
MALAT1
CD81
PFN1
CXCR3
S100A4
SH3BGRL3
RPS24
PIK3R1
EMP3
HSPA8
EEF1D
H1FX
CNN2
CXCR4
EIF4E3
IL32
PCBP1
PABPC1
AOAH
Not sig.
Log(2)FC
p-value
p-value & Log(2)FC
40
30
20
10
0
-1
0
1
– Log10 P
Log2 fold change


C
Down upon pH6.5
Up upon pH6.5
MALAT1
150
100
50
0
− Log10 P
CD81
PFN1
S100A4
SH3BGRL3
CXCR3
EMP3
PCBP1
PTPRCAP
JUND
CORO1A
SLC38A2
SRM
BRD4
PPP1R14B
GIMAP5
ITM2C
TIMP1
PPDPF
PLAAT4
H3F3B
TXNIP
RPS4Y1
H1FX
SYTL3
PIK3R1
HIST1H1D
ODC1
Not sig.
Log(2)FC
p-value
p-value & Log(2)FC
-1.5
-1.0
-0.5
0.0
0.5
1.0
Log2 fold change

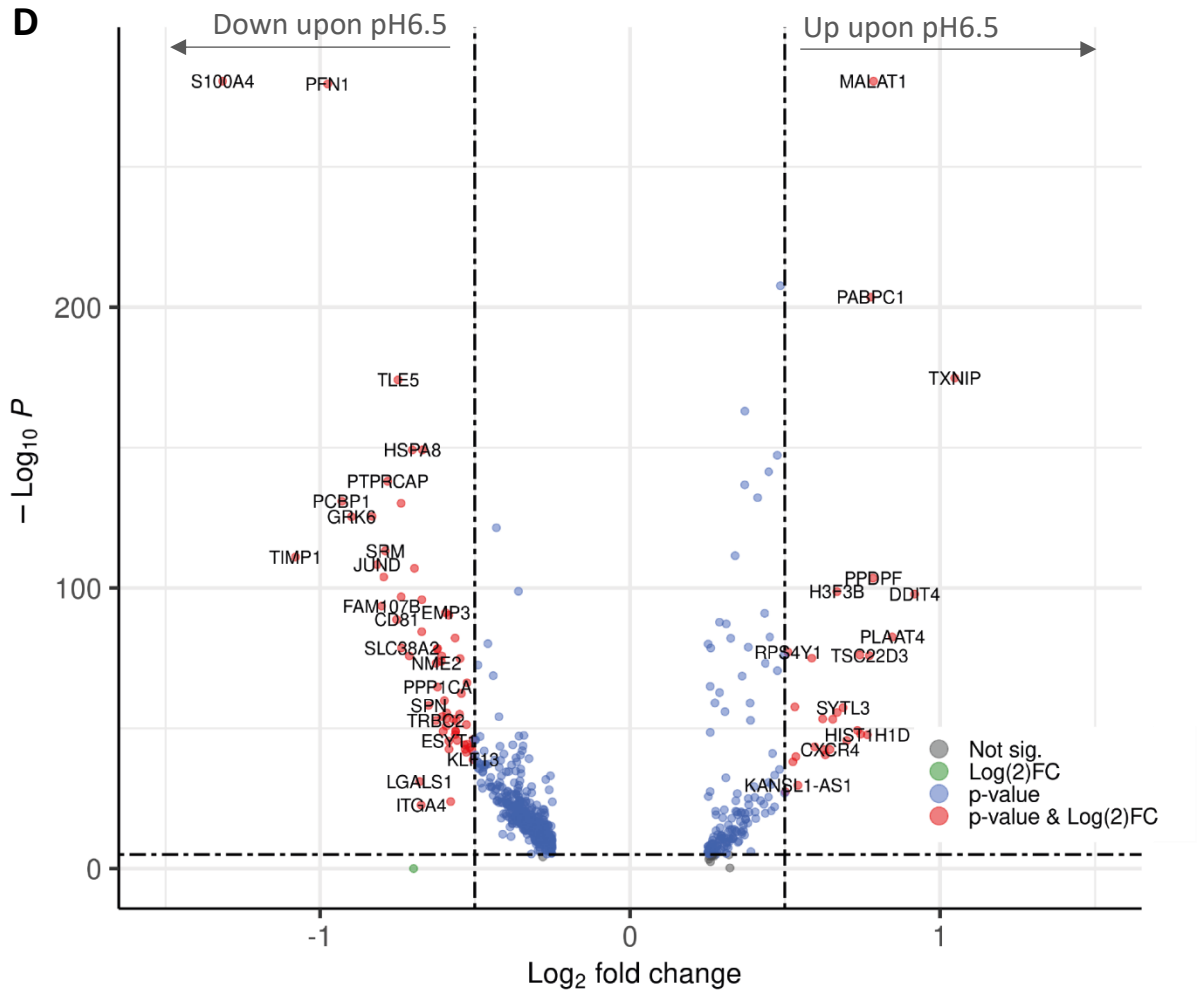


Figure 4-15 – Changes in expression level of genes associated with T cell migration following culture at pH 6.5

Volcano plots indicating genes upregulated and downregulated in MAIT cells (A), γδT cells (B), conventional $CD8^+$ T cells (C) and Th17 cells (D) at low pH, compared to those at neutral pH, without stimulation. Coloured arrows depict genes referenced in the text.

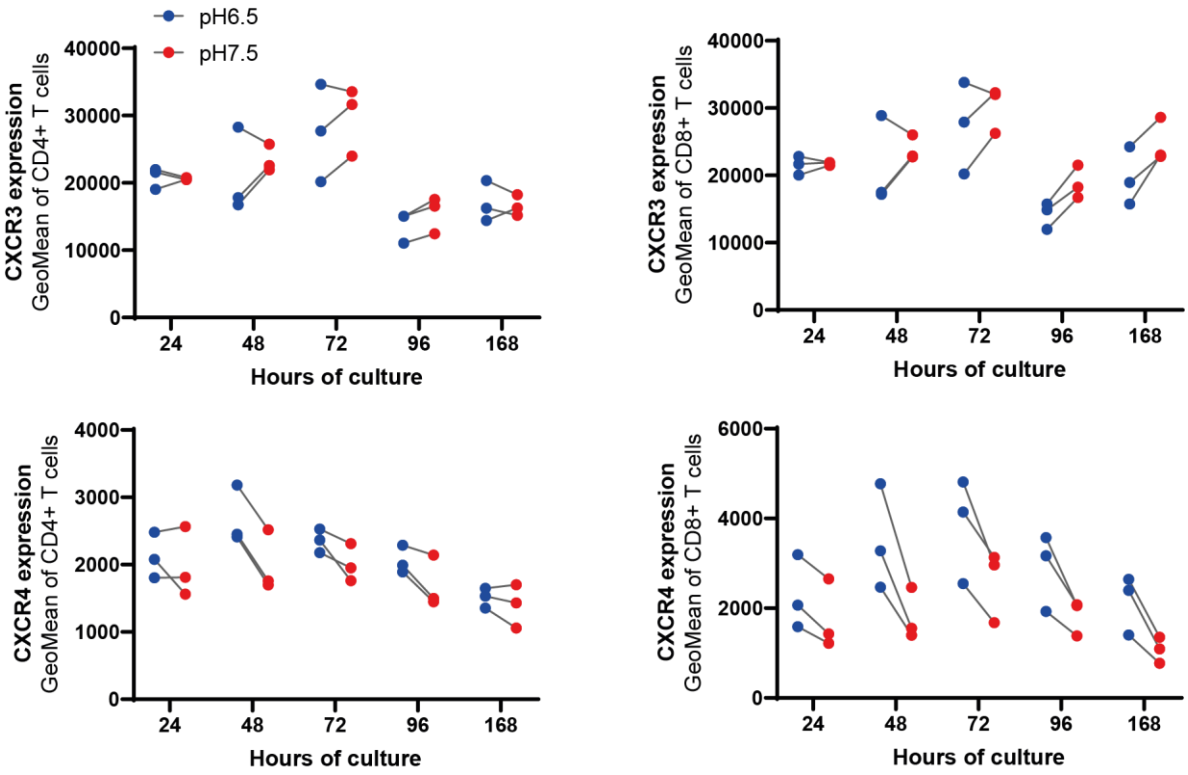
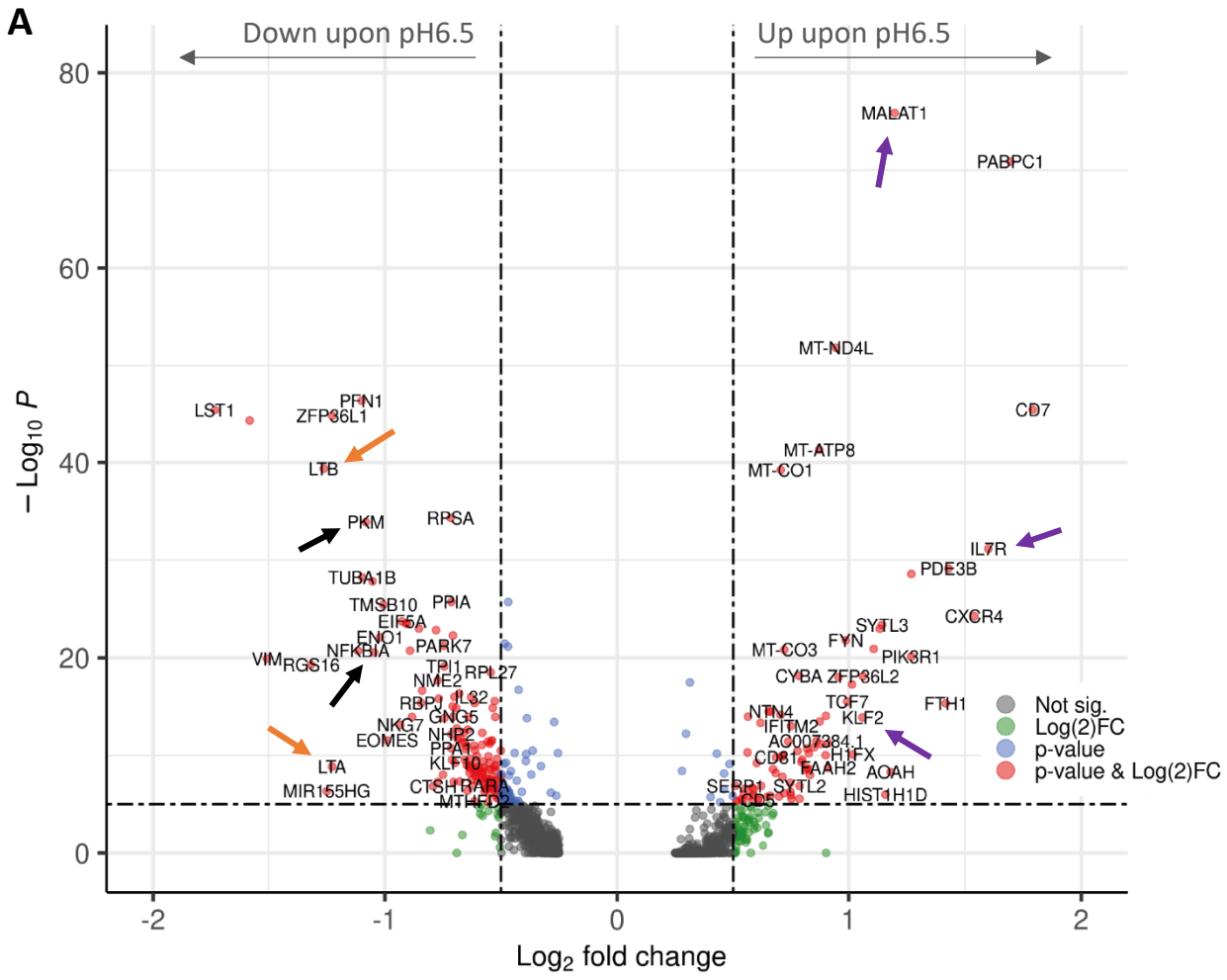
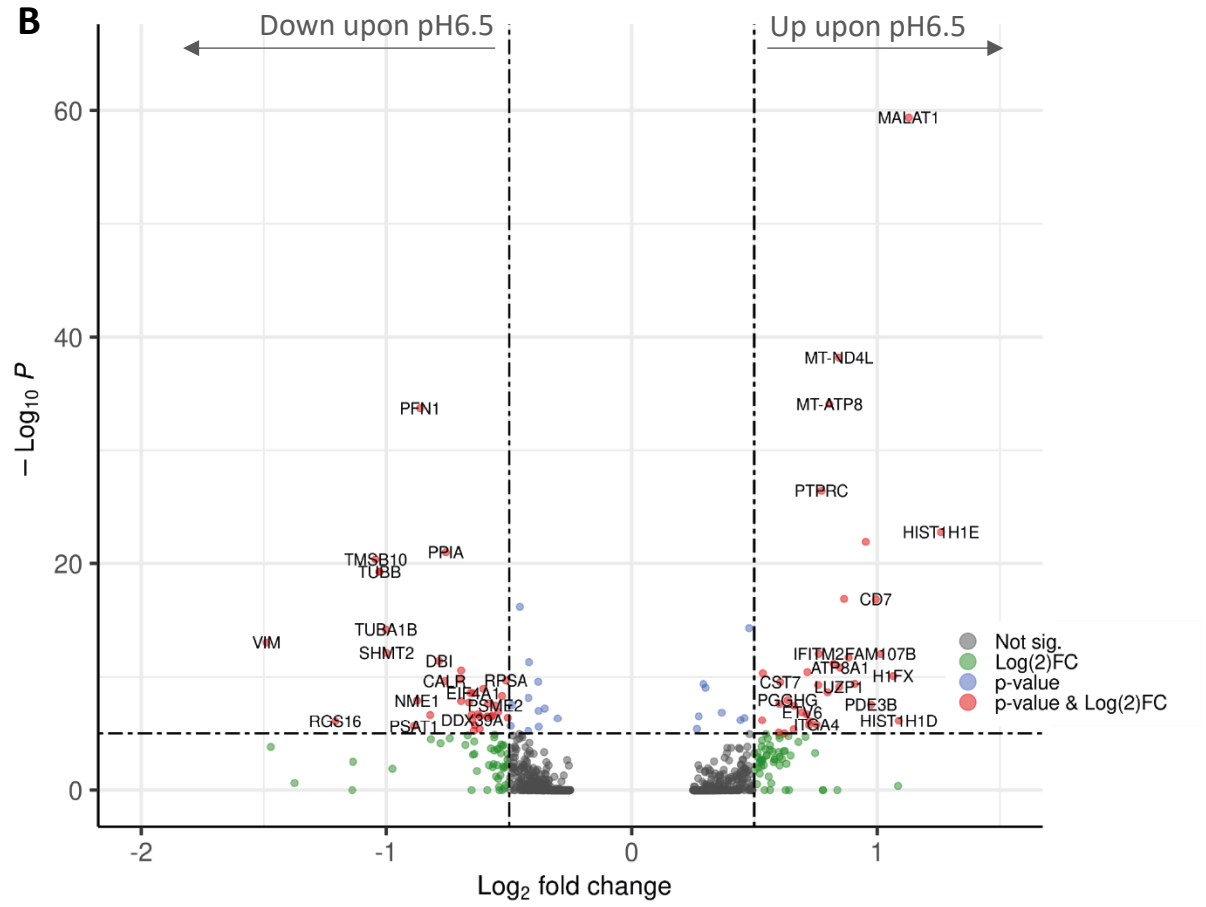
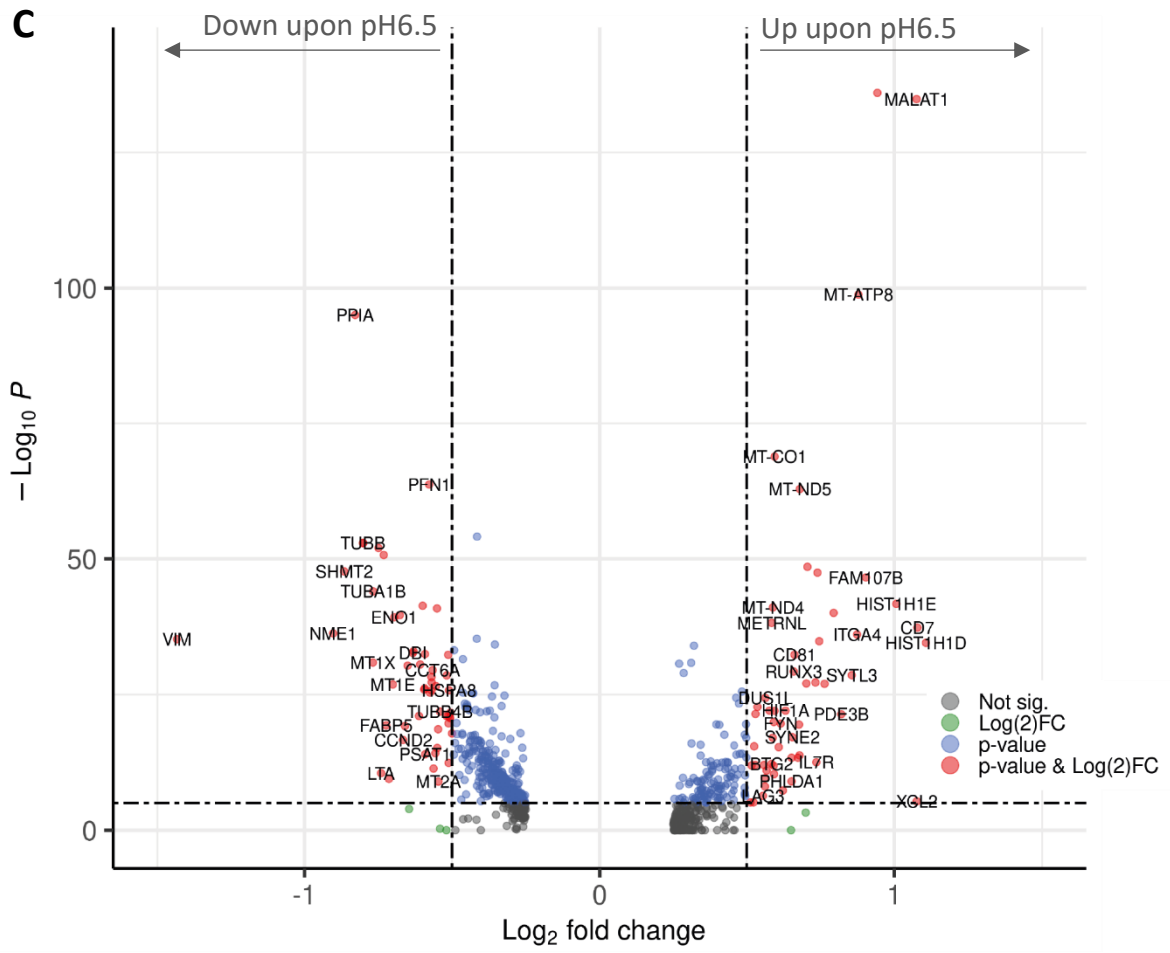


Figure 4-16 – Low pH had different effects on $CD4^+$ and $CD8^+$ T cell expression of CXCR3 and CXCR4

PBMCs were isolated and cultured for up to 7 days (n=3). The geometric mean of extracellular CXCR3 and CXCR4 expression on $CD3^+$ T cells subsets were assessed. Cells cultured at a low pH are depicted in blue, whilst those at pH 7.5 are in red. Statistical significance was not observed upon performing a paired Student's t-test between culture conditions.


A
Down upon pH6.5
Up upon pH6.5
80
60
40
20
0
− Log10 P
-2
-1
0
1
2
Log2 fold change
MALAT1
PABPC1
MT-ND4L
CD7
MT-ATP8
MT-CO1
IL7R
PDE3B
CXCR4
SYTL3
FYN
PIK3R1
MT-CO3
CYBA
ZFP36L2
FTH1
TCF7
KLF2
NTN4
IFITM2
AC007384.1
CD81
H1FX
FAAH2
AOAH
SERPR1
SYTL2
HIST1H1D
CD5
LST1
PFN1
ZFP36L1
LTB
PKM
RPSA
TUBA1B
TMSB10
PPIA
EIF5A
ENO1
PARK7
NFKBIA
VIM
RGS16
TPI1
RPL27
NME2
RBPJ
IL32
NKG7
GNG5
EOMES
NHP2
PPA1
KLF10
LTA
MIR155HG
CTSH
RARA
MTHFD2
Not sig.
Log(2)FC
p-value
p-value & Log(2)FC


B
Down upon pH6.5
Up upon pH6.5
60
40
20
0
− Log10 P
-2
-1
0
1
Log2 fold change
MALAT1
MT-ND4L
MT-ATP8
PFN1
PTPRC
HIST1H1E
PPIA
TMSB10
TUBB
CD7
TUBA1B
VIM
SHMT2
DBI
CALR
RPSA
EIF4A1
NME1
PSME2
RGS16
PSAT1
DDX39A
IFITM2
FAM107B
ATP8A1
H1FX
CST7
LUZP1
PGGHG
PDE3B
ETV6
ITGA4
HIST1H1D
Not sig.
Log(2)FC
p-value
p-value & Log(2)FC


C
Down upon pH6.5
Up upon pH6.5
MALAT1
MT-ATP8
PPIA
MT-CO1
PFN1
MT-ND5
TUBB
SHMT2
TUBA1B
FAM107B
HIST1H1E
ENO1
MT-ND4
METRNL
CD7
ITGA4
HIST1H1D
VIM
NME1
CD81
DBI
MT1X
CCT6A
RUNX3
SYTL3
MT1E
HSPA8
DUS1L
HIF1A
PDE3B
TUBB4B
FABP5
RYR
CCND2
SYNE2
PSAT1
BTG2
IL7R
LTA
MT2A
PHLDA1
LAG3
XCL2
Not sig.
Log(2)FC
p-value
p-value & Log(2)FC
100
50
0
-1
0
1
$-\mathrm{Log}_{10}\,P$
Log_2 fold change

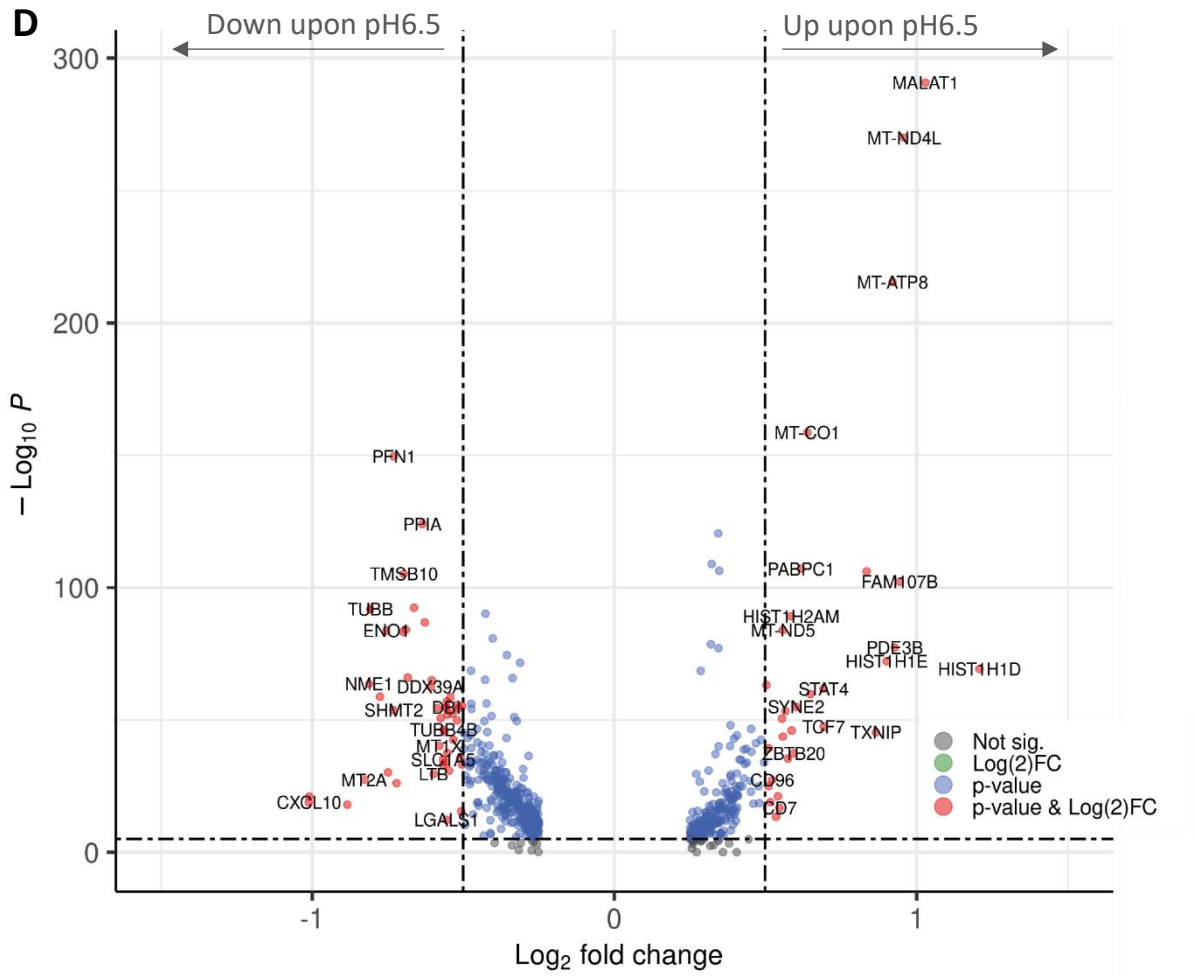


Figure 4-17 – Transcriptional changes in MAIT cells were consistent with the suppression of TCR-driven inflammation in a low pH environment

Volcano plots indicating genes upregulated and downregulated in MAIT cells (A), γδT cells (B), conventional $CD8^+$ T cells (C) and Th17 cells (D) at low pH, compared to those at neutral pH, upon stimulation through the TCR. Coloured arrows depict genes referenced in the text.

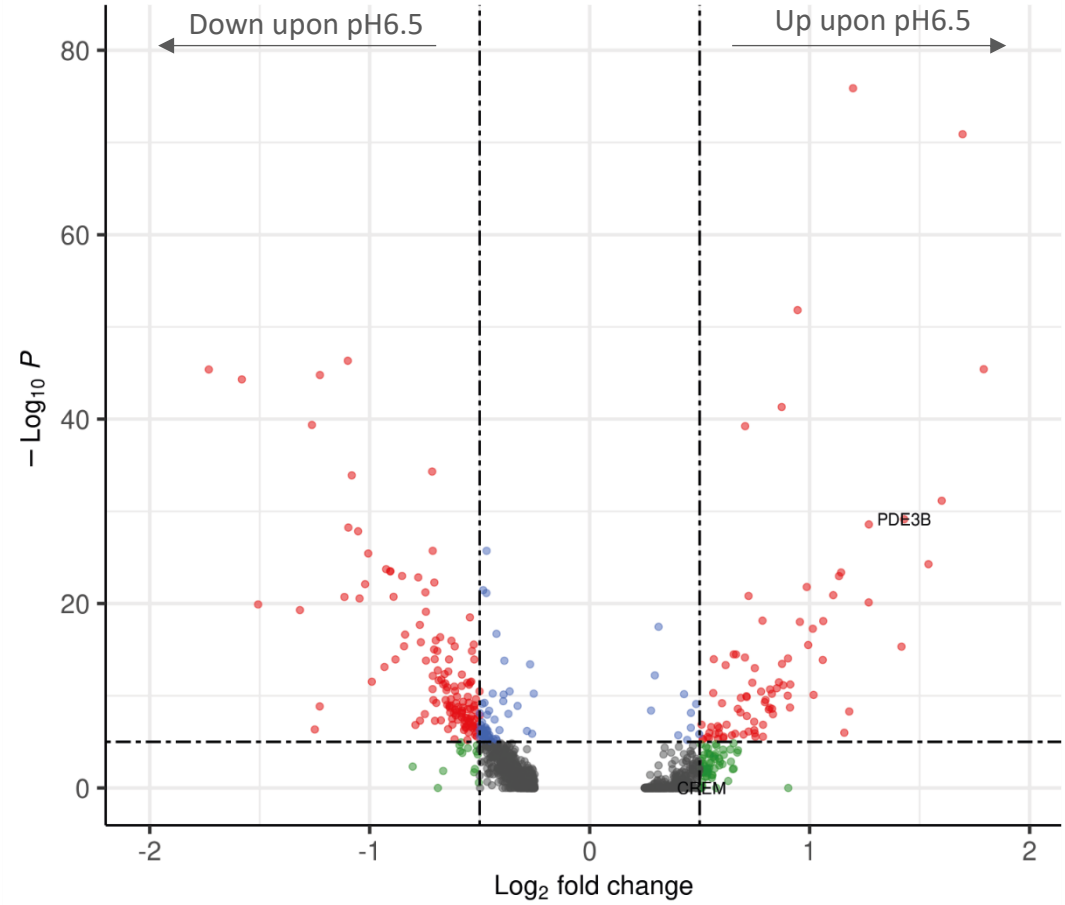


Figure 4-18 – *PDE3B* and *CREM* genes are upregulated in an acidic environment

Volcano plot indicating the upregulation of *PDE3B* and *CREM* in MAIT cells compared to those at neutral pH, upon stimulation through the TCR. This plot is representative of all other cell types assessed.

4.4 Discussion

Extracellular acidosis is a feature of tumour microenvironments, infection response and inflammatory processes[292,309]. Although a wealth of literature discusses the acidic nature of cancers, including solid tumours and lymphomas with high glycolytic activity[310,311], more relevant studies have shown a low pH signature from synovial fluid in the joints of rheumatoid arthritis patients[203,312,313]. In this chapter, through the development of a stable bicarbonate-based culture system, I have reliably shown the suppression of inflammation from immune cells when exposed to an acidic extracellular environment, particularly MAIT cells.

The improved survival of T cells cultured at a low pH, compared to neutral conditions, provides further interest into investigating GPR65's response to extracellular pH changes (to be discussed in Chapter 5), as the receptor is thought to trap cells at the G_0/G_1 phase of the cell cycle, and promote proliferation[178,314,315]. Broadly, T cells were the focus of this work and as such data was not collected for alternative PBMC subtypes; however, it would have been interesting to assess if others also shared improved viability at a low pH environment, as well as further investigating the biology behind the difference, such as if cells were protected from apoptosis.

Functional effects of extracellular pH have been studied across multiple immune cells, reporting both stimulatory and inhibitory effects, depending on the cell type and function analysed. Two of the key cell types within the innate immune system, neutrophils, and dendritic cells, have been shown to become activated and enhance their antigen presentation properties upon incubation at pH 6.5[316,317]. Here I show the suppression of inflammation from monocytes in response to low extracellular pH. Upon stimulation with LPS, an agonist of TLR4, monocytes cultured at pH 6.5 had reduced TNFα and IL-6 production, compared to pH 7.5.

My data reproduces the inhibition of TNFα observed in isolated macrophages by Heming *et al*[318], whilst consistent with the selective increase of IL-1β from the same cells. However, the change to IL-1β production is thought to be due to changes of intracellular pH, rather than be driven by the recognition of excess protons outside the cell[319–321].

As for another key innate cell type, the data presented here mirrors the repression of Th1-driven cytokine release from NK cells upon culturing at a low pH[322], as well as suppression of GM-CSF, a reported driver of inflammatory arthritis[323]. These results were achieved through methods of stimulation not directly activating this cell type, suggesting the importance of studying immune cell function in the context of a mixed cellular system. Notwithstanding GPR65 mRNA expression levels within NK cells, there is still little evidence of their involvement in AS, thus I focused my efforts on T cells.

The role of extracellular pH on T cell function is less contested, with $CD8^+$ T cells in particular presenting consistent constrained activation (reduced CD69 expression compared with cells cultured at neutral pH) and inhibition of TNFα and IFNγ release in acidic conditions[324–326]. My data supports the suppression of Th1 driven cytokines for all T cell types assessed, regardless of stimulation or cells cultured in isolation, and digs deeper into subsets of $CD8^+$ T cells to show the most striking suppressive effects of low pH on MAIT cells, compared to less inflammatory cells expressing lower levels of CD161. To my knowledge, the MAIT cell response to pH has not specifically been reported before. However, it does reflect the results of bile acid, assumed to lower the pH of the extracellular environment, having been shown to hinder MAIT cell activation and pro-inflammatory cytokine release, upon stimulation[327].

GM-CSF and IL-17A are each reported to possess anti- and pro-inflammatory properties, dependent on their location and disease context[328–330]. This complicated biology could explain

why a low pH environment results in different profiles of their release between cell types, perhaps between more conventional lymphocytes and those which are slightly more innate-like in their function; $CD4^+$ T cells were confirmed to increase GM-CSF production in response to extracellular acidosis[75], whilst from MAIT cells and NK cells, GM-CSF was suppressed. So, continuing to address the role of low pH on immune cells, I decided to focus my attention on understanding acidosis on type 1 inflammation.

My data confirmed the strongest activation through the combination of TCR and IL-12+IL-18 stimulation[303,331], particularly for IL-17 production. However, it has been shown that MAIT cell activation by TCR-dependent and TCR-independent methods are transcriptionally distinct[304,332]. Therefore, when using scRNAseq to address my primary question of unravelling GPR65 function in immune cells, I decided to keep both activation methods separate and investigate whether the receptors activity differed upon distinct activation of this innate-like T cell.

Using an unsupervised approach for clustering of cell types within the experiment, a wide range of cell types were included within my assay. As established gene markers were present (eg. *FOXP3* for Treg cells, *CXCR5* for T follicular helper cells[333] and CCR6 and CXCR3 for Th17.1 cells[334]) and generated clustering which made biological sense, I did not believe siRNA treatment within the samples affected the identification of cell type clusters.

Multiple cell types have been implicated in ankylosing spondylitis pathology, particularly those capable of producing an IL-17 signature. When deciding to assess various cell types within the scRNAseq experiment, I compared subsets which have been reported to be involved in AS inflammation (γδT and Th17 cells[96,131]) to conventional $CD8^+$ T cells. By

including γδT, along with the MAIT cells, I was also able to address the question of whether pH effects differed between innate-like cells, and conventional T cells.

A limitation within my experiment is the lack of a control group for $CD161^-$ T cells. Cells expressing CD161 have been shown to possess a pro-inflammatory phenotype, with a shared transcriptional phenotype reported[116]. Although a key marker of MAIT cells, the other cell types included and compared to, will not be a true representation of that whole cell type. For example, the effects of the more inflammatory, Vδ2 γδT cells have likely been captured through the sorting method, but not Vδ1 γδT cells[129], although without the ability to sequence their TCR, one cannot be sure.

It is of note, the three MAIT cell subclusters identified in non-target siRNA treated cells at pH 7.5 were not reflective of those recently reported by Garner and colleagues[304]. Although I used the same timepoints and comparative stimulation concentrations, many other factors could explain the differences, including the presence of other cell types within the assay and with the addition of siRNA in the culture, which could have altered gene transcription.

Upon stimulation, not only were there convincing features of activation and functional changes, but key genes identified to be TCR stimulation specific were also upregulated in those cells cultured with anti-CD3 and anti-CD28 (*CCL4, TNFRSF9* and *TNF*), providing confidence in the assay, as well as suggesting the non-target siRNA did not affect the cells' ability to successfully respond to TCR engagement[304].

GPCRs coupled to $G_{q/11}$ subunits have been shown to signal through the PI3K/AKT pathway and promote cell proliferation and survival[335,336]. As upregulation of *PI3KR1* was observed in a low pH environment, one could hypothesise the improved cell survival reported at the beginning of this chapter could be through active signalling of the PI3K pathway. Recent work

by Pillai and colleagues support this by showing activation of GPR68 at pH 6.5, a close relative of GPR65, and subsequent phosphorylation of Akt in a breast cancer cell line[337]. Nevertheless, further work on identifying the proton-sensing receptor responsible here would be required to answer this theory, particularly as activation of TRPV1 can also signal through the same pathway[338].

Even without a stimulatory signal to the cells, at pH 6.5 gene changes were already directing cells to become less susceptible to activation and subsequent differentiation into pathogenic Th1 and Th17 cells, through altered expression of *CD81* and *MALAT1*[339], overall supporting an anti-inflammatory effect of extracellular acidosis. As a chemokine receptor, CXCR3 is involved in the recruitment of immune cells to inflamed sites and as such is associated with poor prognosis of chronic diseases[340]. Here, I have validated that a low pH environment reduced expression of *CXCR3,* further suggesting its anti-inflammatory effects on cell phenotype. Effects to migration-related chemokine receptors were of interest, particularly considering this finding in the context of GPR65, as aberrant GPR65 expression has been shown to influence immune cell recruitment[191,192,209].

In support of the functional data obtained, an overall suppression of cell activation and function was observed, favouring a resting transcriptional profile at low pH; also speaking to the loss of clustering within stimulated MAIT cells at pH 6.5.

As discussed, a caveat of this gene data set was that it only assessed changes in $CD161^{+}$ T cells, so the question remains whether these striking effects of pH 6.5 are hallmark changes to already probed inflammatory phenotypes. However, when considering the functional data from $CD8^{+}$, $CD161^{lo}$ T cells, the suppressive nature of extracellular acidosis is believed to be true for more naïve-like T cell types too.

I have previously introduced how activation of GPR65 signals through the cAMP pathway (section 1.2.2). It was exciting to see an upregulation of cAMP-related genes from those cells cultured in a low pH environment, and potentially being driven through GPR65 pH sensing. cAMP levels were not assessed from primary cells cultured at pH 6.5, but high levels were suggested due to the increase of *PDE3B*; this phosphodiesterase inhibits cAMP as part of an internal feedback loop to regulate the complex pathway[341].

The cAMP-responsive element modulator, CREM, becomes phosphorylated through the binding of PKA, dependent on high levels of cAMP in the cell. This gene has been shown to be upregulated in tumour associated macrophages (TAM) taken from advanced hepatocarcinoma patients, which bare an acidic signature[342,343]. And as IL-2 production from T cells is inhibited (and subsequent attenuation of response) upon CREM binding the IL-2 promoter[344,345], this further supported a reduced T cell activation state in acidic conditions.

Depending on the context, it appears some immune cells can recognise acidosis as a 'danger' signal, therefore activating part of the innate response. While cells of the adaptive system are likely to become suppressed, and in turn reduce and control inflammation. In the context of the widely studied effect of acidosis in cancer, its suppressive nature is believed to be the tumours way of defending itself from the host immune system and promoting cancer cell survival. An increase of immune checkpoint receptors has been reported on T cells from oesophageal adenocarcinoma patients in a low pH environment, downregulating their inflammatory response[326]. Additionally, Bohn and colleagues observed acidosis to alter the TAM phenotype in melanoma, thereby promoting tumour growth[225]. As a result of this, marketed therapeutics, and drugs in development are either targeting direct low pH changes on immune cells or preventing H+ ion export from the tumour cells[346,347].

When considering the role of pH in immune mediated diseases, although very rare, negative outcomes on the function of the immune system due to renal tubular acidosis have been reported in systemic lupus erythematosus and Sjögren's Syndrome[348,349]. Although there is no direct evidence of low pH at inflammatory sites within ankylosing spondylitis, in other diseases where joint inflammation occurs, acidity of the synovial fluid has been observed[350,351], with this low pH environment likely driven by highly glycolytic synovial lymphocytes[75,352]; moreover, the pH of local inflamed tissue is yet to been reported. We know that circulating lymphocytes in AS patients exhibit a proinflammatory phenotype[97] and their migration to inflamed joints is likely. In a closely related SpA, it has been reported that the diseased synovial fluid taken from PsA patients is enriched with the CXCR3 ligands, CXCL9 and CXCL10[108]. Together with reports that $CD8^+$ T cells from the same joint have been shown to highly express CXCR3[108,353], it is reasonable to think these pathogenic cells have been recruited from the periphery.

In the context of local pockets of acidity identified in the lymph node, Wu and colleagues suggest the low pH environment, created by the T cells themselves, acted in a negative feedback manner, to protect the undesired release of cytokines[354]. So, from work presented here, one could hypothesise that the low pH environment of the joint, particularly seen in disease, acts in a self-protective nature. This local acidosis would prevent lymphocytes becoming further activated and reduce excessive inflammation, in turn restricting how much damage is inflicted to the already compromised joint.

Having provided evidence of suppression of inflammation in acidic environments in this chapter, the next will assess to what extent the immune-expressed, proton-sensing GPR65 is responsible for that effect.

Chapter 5 : Exploring effects of GPR65 function in immune cells

5.1 Introduction

I have established the largely suppressive nature of an acidic extracellular environment on the activation and function of T cells (detailed in Chapter 4). Here, I develop previously used pH-based assays, dedicating this chapter to exploring the role of GPR65 in mediating this effect.

Within the literature, the role of GPR65 is conflicting, with evidence of both pro- and anti-inflammatory activity. On one hand, GPR65 knockout mice exhibited exacerbated colitis[192,206], as well as reports of reduced GPR65 signalling leading to a severe atopic dermatitis[209]. In contrast, gene deletion in $CD4^+$ T cells protected mice from EAE[213], as well as reports of a decrease of IFNγ and IL-17A production[210]. This ambiguity within the field highlights the need for further investigation into GPR65 activity.

Over the last two decades or so, advances in microfluidics have led to the development of next generation sequencing technology and made it possible to profile the transcription of individual cells simultaneously[355], in a high throughput manner and building upon established cellular characterisation using conventional flow cytometry assays, revealing important cellular differences not manifested at the cell surface. With little known about *how* GPR65 activation leads to its ultimate function, I used this technology to uncover the transcriptional changes dependent on GPR65 signalling, to further address its role in the immune system.

5.2 Aim

As the greatest impact of pH-dependent immune suppression was observed in MAIT cells (4.3.1.3), the aim of this chapter was to characterise the role of GPR65 in MAIT cells, in both neutral and acidic pH cultures. Here, I discuss the use of GPR65 silencing within established

functional assays and explore the response of clinically validated, inflammatory cytokine production. Single cell RNA sequencing analysis was used to determine which gene expression profiles were altered upon the loss of GPR65.

5.3 Results

5.3.1 GPR65 expression profiling on immune cell subsets

Before investigating the role of GPR65 on the immune response, it was first useful to understand which cells expressed this pH sensing receptor. Using publicly available RNA sequencing data from healthy control PBMCs[356], MAIT cells were shown to express the highest levels of GPR65, with expression also observed on $CD16^+$ NK cells, γδT cells and non-classical monocytes (Figure 5-1).

Next, I wanted to validate these findings in my hands, alongside co-expression of the other proton sensing family members (introduced in 1.2.2); as well as address if gender differences were apparent on GPR65 expression, due to the disparity of AS inflammation in men[12]. Supporting the scRNAseq data, $CD8^+$ T cells (containing MAIT cells) and $CD56^+$ NK cells (containing $CD16^+$ NK cells) were observed to express the highest levels of GPR65 mRNA, with seemingly no separation between male and female expression (Figure 5-2). GPR4 was not detected on these immune cells (data not shown), whilst NK cells and monocytes had relatively less expression of GPR68 compared to GPR65.

So far, published data reporting GPR65 expression has been obtained through mRNA analysis. However, throughout the duration of this project, antibody reagents have become commercially available. Upon testing the only monoclonal anti-GPR65, a right shift indicative of binding was observed on all the PBMC subsets tested (Figure 5-3A); but as the secondary antibody control also traced the same right shift, GPR65 specific binding was ruled out. Moreover, a FACS-validated polyclonal antibody for GPR65 suggested a lack of binding to T lymphocytes, whilst those cells expressing CD16 ($CD16^+$ NK cells and non-classical monocytes) saw a positive signal (Figure 5-3B). As the corresponding manufacturer isotype control also

shifted to the right on the same cell subsets, I decided to not continue to use the commercial GPR65 antibodies within my project.

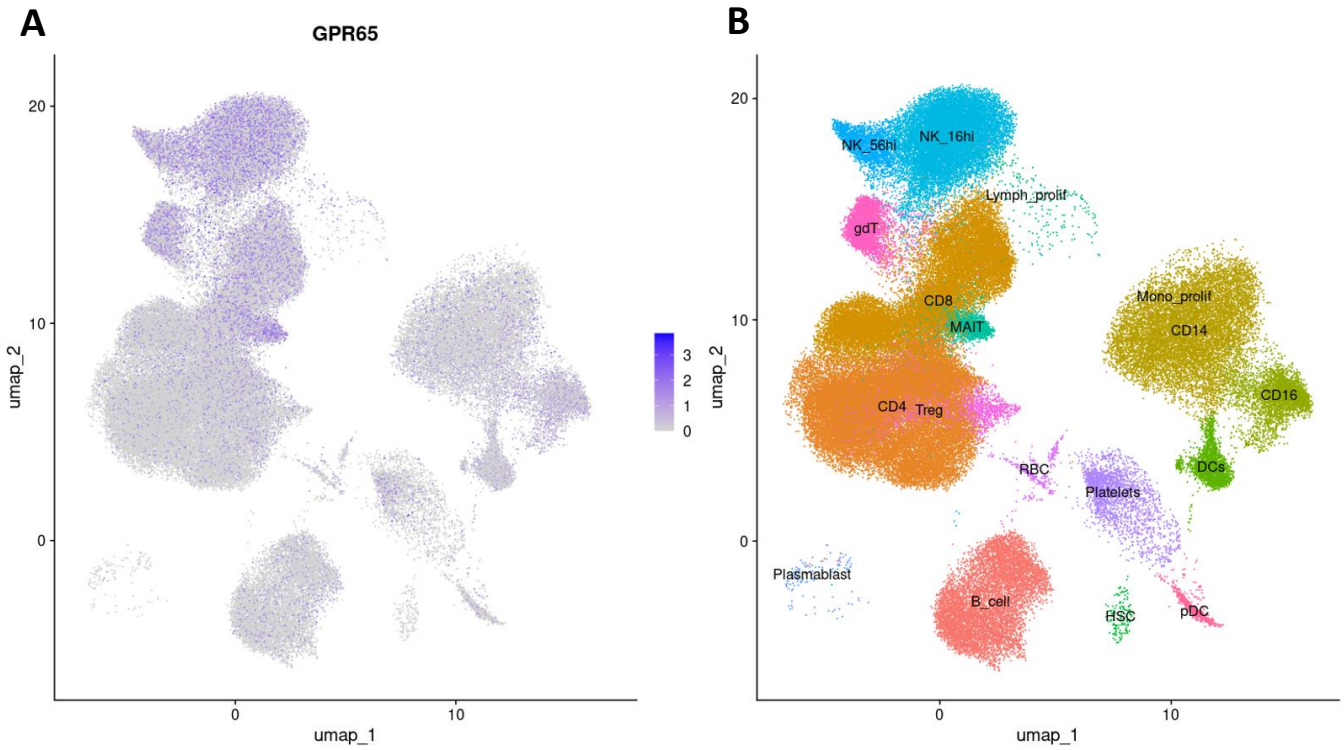


Figure 5-1 – GPR65 expression in healthy control PBMC subsets[n]

Single cell RNA sequencing data from heathy control individuals within the COMBAT dataset[356]. UMAP identifying cellular populations (B) and the corresponding relative expression of GPR65 of each cell type (A).

[n] Analysis performed by Feng Liu.

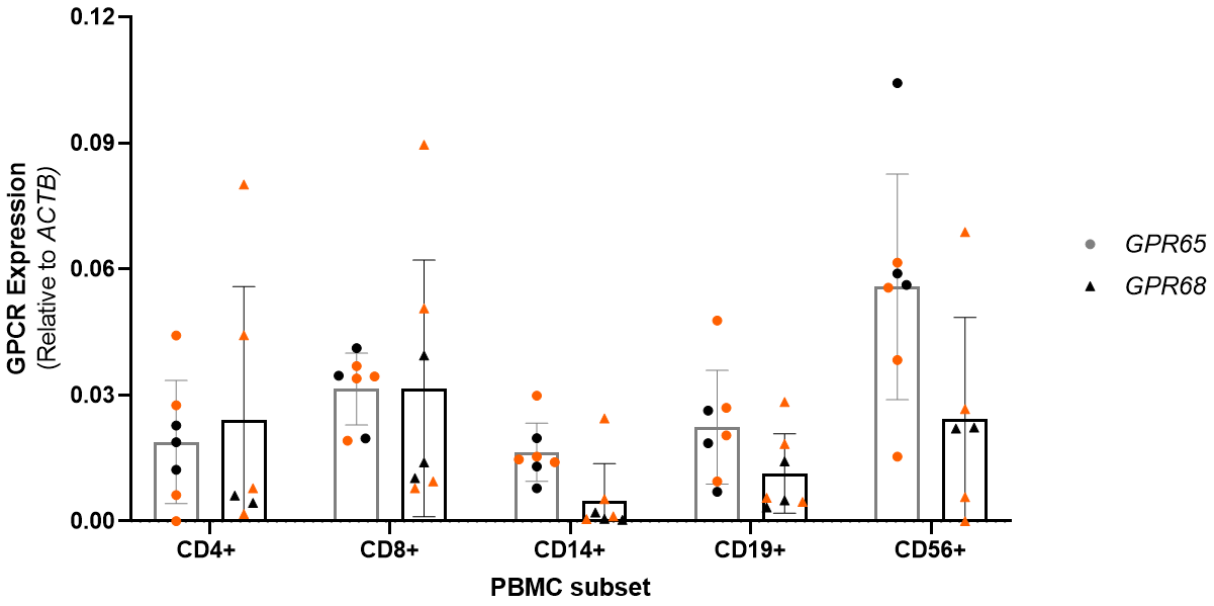
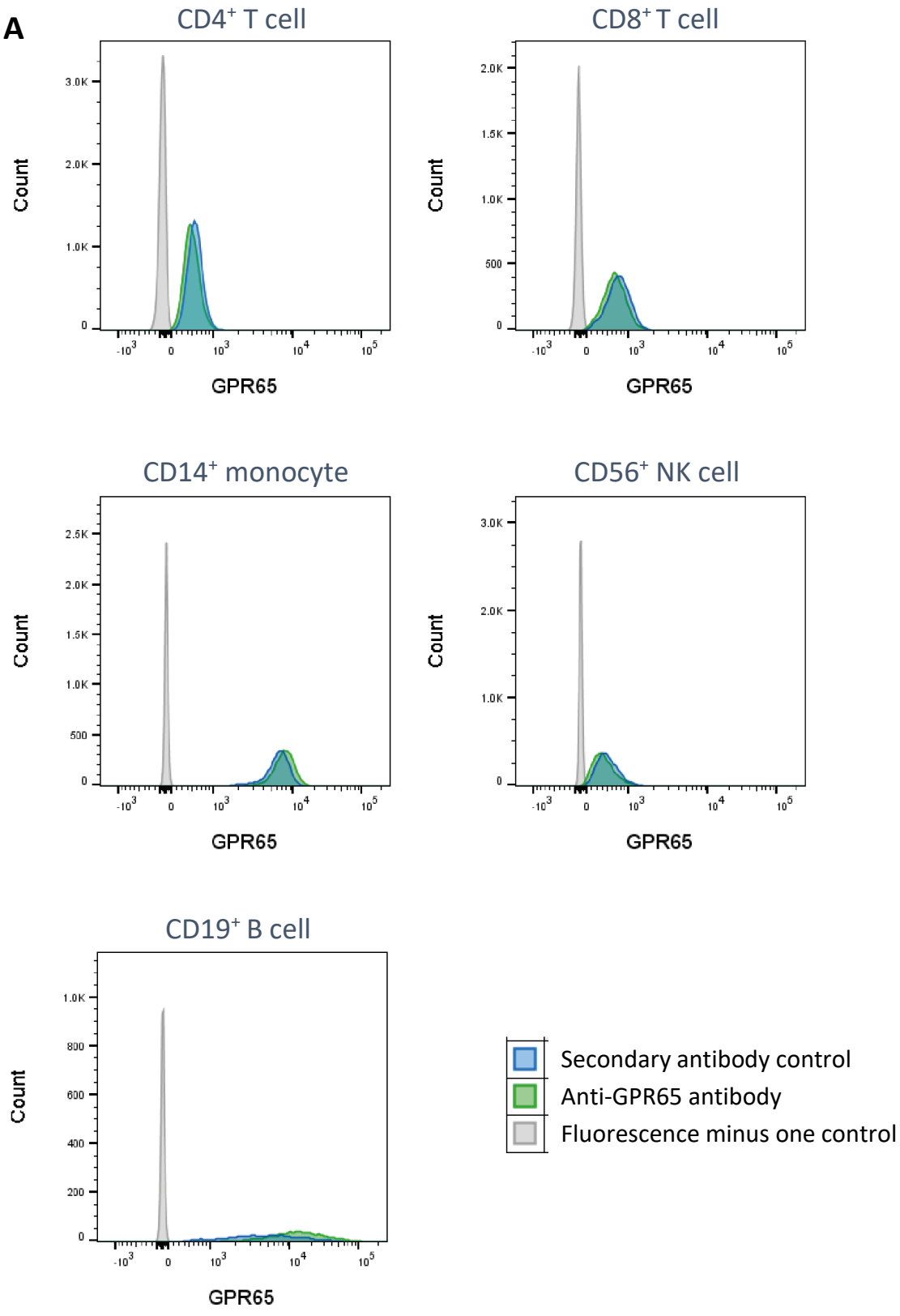


Figure 5-2 – GPR65 expression was equal across genders

PBMCs were isolated from 7 healthy donors (4 females represented by orange symbols, 3 males represented by black symbols). Monocytes were isolated through $CD14^+$ MACS separation and other cell types further isolated by FACS sorting[o]. RNA was extracted and cDNA generated, prior to qPCR analysis for GPCR expression.

[o] Sort performed by Catherine Simpson.


A
CD4+ T cell
CD8+ T cell
CD14+ monocyte
CD56+ NK cell
CD19+ B cell
Count
GPR65
Secondary antibody control
Anti-GPR65 antibody
Fluorescence minus one control

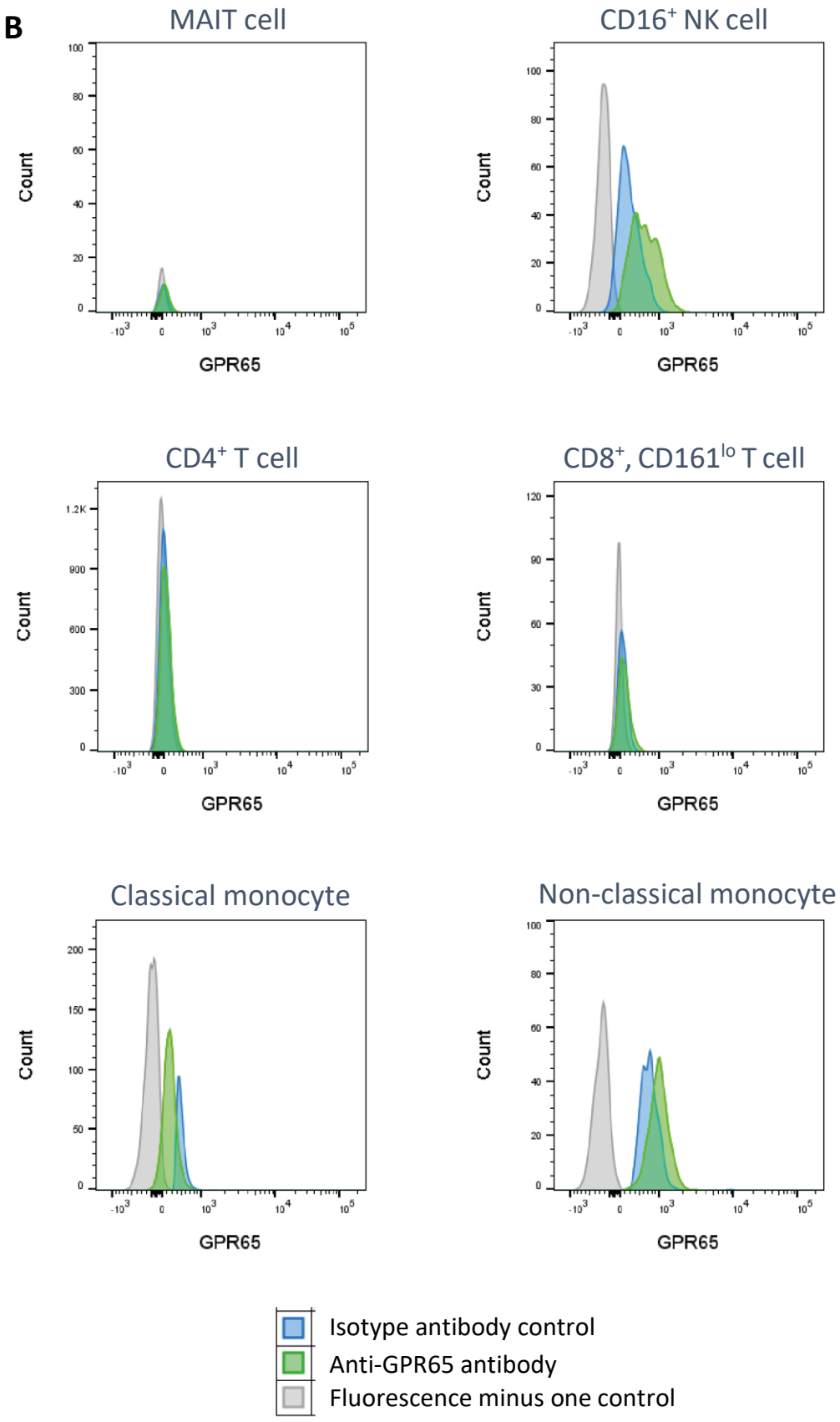

B
MAIT cell
CD16+ NK cell
CD4+ T cell
CD8+, CD161lo T cell
Classical monocyte
Non-classical monocyte
Count
GPR65
Isotype antibody control
Anti-GPR65 antibody
Fluorescence minus one control

Figure 5-3 – Commercial anti-GPR65 antibodies show no evidence of specific binding

PBMCs were isolated (n=3) and treated with Fc block for 10 minutes. (A) Cells were incubated with 1:100 R&D Systems™ anti-GPR65 for 1 hour, before goat anti-mouse IgG binding was assessed by flow cytometry. (B) Cells were incubated with either 1:50 Alomone Labs anti-GPR65, or the relevant Alomone isotype control for 1 hour, before receptor expression was assessed by flow cytometry. Cell surface markers were included in the cell staining step to identify PBMC subsets. A fluorescence minus one control was analysed (grey peaks) to identify a negative signal in the channel of interest. GPR65 binding is identified by green peaks shifting to the right of the plot, with the corresponding isotype/secondary antibody control peak in blue. The plots are from one donor, per antibody tested, and is representative of all three donors analysed.

5.3.2 Establishing the functional role of GPR65 in primary cells

Without the ability to neutralise, agonise or block a target with an antibody, functional effects of a specific protein can be investigated through the genetic manipulation of its expression. To address whether GPR65 was in part responsible for the functional effects of pH discussed in Chapter 4, I decided to silence GPR65 in primary cells.

Of the two methods available, both the CRISPR and siRNA approaches have their advantages and disadvantages, with success largely depending on the gene and the cell type of interest. So, I decided to run both in parallel to see which would be most effective in silencing GPR65 in MAIT cells.

5.3.2.1 CRISPR gene editing in T cells

$CD3^+$ T cells were negatively isolated from PBMCs by magnetic separation, prior to transfection with a GPR65 specific CRISPR/Cas9 ribonucleoprotein (RNP) complex. Three days post gene knockout, a portion of cells were processed for determining silencing efficiency, whilst others remained in the assay and further stimulated for 24 hours with a favoured MAIT cell stimulation (Figure 5-4). Preliminary functional outcomes were assessed by intracellular cytokine analysis from $CD4^+$ and $CD8^+$ T cells by flow cytometry.

Active Cas9 was confirmed when assessing the knockdown of the positive control, CD28 (Figure 5-5A), in turn confirming the technical success of the experiment. To define a suitable ratio of guide RNA (gRNA): Cas9, a titration was performed, and PCR carried out using primers flanking the intended edit locus (represented in Figure 2-1), to assess which ratio resulted in a more robust edit and would likely disrupt protein translation. The bands smeared appearance, indicative of unequal genetic cuts, suggested that for both ratios tested, editing had occurred at this position (Figure 5-5B); with the 3:1 ratio appearing to introduce a

deletion at this position of the gene more successfully than 1:1, as evident by the migration of the band on the agarose gel. However, one could not know for certain if GPR65 had been knocked out by assessing bands on the gel alone. Regrettably, inconclusive sequencing could not confirm the success of gene knockout, and without GPR65-specific tools to assess protein changes, further validation could not be sourced at the time.

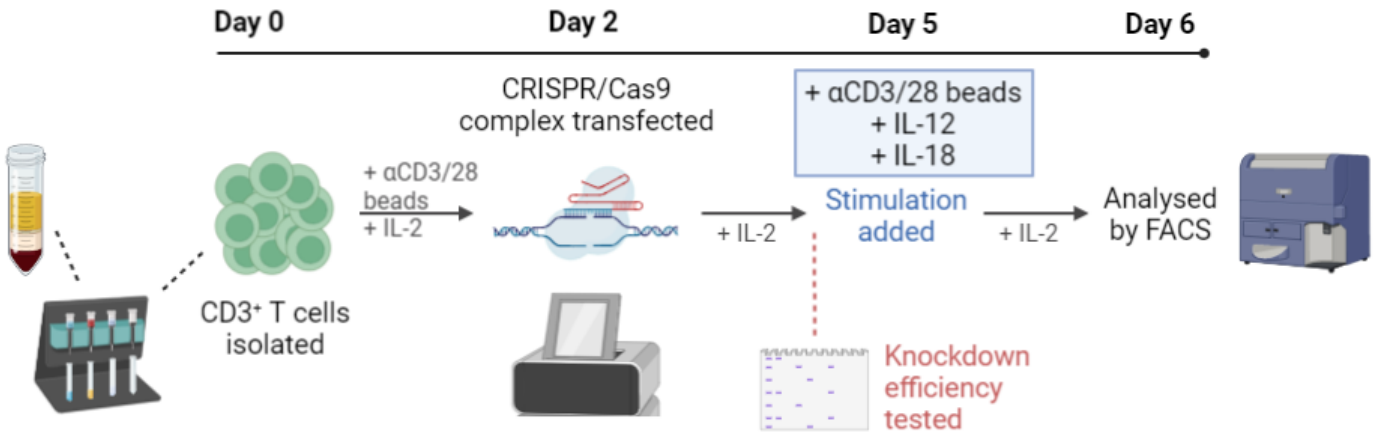


Figure 5-4 – Experimental plan of GPR65 knockout, using CRISPR/Cas9 technology in isolated T cells

$CD3^+$ T cells were isolated from PBMCs and stimulated for 48 hours (n=1), in the presence of IL-2 [50U/mL]. GPR65 specific RNP complexes were transfected into the pre-stimulated T cells and cultured, again with IL-2, for a further 72 hours. A portion of cells were taken for the confirmation of GPR65 knockout, whilst the remaining cells were stimulated with αCD3 and αCD28, plus IL-12 [10ng/mL] and IL-18 [10ng/mL] for 24 hours. Intracellular cytokine analysis by flow cytometry was performed to assess function.

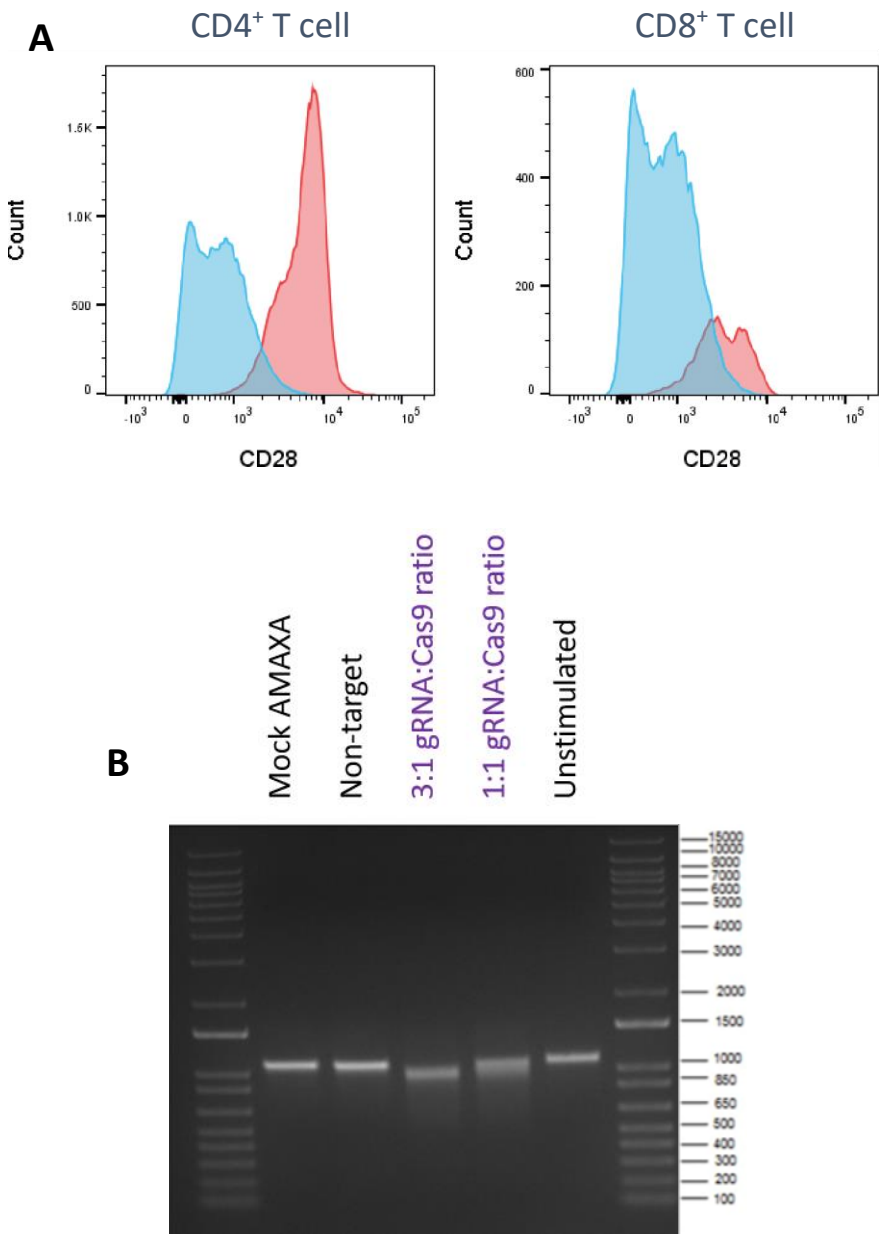


Figure 5-5 – GPR65 knock out using CRISPR/Cas9 complexes

(A) CD28 surface expression was observed on day 5 by flow cytometry. Red peaks depict wild type CD28 expression, whilst blue peaks represent those treated with CD28 gRNA/Cas9 complexes. (B) 72 hours post knockout, DNA was extracted, and PCR was performed with GPR65-specific primers, prior to samples being run on a gel for visualisation of the sequence length. A ladder and corresponding base pair sizes are to the right of the gel, whilst lanes of interest for GPR65 knockout are written in purple, and controls in black.

Despite not being able to confidently know that GPR65 had been knocked out, preliminary data for changes in T cell function was recorded. Strikingly, poor viability of the cells was seen after 6 days in the assay, with all conditions having less than 50% of cells alive (Figure 5-6A); but this data did suggest the transfection procedure itself did not affect viability. At a first glance of the functional data, the pro-inflammatory cytokines assessed were increased upon GPR65 silencing at the 1:1 condition (Figure 5-6), suggesting that GPR65 restricts the release of these cytokines and possesses an anti-inflammatory role in T cells. Yet, no dramatic changes of function were observed from the 3:1 ratio, compared to the non-target control. Moreover, in the non-target control condition, whilst IL-17A and IL-17F expression (Figure 5-6E and F) were in the expected range from stimulated T cells, lower than expected production of TNFα (< 2%) and IFNγ (< 20%) was concerning (Figure 5-6B and C).

Overall, substantial optimisation would have been required to draw firm conclusions about the effects of GPR65 knockout, including improvements for assessing change at the genetic level, as well as reworking the integrated protocol to assess function, not only to achieve better cell health, but also improve functional readouts. Therefore, work here was not continued; this decision was also in part due to the simultaneous success being had for siRNA gene knockdown.

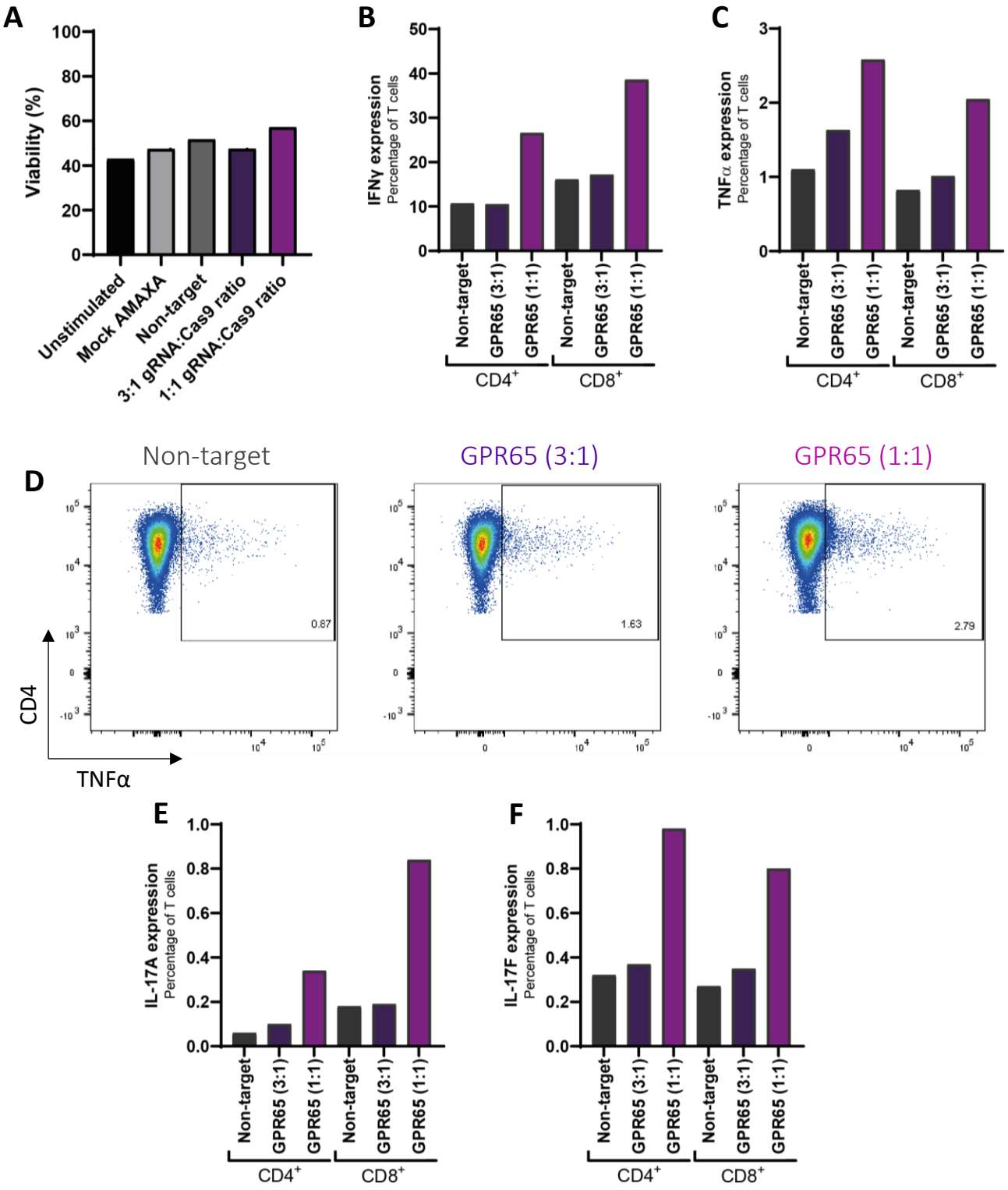


Figure 5-6 – Pro-inflammatory cytokine release was increased by T cells treated with GPR65 specific RNP complexes

(A) Viability of $CD3^+$ T cells at day 6 of the CRISPR/Cas9 protocol (described in Figure 5-4, n = 1). (B) Expression of intracellular cytokines IFNγ (B), TNFα (C), IL-17A (E) and IL-17F (F) was determined in $CD4^+$ and $CD8^+$ T cells by flow cytometry; with representative FACS plots from $CD4^+$ T cells expressing TNFα (D).

5.3.2.2 siRNA knockdown in MAIT cells

Notoriously, primary T cells have been difficult to treat with siRNA. Here, I used the Accell siRNA system, for hard-to-treat cells, to test whether GPR65 can be knocked down in T cells.

5.3.2.2.1 Optimisation in isolated $CD8^+$ T cells

I started by assessing a 3-day time course of GPR65 knockdown in positively isolated $CD8^+$ T cells. Treatment of cells with siRNA transfection reagents did not alter viability (Figure 5-7A) and was instead noted to improve cell survival in GPR65 siRNA treated cells, compared to both negative controls (siRNA untreated and non-target siRNA treated).

The efficiency of GPR65 knockdown reaching a loss of greater than 70% expression was deemed a success after 24 hours (Figure 5-7B), with better results seen after 48 hours (78% knockdown). Knockdown efficiency had decreased by 72 hours, speaking to the transient nature of the siRNA treatment. This supported the rationale of using siRNA for knockdown for up to 48 hours, as well as the redundancy of using an untreated control.

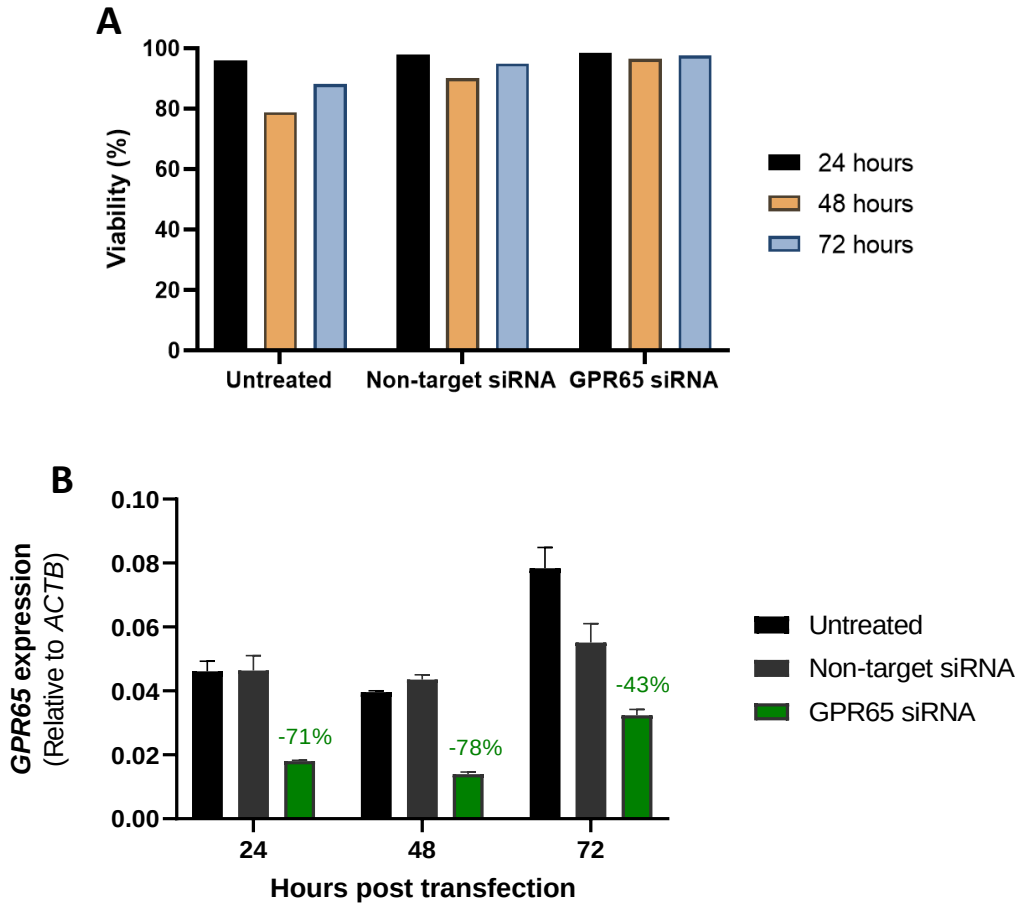


Figure 5-7 – GPR65 was successfully knocked down by siRNA treatment in CD8⁺ T cells after 24 hours

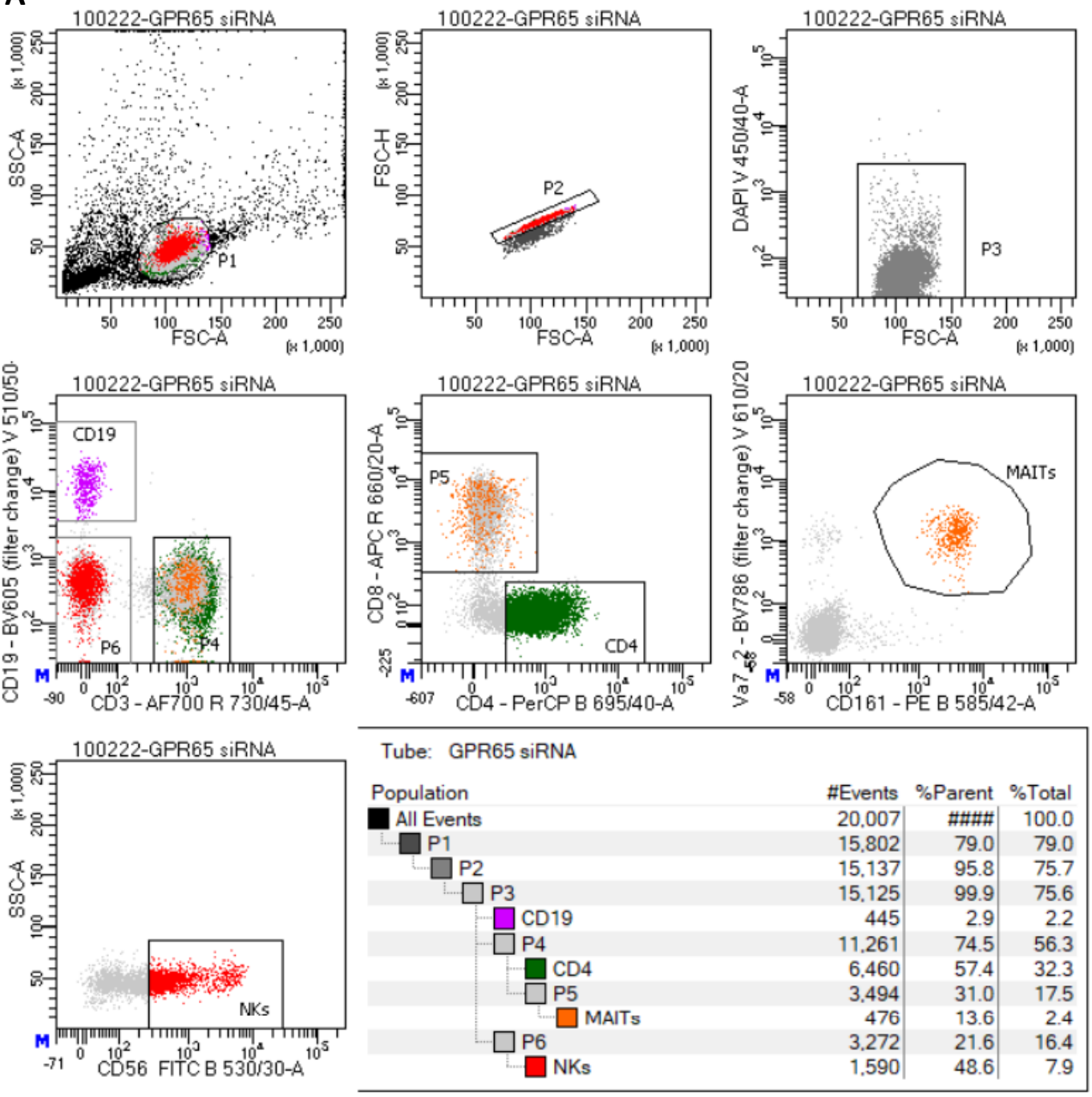
CD8⁺ T cells were positively isolated using magnetic separation from PBMCs. 1µM non-target or GPR65 siRNA was cultured with cells for up to 72 hours. (A) Viability was assessed daily using DAPI, by flow cytometry. (B) RNA was extracted, cDNA generated, and GPR65 mRNA expression was analysed by qPCR, relative to the housekeeping gene, *ACTB*. Untreated cells acted as a negative control for effects of siRNA. Data presented is from one donor and is a representation of 4 donors with the same conditions.

5.3.2.2.2 GPR65 knockdown in PBMCs

I have previously shown that MAIT cells were more functional in a mixed cell population, compared to isolated $CD8^+$ T cells alone (section 4.3.2). So, I next wanted to test whether GPR65 silencing by siRNA was successful in the context of PBMCs.

Using the optimised conditions established within isolated $CD8^+$ T cells, 1µM siRNA was cultured with PBMCs for 48 hours, prior to isolating cell subsets via magnetic and FACS based sorting (Figure 5-8A). Cells shown to express the highest levels of GPR65 expression, MAIT and NK cells, saw efficient receptor knockdown (65% and 47%, respectively) (Figure 5-8B). Alternative cell types saw reduced GPR65 expression, but to varying and less convincing degrees.

A


100222-GPR65 siRNA
SSC-A
FSC-A
P1
FSC-H
P2
DAPI V 450/40-A
P3
CD19 - BV605 (filter change) V 510/50
CD3 - AF700 R 730/45-A
CD19
P6
P4
CD8 - APC R 660/20-A
CD4 - PerCP B 695/40-A
P5
CD4
Va7.2 - BV786 (filter change) V 610/20
CD161 - PE B 585/42-A
MAITs
CD56 FITC B 530/30-A
NKs
Tube: GPR65 siRNA
Population #Events %Parent %Total
All Events 20,007 #### 100.0
P1 15,802 79.0 79.0
P2 15,137 95.8 75.7
P3 15,125 99.9 75.6
CD19 445 2.9 2.2
P4 11,261 74.5 56.3
CD4 6,460 57.4 32.3
P5 3,494 31.0 17.5
MAITs 476 13.6 2.4
P6 3,272 21.6 16.4
NKs 1,590 48.6 7.9

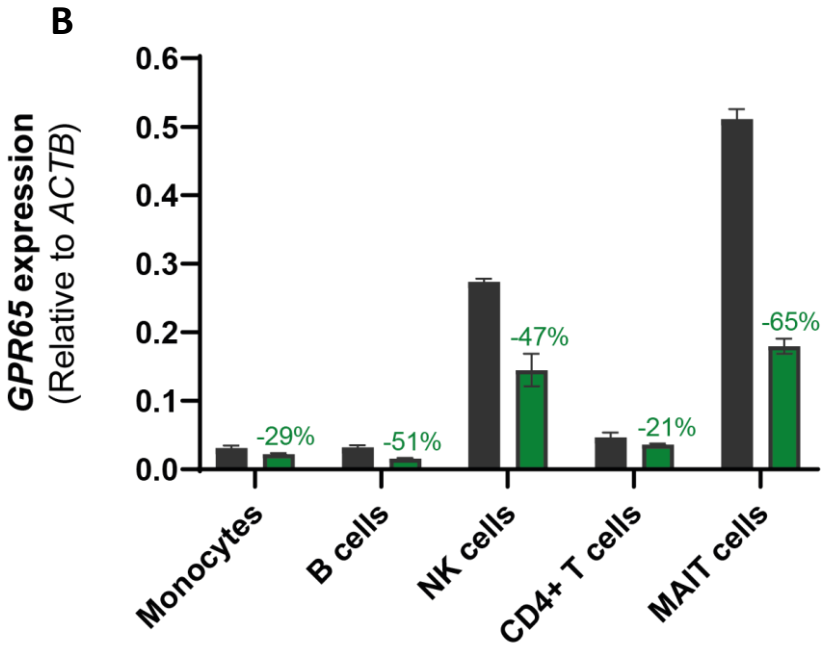


Figure 5-8 – GPR65 expression was efficiently reduced in MAIT cells upon PBMC siRNA knockdown

PBMCs were cultured with 1µM non-target or GPR65 siRNA for 48 hours. Monocytes were purified through magnetic separation, with remaining cells undergoing FACS sorting to isolate out alternative populations. (A) The FACS sort report depicting the gating strategy to identify $CD19^+$ B cells, $CD56^+$ NK cells, $CD4^+$ T cells and $CD8^+$, $CD161^+$, $V\alpha7.2^+$ MAIT cells.[p] (B) For each cell subset collected, RNA was extracted, cDNA generated, and GPR65 mRNA expression was analysed by qPCR, relative to the housekeeping gene, *ACTB*. Data is an n=1 and representative of 2 donors with the same conditions.

[p] FACS sort performed by Catherine Simpson.

5.3.2.2.3 Assessing GPR65 function in MAIT cells

I have described a reduced inflammatory profile of MAIT cells upon their culture in an acidic environment (Figure 4-4). Using optimised gene modifying siRNA, I could interrogate the role of GPR65 on the low pH-dependent suppression seen. PBMCs were treated with either 1μM non-target or GPR65 siRNA for 24 hours, prior to stimulation with αCD3 and αCD28, plus IL-18, for a further 24 hours, in pH 6.5 and pH 7.5 culture conditions. BFA was used in the final 4 hours of culture and intracellular cytokine production from T cells was determined by flow cytometry.

Firstly, suppression of cytokine release from MAIT cells by acidic conditions was confirmed, such as IFNγ production dropping from ~90% at pH7.5, to ~20% when cultured at pH 6.5 (Figure 5-9). On the other hand, granzyme B production from $CD8^+$, $CD161^{lo}$ cells was consistent between the two pH cultures. Remarkably, when looking at effects upon silencing GPR65, an increase of IFNγ expression from both $CD8^+$ T cell subsets assessed was shown when cells were cultured at pH 6.5 (Figure 5-9A and B), albeit not back to baseline pH 7.5 levels. Together with an increase of corresponding IFNγ protein in the supernatant (Figure 5-9D), this suggested that GPR65 was in part responsible for the restriction of this Th1 family cytokine in an acidic environment. A trend in the partial rescue of low pH-dependent granzyme B was also noted from MAIT cells (Figure 5-9A). In comparison, effects of GPR65 knockdown in $CD4^+$ T cells at pH 6.5 appeared to have no effect on cytokine release (Figure 5-9C).

Considering the function of GPR65 at neutral pH, its silencing was redundant for all the cytokines studied, except for IL-17A. Decreased expression of IL-17A was seen from

lymphocytes upon silencing (Figure 5-9). This data supported a pro-inflammatory role of GPR65 in immune cell function.

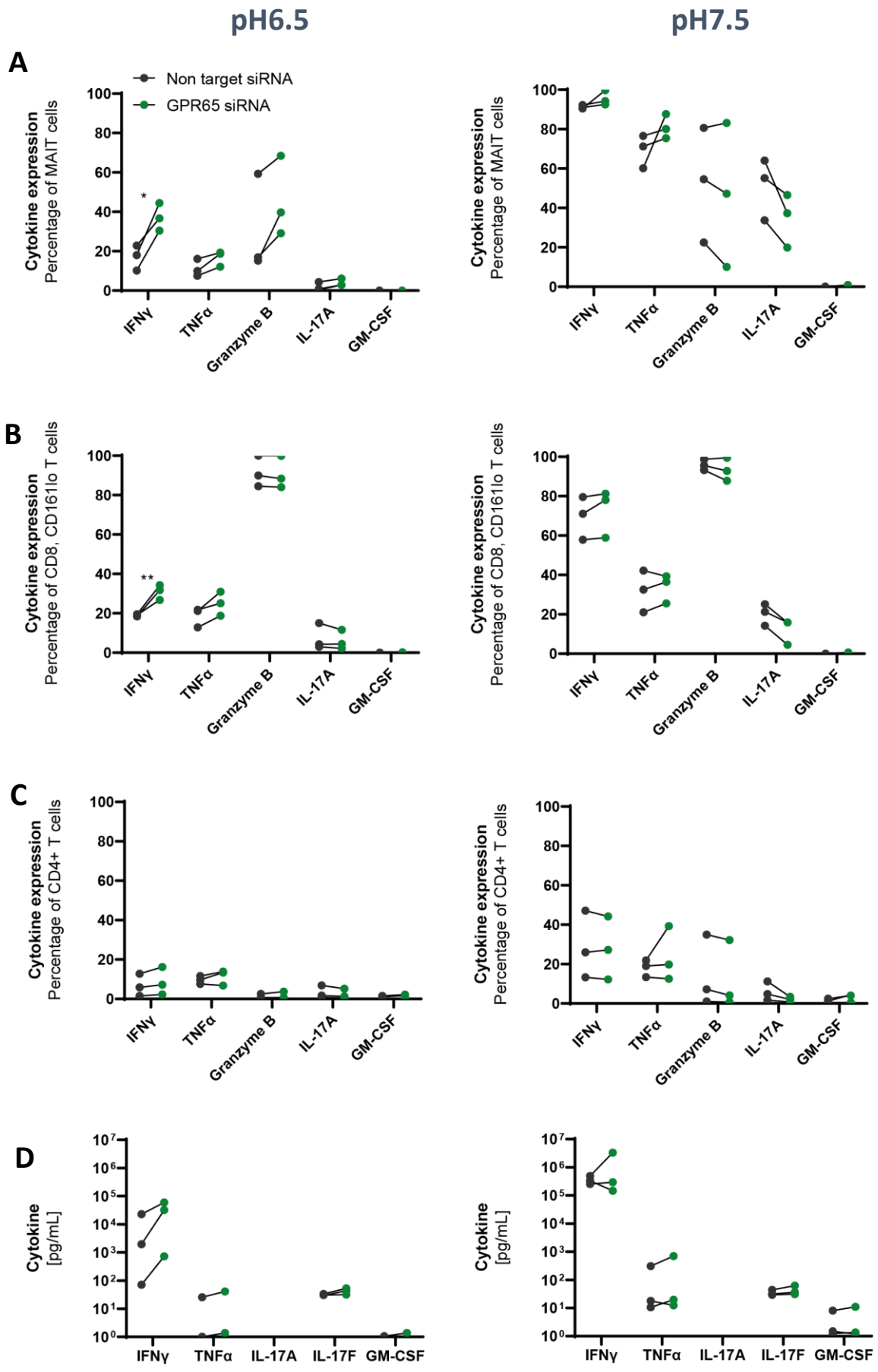

pH6.5
pH7.5
A
Non target siRNA
GPR65 siRNA
Cytokine expression
Percentage of MAIT cells
B
Cytokine expression
Percentage of CD8, CD161lo T cells
C
Cytokine expression
Percentage of CD4+ T cells
D
Cytokine
[pg/mL]
IFNγ
TNFα
Granzyme B
IL-17A
IL-17F
GM-CSF

Figure 5-9 - IFNγ pH-dependent inhibition was attenuated by GPR65 knockdown in $CD8^+$ T cells

PBMCs were isolated and treated with 1µM non-target or GPR65 siRNA for 24 hours. Cells were then stimulated with αCD3 and αCD28 [1µg/mL], plus IL-18 [50 ng/mL] for a further 24 hours (n=3), at two pH cultures, pH 6.5 (all graphs on the left) and pH 7.5 (all graphs on the right). Expression of intracellular cytokines was determined in MAIT cells (A), $CD8^+$, $CD161^{lo}$ T cells (B) and $CD4^+$ T cells (C), with supernatant protein also quantified (D). Cells treated with non-target siRNA are depicted in grey, whilst those treated with GPR65 siRNA are in green. Data represents the mean of three technical replicates, for each of the three biological replicates. Statistical significance was performed using a paired Student's t-test between culture conditions. *p≤0.05, **p≤0.01.

5.3.3 Identification of transcriptional changes within lymphocytes upon the knockdown of GPR65

To uncover novel GPR65 biology in immune cells, I needed to go deeper than just considering functional protein outcomes, and further explore transcriptional changes to identify important mechanisms of the role of GPR65 activity. The strength of single cell RNA sequencing comes with the number of cells that can be investigated and the transcriptional information for each cell, thereby increasing power and confidence in the findings. As GPR65 was not expressed on all PBMC subsets, a way of enriching GPR65^{+} cells was required.

5.3.3.1 GPR65 and KLRB1 are co-expressed on cells of interest

Through analysis of publicly available RNA sequencing data from healthy control PBMCs[357], KLRB1, the gene responsible for CD161, was identified as being co-expressed on many of the same immune cell types as GPR65, including MAIT cells, γδT cells and NK cells (Figure 5-10[q]).

[q] Analysis performed by Feng Liu.

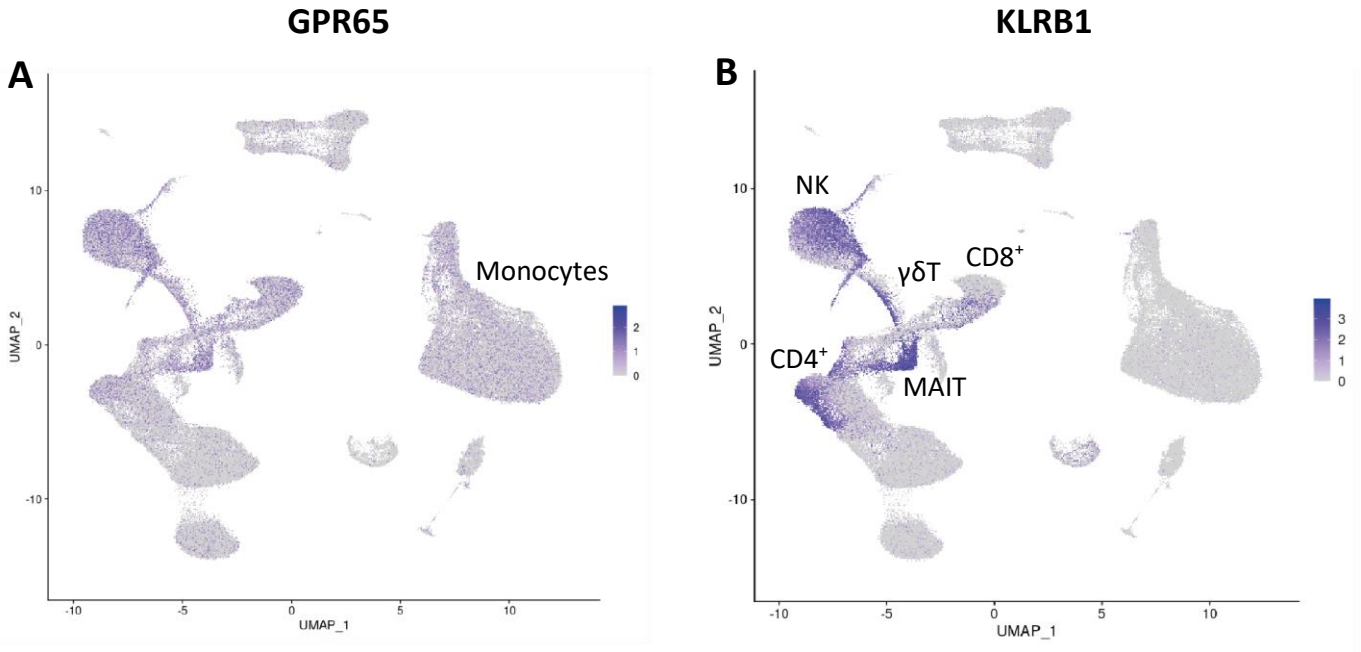


Figure 5-10 – GPR65 co-expressed with KLRB1 in lymphocytes[r]

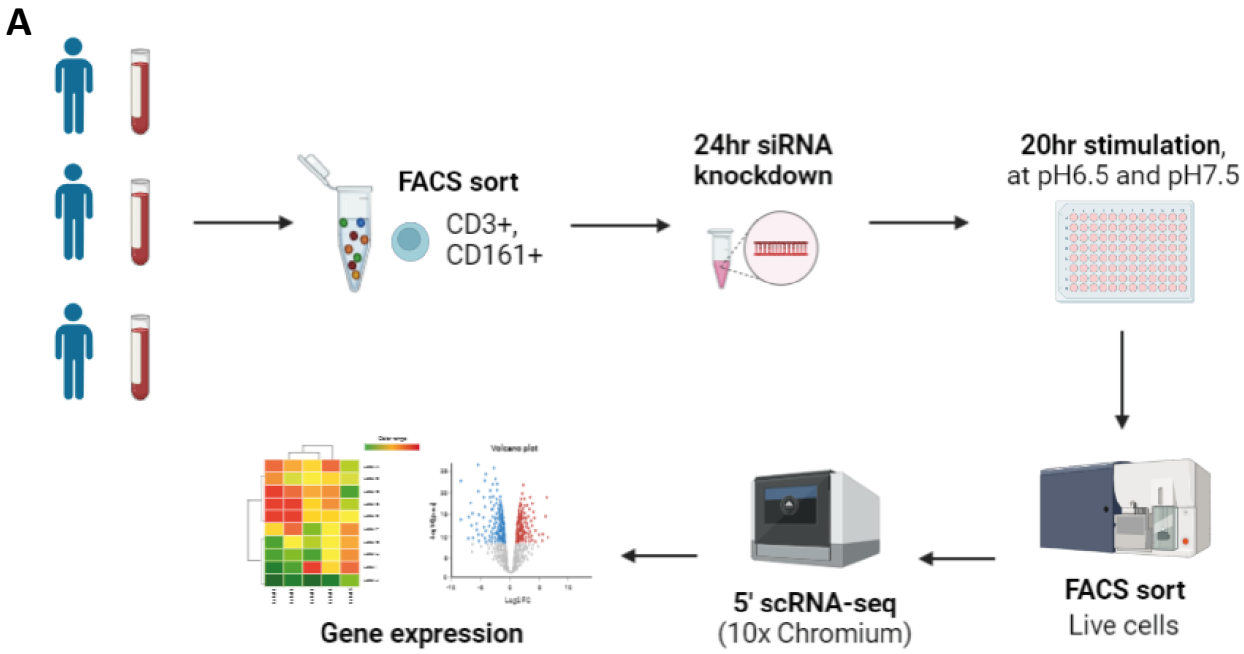
Single cell RNA sequencing data obtained from heathy control individuals[357]. UMAPs of relative gene expression for GPR65 (A) and KLRB1 (B), with cell subsets of interest labelled.

[r] Analysis performed by Feng Liu.

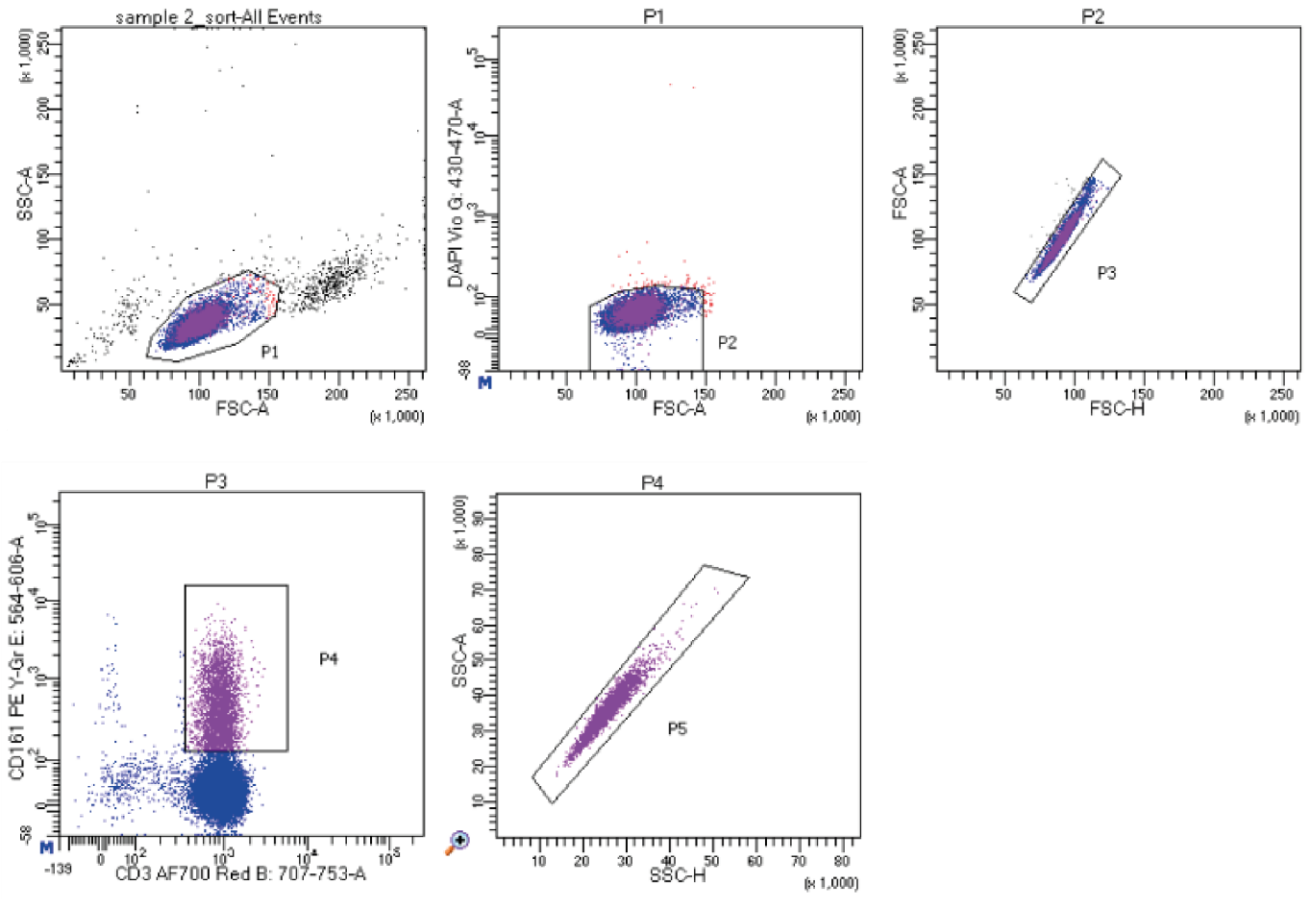
5.3.3.2 Experimental conditions for scRNAseq analysis

Upon the decision to purify cells expressing the extracellular marker CD161, as a surrogate for GPR65 expression, I also focused on T cell subsets. Thus, GPR65 expressing NK cells and monocytes were not included in this experiment.

Peripheral blood was taken from 3 male healthy donors, and $CD3^+$, $CD161^+$ cells were sorted using flow cytometry (Figure 5-11B). Cells were subject to siRNA treatment for 24 hours, then left unstimulated or stimulated with cytokines IL-12 and IL-18, or αCD3 and αCD28, at both pH 6.5 and pH 7.5. After 20 hours, live cells were sorted for scRNAseq (Figure 5-11A). This experimental plan generated 12 test conditions and can be seen within Table 8.


A
FACS sort
CD3+,
CD161+
24hr siRNA
knockdown
20hr stimulation,
at pH6.5 and pH7.5
FACS sort
Live cells
5' scRNA-seq
(10x Chromium)
Gene expression

B



Tube: sample 2_sort

Population	#Events	%Parent	%Total
All Events	20,000	####	100.0
P1	19,304	96.5	96.5
P2	19,227	99.6	96.1
P3	19,186	99.8	95.9
P4	3,393	17.7	17.0
P5	3,393	100.0	17.0

Figure 5-11 - Experimental plan of single cell RNA sequencing conditions

(A) A cartoon showing the experimental protocol; PBMCs were isolated from three male healthy donors and $CD3^+$, $CD161^+$ cells isolated by flow cytometry[s] (B). These cells were subjected to 1µM GPR65 or non-targeting siRNA for 24 hours, prior to stimulation at 2x pH culture conditions for a further 20 hours. $DAPI^+$ live cells were then sorted[t] and processed for sequencing, as per the 10x Genomics manufacturers guidance.

[s] $CD3^+$, $CD161^+$ isolating FACS sort performed by Helen Ferry.
[t] Live cell FACS sort performed by Jonathan Webber.

Sample	Knockdown	pH	Stimulation
1	Non-target siRNA	pH 6.5	Unstimulated
2	Non-target siRNA	pH 6.5	αCD3 and αCD28
3	Non-target siRNA	pH 6.5	IL-12 and IL-18
4	Non-target siRNA	pH 7.5	Unstimulated
5	Non-target siRNA	pH 7.5	αCD3 and αCD28
6	Non-target siRNA	pH 7.5	IL-12 and IL-18
7	GPR65 siRNA	pH 6.5	Unstimulated
8	GPR65 siRNA	pH 6.5	αCD3 and αCD28
9	GPR65 siRNA	pH 6.5	IL-12 and IL-18
10	GPR65 siRNA	pH 7.5	Unstimulated
11	GPR65 siRNA	pH 7.5	αCD3 and αCD28
12	GPR65 siRNA	pH 7.5	IL-12 and IL-18

Table 8 – Experimental samples subject to RNA sequencing

Colours are representative of differences between the samples.

5.3.3.3 GPR65 was successfully knocked down in unstimulated lymphocytes, at pH 7.5

Primary analysis of the sequencing has already been discussed within section 4.3.3, identifying 17 cell clusters (Figure 4-8A). Of the cell types included in this experiment, MAIT cells were observed to express the highest levels of GPR65 (Figure 5-12).

Before addressing the transcriptional effects of GPR65 knockdown, it was important to assess the efficiency of siRNA treatment. Relative GPR65 expression levels across all cells, per experimental condition, were investigated (Table 9). Receptor knockdown was considered a success at pH 7.5 in unstimulated cells, with 56.4% vs 20% percentage expressed, for non-target and GPR65 siRNA, respectively (Figure 5-13, black box). However, the final 20 hours of stimulation subsequently altered its expression; cells cultured within acidic conditions reported an increase of GPR65 expression (Figure 5-13, blue box), whilst those stimulated with αCD3 and αCD28 suggested reduced gene expression (Figure 5-13, red box), and in general reduced the ability to identify siRNA effects.

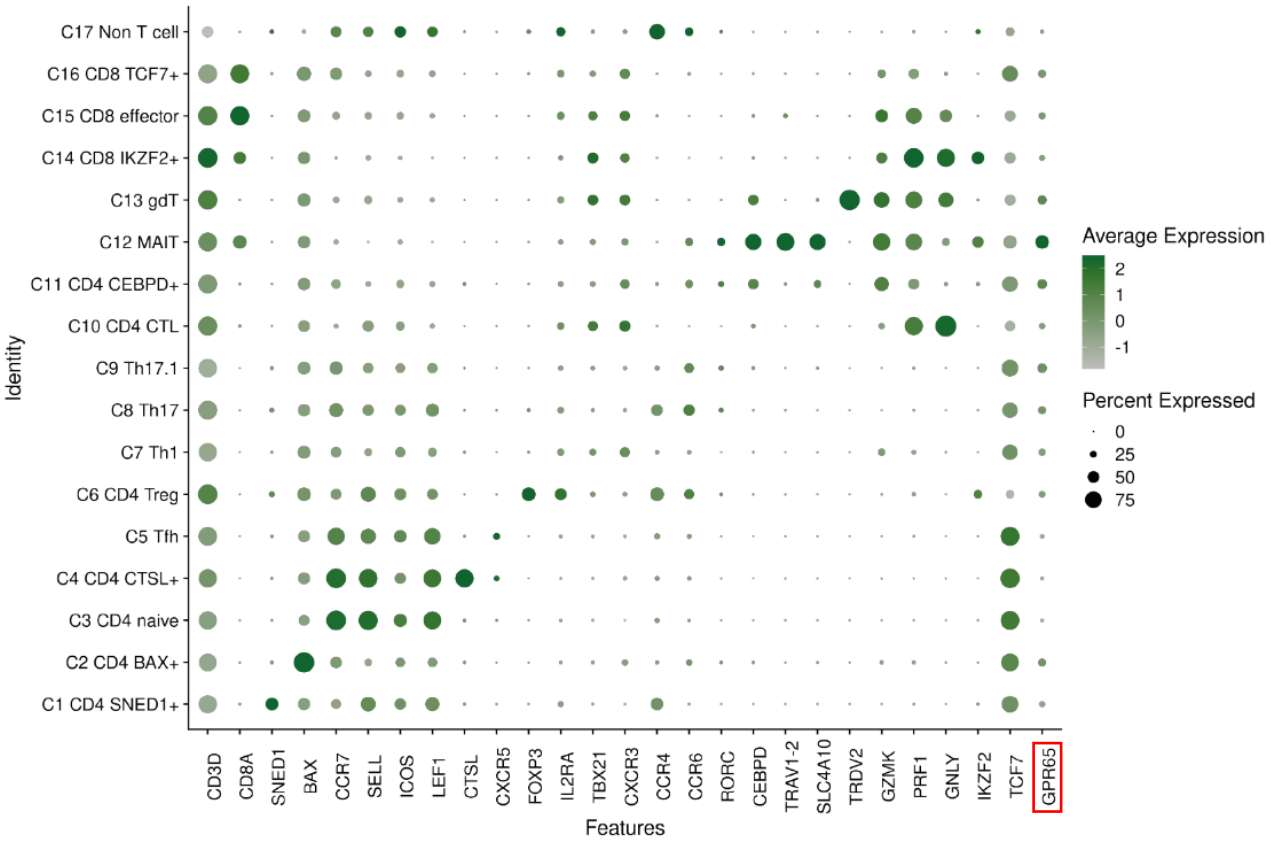
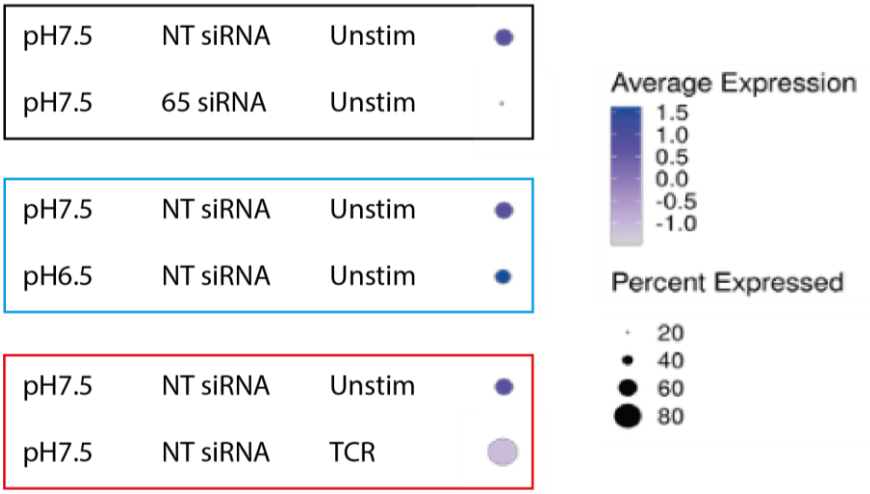


Figure 5-12 - MAIT cells were confirmed to express the highest levels of GPR65 mRNA

Dot plots of the expression of established gene markers to identify each cluster (as highlighted in section 4.3.3), with GPR65 expression depicted by the red box. Dot size indicates the percentage of cells expressing the gene, whilst dot colour represents the intensity of expression.



Sample	Knockdown	pH	Stimulation	Average expression	Percentage expressed %
1	Non-target siRNA	pH 6.5	Unstimulated	0.56	47.5
2	Non-target siRNA	pH 6.5	αCD3 and αCD28	0.42	78.6
3	Non-target siRNA	pH 6.5	IL-12 and IL-18	0.47	64.0
4	Non-target siRNA	pH 7.5	Unstimulated	0.52	56.4
5	Non-target siRNA	pH 7.5	αCD3 and αCD28	0.42	76.7
6	Non-target siRNA	pH 7.5	IL-12 and IL-18	0.49	63.4
7	GPR65 siRNA	pH 6.5	Unstimulated	0.55	57.4
8	GPR65 siRNA	pH 6.5	αCD3 and αCD28	0.42	77.2
9	GPR65 siRNA	pH 6.5	IL-12 and IL-18	0.48	58.9
10	GPR65 siRNA	pH 7.5	Unstimulated	0.51	20.0
11	GPR65 siRNA	pH 7.5	αCD3 and αCD28	0.40	83.3
12	GPR65 siRNA	pH 7.5	IL-12 and IL-18	0.48	70.6

Figure 5-13 and Table 9 – GPR65 was successfully knocked down in unstimulated cells cultured at pH 7.5

Expression of relative GPR65 mRNA expression from all cells. The dot plots indicate the percentage of cells expressing the gene by size, whilst their colour represents the intensity of expression. Coloured boxes depict comparisons referenced in the text. The table includes all the samples within the scRNAseq experiment (colours are representative of differences between the conditions tested), with corresponding expression values for the dots.

5.3.3.4 Sub clustering of MAIT cells change upon GPR65 knockdown

Having confirmed that MAIT cells expressed the highest levels of GPR65 (Figure 5-12) and showed their function to be altered upon silencing the receptor (Figure 5-9), I again focused the transcriptional analysis on these innate-like T cells.

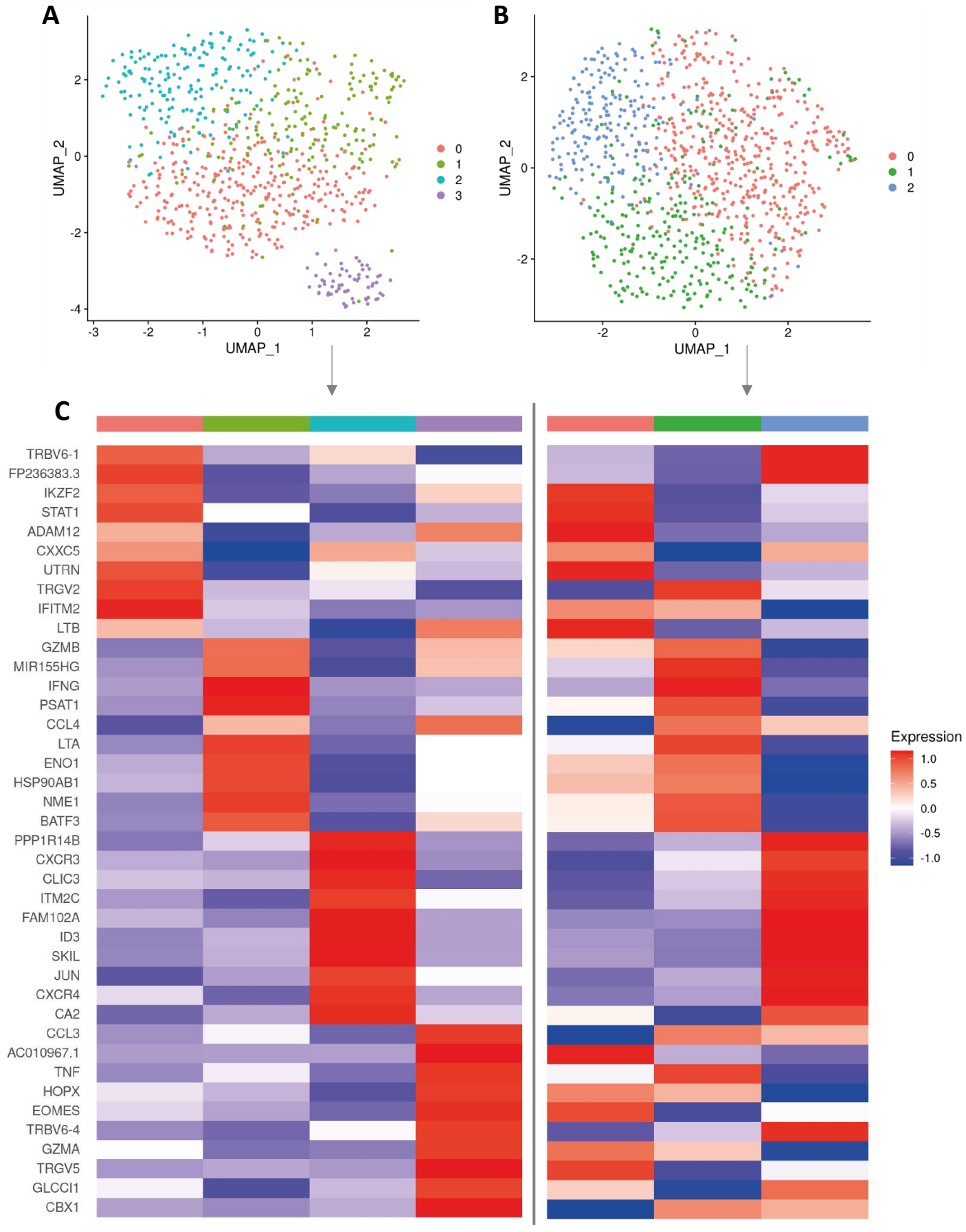
Before seeking differentially expressed genes between the two siRNA treatment groups, I asked if MAIT clustering was affected by this genetic manipulation, just as was seen by a change in pH condition (Figure 4-10). The UMAP algorithm identified 4 subclusters for stimulated, non-target siRNA treated MAIT cells at neutral pH (Figure 5-14A). Upon running the exact same code, with the clustering resolution set at 0.8, on equivalent stimulated cells this time subject to GPR65 siRNA, 3 subclusters were generated (Figure 5-14B).

Visually cluster 3 appeared to be the 'missing' cluster from the cells where GPR65 had been silenced, but I was unsure whether the genes responsible for the generation of this cluster were not expressed at all, or whether the genes were not as highly expressed, and instead present within alternative clusters. So, I identified the top 10 key cluster specific genes for the stimulated, non-target siRNA treated samples at pH 7.5 (Figure 5-14C, left-hand side heatmap). Cluster 0, the biggest of the clusters, expressed genes which were associated with early signs of activation (*STAT1, IFITM2, ADAM12*[358]). Cluster 1 overexpressed cytotoxic, effector genes (*GZMB, LTA, IFNG*[359]) relative to all other clusters. Cluster 2 possessed the highest levels of genes with tissue-infiltrating and innate-like properties (*JUN*, *ITM2C, CXCR3*[359]). Cluster 3 represented cells with prolonged activation, overexpressing *TNF, HOPX* and *EOMES*.

For comparison, I produced another heatmap for stimulated, GPR65 siRNA treated samples at pH 7.5, with those same 40 genes (Figure 5-14C, right hand side heatmap). Here, clusters 1

and 2 were very similar between the two siRNA treated groups, and those genes of cluster 1 where an increase of expression was also visible in cluster 3 for non-target siRNA treated cells, appeared to fall back into cluster 1 for GPR65 siRNA treated cells (E.g, *ENO1, NME1, BATF3*). Cluster 0 reported variation, particularly for T cell receptor genes *TRBV6-1* and *TRGV2*, but for the most part, the same genes located in this cluster for both non-target and GPR65 siRNA treated cells. In contrast, effector genes (*HOPX, EOMES, GZMA*) originally located in cluster 3 appeared to locate into their closest neighbouring cluster, cluster 0, whilst the pro-inflammatory cytokine *TNF* was found in the cytotoxic effector cluster 1. Interestingly, T cell receptor genes within cluster 3 (*TRBV6-4, TRGV5*) were also displaced into alternative clusters.

When combining all the stimulated MAIT cells cultured at pH 7.5, now with an altered clustering resolution of 0.4, to reflect the change in cell number, 4 subclusters were created (Figure 5-14D). Both siRNA treatments were seen to populate all four clusters, but less than 10% of GPR65 siRNA treated cells were represented in cluster 3, with an increase in cluster 1, compared to non-target siRNA treated cells (Figure 5-14E).


A
UMAP_2
UMAP_1
0
1
2
3
B
UMAP_2
UMAP_1
0
1
2
C
TRBV6-1
FP236383.3
IKZF2
STAT1
ADAM12
CXXC5
UTRN
TRGV2
IFITM2
LTB
GZMB
MIR155HG
IFNG
PSAT1
CCL4
LTA
ENO1
HSP90AB1
NME1
BATF3
PPP1R14B
CXCR3
CLIC3
ITM2C
FAM102A
ID3
SKIL
JUN
CXCR4
CA2
CCL3
AC010967.1
TNF
HOPX
EOMES
TRBV6-4
GZMA
TRGV5
GLCCI1
CBX1
Expression
1.0
0.5
0.0
-0.5
-1.0

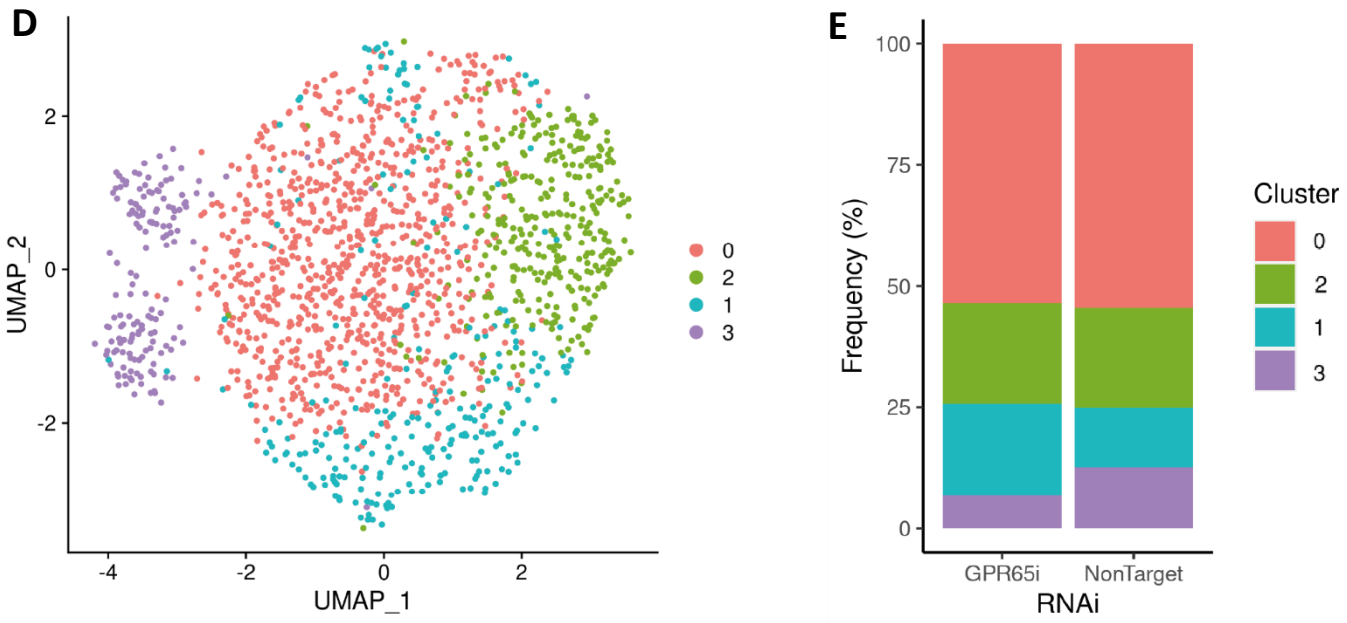


Figure 5-14 - GPR65 siRNA treatment impaired MAIT cell sub clustering

(A) UMAP of non-target siRNA treated MAIT cells, consisting of all three stimulation conditions, at neutral pH. (B) UMAP of GPR65 siRNA treated MAIT cells, consisting of all three stimulation conditions, at neutral pH. (C) The left-hand side heatmap shows row-scaled, average, log-transformed normalised expression of the top 10 significant marker genes for each cluster identified in UMAP A. The right-hand side heatmap shows those same 40 genes from the left, but for each of the clusters identified in UMAP B. (D) UMAP of all MAIT cells, consisting of all three stimulation conditions, at neutral pH. (E) Proportion of cells in each cluster from UMAP D.

Note, cluster naming is correct for figures D and E, but representative colours have changed from those depicted in figure A.

5.3.3.5 Preliminary data suggested tonic GPR65 signalling to be implicated in CD28 co-stimulatory pathways

To discover GPR65-dependent biology in immune cells, I identified differentially expressed genes between non-target and GPR65 siRNA treated cells, with or without TCR stimulation, and within different pH culture conditions.

Assessing GPR65 silencing in unstimulated MAIT cells at pH 7.5, found less than 10 transcriptional changes compared to non-target siRNA treated cells (Figure 5-15A); at an FDR-adjusted p-value < 0.05 and minimum log2FC of ±0.5. In keeping with previous analysis (detailed in 4.3.3.2), I further compared the effects of GPR65 knockdown on alternative cell types (γδT cells, conventional $CD8^+$ T cells and Th17 cells). Despite lower GPR65 expression levels on these cells (Figure 5-12), the genes reported in MAIT cells were similarly identified as being differentially expressed, regardless of whether the cells were conventional or innate-like, or due to their $CD4^+$ v $CD8^+$ phenotype (Figure 5-15B-D). As genes were similar across the cell types, and as power was weak within this analysis due to limitations of only 2 experimental conditions being compared, I repeated the DEG analysis on all $CD3^+$ $CD161^+$ T cells. Again, only a handful of transcriptional changes were reported between GPR65 knockdown and its control, with many of the DEG located below thresholds set (Figure 5-15E; within the orange box). After resetting the cut off to a minimum log2FC of ±0.25, GPR65 silencing in unstimulated cells at pH 7.5 reported 185 transcriptional changes compared to non-target siRNA treated cells (Figure 5-16A). Reactome pathway analysis of > 140 genes downregulated in GPR65 knockdown cells suggested involvement of this proton-sensing receptor in CD28 co-stimulation and PI3K/AKT signalling (Figure 5-16B).

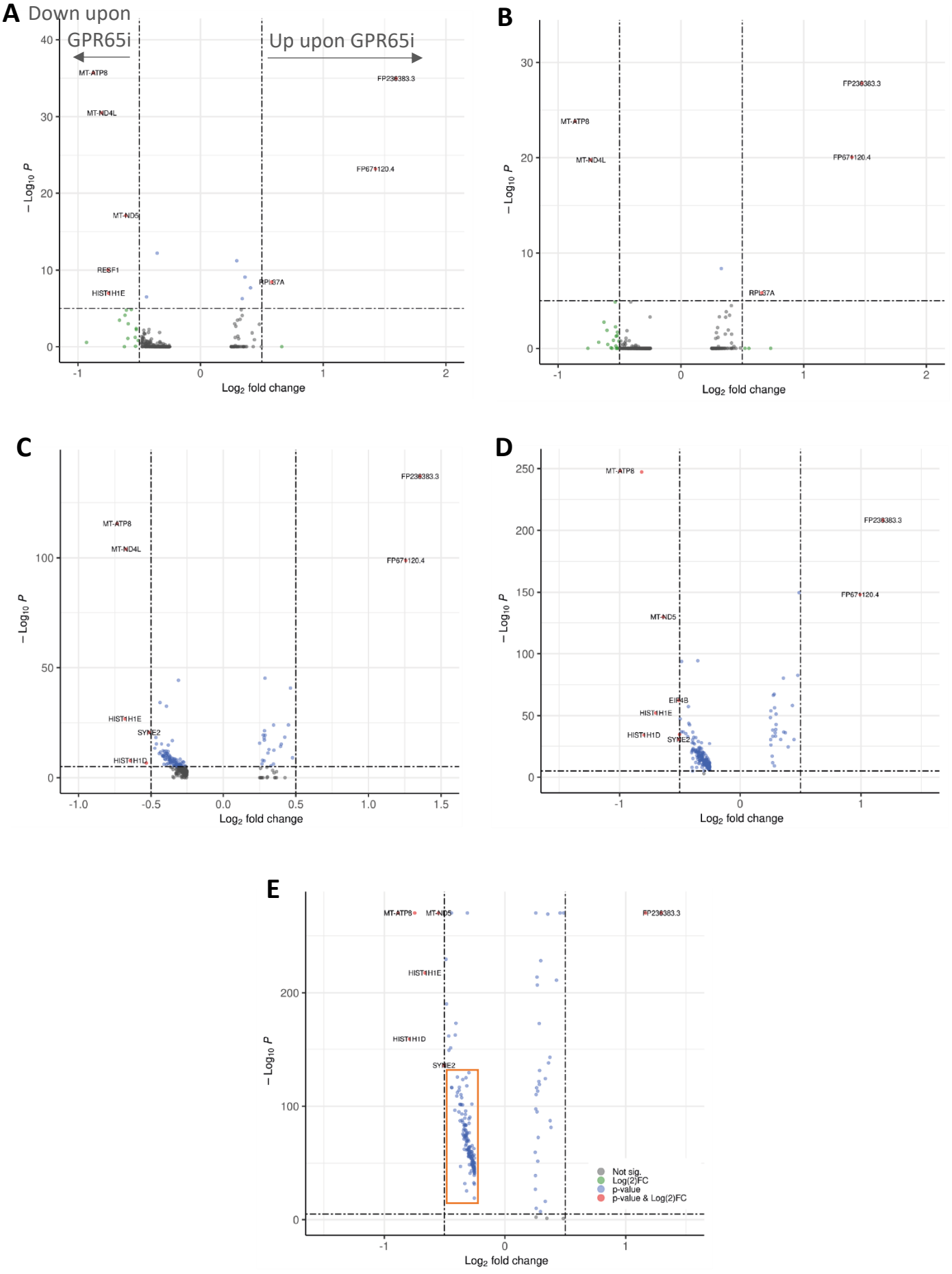

A
Down upon GPR65i
Up upon GPR65i
MT-ATP8
MT-ND4L
MT-ND5
RESF1
HIST1H1E
FP236383.3
FP671120.4
RPL37A
− Log10 P
Log2 fold change
B
MT-ATP8
MT-ND4L
FP236383.3
FP671120.4
RPL37A
C
MT-ATP8
MT-ND4L
HIST1H1E
SYNE2
HIST1H1D
FP236383.3
FP671120.4
D
MT-ATP8
MT-ND5
EIF4B
HIST1H1E
HIST1H1D
SYNE2
FP236383.3
FP671120.4
E
MT-ATP8
MT-ND5
HIST1H1E
HIST1H1D
SYNE2
FP236383.3
Not sig.
Log(2)FC
p-value
p-value & Log(2)FC

Figure 5-15 – Differentially expressed genes of unstimulated GPR65 siRNA and non-target siRNA treated T cell subsets, at pH 7.5

Volcano plots indicating genes upregulated and downregulated in GPR65 siRNA treated (GPR65i) unstimulated MAIT cells (A), γδT cells (B), $CD8^+$ T cells (C), Th17 cells (D), and all $CD3^+$ $CD161^+$ T cells (E) at neutral pH, compared to non-target siRNA treated cells. The orange box depicts a reference within the text.

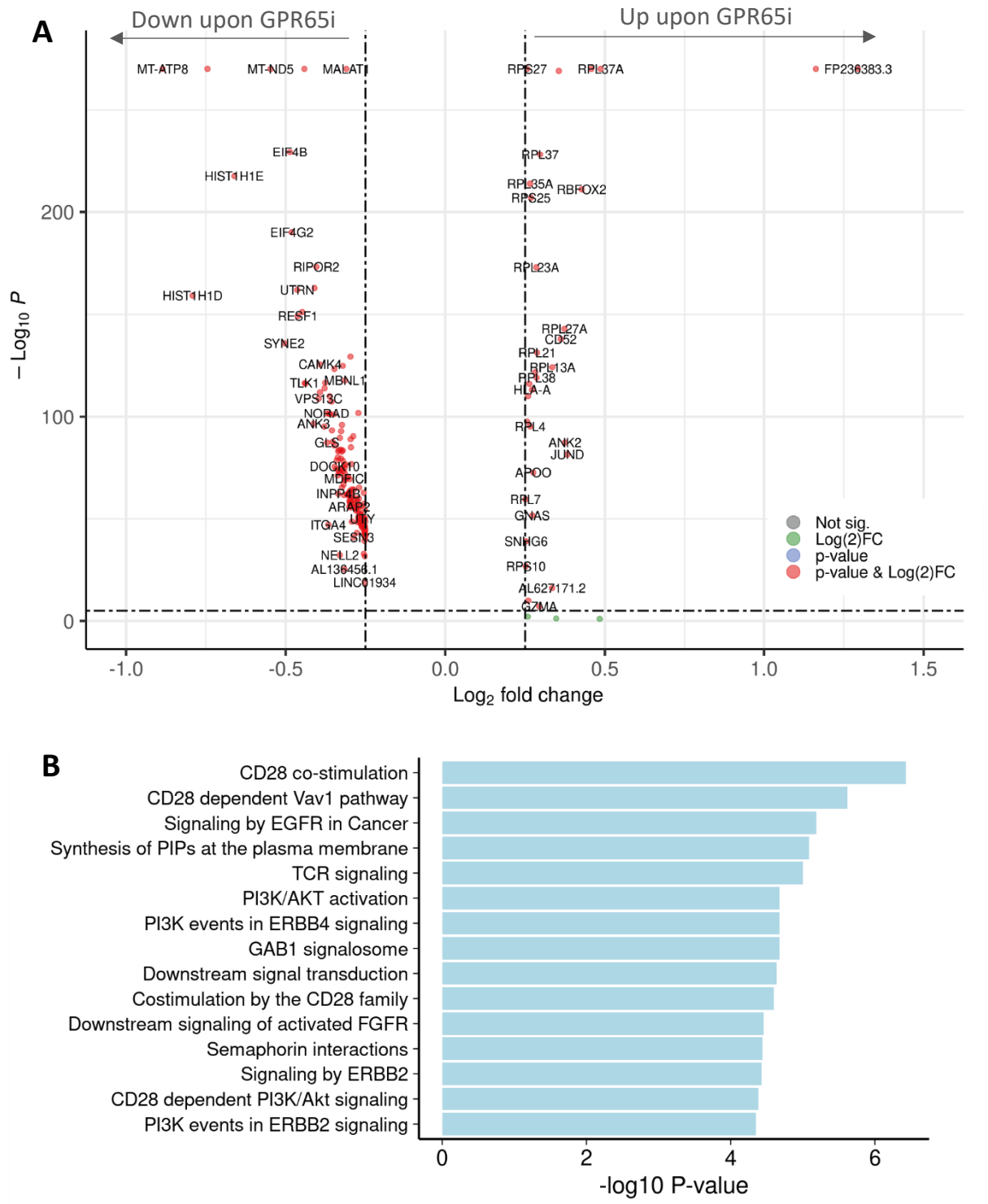


Figure 5-16 – GPR65 is suggested to be implicated with CD28 activation in a neutral pH environment

Volcano plot indicating genes upregulated and downregulated in GPR65 siRNA treated unstimulated $CD3^+$ $CD161^+$ T cells (A) at neutral pH, compared to non-target siRNA treated cells; with a false discovery rate (FDR) -adjusted p-value < 0.05 and minimum log2FC of ±0.25. (B) Reactome pathway analysis of all downregulated genes within plot A.

Henceforth, variable genes reported between non-target siRNA and GPR65 siRNA treated cells were assessed in all $CD3^+$, $CD161^+$ cells and the log2FC threshold set at ±0.25.

Assessing cells treated with GPR65 siRNA in TCR-stimulated cells at pH 7.5, identified 48 upregulated genes compared to non-target siRNA treated cells (Figure 5-17). Markers of T cell proliferation (*NFKB1, MAP2K2, JUND* (orange arrows)) were upregulated in cells with silenced GPR65, as well as the co-stimulatory receptor gene *CD81* (black arrow). Additionally, genes associated with cytotoxicity (*LTA, RUNX3* (purple arrows)) were shown to be increased in cells with reduced GPR65 expression.

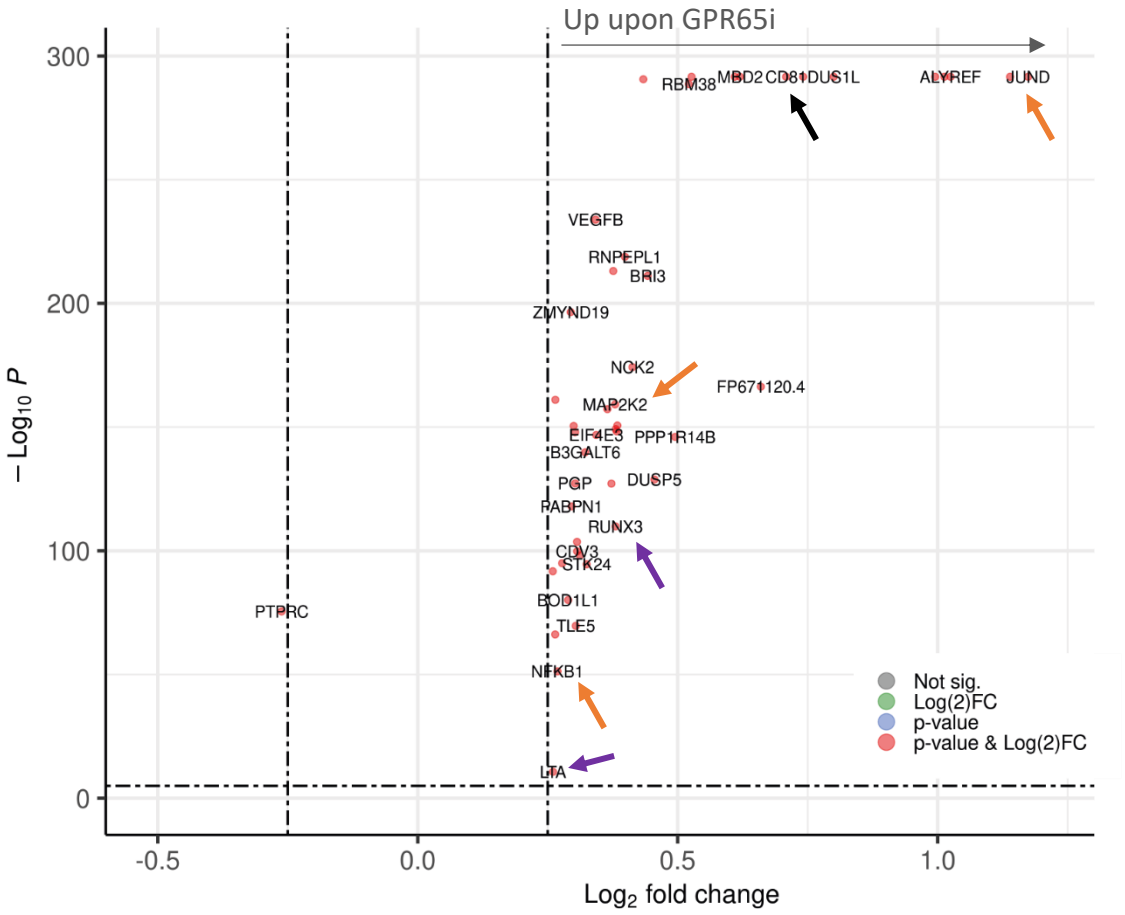


Figure 5-17 – Changes in gene expression upon GPR65 silencing in αCD3 and αCD28 stimulated CD161$^+$ T cells

Volcano plot indicating genes upregulated and downregulated in GPR65 siRNA treated, αCD3 and αCD28 stimulated CD3$^+$ CD161$^+$ T cells, at neutral pH, compared to non-target siRNA treated cells; with an FDR-adjusted p-value < 0.05 and minimum log2FC of ±0.25. Coloured arrows depict genes referenced in the text.

5.3.3.6 Increased expression of genes associated with activation and effector function upon GPR65 silencing in T cells when cultured in an acidic environment

Having explored the effects of GPR65 silencing in neutral pH, it was key to assess the proton sensing receptor's role in an acidic pH environment, given the hypothesis and functional changes observed (data within 5.3.2.2.3).

Of the 31 variable genes upregulated in unstimulated cells cultured at pH 6.5, 24 genes (77% of total DEGs) were upregulated within TCR stimulated cells cultured at pH 7.5 (Table 10).

Following TCR stimulation, despite the report of < 20 variable genes from cells cultured at pH 6.5 treated with GPR65 siRNA, compared to non-target siRNA, those identified were biologically relevant (Figure 5-18). An increase of activation (*IL2RA*) and effector genes (*GZMB, IFNG, HOPX*) was observed in cells with silenced GPR65, alongside a decrease of the resting T cell marker, *IL7R*. Overall, suggesting an anti-inflammatory role for GPR65 in activated $CD161^{+}$ T cells, when exposed to an acidic environment.

Low numbers of variable genes presented could suggest functional redundancy in the form of other proton sensing receptors. The assessment of alternative proteins only reported the presence of GPR68, ASIC3 and TRPV1 within these cells (expression of other ASIC family members were not detected). In comparison to GPR65 expression, relative expression levels were much reduced, with very little ASIC3 and TRPV1 observed (Figure 5-19).

CD81	*FAM107B*	*TMEM238*	*DUS1L*	*UBALD2*	*RBM38*
FP671120.4	*RNPEPL1*	*EIF4E3*	*NCK2*	*JUND*	*PABPN1*
SRM	*GRK6*	*RUNX3*	*CTBP1*	*BRD4*	*VEGFB*
LFNG	*ALYREF*	*PIP4K2A*	*CDV3*	*BRI3*	*BRD7*

Table 10 – List of upregulated genes in GPR65 silenced cells, observed in both unstimulated CD161$^+$ T cells at pH 6.5, and cells stimulated with αCD3 and αCD28 at pH 7.5, compared to non-target siRNA treated cells.

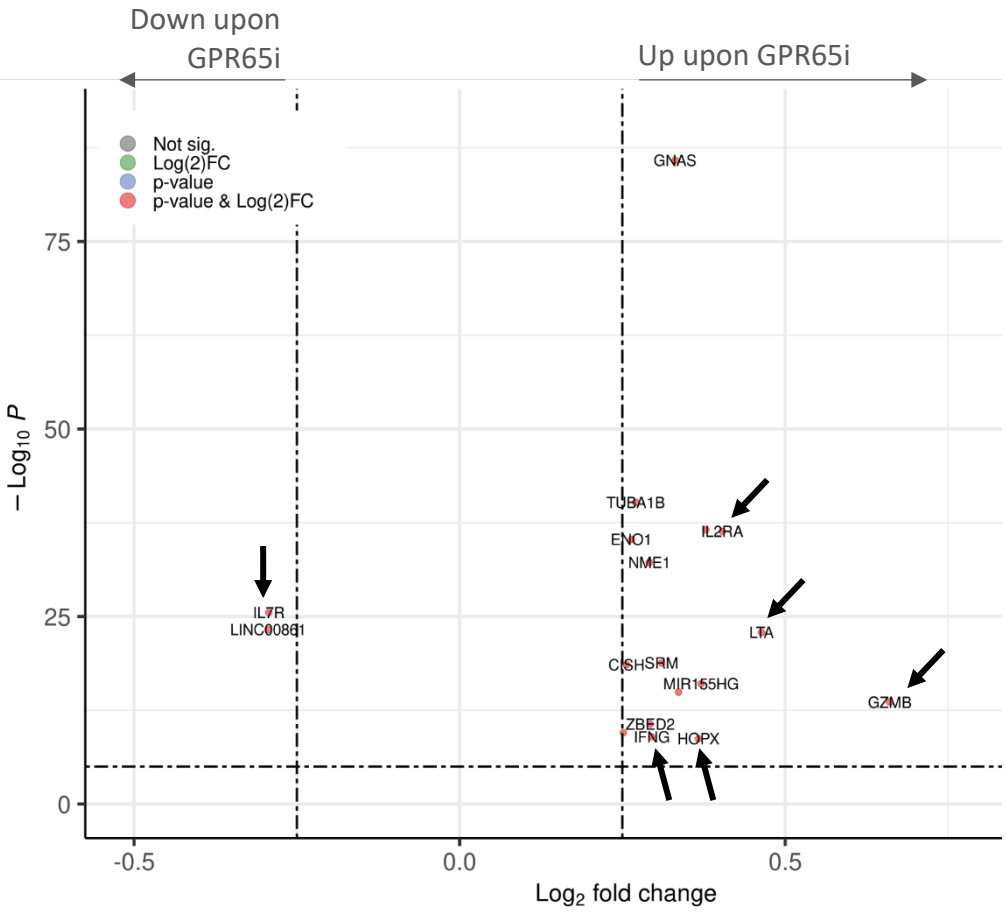


Figure 5-18 – GPR65 silencing at pH 6.5 upregulated T cell activation and effector genes, upon TCR stimulation

Volcano plot indicating genes upregulated and downregulated in GPR65 siRNA treated (GRP65i), αCD3 and αCD28 stimulated CD3$^+$ CD161$^+$ T cells, at pH 6.5, compared to non-target siRNA treated cells; with an FDR-adjusted p-value < 0.05 and minimum log2FC of ±0.25. Black arrows depict genes referenced in the text.

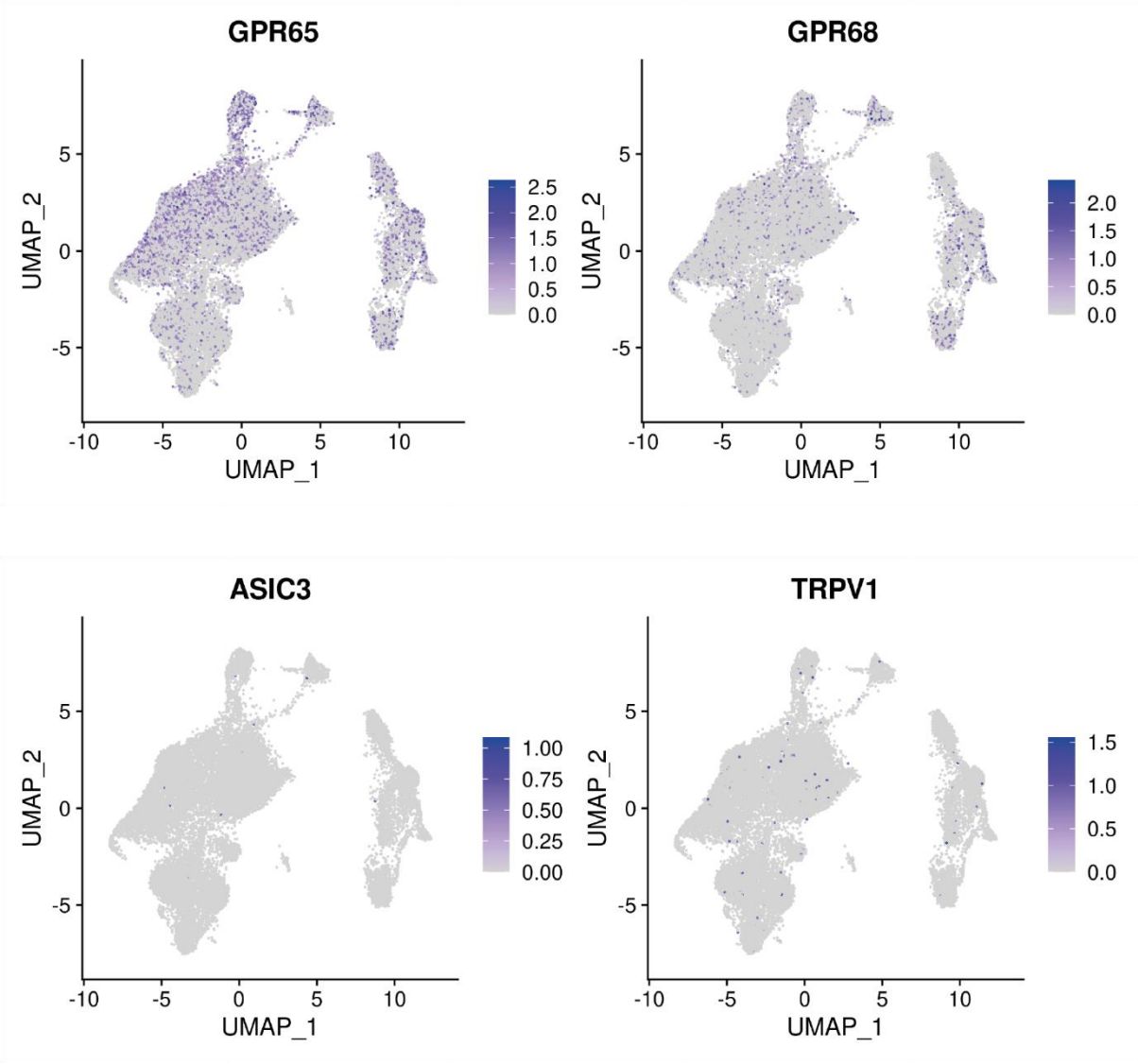


Figure 5-19 – Relative proton sensing receptor expression levels in CD161^{+} T cells

UMAP plots showing the relative gene expression of each detected proton sensing gene. The intensity of purple colour represents the normalised transcript frequency, with each dot representing a cell.

5.4 Discussion

Ankylosing spondylitis has been associated with > 100 loci through GWAS[58,59]; however, the function of the genes implicated are not always known, and often there is limited understanding of how they influence biology of health and disease[360]. Of those genes, GPR65 has been shown to be overexpressed in $CD4^+$ T cells of AS patients[75], with further eQTL analysis showing the AS-associated genotype-dependent expression of GPR65 in immune cells[201,202]. As GPR65 activity is not well defined, the primary aim of this chapter was to investigate how this proton sensing receptor impacts immune cell function, particularly as an acidic environment suppresses inflammation (Chapter 4). Here, I present evidence for GPR65 having a dual inflammatory role. This proton sensing receptor has anti-inflammatory effects in Th1-driven lymphocyte biology, through its activation upon an acidic cue (particularly for IFNγ production by TCR-stimulated MAIT cells), while GPR65 silencing at neutral pH indicates a pro-inflammatory function in IL-17A producing T cells.

Without a reliable anti-GPR65 monoclonal antibody, receptor protein levels expressed on the surface are unclear. Published work has relied upon mRNA analysis to determine GPR65 expression profiles, with expression reported in the lung, spleen, liver, cancer cells and most interestingly immune cells[361]. When assessing relative expression across the immune cell populations, $CD16^+$ NK cells, non-classical monocytes and MAIT cells expressed the highest levels of GPR65 at baseline[362]. In my hands, MAIT cells and NK cells were confirmed to express the highest levels of GPR65, whilst the monocytes did not show such a strong profile, likely due to the lack of defined subsetting. Non-classical monocytes express low, if any, levels of CD14, so were likely lost through the $CD14^+$ method of bead isolation and their expression was therefore not analysed within the monocyte population reported here.

The lack of GPR4 expressed on immune cells analysed was expected, with its expression profile primarily associated with endothelial cells of the lung, kidney, and heart[363]. Comparatively, relative to GPR65, GPR68 was expressed at lower levels on immune cells, perhaps suggesting GPR65 as the dominant proton sensing receptor in the immune system. Although GPR68 has been shown to promote pro-inflammatory cytokine release from pancreatic β-cells upon pH-dependent activation[299], alternative reports of its activity in neurones confirm its role beyond inflammation[364].

Upon testing commercial GPR65 antibodies on immune cells *ex-vivo*, the single monoclonal antibody presented non-specific binding, whilst extracellular expression was observed on $CD16^+$ NK cells and monocytes using the polyclonal antibody. Interestingly this binding profile supported observations from phage derived antibodies previously raised (Figure 3-13). Despite the right shift of antibody binding, the isotype control also bound the same cell types, albeit with slightly less of a signal. These signals could be real; however, I remain wary in trusting them due to tracking with Fc expression. CD16, also known as FcγRIII, can interact with the Fc portion of an antibody and is a likely target for binding on $CD16^+$ NK cells and non-classical monocytes, seen here.

It is not unusual to observe discrepancies between mRNA and protein expression of a given target, with transcripts not sufficient to predict protein levels alone[365]. However, if mRNA expression is high there is correlation for protein to be produced, even if not to the same high level. So, here with no signal of antibody binding to MAIT cells recorded, yet evidence of high GPR65 mRNA expression in these cells, it created further doubt in the validity of the binding profiles observed from the commercial antibody. Upon reviewing all my work whilst writing this thesis, I acknowledge the phage-derived antibodies (discovered in 3.3.2.3) could have

been tested within a functional setting, to further understand if they were specific and could modulate function in anyway, instead of being led too strongly by their primary cell binding profiles.

To address the biological questions around the functional role of the receptor in immune cells, I genetically manipulated GPR65. By blocking or overexpressing a gene, one can interrogate its phenotypic effect. Overexpression studies are well established and informative when using cell lines, however there are challenges when it comes to increasing mRNA in primary cells. Therefore, I focused my attention on assessing the function of GPR65 by silencing its expression.

There are two key methods of blocking gene expression: the CRISPR system, and RNA interference technology. Highly specific siRNA associates with the RNA-induced silencing complex, leading to cleaved mRNA and inhibition of protein expression[366]. Due to the change at the RNA level, this gene knockdown is transient and reversible. In contrast, CRISPR permanently silences the gene of interest through its knockout at the DNA level. The CRISPR-associated endonuclease protein (Cas9) is directed to the specific target gene by the corresponding guide RNA (gRNA), causing a double strand break in the DNA and ultimate protein disruption[367].

Here, I utilised the Synthego gene knockout system which used a pool of 3 gRNA specifically for GPR65, resulting in a fragment deletion. T cells were initially activated before transfection of the ribonucleoprotein (RNP) complex. However, the desired ratio of gRNA:Cas9 for this target was unknown, hence the trial of two ratios; for which my preliminary data suggested gene edits from both. Upon knockout, these cells were subject to TCR stimulation to assess the impact of gene silencing on cellular function.

After 6 days in culture, 2 rounds of stimulation and an electroporation shock, the cells were less than 50% viable. Therefore, it was unsurprising to see such low levels of intracellular cytokine expression, perhaps indicative of an exhausted phenotype. Although this method of silencing is popular in the field, I felt substantial optimisation would have been required before trusting outcomes of the functional data. It is believed that knockout efficiency is reduced without activation of the cell cycle. However, even if cell numbers were increased to improve power, without a specific antibody I would still have no way of enriching for cells with successful GPR65 silencing. The decision to stop work on the CRISPR method was aided by the parallel success of the alternative siRNA knockdown method, where inhibition of GPR65 mRNA expression was observed in MAIT cells and was reproducibly shown to have at least > 50% efficiency, repeated over multiple donors. Having achieved silencing of GPR65 mRNA for up to 48 hours, I combined previously optimised 24-hour pH stimulation experiments (detailed in 4.3.2) to explore the role of the receptor.

To strengthen functional data discoveries, I wanted to explore the transcriptional changes driven by the knockdown of GPR65 in both neutral and acidic cultures. Restrictions in the number of cells that could be sequenced per channel using the 10x chromium chip, highlighted the need to enrich for cells of interest. Here, to assess the effects of GPR65 silencing it was important to select cells expressing GPR65. Usually, one would isolate required cells using specific antibodies; however, without the option of this tool (discussed in Chapter 3), a surrogate marker in the form of CD161 was adopted.

At this stage, MAIT cells were my primary cell type of interest, due to their GPR65 expression profile and functional responses to both acidic cues and receptor silencing. As an identifying feature of MAIT cells, these cells were entirely captured through the selection of $CD161^{+}$

(encoded by KLRB1) cells, as well as alternative T cell subsets and NK cells. Nevertheless, the NK cells represented up to 40% of KLRB1 expressing cells, so the additional selection of $CD3^+$ cells was included in the sort, to not further dilute MAIT cells in the sequencing analysis. GPR65 knockdown was confirmed a success, with the expectation of altered expression when culturing in an acidic environment, and upon cell stimulation.

Acidosis at sites of inflammation has been long observed, but only over the last decade or so has the way immune cells sense this change in extracellular pH been studied. As one of many receptors with the ability to respond to proton concentration[177], GPR65 function has been assessed through a variety of methods, including mouse models of disease with silenced GPR65[204], as well as analysis of cells possessing a missense variant of the gene[206]. Together the *in vivo* and *in vitro* models have reported GPR65 to have pro- and anti-inflammatory roles, alluding to the complexity of the biology of this receptor[206,210].

As GPR65 is genetically associated with IBD, much of the functional characterisation has been performed in mouse models of colitis. An increase of proinflammatory cytokines (IFNγ, TNFα, IL-17A and IL-6) have been reported in gut tissue, alongside exacerbated disease pathology upon GPR65 knockout, with authors concluding a protective role for the receptor, at least in the context of IBD[206,368]. However, this method of cytokine analysis does not provide information on the cell types responsible for these effects.

In acidic conditions, partial rescue of TNFα and IL-6 was observed upon GPR65 knockout in LPS-primed macrophages[182]. Using alternative disease models understood to be dependent on myeloid cell biology, GPR65 knockout was associated with exacerbation of rheumatoid arthritis and myocardial infarctions[191,204], strengthening GPR65's anti-inflammatory properties, at least within macrophages.

As for GPR65 activity in T cells, its role in inflammation is conflicting. On one hand receptor silencing in $CD4^+$ T cells led to a decrease of GM-CSF production[75], as well as single cell RNA sequencing analysis providing evidence for GPR65 facilitating Th17 pathogenicity [213]. In contrast, manipulated GPR65 expression rescued pH-dependent effects on TNFα and IFNγ production by lymphocytes[192,214]. It was this contradiction of the literature that led me to want to evaluate the role of GPR65 in T cells. Deciding to focus on MAIT cells, upon the knowledge of their relatively high mRNA expression levels, I wanted to answer two questions using my data:

- What function (if any) does GPR65 have at a steady state?
- Does GPR65 play a part in the suppression of the immune cell response when exposed to an acidic environment?

When $CD161^+$ T cells were at a steady state, transcriptional analysis implied an influence of GPR65 on TCR co-stimulation and the PI3K/AKT pathway, reaffirming GPR65 activity in promoting cell survival. The silencing of GPR65 and association with PI3K signalling could imply the observed upregulation of *PI3KR1* in a low pH environment (Figure 4-17), was dependent on GPR65 sensing. Cellular activation through the TCR proposed the impact on co-stimulation was subtle, as αCD3 and αCD28 stimulation appeared to override the transcriptional signature. Instead, a loss of GPR65 in TCR activated cells at steady state resulted in an increase of a different set of variable genes, compared to the siRNA control.

A large proportion of these genes are yet to have their function revealed, whilst others infer GPR65 to influence MAPK signalling (*DUSP5, MAP2K2, STK24*). Through GPR65's coupling to G_s, the MAPK pathway can be inhibited[210,369]; therefore, the upregulation of these genes in T

cells where GPR65 has been silenced suggests receptor activation, even upon sensing a low concentration of extracellular H^+.

Additional analysis of GPR65-silenced MAIT cells at pH 7.5, showed the loss of a 'prolonged activation' subcluster, presenting an inflammatory signature including, *HOPX, TNF and EOMES,* for which these have been shown to be associated with SpA[58,75]. Together with the results from the *in vitro* functional experiment at pH 7.5, where IL-17A was reduced in GPR65 siRNA treated $CD4^+$ and $CD8^+$ T cells, compared to the non-target control, work presented here suggests GPR65 to be pro-inflammatory in T cells, in neutral conditions.

Next, the assessment of lymphocytes cultured in acidic conditions without stimulation interestingly revealed many of the same upregulated differentially expressed genes as those observed upon TCR-stimulated, GPR65 siRNA treated, $CD161^+$ T cells at pH 7.5. Several of these genes are yet to have their function described, but this independent finding advocates their involvement in GPR65 biology. Furthermore, and perhaps more importantly, this observation could imply that activated cells in neutral conditions generate a very localised low pH environment, likely through their own metabolic activity, leading to GPR65 signalling.

The silencing of GPR65 in TCR-stimulated $CD8^+$ T cells was able to partially rescue IFNγ and granzyme B at pH 6.5, suggesting that the receptor was in part responsible for the reduced cytokine response in acidic conditions. These effects however did not appear to be restricted to $CD8^+$ T cells when considering transcriptional changes, with *IFNG* and *GZMB*, amongst other inflammation associated effector genes, upregulated upon GPR65 knockdown.

Poignantly, whilst I was analysing the sequencing data a very relevant and supporting study was published. Chen and colleagues were using bacterial induced colitis models to address the impact of GPR65 on tissue homeostasis in the gut[192]. Not only did they include mice with

a full GPR65 knockout (KO) to assess disease, but they also compared the effects of the IBD associated SNP (rs3742704) which causes a partial loss of function. Therefore, is translatable to my partially effective siRNA driven GPR65 knockdown. $CD4^+$ T cells from these and WT mice cultured at both pH 7.4 and pH 6.8 replicated my findings of GPR65 rescuing IFNγ suppression in acidic conditions, and the additional partial rescue of TNFα, although to a lesser extent. Along with the observation of GPR65 knockdown restricting IL-17A production.

Additional too wet lab assessment of function, the group further incorporated single cell RNA sequencing of Th17 and Th22 cells from the KO and WT mice, and report that GPR65 signalling impacts metabolism pathways. Data collected here has independently reproduced this with the observation of the upregulation of *SRM*, a polyamine pathway gene, observed in GPR65 siRNA treated cells, independent of stimulation or pH. Furthermore, Chen *et al's* sequencing was performed on $CD4^+$ T cells in neutral conditions, without any prior activation and confirm my observations of GPR65 influencing T cell receptor signalling[192].

In general, low numbers of variation in gene expression levels presented in my work comparing GPR65 siRNA and its non-target control at low pH, could suggest the pH effect or stimulation was too strong to see subtle activity of GPR65. Alternatively, the nature of only partially rescuing pH-dependent suppression speaks to activity of other proteins driving this response. Although relatively lower than GPR65 expression, the presence of GPR68 is interesting. GPR68 knockout in mouse models of IBD have suggested that it primarily reacts to acidosis in a pro-inflammatory manner and is a potential 'counter player' to GPR65[370,371]. Therefore, it would be plausible that upon GPR65 redundancy, GPR68 becomes the dominant proton sensing GPCR and masks the anti-inflammatory effects from GPR65.

A caveat of work presented in this chapter using siRNA to assess gene function, could also explain the lack of highly definitive conclusions throughout this chapter. Without an approach to assess corresponding protein expression, it is unclear how much knockdown has been translated to the surface. Alternative GPCR family members have a reported half-life between 24-72 hours on human immune cells[372]; however, the field is lacking knowledge around the turnover of GPR65 specifically. Therefore, if GPR65 half-life is at the higher end of the range, it is possible that effective protein knockdown was not achieved in the time frame of the assays described here. This current gap of knowledge indeed places importance on the continuation of the discovery of a reliable GPR65 specific antibody.

Here, conclusions have been made upon seeing a partial loss of mRNA expression, with the assumption of a similar loss of protein, but this incomplete knockdown will likely present confounding effects from the remnant low levels of protein still expressed. Developments for using CRISPR technology here would be beneficial to understand the true function of the receptor, but one could argue not have the ability to assess how gene dysregulation influences disease.

GPR65 is primarily expressed on cells that can respond to stimulus in an innate fashion. Proposed GPR65 function on MAIT cells, γδT cells and myeloid cells have already been discussed, but high mRNA expression is also observed in NK cells. Using a mouse model of multiple sclerosis, disease was exacerbated in GPR65 knockout mice and was discovered to be dependent on iNKT cells[190]. As the pH of the central nervous system in the EAE model has been reported to be pH 6.6[373], this study further supports a protective role for GPR65 expressed on innate immune cells in acidic environments.

In general, $CD161^{+}$ expressing cells are associated with pathogenic cell types, particularly those capable of IL-17A secretion[374]; so, as GPR65 appears to correlate with its corresponding gene expression, does this proton sensing receptor serve as a brake on inflammation when those cells reach infection or inflammatory sites presenting acidosis?

Overall, my lymphocyte data supports GPR65 possessing both pro- and anti-inflammatory properties, dependent on the environment. One could even theorise perhaps a favoured Th1-like suppression in acidic environments, while promoting a Th17 signature at steady state. Unfortunately, assessment of IL-17A related biology was not captured by sequencing methods. With the restraint of costs associated with scRNAseq, only one timepoint was analysed, so this limitation of the work presented could provide an explanation for the lack of detecting *IL17A, IL17F* and *RORC* expression.

Chapter 6 : Overall Discussion and Future Directions

6.1 Main findings

The focus of this project was to investigate the role of GPR65 on immune function, incorporating antibody discovery, with the aim to identify a tool reagent, to address key biological questions.

My initial focus was the generation of a GPR65 specific monoclonal antibody, which as a GPCR with an unidentified complex structure, I knew would be a challenge. Established antibody discovery methods were productive, raising specific antibodies against the antigen used. However, there was a high level of attrition across all campaigns, resulting in only one potential, conformationally sensitive, GPR65 specific antibody, speaking to the general lack of understanding of the receptors structure and its behaviours. It is likely a great deal of optimisation and novel techniques are required to fully identify the true structure of this orphan GPCR and allow subsequent studies to be performed to understand its expression properties, as well as details of its various conformations within specific environments, especially in response to changes of extracellular pH. Not only would knowing more about the GPCR structure offer insight into mechanisms of function, it would also provide a basis for drug design.

Within the context of GPCR antibody discovery I have provided evidence of a scaffold-based approach for displaying looped antigen, resulting in the identification of loop-specific antibodies. Therefore, providing promise for future antibody campaigns to utilise this presentation of targets with unstable structures, in displaying extracellular loops of interest. With enhancements of research on basic structure, as well as developments of novel

approaches for antibody discovery against difficult structures, the generation of functional antibodies against difficult to target GPCRs is closer than ever before.

This project approached exploring the function of the pH sensing GPR65 receptor in two halves; the first to establish the role of pH on immune function, then to address the specific role of GPR65 in mediating the effects observed, utilising genetic manipulation in the absence of reliable antibody reagents. This thesis confirms the consensus of a low pH environment negatively impacting immune cell function, inhibiting pro-inflammatory responses from T lymphocytes.

I have highlighted that GPR65 can signal through the G_s coupled protein, leading to an increase of cAMP production and in turn phosphorylating CREB. This post translational modification is understood to inhibit its own binding to the NFκB complex, resulting in the restriction of the inflammatory response[188]. Therefore, one would predict the activation of GPR65 to drive anti-inflammatory effects, as supported by GPR65 functional studies on myeloid cells[182]. Nevertheless, given the reported immune regulatory effects of GPR65 in T cells associated with SpA[75,213] and its genetic association through GWAS[58], I initially hypothesised that GPR65 would be exacerbating the already inflammatory milieu in a diseased environment. However, work presented in this thesis has suggested a more complex function of GPR65 than originally envisaged.

GPR65 is understood to be most highly expressed on innate-like T cells and monocytes, from their relative mRNA expression profiles. Inflammatory sites, including solid tumours, are often accompanied by acidic conditions, driven through resident metabolic activity, including glycolysis[375]. Data presented in this thesis shows a reduced inflammatory profile from MAIT cells when cultured in acidic environments; for which GPR65 appears to be somewhat

implicated, with evidence at both protein (the rescue of low pH dependent IFNγ and granzyme B suppression) and mRNA levels (GPR65 silencing lead to the upregulation of *IL2RA, IFNG, GZMB, HOPX*). It is worth considering the relatively few differentially expressed genes, and their small fold changes observed through RNA sequencing perhaps speaks to a degree of redundancy in the system, with alternative proton sensing GPCRs, such as GPR68 potentially also playing a role. This is a limitation of my work and to overcome this, one could either knockout GPR68 and assess GPR65 silencing on immune function, or alternatively use GPR65 specific agonists or antagonists (as previously described[264,376]) to validate the findings seen.

A couple of explanations for opposing immune activity of GPR65 reported in the literature could be through differences of achieving full or partial knockout, or even disease model-specific variances. Remarkably, this conflicting evidence is likely proposing the theory that GPR65 acts differently on alternative cell types and perhaps provides innate-adaptive immune cell crosstalk. Global knockout mice suggest GPR65 to be anti-inflammatory[206], whilst conditional knockout models in $CD4^+$ T cells provide evidence for the receptor's pro-inflammatory role[210], both within in IBD models. A clear difference here is the presence of GPR65 expression on both myeloid cells and NK cells, as well as T lymphocytes.

I observed stronger functional effects of GPR65 silencing in MAIT cells within a mixed culture, compared to in isolated T cell conditions (and arguably a potential reason for weak findings from the RNA sequencing). This implicates an indirect effect from alternative cells in the system (likely to be soluble factors released by monocytes), which importantly also would have displayed some degree of GPR65 knockdown. Within inflamed joints of AS patients, the presence of a variety of immune cells have been reported, with cell-cell crosstalk likely, and

each responding in their own way to the local environment, but also have the potential to indirectly affect each other. Whilst performing GPR65 functional studies in specific isolated cell populations to identify its exact function is appropriate, to understand the role of GPR65 specifically within the disease context, future studies of GPR65 should be performed in a mixed cell system.

Arguably, the most significant finding of my work is that GPR65 has opposing effects on T cell receptor driven inflammation, dependent on the extracellular hydrogen ion concentration, thus highlighting the importance of understanding immune function in the right environment. Often, most *in-vitro* human work is carried out at neutral pH, so future studies should keep in mind the environment in which immune cells need to function, and the likely impact of that. Here, I have shown that GPR65 serves as a brake on inflammation in acidic conditions, whilst its tonic signalling at neutral conditions potentiated IL-17 production. Based on the observations in this thesis, a model describing the activity of GPR65 was developed, and is shown in Figure 6-1. Further research is required to understand the differences between effects on Th1 versus Th17 related functions. GPR65 is reported to have a RORγt binding site in its promoter[377], so the question becomes; how does GPR65 signalling impact the regulation of RORC, and potentially other immune transcription factors, such as TXB21?

In the context of spondyloarthritis, I propose a role for innate-like lymphocytes expressing GPR65. Although MAIT cell numbers have been reported to be lower in the blood of AS patients compared to healthy controls, they had increased production of IL-17A[119]. From data presented here, MAIT cells in the periphery may be tonically activated through their high expression of GPR65, and in part be responsible for the increased IL-17 phenotype. Upon their recruitment and migration to the joint, these already primed cells respond to acidosis through

the substantial activation of GPR65, suppressing clinically validated pro-inflammatory cytokines and protecting the joint from further tissue damage.

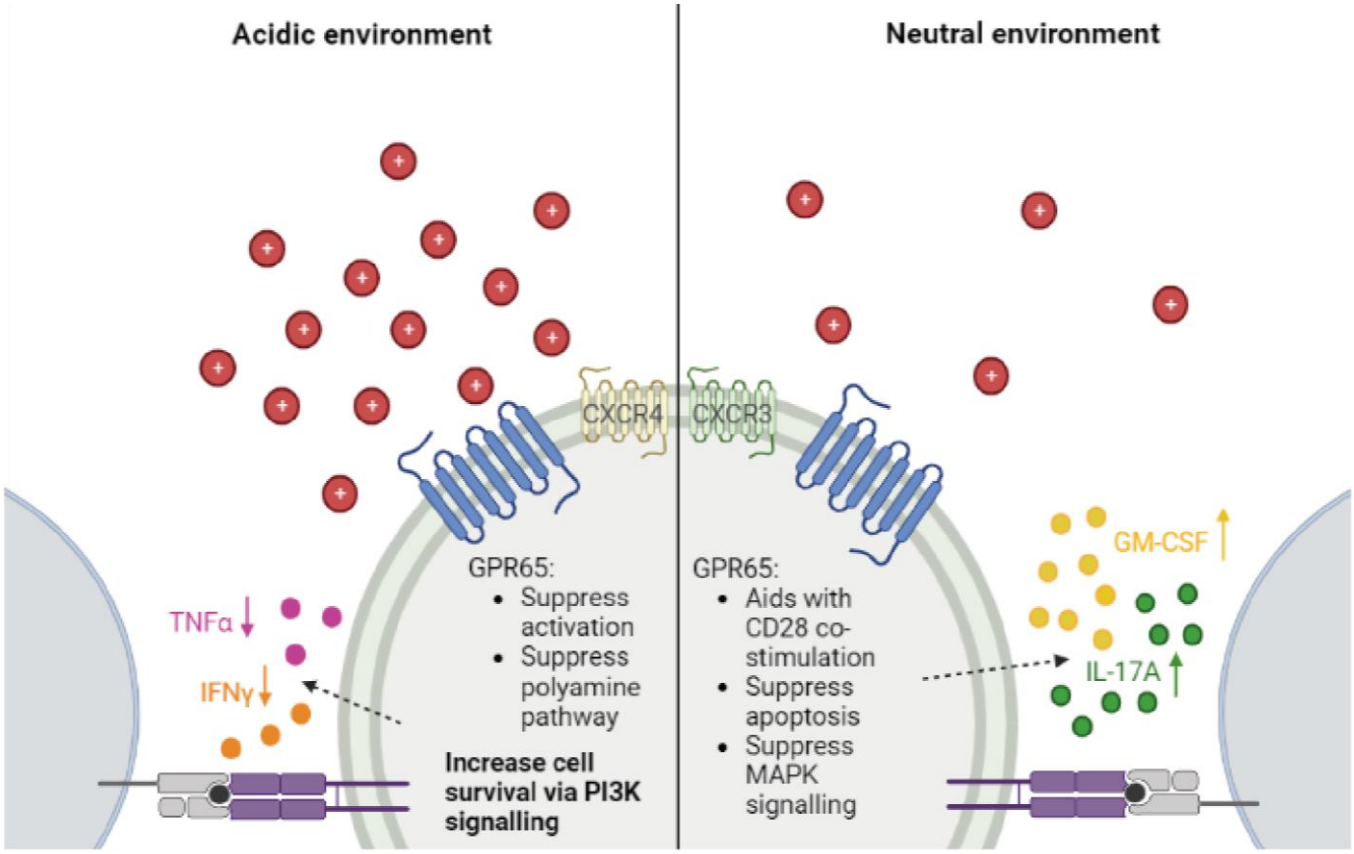


Figure 6-1 – Model of GPR65 function in TCR stimulated T cells, in neutral and low pH extracellular environments

In neutral pH conditions, tonic GPR65 signalling in TCR stimulated T cells augments the CD28 co-stimulation pathway, promotes the production of GM-CSF and IL-17A, and suppresses apoptosis. In contrast, GPR65 activation through acidosis on TCR stimulated T cells mediates the suppression of cellular activation and Th1-related cytokine release, favours CXCR4 expression over CXCR3 expression and increases cell survival through PI3K signalling. Diagram created with BioRender.

6.2 Overall conclusion

Although there are proven treatments for ankylosing spondylitis, a great unmet clinical need remains, with low remission rates still seen. Important biological pathways have been associated with disease through genome wide association studies but understanding how relevant they are at a functional level is crucial to propose new therapeutic targets with confidence. Evidence provided here on the complex functional activity of GPR65 on immune cells makes it challenging to decide whether blocking or enhancing its effects would be advantageous for AS. I believe I have generated some important new questions, which will hopefully be the subject of future research.

6.3 Future directions

Validation of single cell RNA sequencing findings

The relatively limited sample size for the scRNAseq experiment could be considered a limitation of this study. However, this number of samples (n=3) is not uncommon for observational studies. The analysis highlighted genes which appeared to be dependent on GPR65 activity, but I unfortunately ran out of time to follow these up. To gain confidence in the genes implicated, my next steps would have been to perform a follow up bulk RNA sequencing experiment, with repeated conditions of TCR stimulation on non-target and GPR65 siRNA treated $CD3^+$, $CD161^+$ T cells, cultured at the two pH of interest, isolating then only the MAIT cells and γδT cell populations for analysis. Upon the confirmation of these dependent genes, I would have then gone on to validate them *in vitro*.

Alternatively, it would be interesting to follow up with RNA sequencing on $CD161^+$ T cells, having been cultured within a mixed PBMC system, and assess how transcriptional changes differ to data recorded here, to unpick how important cell cross talk is for GPR65 biology.

Assess GPR65 function in ankylosing spondylitis patients

My research has been based exclusively on samples from heathy volunteers and focused on MAIT cells in particular, due to their GPR65 expression profile and effect on function observed upon their culture in an acidic environment. As these cells are similar in phenotype and function to γδT cells[129], and both these innate-like cells are enriched in the inflamed joint[119,132], the next stage of this research would be to assess whether GPR65 function in these cells from AS patients is the same as in health.

Firstly, it would be interesting to compare the function of both cells derived from the periphery to those isolated from the synovial fluid from patients, to assess if cells in the joint are primed for the response of GPR65, through their consistent exposure to acidosis. Secondly, the specifics of how a missense mutation in GPR65 affects disease in IBD is reported, through the use of patient cells displaying the SNP rs3742704[192,206]. It would be informative to assess the function of the AS associated SNP rs11624293 (in LD with rs3742704) in patients, to hypothesise the extent to which GPR65 is altering the immune response in disease; particularly as results here showed GPR65 knockdown led to the differential expression of several genes associated with AS (*IL7R, EOMES RUNX3, TBX21*).

Appendix

How COVID has impacted this DPhil

Despite the breadth of work achieved throughout this DPhil, the initial proposal has changed somewhat due to global challenges faced.

I originally had proposed to run all functional experiments in ankylosing spondylitis PBMCs, in parallel with healthy donors. However, through restrictions and prioritisation of telemed consultations, access to patient samples was not possible for a long time. Ideally, I would have also used more than 3 healthy controls per experiment, but with less volunteers on site to donate fresh blood, this was also challenging throughout.

The first of the COVID lockdowns came into effect less than a year into my DPhil. Although I was fortunate to gain eventual access into UCB labs, just under 3 months of lab time was lost. The skeleton staff in labs at this time left little technical support available whilst I was tackling the unfamiliar antibody discovery process, although I did have virtual advice if things were not quite as expected.

Finally, worldwide shortages of consumables through impacts from COVID and Brexit were also felt, and plans were altered accordingly. For example, I could not source low binding plates to continue additional FACS based analysis of monocyte function, and general reagents were often substituted for less reliable alternatives, such as swapping the established tips for non-low retention tips.

References

1. Dougados, M. & Baeten, D. Spondyloarthritis. *Lancet* 377, 2127–2137 (2011).

2. McGonagle, D., Gibbon, W. & Emery, P. Classification of inflammatory arthritis by enthesitis. *Lancet Lond Engl* 352, 1137–40 (1998).

3. Navarro-Compán, V., Sepriano, A., El-Zorkany, B. & Heijde, D. van der. Axial spondyloarthritis. *Ann Rheum Dis* 80, 1511–1521 (2021).

4. Wang, C.-R. *et al.* Rare occurrence of inflammatory bowel disease in a cohort of Han Chinese ankylosing spondylitis patients- a single institute study. *Sci Rep-uk* 7, 13165 (2017).

5. Rosenbaum, J. T., Pisenti, L., Park, Y. & Howard, R. A. Insight into the Quality of Life of Patients with Ankylosing Spondylitis: Real-World Data from a US-Based Life Impact Survey. *Rheumatology Ther* 6, 353–367 (2019).

6. Dean, L. E. *et al.* Global prevalence of ankylosing spondylitis. *Rheumatology* 53, 650–657 (2014).

7. Baum, J. & Ziff, M. The Rarity of Ankylosing Spondylitis in the Black Race. *Arthritis Rheumatism* 14, 12–18 (1971).

8. Reveille, J. D., Hirsch, R., Dillon, C. F., Carroll, M. D. & Weisman, M. H. The prevalence of HLA–B27 in the US: Data from the US National Health and Nutrition Examination Survey, 2009. *Arthritis Rheumatism* 64, 1407–1411 (2012).

9. Jamalyaria, F. *et al.* Ethnicity and disease severity in ankylosing spondylitis a cross-sectional analysis of three ethnic groups. *Clin Rheumatol* 36, 2359–2364 (2017).

10. Ogdie, A. *et al.* Real-World Patient Experience on the Path to Diagnosis of Ankylosing Spondylitis. *Rheumatology Ther* 6, 255–267 (2019).

11. HAWLEY, S., SACKS, S., BOWNESS, P. & PRIETO-ALHAMBRA, D. Incidence of Total Hip and Knee Replacement in UK Patients with Ankylosing Spondylitis. *J Rheumatology* 45, 1334–1336 (2018).

12. Gracey, E. *et al.* Sexual Dimorphism in the Th17 Signature of Ankylosing Spondylitis. *Arthritis Rheumatol* 68, 679–689 (2016).

13. Hay, C. A. *et al.* Diagnostic delay in axial spondyloarthritis: a systematic review. *Clin Rheumatol* 41, 1939–1950 (2022).

14. Zhu, W. *et al.* Ankylosing spondylitis: etiology, pathogenesis, and treatments. *Bone Res* 7, 22 (2019).

15. Murphy, S. N. *et al.* A brief human history of ankylosing spondylitis: A scoping review of pathogenesis, diagnosis, and treatment. *Surg Neurology Int* 13, 297 (2022).

16. Linden, S. V. D., Valkenburg, H. A. & Cats, A. Evaluation of Diagnostic Criteria for Ankylosing Spondylitis. *Arthritis Rheumatism* 27, 361–368 (1984).

17. Sieper, J. *et al.* The Assessment of SpondyloArthritis international Society (ASAS) handbook: a guide to assess spondyloarthritis. *Ann Rheum Dis* 68, ii1 (2009).

18. Sieper, J. *et al.* Systematic review of clinical, humanistic, and economic outcome comparisons between radiographic and non-radiographic axial spondyloarthritis. *Semin Arthritis Rheu* 46, 746–753 (2017).

19. Rudwaleit, M. *et al.* The Assessment of SpondyloArthritis international Society classification criteria for peripheral spondyloarthritis and for spondyloarthritis in general. *Ann Rheum Dis* 70, 25 (2011).

20. Brown, M. A. *et al.* Susceptibility to ankylosing spondylitis in twins the role of genes, HLA, and the environment. *Arthritis Rheumatism* 40, 1823–1828 (1997).

21. Rudwaleit, M. & Baeten, D. Ankylosing spondylitis and bowel disease. *Best Pract Res Clin Rheumatology* 20, 451–471 (2006).

22. Stolwijk, C. *et al.* The epidemiology of extra-articular manifestations in ankylosing spondylitis: a population-based matched cohort study. *Ann Rheum Dis* 74, 1373 (2015).

23. Vos, M. D. *et al.* Ileocolonoscopy in Seronegative Spondylarthropathy. *Gastroenterology* 96, 339–344 (1989).

24. Praet, L. V. *et al.* Microscopic gut inflammation in axial spondyloarthritis: a multiparametric predictive model. *Ann Rheum Dis* 72, 414 (2013).

25. Campos, J. F. *et al.* Fecal calprotectin as a biomarker of microscopic bowel inflammation in patients with spondyloarthritis. *Int J Rheum Dis* 25, 1078–1086 (2022).

26. Fragoulis, G. E. *et al.* Inflammatory bowel diseases and spondyloarthropathies: From pathogenesis to treatment. *World J Gastroentero* 25, 2162–2176 (2019).

27. Rehaume, L. M. *et al.* ZAP-70 Genotype Disrupts the Relationship Between Microbiota and Host, Leading to Spondyloarthritis and Ileitis in SKG Mice. *Arthritis Rheumatol* 66, 2780–2792 (2014).

28. Taurog, J. D. *et al.* The germfree state prevents development of gut and joint inflammatory disease in HLA-B27 transgenic rats. *J Exp Medicine* 180, 2359–2364 (1994).

29. Qin, J. *et al.* A human gut microbial gene catalogue established by metagenomic sequencing. *Nature* 464, 59–65 (2010).

30. Huttenhower, C., Kostic, A. D. & Xavier, R. J. Inflammatory Bowel Disease as a Model for Translating the Microbiome. *Immunity* 40, 843–854 (2014).

31. Berland, M. *et al.* Both disease activity and HLA-B27 determine gut microbiome dysbiosis in spondyloarthritis. *Arthritis Rheumatol* (2022) doi:10.1002/art.42289.

32. Costello, M. *et al.* Brief Report: Intestinal Dysbiosis in Ankylosing Spondylitis. *Arthritis Rheumatol* 67, 686–691 (2015).

33. Sternes, P. R. *et al.* Distinctive gut microbiomes of ankylosing spondylitis and inflammatory bowel disease patients suggest differing roles in pathogenesis and correlate with disease activity. *Arthritis Res Ther* 24, 163 (2022).

34. Schlosstein, L., Terasaki, P. I., Bluestone, R. & Pearson, C. M. High Association of an HL-A Antigen, W27, with Ankylosing Spondylitis. *New Engl J Medicine* 288, 704–706 (1973).

35. Brewerton, D. A. *et al.* ANKYLOSING SPONDYLITIS AND HL-A 27. *Lancet* 301, 904–907 (1973).

36. Gofton, J., Chalmers, A., Price, G. & Reeve, C. HL-A 27 and ankylosing spondylitis in B.C. Indians. *J Rheumatol* 11, 572–3 (1984).

37. Bowness, P. HLA-B27. *Annu Rev Immunol* 33, 29–48 (2015).

38. D'amato, M. *et al.* Relevance of residue 116 of HLA-B27 in determining susceptibility to ankylosing spondylitis. *Eur J Immunol* 25, 3199–3201 (1995).

39. Braun, J. *et al.* Prevalence of spondylarthropathies in HLA-B27 positive and negative blood donors. *Arthritis Rheumatism* 41, 58–67 (1998).

40. Wordsworth, B. P., Cohen, C. J., Davidson, C. & Vecellio, M. Perspectives on the Genetic Associations of Ankylosing Spondylitis. *Front Immunol* 12, 603726 (2021).

41. Hermann, E., Büschenfelde, K.-H. M. zum, Fleischer, B. & Yu, D. T. Y. HLA-B27-restricted CD8 T cells derived from synovial fluids of patients with reactive arthritis and ankylosing spondylitis. *Lancet* 342, 646–650 (1993).

42. Taurog, J. D. *et al.* Spondylarthritis in HLA–B27/human β2-microglobulin–transgenic rats is not prevented by lack of CD8. *Arthritis Rheumatism* 60, 1977–1984 (2009).

43. RL, A., CA, O., AJ, M. & P, B. Cutting edge: HLA-B27 can form a novel beta 2-microglobulin-free heavy chain homodimer structure. *J Immunol* 162, 5045–8 (1999).

44. Bird, L. A. *et al.* Lymphoblastoid cells express HLA-B27 homodimers both intracellularly and at the cell surface following endosomal recycling. *Eur J Immunol* 33, 748–759 (2003).

45. Kollnberger, S. *et al.* Cell-surface expression and immune receptor recognition of HLA–B27 homodimers. *Arthritis Rheumatism* 46, 2972–2982 (2002).

46. Rysnik, O. *et al.* Non-conventional forms of HLA-B27 are expressed in spondyloarthritis joints and gut tissue. *J Autoimmun* 70, 12–21 (2016).

47. Bowness, P. *et al.* Th17 Cells Expressing KIR3DL2+ and Responsive to HLA-B27 Homodimers Are Increased in Ankylosing Spondylitis. *J Immunol* 186, 2672–2680 (2011).

48. Chan, A. T., Kollnberger, S. D., Wedderburn, L. R. & Bowness, P. Expansion and enhanced survival of natural killer cells expressing the killer immunoglobulin-like receptor KIR3DL2 in spondylarthritis. *Arthritis Rheumatism* 52, 3586–3595 (2005).

49. Payeli, S. K. *et al.* Inhibiting HLA–B27 homodimer–driven immune cell inflammation in spondylarthritis. *Arthritis Rheumatism* 64, 3139–3149 (2012).

50. Sian, T. C. C. L. K. *et al.* Allelic association with ankylosing spondylitis fails to correlate with human leukocyte antigen B27 homodimer formation. *J Biol Chem* 294, 20185–20195 (2019).

51. Mear, J. *et al.* Misfolding of HLA-B27 as a result of its B pocket suggests a novel mechanism for its role in susceptibility to spondyloarthropathies. *J Immunol* 163, 6665–70 (1999).

52. Goodall, J. C. *et al.* Endoplasmic reticulum stress-induced transcription factor, CHOP, is crucial for dendritic cell IL-23 expression. *Proc National Acad Sci* 107, 17698–17703 (2010).

53. Turner, M. J. *et al.* HLA-B27 Misfolding in Transgenic Rats Is Associated with Activation of the Unfolded Protein Response. *J Immunol* 175, 2438–2448 (2005).

54. Rezaiemanesh, A. *et al.* Upregulation of Unfolded Protein Response and ER Stress–Related IL-23 Production in M1 Macrophages from Ankylosing Spondylitis Patients. *Inflammation* 45, 665–676 (2022).

55. Zeng, L., Lindstrom, M. J. & Smith, J. A. Ankylosing spondylitis macrophage production of higher levels of interleukin-23 in response to lipopolysaccharide without induction of a significant unfolded protein response. *Arthritis Rheumatism* 63, 3807–3817 (2011).

56. Ciccia, F. *et al.* Evidence that autophagy, but not the unfolded protein response, regulates the expression of IL-23 in the gut of patients with ankylosing spondylitis and subclinical gut inflammation. *Ann Rheum Dis* 73, 1566 (2014).

57. Sieper, J., Braun, J., Dougados, M. & Baeten, D. Axial spondyloarthritis. *Nat Rev Dis Primers* 1, 15013 (2015).

58. (IGAS), I. G. of A. S. C. *et al.* Identification of multiple risk variants for ankylosing spondylitis through high-density genotyping of immune-related loci. *Nat Genet* 45, 730–738 (2013).

59. Ellinghaus, D. *et al.* High-density genotyping study identifies four new susceptibility loci for atopic dermatitis. *Nat Genet* 45, 808–812 (2013).

60. Chen, L. *et al.* Silencing or inhibition of endoplasmic reticulum aminopeptidase 1 (ERAP1) suppresses free heavy chain expression and Th17 responses in ankylosing spondylitis. *Ann Rheum Dis* 75, 916 (2016).

61. Danoy, P. *et al.* Association of Variants at 1q32 and STAT3 with Ankylosing Spondylitis Suggests Genetic Overlap with Crohn's Disease. *Plos Genet* 6, e1001195 (2010).

62. (IIBDGC), T. I. I. G. C. *et al.* Host–microbe interactions have shaped the genetic architecture of inflammatory bowel disease. *Nature* 491, 119–124 (2012).

63. Rock, K. L., Lai, J. & Kono, H. Innate and adaptive immune responses to cell death. *Immunol Rev* 243, 191–205 (2011).

64. Uribe-Querol, E. & Rosales, C. Phagocytosis: Our Current Understanding of a Universal Biological Process. *Front Immunol* 11, 1066 (2020).

65. Pegram, H. J., Andrews, D. M., Smyth, M. J., Darcy, P. K. & Kershaw, M. H. Activating and inhibitory receptors of natural killer cells. *Immunol Cell Biol* 89, 216–224 (2011).

66. Adams, N. M., Grassmann, S. & Sun, J. C. Clonal expansion of innate and adaptive lymphocytes. *Nat Rev Immunol* 20, 694–707 (2020).

67. Mauro, D. *et al.* Ankylosing spondylitis: an autoimmune or autoinflammatory disease? *Nat Rev Rheumatol* 17, 387–404 (2021).

68. Baerlecken, N. T. *et al.* Autoantibodies against CD74 in spondyloarthritis. *Ann Rheum Dis* 73, 1211 (2014).

69. Chen, L. & Flies, D. B. Molecular mechanisms of T cell co-stimulation and co-inhibition. *Nat Rev Immunol* 13, 227–242 (2013).

70. Abdoli, R. & Najafian, N. T Helper Cells Fate Mapping by Co-stimulatory Molecules and its Functions in Allograft Rejection and Tolerance. *Int J Organ Transplant Medicine* 5, 97–110 (2014).

71. Zeng, H. & Chi, H. mTOR signaling and transcriptional regulation in T lymphocytes. *Biochem Soc Symp* 5, e28263 (2014).

72. Lee, Y. K. *et al.* Late Developmental Plasticity in the T Helper 17 Lineage. *Immunity* 30, 92–107 (2009).

73. Nistala, K. *et al.* Th17 plasticity in human autoimmune arthritis is driven by the inflammatory environment. *Proc National Acad Sci* 107, 14751–14756 (2010).

74. Cohen, C. J. *et al.* Human Th1 and Th17 Cells Exhibit Epigenetic Stability at Signature Cytokine and Transcription Factor Loci. *J Immunol* 187, 5615–5626 (2011).

75. Al-Mossawi, M. H. *et al.* Unique transcriptome signatures and GM-CSF expression in lymphocytes from patients with spondyloarthritis. *Nat Commun* 8, 1510 (2017).

76. Ciccia, F. *et al.* Expansion of intestinal CD4+CD25high Treg cells in patients with ankylosing spondylitis: A putative role for interleukin-10 in preventing intestinal Th17 response. *Arthritis Rheumatism* 62, 3625–3634 (2010).

77. Appel, H. *et al.* Analysis of IL-17+cells in facet joints of patients with spondyloarthritis suggests that the innate immune pathway might be of greater relevance than the Th17-mediated adaptive immune response. *Arthritis Res Ther* 13, R95 (2011).

78. Lochner, M. *et al.* In vivo equilibrium of proinflammatory IL-17+ and regulatory IL-10+ Foxp3+ RORγt+ T cells. *J Exp Medicine* 205, 1381–1393 (2008).

79. Lee, D.-G., Woo, J.-W., Kwok, S.-K., Cho, M.-L. & Park, S.-H. MRP8 promotes Th17 differentiation via upregulation of IL-6 production by fibroblast-like synoviocytes in rheumatoid arthritis. *Exp Mol Medicine* 45, e20–e20 (2013).

80. Simone, D. *et al.* Single cell analysis of spondyloarthritis regulatory T cells identifies distinct synovial gene expression patterns and clonal fates. *Commun Biology* 4, 1395 (2021).

81. Komatsu, N. *et al.* Pathogenic conversion of Foxp3+ T cells into TH17 cells in autoimmune arthritis. *Nat Med* 20, 62–68 (2014).

82. Cao, D., Vollenhoven, R. van, Klareskog, L., Trollmo, C. & Malmström, V. CD25brightCD4+regulatory T cells are enriched in inflamed joints of patients with chronic rheumatic disease. *Arthritis Res Ther* 6, R335 (2004).

83. LIMÓN-CAMACHO, L. *et al.* In Vivo Peripheral Blood Proinflammatory T Cells in Patients with Ankylosing Spondylitis. *J Rheumatology* 39, 830–835 (2012).

84. Gracey, E., Haroon, N. & Inman, R. D. Editorial: HLA–B27, Cytokines, and Spondyloarthritis: Noncanonical Functions of a Curious Class I Major Histocompatibility Complex Gene. *Arthritis Rheumatol* 66, 783–785 (2014).

85. Ma, C. S. *et al.* Deficiency of Th17 cells in hyper IgE syndrome due to mutations in STAT3. *J Exp Medicine* 205, 1551–1557 (2008).

86. Milner, J. D. *et al.* Impaired TH17 cell differentiation in subjects with autosomal dominant hyper-IgE syndrome. *Nature* 452, 773–776 (2008).

87. Aggarwal, S., Ghilardi, N., Xie, M.-H., Sauvage, F. J. de & Gurney, A. L. Interleukin-23 Promotes a Distinct CD4 T Cell Activation State Characterized by the Production of Interleukin-17*. *J Biol Chem* 278, 1910–1914 (2003).

88. Ghoreschi, K. *et al.* Generation of pathogenic TH17 cells in the absence of TGF-β signalling. *Nature* 467, 967–971 (2010).

89. Oppmann, B. *et al.* Novel p19 Protein Engages IL-12p40 to Form a Cytokine, IL-23, with Biological Activities Similar as Well as Distinct from IL-12. *Immunity* 13, 715–725 (2000).

90. Chang, S. H. & Dong, C. A novel heterodimeric cytokine consisting of IL-17 and IL-17F regulates inflammatory responses. *Cell Res* 17, 435–440 (2007).

91. Yao, Z. *et al.* Human IL-17: a novel cytokine derived from T cells. *J Immunol Baltim Md 1950* 155, 5483–6 (1995).

92. Shahrara, S. *et al.* IL-17–Mediated Monocyte Migration Occurs Partially through CC Chemokine Ligand 2/Monocyte Chemoattractant Protein-1 Induction. *J Immunol* 184, 4479–4487 (2010).

93. Liang, S. C. *et al.* Interleukin (IL)-22 and IL-17 are coexpressed by Th17 cells and cooperatively enhance expression of antimicrobial peptides. *J Exp Medicine* 203, 2271–2279 (2006).

94. Braem, K. & Lories, R. J. Insights into the pathophysiology of ankylosing spondylitis: Contributions from animal models. *Joint Bone Spine* 79, 243–248 (2012).

95. Ridley, A. *et al.* Activation-Induced Killer Cell Immunoglobulin-like Receptor 3DL2 Binding to HLA–B27 Licenses Pathogenic T Cell Differentiation in Spondyloarthritis. *Arthritis Rheumatol* 68, 901–914 (2016).

96. Jandus, C. *et al.* Increased numbers of circulating polyfunctional Th17 memory cells in patients with seronegative spondylarthritides. *Arthritis Rheumatism* 58, 2307–2317 (2008).

97. Shen, H., Goodall, J. C. & Gaston, J. S. H. Frequency and phenotype of peripheral blood Th17 cells in ankylosing spondylitis and rheumatoid arthritis. *Arthritis Rheumatism* 60, 1647–1656 (2009).

98. Xueyi, L. *et al.* Levels of Circulating Th17 Cells and Regulatory T Cells in Ankylosing Spondylitis Patients with an Inadequate Response to Anti−TNF-α Therapy. *J Clin Immunol* 33, 151–161 (2013).

99. Mei, Y. *et al.* Increased serum IL-17 and IL-23 in the patient with ankylosing spondylitis. *Clin Rheumatol* 30, 269–273 (2011).

100. Zrioual, S. *et al.* IL-17RA and IL-17RC Receptors Are Essential for IL-17A-Induced ELR+ CXC Chemokine Expression in Synoviocytes and Are Overexpressed in Rheumatoid Blood. *J Immunol* 180, 655–663 (2008).

101. Teunissen, M. B. M., Bos, J. D., Koomen, C. W., Malefyt, R. de W. & Wierenga, E. A. Interleukin-17 and Interferon-γ Synergize in the Enhancement of Proinflammatory Cytokine Production by Human Keratinocytes. *J Invest Dermatol* 111, 645–649 (1998).

102. Lee, J. S. *et al.* Interleukin-23-Independent IL-17 Production Regulates Intestinal Epithelial Permeability. *Immunity* 43, 727–738 (2015).

103. Gagliani, N. *et al.* Th17 cells transdifferentiate into regulatory T cells during resolution of inflammation. *Nature* 523, 221–225 (2015).

104. Ciccia, F. *et al.* Overexpression of interleukin-23, but not interleukin-17, as an immunologic signature of subclinical intestinal inflammation in ankylosing spondylitis. *Arthritis Rheumatism* 60, 955–965 (2009).

105. Gracey, E. *et al.* Altered Cytotoxicity Profile of CD8+ T Cells in Ankylosing Spondylitis. *Arthritis Rheumatol* 72, 428–434 (2020).

106. Steel, K. J. A. *et al.* Polyfunctional, Proinflammatory, Tissue-Resident Memory Phenotype and Function of Synovial Interleukin-17A+CD8+ T Cells in Psoriatic Arthritis. *Arthritis Rheumatol* 72, 435–447 (2020).

107. Qaiyum, Z., Gracey, E., Yao, Y. & Inman, R. D. Integrin and transcriptomic profiles identify a distinctive synovial CD8+ T cell subpopulation in spondyloarthritis. *Ann Rheum Dis* 78, 1566 (2019).

108. Penkava, F. *et al.* Single-cell sequencing reveals clonal expansions of pro-inflammatory synovial CD8 T cells expressing tissue-homing receptors in psoriatic arthritis. *Nat Commun* 11, 4767 (2020).

109. Sherlock, J. P. *et al.* IL-23 induces spondyloarthropathy by acting on ROR-γt+ CD3+CD4−CD8− entheseal resident T cells. *Nat Med* 18, 1069–1076 (2012).

110. Wencker, M. *et al.* Innate-like T cells straddle innate and adaptive immunity by altering antigen-receptor responsiveness. *Nat Immunol* 15, 80–87 (2014).

111. Porcelli, S., Yockey, C. E., Brenner, M. B. & Balk, S. P. Analysis of T cell antigen receptor (TCR) expression by human peripheral blood CD4-8- alpha/beta T cells demonstrates preferential use of several V beta genes and an invariant TCR alpha chain. *J Exp Medicine* 178, 1–16 (1993).

112. Provine, N. M. & Klenerman, P. MAIT Cells in Health and Disease. *Annu Rev Immunol* 38, 1–26 (2020).

113. Garner, L. C., Klenerman, P. & Provine, N. M. Insights Into Mucosal-Associated Invariant T Cell Biology From Studies of Invariant Natural Killer T Cells. *Front Immunol* 9, 1478 (2018).

114. Treiner, E. *et al.* Selection of evolutionarily conserved mucosal-associated invariant T cells by MR1. *Nature* 422, 164–169 (2003).

115. Kjer-Nielsen, L. *et al.* MR1 presents microbial vitamin B metabolites to MAIT cells. *Nature* 491, 717–723 (2012).

116. Fergusson, J. R. *et al.* CD161 Defines a Transcriptional and Functional Phenotype across Distinct Human T Cell Lineages. *Cell Reports* 9, 1075–1088 (2014).

117. Maggi, L. *et al.* CD161 is a marker of all human IL-17-producing T-cell subsets and is induced by RORC. *Eur. J. Immunol.* 40, 2174–2181 (2010).

118. Hayashi, E. *et al.* Involvement of Mucosal-associated Invariant T cells in Ankylosing Spondylitis. *J Rheumatology* 43, 1695–1703 (2016).

119. Gracey, E. *et al.* IL-7 primes IL-17 in mucosal-associated invariant T (MAIT) cells, which contribute to the Th17-axis in ankylosing spondylitis. *Ann Rheum Dis* 75, 2124 (2016).

120. Duurland, C. L. *et al.* CD161 expression and regulation defines rapidly responding effector CD4+ T cells associated with improved survival in HPV16-associated tumors. *J Immunother Cancer* 10, e003995 (2022).

121. Toussirot, E. & Saas, P. MAIT cells: potent major cellular players in the IL-17 pathway of spondyloarthritis? *Rmd Open* 4, e000821 (2018).

122. Koppejan, H. *et al.* Altered composition and phenotype of mucosal-associated invariant T cells in early untreated rheumatoid arthritis. *Arthritis Res Ther* 21, 3 (2019).

123. M, Lefton., N, Sharma., AR, Patel., JA, Sparks. & J, Ermann. Polyfunctional IL-17A+ MAIT cells are expanded in the peripheral blood of patients with HLA-B27+ axial spondyloarthritis. *bioRxiv* (2022) doi:https://doi.org/10.1101/2022.01.17.475829.

124. Rosine, N. *et al.* Characterization of Blood Mucosal-Associated Invariant T Cells in Patients With Axial Spondyloarthritis and of Resident Mucosal-Associated Invariant T Cells

From the Axial Entheses of Non-Axial Spondyloarthritis Control Patients. *Arthritis Rheumatol* (2022) doi:10.1002/art.42090.

125. Amini, A., Pang, D., Hackstein, C.-P. & Klenerman, P. MAIT Cells in Barrier Tissues: Lessons from Immediate Neighbors. *Front Immunol* 11, 584521 (2020).

126. Vermijlen, D., Gatti, D., Kouzeli, A., Rus, T. & Eberl, M. γδ T cell responses: How many ligands will it take till we know? *Semin Cell Dev Biol* 84, 75–86 (2018).

127. Bank, I. The Role of Gamma Delta T Cells in Autoimmune Rheumatic Diseases. *Cells* 9, 462 (2020).

128. Lawand, M., Déchanet-Merville, J. & Dieu-Nosjean, M.-C. Key Features of Gamma-Delta T-Cell Subsets in Human Diseases and Their Immunotherapeutic Implications. *Front Immunol* 8, 761 (2017).

129. Provine, N. M. *et al.* Unique and Common Features of Innate-Like Human Vδ2+ γδT Cells and Mucosal-Associated Invariant T Cells. *Front Immunol* 9, 756 (2018).

130. Kenna, T. J. *et al.* Enrichment of circulating interleukin-17–secreting interleukin-23 receptor–positive γ/δ T cells in patients with active ankylosing spondylitis. *Arthritis Rheumatism* 64, 1420–1429 (2012).

131. Cuthbert, R. J. *et al.* Evidence that tissue resident human enthesis γδT-cells can produce IL-17A independently of IL-23R transcript expression. *Ann Rheum Dis* 78, 1559 (2019).

132. Venken, K. *et al.* RORγt inhibition selectively targets IL-17 producing iNKT and γδ-T cells enriched in Spondyloarthritis patients. *Nat Commun* 10, 9 (2019).

133. Reinhardt, A. *et al.* Interleukin-23–Dependent γ/δ T Cells Produce Interleukin-17 and Accumulate in the Enthesis, Aortic Valve, and Ciliary Body in Mice. *Arthritis Rheumatol* 68, 2476–2486 (2016).

134. Ono, T. *et al.* IL-17-producing γδ T cells enhance bone regeneration. *Nat Commun* 7, 10928 (2016).

135. Akalın, N. & Soy, M. Natural Killer and Natural Killer T Cells as a Prognostic Factor for Rheumatoid Arthritis and Ankylosing Spondylitis. *Int J Biomed Res* 6, 301–308 (2015).

136. Mousavi, T. *et al.* Phenotypic study of natural killer cell subsets in ankylosing spondylitis patients. *Iranian J Allergy Asthma Immunol* 8, 193–8 (2009).

137. Ren, C. *et al.* Single-cell RNA-seq reveals altered NK cell subsets and reduced levels of cytotoxic molecules in patients with ankylosing spondylitis. *J Cell Mol Med* 26, 1071–1082 (2022).

138. Wong-Baeza, I. *et al.* KIR3DL2 Binds to HLA-B27 Dimers and Free H Chains More Strongly than Other HLA Class I and Promotes the Expansion of T Cells in Ankylosing Spondylitis. *J Immunol* 190, 3216–3224 (2013).

139. Ciccia, F. *et al.* Interleukin-22 and interleukin-22–producing NKp44+ natural killer cells in subclinical gut inflammation in ankylosing spondylitis. *Arthritis Rheumatism* 64, 1869–1878 (2012).

140. Liu, J. *et al.* Single-cell analysis reveals innate immunity dynamics in ankylosing spondylitis. *Clin Transl Medicine* 11, e369 (2021).

141. Kim, T.-J. *et al.* Immune cells and bone formation in ankylosing spondylitis. *Clin Exp Rheumatol* 30, 469–75 (2011).

142. Surdacki, A. *et al.* Blood Monocyte Heterogeneity and Markers of Endothelial Activation in Ankylosing Spondylitis. *J Rheumatology* 41, 481–489 (2014).

143. Wright, C. *et al.* Ankylosing spondylitis monocytes show upregulation of proteins involved in inflammation and the ubiquitin proteasome pathway. *Ann Rheum Dis* 68, 1626 (2009).

144. Conrad, K., Wu, P., Sieper, J. & Syrbe, U. In vivo pre-activation of monocytes in patients with axial spondyloarthritis. *Arthritis Res Ther* 17, 179 (2015).

145. Ciccia, F. *et al.* Proinflammatory CX3CR1+CD59+Tumor Necrosis Factor–Like Molecule 1A+Interleukin-23+ Monocytes Are Expanded in Patients With Ankylosing Spondylitis and Modulate Innate Lymphoid Cell 3 Immune Functions. *Arthritis Rheumatol* 70, 2003–2013 (2018).

146. Rycke, L. D. *et al.* Tumor necrosis factor α blockade treatment down-modulates the increased systemic and local expression of toll-like receptor 2 and toll-like receptor 4 in spondylarthropathy. *Arthritis Rheumatism* 52, 2146–2158 (2005).

147. Shi, H. *et al.* GM-CSF Primes Proinflammatory Monocyte Responses in Ankylosing Spondylitis. *Front Immunol* 11, 1520 (2020).

148. Ciccia, F. *et al.* Dysbiosis and zonulin upregulation alter gut epithelial and vascular barriers in patients with ankylosing spondylitis. *Ann Rheum Dis* 76, 1123 (2017).

149. Bridgewood, C. *et al.* Identification of myeloid cells in the human enthesis as the main source of local IL-23 production. *Ann Rheum Dis* 78, 929 (2019).

150. Rezaiemanesh, A. *et al.* Ankylosing spondylitis M-CSF-derived macrophages are undergoing unfolded protein response (UPR) and express higher levels of interleukin-23. *Mod Rheumatol* 27, 1–17 (2016).

151. Heijde, D. van der *et al.* 2016 update of the ASAS-EULAR management recommendations for axial spondyloarthritis. *Ann Rheum Dis* 76, 978 (2017).

152. Lambert, R. G. W. *et al.* Adalimumab significantly reduces both spinal and sacroiliac joint inflammation in patients with ankylosing spondylitis: A multicenter, randomized, double-blind, placebo-controlled study. *Arthritis Rheumatism* 56, 4005–4014 (2007).

153. Heijde, D. van der *et al.* Efficacy and safety of infliximab in patients with ankylosing spondylitis: Results of a randomized, placebo-controlled trial (ASSERT). *Arthritis Rheumatism* 52, 582–591 (2005).

154. Calin, A. *et al.* Outcomes of a multicentre randomised clinical trial of etanercept to treat ankylosing spondylitis. *Ann Rheum Dis* 63, 1594 (2004).

155. Landewé, R. *et al.* Efficacy of certolizumab pegol on signs and symptoms of axial spondyloarthritis including ankylosing spondylitis: 24-week results of a double-blind randomised placebo-controlled Phase 3 study. *Ann Rheum Dis* 73, 39 (2014).

156. Deodhar, A. *et al.* Safety and Efficacy of Golimumab Administered Intravenously in Adults with Ankylosing Spondylitis: Results through Week 28 of the GO-ALIVE Study. *J Rheumatology* 45, jrheum.170487 (2017).

157. Dougados, M. *et al.* Efficacy and safety of ixekizumab through 52 weeks in two phase 3, randomised, controlled clinical trials in patients with active radiographic axial spondyloarthritis (COAST-V and COAST-W). *Ann Rheum Dis* 79, 176 (2020).

158. Heijde, D. van der *et al.* Dual neutralisation of interleukin-17A and interleukin-17F with bimekizumab in patients with active ankylosing spondylitis: results from a 48-week phase IIb, randomised, double-blind, placebo-controlled, dose-ranging study. *Ann Rheum Dis* 79, 595 (2020).

159. Wei, J. C.-C. *et al.* Efficacy and safety of brodalumab, an anti-IL17RA monoclonal antibody, in patients with axial spondyloarthritis: 16-week results from a randomised, placebo-controlled, phase 3 trial. *Ann Rheum Dis* 80, 1014–1021 (2021).

160. Pavelka, K. *et al.* Efficacy, safety, and tolerability of secukinumab in patients with active ankylosing spondylitis: a randomized, double-blind phase 3 study, MEASURE 3. *Arthritis Res Ther* 19, 285 (2017).

161. Deodhar, A. *et al.* Three Multicenter, Randomized, Double-Blind, Placebo-Controlled Studies Evaluating the Efficacy and Safety of Ustekinumab in Axial Spondyloarthritis. *Arthritis Rheumatol* 71, 258–270 (2019).

162. Baeten, D. *et al.* Risankizumab, an IL-23 inhibitor, for ankylosing spondylitis: results of a randomised, double-blind, placebo-controlled, proof-of-concept, dose-finding phase 2 study. *Ann Rheum Dis* 77, 1295 (2018).

163. Sieper, J., Porter-Brown, B., Thompson, L., Harari, O. & Dougados, M. Assessment of short-term symptomatic efficacy of tocilizumab in ankylosing spondylitis: results of randomised, placebo-controlled trials. *Ann Rheum Dis* 73, 95 (2014).

164. Al-Mossawi, M. H. *et al.* A first in disease phase 2A trial of granulocyte monocyte colony stimulating factor neutralisation for axial spondyloarthritis (NAMASTE study). *Clinical and Experimental Rheumatology* 35, 1161 (2021).

165. Heijde, D. van der *et al.* Efficacy and safety of upadacitinib for active ankylosing spondylitis refractory to biological therapy: a double-blind, randomised, placebo-controlled phase 3 trial. *Ann Rheum Dis* 81, 1515–1523 (2022).

166. Deodhar, A. *et al.* Tofacitinib for the treatment of ankylosing spondylitis: a phase III, randomised, double-blind, placebo-controlled study. *Ann Rheum Dis* 80, 1004–1013 (2021).

167. Yang, D. *et al.* G protein-coupled receptors: structure- and function-based drug discovery. *Signal Transduct Target Ther* 6, 7 (2021).

168. Hauser, A. S., Attwood, M. M., Rask-Andersen, M., Schiöth, H. B. & Gloriam, D. E. Trends in GPCR drug discovery: new agents, targets and indications. *Nat Rev Drug Discov* 16, 829–842 (2017).

169. Zhao, M. *et al.* The Roles of Orphan G Protein-Coupled Receptors in Autoimmune Diseases. *Clin Rev Allerg Immu* 60, 220–243 (2021).

170. Rasmussen, S. G. F. *et al.* Crystal structure of the β2 adrenergic receptor–Gs protein complex. *Nature* 477, 549–555 (2011).

171. Wootten, D., Christopoulos, A., Marti-Solano, M., Babu, M. M. & Sexton, P. M. Mechanisms of signalling and biased agonism in G protein-coupled receptors. *Nat Rev Mol Cell Bio* 19, 638–653 (2018).

172. Calebiro, D. & Godbole, A. Internalization of GPCRs: implication in receptor function, physiology and diseases. *Best Pract Res Cl En* 32, 83–91 (2018).

173. Choi, J.-W., Lee, S. Y. & Choi, Y. Identification of a Putative G Protein-Coupled Receptor Induced during Activation-Induced Apoptosis of T Cells. *Cell Immunol* 168, 78–84 (1996).

174. Rowe, J. B., Kapolka, N. J., Taghon, G. J., Morgan, W. M. & Isom, D. G. The evolution and mechanism of GPCR proton sensing. *J Biol Chem* 296, 100167 (2021).

175. Ludwig, M.-G. *et al.* Proton-sensing G-protein-coupled receptors. *Nature* 425, 93–98 (2003).

176. Wang, J.-Q. *et al.* TDAG8 Is a Proton-sensing and Psychosine-sensitive G-protein-coupled Receptor*. *J Biol Chem* 279, 45626–45633 (2004).

177. Radu, C. G., Nijagal, A., McLaughlin, J., Wang, L. & Witte, O. N. Differential proton sensitivity of related G protein-coupled receptors T cell death-associated gene 8 and G2A expressed in immune cells. *Proc National Acad Sci* 102, 1632–1637 (2005).

178. Ihara, Y. *et al.* The G protein-coupled receptor T-cell death-associated gene 8 (TDAG8) facilitates tumor development by serving as an extracellular pH sensor. *Proc National Acad Sci* 107, 17309–17314 (2010).

179. Im, D.-S., Heise, C. E., Nguyen, T., O'Dowd, B. F. & Lynch, K. R. Identification of a Molecular Target of Psychosine and Its Role in Globoid Cell Formation. *J Cell Biology* 153, 429–434 (2001).

180. Ishii, S., Kihara, Y. & Shimizu, T. Identification of T Cell Death-associated Gene 8 (TDAG8) as a Novel Acid Sensing G-protein-coupled Receptor*. *J Biol Chem* 280, 9083–9087 (2005).

181. Pándy-Szekeres, G. *et al.* GPCRdb in 2018: adding GPCR structure models and ligands. *Nucleic Acids Res* 46, gkx1109- (2017).

182. Mogi, C. *et al.* Involvement of Proton-Sensing TDAG8 in Extracellular Acidification-Induced Inhibition of Proinflammatory Cytokine Production in Peritoneal Macrophages. *J Immunol* 182, 3243–3251 (2009).

183. Jin, Y. *et al.* Inhibition of interleukin-1β production by extracellular acidification through the TDAG8/cAMP pathway in mouse microglia. *J Neurochem* 129, 683–695 (2014).

184. Tcymbarevich, I. V. *et al.* The impact of the rs8005161 polymorphism on G protein-coupled receptor GPR65 (TDAG8) pH-associated activation in intestinal inflammation. *Bmc Gastroenterol* 19, 2 (2019).

185. Siehler, S. G12/13-dependent signaling of G-protein-coupled receptors: disease context and impact on drug discovery. *Expert Opin Drug Dis* 2, 1591–1604 (2007).

186. KYAW, H. *et al.* Cloning, Characterization, and Mapping of Human Homolog of Mouse T-Cell Death-Associated Gene. *Dna Cell Biol* 17, 493–500 (1998).

187. Kottyan, L. C. *et al.* Eosinophil viability is increased by acidic pH in a cAMP- and GPR65-dependent manner. *Blood* 114, 2774–2782 (2009).

188. Wen, A. Y., Sakamoto, K. M. & Miller, L. S. The Role of the Transcription Factor CREB in Immune Function. *J Immunol* 185, 6413–6419 (2010).

189. Hsieh, W.-S., Kung, C.-C., Huang, S.-L., Lin, S.-C. & Sun, W.-H. TDAG8, TRPV1, and ASIC3 involved in establishing hyperalgesic priming in experimental rheumatoid arthritis. *Sci Rep-uk* 7, 8870 (2017).

190. Wirasinha, R. C. *et al.* GPR65 inhibits experimental autoimmune encephalomyelitis through CD4+ T cell independent mechanisms that include effects on iNKT cells. *Immunol Cell Biol* 96, 128–136 (2018).

191. Nagasaka, A. *et al.* The proton-sensing G protein-coupled receptor T-cell death-associated gene 8 (TDAG8) shows cardioprotective effects against myocardial infarction. *Sci Rep-uk* 7, 7812 (2017).

192. Chen, X. *et al.* pH sensing controls tissue inflammation by modulating cellular metabolism and endo-lysosomal function of immune cells. *Nat Immunol* 1–13 (2022) doi:10.1038/s41590-022-01231-0.

193. Ma, X. D. *et al.* TDAG8 activation attenuates cerebral ischaemia-reperfusion injury via Akt signalling in rats. *Exp Neurol* 293, 115–123 (2017).

194. Chen, L.-D. *et al.* T-cell death-associated gene 8 accelerates atherosclerosis by promoting vascular smooth muscle cell proliferation and migration. *Atherosclerosis* 297, 64–73 (2020).

195. Ail, D. *et al.* Increased expression of the proton-sensing G protein-coupled receptor Gpr65 during retinal degeneration. *Neuroscience* 301, 496–507 (2015).

196. McMurray, K. M. J. *et al.* Immunomodulatory T cell death associated gene-8 (TDAG8) receptor in depression-associated behaviors. *Physiol Behav* 209, 112598 (2019).

197. Dai, S.-P. *et al.* TDAG8 involved in initiating inflammatory hyperalgesia and establishing hyperalgesic priming in mice. *Sci Rep-uk* 7, 41415 (2017).

198. Hikiji, H. *et al.* TDAG8 activation inhibits osteoclastic bone resorption. *Faseb J* 28, 871–879 (2014).

199. Franke, A. *et al.* Genome-wide meta-analysis increases to 71 the number of confirmed Crohn's disease susceptibility loci. *Nat Genet* 42, 1118–1125 (2010).

200. Consortium, I. M. S. G. *et al.* Genetic risk and a primary role for cell-mediated immune mechanisms in multiple sclerosis. *Nature* 476, 214–219 (2011).

201. Kasela, S. *et al.* Pathogenic implications for autoimmune mechanisms derived by comparative eQTL analysis of CD4+ versus CD8+ T cells. *Plos Genet* 13, e1006643 (2017).

202. Fairfax, B. P. *et al.* Innate Immune Activity Conditions the Effect of Regulatory Variants upon Monocyte Gene Expression. *Science* 343, 1246949 (2014).

203. P, Geborek., T, Saxne., H, Pettersson. & Wollheim.FA. Synovial fluid acidosis correlates with radiological joint destruction in rheumatoid arthritis knee joints. *The Journal of Rheumatology* 16, 468–472.

204. Onozawa, Y., Komai, T. & Oda, T. Activation of T cell death-associated gene 8 attenuates inflammation by negatively regulating the function of inflammatory cells. *Eur J Pharmacol* 654, 315–319 (2011).

205. Al-Mossawi, H. *et al.* Context-specific regulation of surface and soluble IL7R expression by an autoimmune risk allele. *Nat Commun* 10, 4575 (2019).

206. Lassen, K. G. *et al.* Genetic Coding Variant in GPR65 Alters Lysosomal pH and Links Lysosomal Dysfunction with Colitis Risk. *Immunity* 44, 1392–1405 (2016).

207. Chen, X. *et al.* pH sensing controls tissue inflammation by modulating cellular metabolism and endo-lysosomal function of immune cells. *Nat Immunol* 1–13 (2022) doi:10.1038/s41590-022-01231-0.

208. Lyu, P. C., Sherman, J. C., Chen, A. & Kallenbach, N. R. Alpha-helix stabilization by natural and unnatural amino acids with alkyl side chains. *Proc National Acad Sci* 88, 5317–5320 (1991).

209. Xie, L. *et al.* pH and Proton Sensor GPR65 Determine Susceptibility to Atopic Dermatitis. *J Immunol* 207, 101–109 (2021).

210. Lin, R. *et al.* GPR65 promotes intestinal mucosal Th1 and Th17 cell differentiation and gut inflammation through downregulating NUAK2. *Clin Transl Medicine* 12, e771 (2022).

211. Lee, H.-S., Lobbestael, E., Vermeire, S., Sabino, J. & Cleynen, I. Inflammatory bowel disease and Parkinson's disease: common pathophysiological links. *Gut* 70, 408–417 (2021).

212. Hui, K. Y. *et al.* Functional variants in the LRRK2 gene confer shared effects on risk for Crohn's disease and Parkinson's disease. *Sci Transl Med* 10, (2018).

213. Gaublomme, J. T. *et al.* Single-Cell Genomics Unveils Critical Regulators of Th17 Cell Pathogenicity. *Cell* 163, 1400–1412 (2015).

214. Xie, L. *et al.* pH and Proton Sensor GPR65 Determine Susceptibility to Atopic Dermatitis. *J Immunol* 207, 101–109 (2021).

215. Neri, D. & Supuran, C. T. Interfering with pH regulation in tumours as a therapeutic strategy. *Nat Rev Drug Discov* 10, 767–777 (2011).

216. Warburg, O., Wind, F. & Negelein, E. THE METABOLISM OF TUMORS IN THE BODY. *J Gen Physiology* 8, 519–530 (1927).

217. Sin, W. C. *et al.* G protein-coupled receptors GPR4 and TDAG8 are oncogenic and overexpressed in human cancers. *Oncogene* 23, 6299–6303 (2004).

218. Klatt, W., Wallner, S., Brochhausen, C., Stolwijk, J. A. & Schreml, S. Expression profiles of proton-sensing G-protein coupled receptors in common skin tumors. *Sci Rep-uk* 10, 15327 (2020).

219. Wang, H.-X. *et al.* Overexpression of G-protein-coupled receptors 65 in glioblastoma predicts poor patient prognosis. *Clin Neurol Neurosur* 164, 132–137 (2018).

220. Ryder, C., McColl, K., Zhong, F. & Distelhorst, C. W. Acidosis Promotes Bcl-2 Family-mediated Evasion of Apoptosis INVOLVEMENT OF ACID-SENSING G PROTEIN-COUPLED RECEPTOR GPR65 SIGNALING TO MEK/ERK*. *J Biol Chem* 287, 27863–27875 (2012).

221. Mori, D. *et al.* Extracellular acidity in tumor tissue upregulates programmed cell death protein 1 expression on tumor cells via proton-sensing G protein-coupled receptors. *Int. J. Cancer* 149, 2116–2124 (2021).

222. Justus, C. R. *et al.* Contextual tumor suppressor function of T cell death-associated gene 8 (TDAG8) in hematological malignancies. *J Transl Med* 15, 204 (2017).

223. Li, Z., Dong, L., Dean, E. & Yang, L. V. Acidosis Decreases c-Myc Oncogene Expression in Human Lymphoma Cells: A Role for the Proton-Sensing G Protein-Coupled Receptor TDAG8. *Int J Mol Sci* 14, 20236–20255 (2013).

224. Cassetta, L. & Pollard, J. W. Targeting macrophages: therapeutic approaches in cancer. *Nat Rev Drug Discov* 17, 887–904 (2018).

225. Bohn, T. *et al.* Tumor immunoevasion via acidosis-dependent induction of regulatory tumor-associated macrophages. *Nat Immunol* 19, 1319–1329 (2018).

226. Cipriani, B. *et al.* Abstract 1631: GPR65 is a critical mediator of low pH induced immunosuppressive signalling in tumor associated macrophages: Human target validation of GPR65 as a novel innate immune checkpoint and discovery of potent, selective GPR65 antagonists. *Cancer Res* 81, 1631–1631 (2021).

227. CA, J., P, T. & M, W. *Immunobiology: The Immune System in Health and Disease*. (2001).

228. Marshall, J. S., Warrington, R., Watson, W. & Kim, H. L. An introduction to immunology and immunopathology. *Allergy Asthma Clin Immunol* 14, 49 (2018).

229. Tangye, S. G., Ferguson, A., Avery, D. T., Ma, C. S. & Hodgkin, P. D. Isotype Switching by Human B Cells Is Division-Associated and Regulated by Cytokines. *J Immunol* 169, 4298–4306 (2002).

230. Stavnezer, J., Guikema, J. E. J. & Schrader, C. E. Mechanism and Regulation of Class Switch Recombination. *Annu Rev Immunol* 26, 261–292 (2008).

231. Porter, R. R. The hydrolysis of rabbit γ-globulin and antibodies with crystalline papain. *Biochem J* 73, 119–127 (1959).

232. Erp, E. A. van, Luytjes, W., Ferwerda, G. & Kasteren, P. B. van. Fc-Mediated Antibody Effector Functions During Respiratory Syncytial Virus Infection and Disease. *Front Immunol* 10, 548 (2019).

233. Schroeder, H. W. & Cavacini, L. Structure and function of immunoglobulins. *J Allergy Clin Immun* 125, S41–S52 (2010).

234. Vidarsson, G., Dekkers, G. & Rispens, T. IgG Subclasses and Allotypes: From Structure to Effector Functions. *Front Immunol* 5, 520 (2014).

235. Übelhart, R. *et al.* Responsiveness of B cells is regulated by the hinge region of IgD. *Nat Immunol* 16, 534–543 (2015).

236. Gould, H. J. *et al.* THE BIOLOGY OF IGE AND THE BASIS OF ALLERGIC DISEASE. *Annu Rev Immunol* 21, 579–628 (2003).

237. KÖHLER, G. & MILSTEIN, C. Continuous cultures of fused cells secreting antibody of predefined specificity. *Nature* 256, 495–497 (1975).

238. Group*, O. M. T. S. A Randomized Clinical Trial of OKT3 Monoclonal Antibody for Acute Rejection of Cadaveric Renal Transplants. *New Engl J Medicine* 313, 337–342 (1985).

239. Lu, R.-M. *et al.* Development of therapeutic antibodies for the treatment of diseases. *J Biomed Sci* 27, 1 (2020).

240. Castelli, M. S., McGonigle, P. & Hornby, P. J. The pharmacology and therapeutic applications of monoclonal antibodies. *Pharmacol Res Perspectives* 7, e00535 (2019).

241. Jiang, X.-R. *et al.* Advances in the assessment and control of the effector functions of therapeutic antibodies. *Nat Rev Drug Discov* 10, 101–111 (2011).

242. Berens, S. J., Wylie, D. E. & Lopez, O. J. Use of a single VH family and long CDR3s in the variable region of cattle Ig heavy chains. *Int Immunol* 9, 189–199 (1997).

243. Macpherson, A. *et al.* The allosteric modulation of complement C5 by knob domain peptides. *Elife* 10, e63586 (2021).

244. Macpherson, A. *et al.* Isolation of antigen-specific, disulphide-rich knob domain peptides from bovine antibodies. *Plos Biol* 18, e3000821 (2020).

245. Zhu, C. *et al.* Rationally designed carbohydrate-occluded epitopes elicit HIV-1 Env-specific antibodies. *Nat Commun* 10, 948 (2019).

246. Marks, J. D. *et al.* By-passing immunization Human antibodies from V-gene libraries displayed on phage. *J Mol Biol* 222, 581–597 (1991).

247. Clargo, A. M. *et al.* The rapid generation of recombinant functional monoclonal antibodies from individual, antigen-specific bone marrow-derived plasma cells isolated using a novel fluorescence-based method. *Mabs* 6, 143–159 (2014).

248. Blighe, K., Rana, K. & Lewis, M. EnhancedVolcano: Publication-ready volcano plots with enhanced colouring and labelling. (2018).

249. Fang, H., Knezevic, B., Burnham, K. L. & Knight, J. C. XGR software for enhanced interpretation of genomic summary data, illustrated by application to immunological traits. *Genome Med* 8, 129 (2016).

250. Monod, J., Wyman, J. & Changeux, J.-P. On the nature of allosteric transitions: A plausible model. *J Mol Biol* 12, 88–118 (1965).

251. Kumar, S., Ma, B., Tsai, C., Sinha, N. & Nussinov, R. Folding and binding cascades: Dynamic landscapes and population shifts. *Protein Sci* 9, 10–19 (2000).

252. Berger, C. *et al.* Antigen recognition by conformational selection. *Febs Lett* 450, 149–153 (1999).

253. Hutchings, C. J. Mini-review: antibody therapeutics targeting G protein-coupled receptors and ion channels. *Antib Ther* 3, 257–264 (2020).

254. King, C. T. *et al.* Discovery of the Migraine Prevention Therapeutic Aimovig (Erenumab), the First FDA-Approved Antibody against a G-Protein-Coupled Receptor. *Acs Pharmacol Transl Sci* 2, 485–490 (2019).

255. Niwa, R. *et al.* Defucosylated Chimeric Anti-CC Chemokine Receptor 4 IgG1 with Enhanced Antibody-Dependent Cellular Cytotoxicity Shows Potent Therapeutic Activity to T-Cell Leukemia and Lymphoma. *Cancer Res* 64, 2127–2133 (2004).

256. Ishida, T. *et al.* The CC Chemokine Receptor 4 as a Novel Specific Molecular Target for Immunotherapy in Adult T-Cell Leukemia/Lymphoma. *Clin Cancer Res* 10, 7529–7539 (2004).

257. Correia, B. E. *et al.* Proof of principle for epitope-focused vaccine design. *Nature* 507, 201–206 (2014).

258. García-Nafría, J. & Tate, C. G. Structure determination of GPCRs: cryo-EM compared with X-ray crystallography. *Biochem Soc T* 49, 2345–2355 (2021).

259. Popot, J.-L. Amphipols, Nanodiscs, and Fluorinated Surfactants: Three Nonconventional Approaches to Studying Membrane Proteins in Aqueous Solutions. *Annu Rev Biochem* 79, 737–775 (2010).

260. Charalambous, K., Miller, D., Curnow, P. & Booth, P. J. Lipid bilayer composition influences small multidrug transporters. *Bmc Biochem* 9, 31–31 (2008).

261. Scheidelaar, S. *et al.* Effect of Polymer Composition and pH on Membrane Solubilization by Styrene-Maleic Acid Copolymers. *Biophys J* 111, 1974–1986 (2016).

262. Lalonde, M. S. & Sundquist, W. I. How HIV finds the door. *Proc National Acad Sci* 109, 18631–18632 (2012).

263. Ho, T. T. *et al.* Method for rapid optimization of recombinant GPCR protein expression and stability using virus-like particles. *Protein Expres Purif* 133, 41–49 (2017).

264. Huang, X.-P. *et al.* Allosteric ligands for the pharmacologically dark receptors GPR68 and GPR65. *Nature* 527, 477–483 (2015).

265. Smith, G. P. Filamentous Fusion Phage: Novel Expression Vectors That Display Cloned Antigens on the Virion Surface. *Science* 228, 1315–1317 (1985).

266. Chan, C. E. Z., Lim, A. P. C., MacAry, P. A. & Hanson, B. J. The role of phage display in therapeutic antibody discovery. *Int Immunol* 26, 649–657 (2014).

267. Kumar, R., Parray, H. A., Shrivastava, T., Sinha, S. & Luthra, K. Phage display antibody libraries: A robust approach for generation of recombinant human monoclonal antibodies. *Int J Biol Macromol* 135, 907–918 (2019).

268. Geoghegan, K. F. *et al.* Spontaneous α-N-6-Phosphogluconoylation of a “His Tag” inEscherichia coli:The Cause of Extra Mass of 258 or 178 Da in Fusion Proteins. *Anal Biochem* 267, 169–184 (1999).

269. Buccitelli, C. & Selbach, M. mRNAs, proteins and the emerging principles of gene expression control. *Nat Rev Genet* 21, 630–644 (2020).

270. Lin, X. *et al.* Structural basis of ligand recognition and self-activation of orphan GPR52. *Nature* 579, 152–157 (2020).

271. Kobilka, B. K. & Deupi, X. Conformational complexity of G-protein-coupled receptors. *Trends Pharmacol Sci* 28, 397–406 (2007).

272. Goldstein, L. D. *et al.* Massively parallel single-cell B-cell receptor sequencing enables rapid discovery of diverse antigen-reactive antibodies. *Commun Biology* 2, 304 (2019).

273. Manz, R., Assenmacher, M., Pflüger, E., Miltenyi, S. & Radbruch, A. Analysis and sorting of live cells according to secreted molecules, relocated to a cell-surface affinity matrix. *Proc National Acad Sci* 92, 1921–1925 (1995).

274. Townsend, S. E., Goodnow, C. C. & Cornall, R. J. Single epitope multiple staining to detect ultralow frequency B cells. *J Immunol Methods* 249, 137–146 (2001).

275. Franz, B., May, K. F., Dranoff, G. & Wucherpfennig, K. Ex vivo characterization and isolation of rare memory B cells with antigen tetramers. *Blood* 118, 348–357 (2011).

276. Starkie, Dale. O., Compson, J. E., Rapecki, S. & Lightwood, D. J. Generation of Recombinant Monoclonal Antibodies from Immunised Mice and Rabbits via Flow

Cytometry and Sorting of Antigen-Specific IgG+ Memory B Cells. *Plos One* 11, e0152282 (2016).

277. Bell, J. & Gray, D. Antigen-capturing Cells Can Masquerade as Memory B Cells. *J Exp Medicine* 197, 1233–1244 (2003).

278. Jo, M. & Jung, S. T. Engineering therapeutic antibodies targeting G-protein–coupled receptors. *Exp Mol Medicine* 48, e207–e207 (2016).

279. Hutchings, C. J., Koglin, M., Olson, W. C. & Marshall, F. H. Opportunities for therapeutic antibodies directed at G-protein-coupled receptors. *Nat Rev Drug Discov* 16, 787–810 (2017).

280. Wilkinson, T. C. I. Discovery of functional monoclonal antibodies targeting G-protein-coupled receptors and ion channels. *Biochem Soc T* 44, 831–837 (2016).

281. Hansen, D. T., Craciunescu, F. M., Fromme, P., Johnston, S. A. & Sykes, K. F. Generation of High-Specificity Antibodies against Membrane Proteins Using DNA-Gold Micronanoplexes for Gene Gun Immunization. *Curr Protoc Protein Sci* 91, 29.20.1-29.20.22 (2018).

282. Liu, S., Wang, S. & Lu, S. Using DNA Immunization to Elicit Monoclonal Antibodies in Mice, Rabbits, and Humans. *Hum Gene Ther* 29, 997–1003 (2018).

283. Pardi, N. *et al.* Zika virus protection by a single low-dose nucleoside-modified mRNA vaccination. *Nature* 543, 248–251 (2017).

284. Polack, F. P. *et al.* Safety and Efficacy of the BNT162b2 mRNA Covid-19 Vaccine. *New Engl J Medicine* 383, NEJMoa2034577 (2020).

285. Alberer, M. *et al.* Safety and immunogenicity of a mRNA rabies vaccine in healthy adults: an open-label, non-randomised, prospective, first-in-human phase 1 clinical trial. *Lancet* 390, 1511–1520 (2017).

286. Petsch, B. *et al.* Protective efficacy of in vitro synthesized, specific mRNA vaccines against influenza A virus infection. *Nat Biotechnol* 30, 1210–1216 (2012).

287. Akinc, A. *et al.* The Onpattro story and the clinical translation of nanomedicines containing nucleic acid-based drugs. *Nat Nanotechnol* 14, 1084–1087 (2019).

288. Lindsay, K. E. *et al.* Visualization of early events in mRNA vaccine delivery in non-human primates via PET–CT and near-infrared imaging. *Nat Biomed Eng* 3, 371–380 (2019).

289. Liang, F. *et al.* Efficient Targeting and Activation of Antigen-Presenting Cells In Vivo after Modified mRNA Vaccine Administration in Rhesus Macaques. *Mol Ther* 25, 2635–2647 (2017).

290. Epstein, F. H., Wolfe, M. M. & Soll, A. H. The Physiology of Gastric Acid Secretion. *New Engl J Medicine* 319, 1707–1715 (1988).

291. Schwalfenberg, G. K. The Alkaline Diet: Is There Evidence That an Alkaline pH Diet Benefits Health? *J Environ Public Heal* 2012, 727630 (2012).

292. Borregaard, N., Schwartz, J. H. & Tauber, A. I. Proton secretion by stimulated neutrophils. Significance of hexose monophosphate shunt activity as source of electrons and protons for the respiratory burst. *J Clin Invest* 74, 455–459 (1984).

293. Ashby, B. S. pH STUDIES IN HUMAN MALIGNANT TUMOURS. *Lancet* 288, 312–315 (1966).

294. Vaupel, P., Kallinowski, F. & Okunieff, P. Blood flow, oxygen and nutrient supply, and metabolic microenvironment of human tumors: a review. *Cancer Research* 49, 6449–65.

295. Deval, E. *et al.* ASIC3, a sensor of acidic and primary inflammatory pain. *Embo J* 27, 3047–3055 (2008).

296. Kweon, H.-J. & Suh, B.-C. Acid-sensing ion channels (ASICs): therapeutic targets for neurological diseases and their regulation. *Bmb Rep* 46, 295–304 (2013).

297. Bertin, S. *et al.* The ion channel TRPV1 regulates the activation and proinflammatory properties of CD4+ T cells. *Nat Immunol* 15, 1055–1063 (2014).

298. Tominaga, M. *et al.* The Cloned Capsaicin Receptor Integrates Multiple Pain-Producing Stimuli. *Neuron* 21, 531–543 (1998).

299. Chandra, V. *et al.* Extracellular acidification stimulates GPR68 mediated IL-8 production in human pancreatic β cells. *Sci Rep-uk* 6, 25765 (2016).

300. Dong, L. *et al.* Acidosis Activation of the Proton-Sensing GPR4 Receptor Stimulates Vascular Endothelial Cell Inflammatory Responses Revealed by Transcriptome Analysis. *Plos One* 8, e61991 (2013).

301. Ussher, J. E. *et al.* CD161++CD8+ T cells, including the MAIT cell subset, are specifically activated by IL-12+IL-18 in a TCR-independent manner. *Eur J Immunol* 44, 195–203 (2014).

302. Cole, S. *et al.* Interleukin (IL)-12 and IL-18 Synergize to Promote MAIT Cell IL-17A and IL-17F Production Independently of IL-23 Signaling. *Front Immunol* 11, 585134 (2020).

303. Slichter, C. K. *et al.* Distinct activation thresholds of human conventional and innate-like memory T cells. *Jci Insight* 1, e86292 (2016).

304. Garner, L. C., Amini, A., FitzPatrick, M. E. B., Provine, N. M. & Klenerman, P. Human MAIT cells show clonal diversity but transcriptional and functional homogeneity. *Biorxiv* 2022.02.26.482031 (2022) doi:10.1101/2022.02.26.482031.

305. Gutierrez-Arcelus, M. *et al.* Lymphocyte innateness defined by transcriptional states reflects a balance between proliferation and effector functions. *Nat Commun* 10, 687 (2019).

306. Lalle, G. *et al.* A T cell-intrinsic function for NF-κB RelB in experimental autoimmune encephalomyelitis. *Sci Rep-uk* 11, 19674 (2021).

307. Lacotte, S., Brun, S., Muller, S. & Dumortier, H. CXCR3, Inflammation, and Autoimmune Diseases. *Ann Ny Acad Sci* 1173, 310–317 (2009).

308. Hinks, T. S. C. & Zhang, X.-W. MAIT Cell Activation and Functions. *Front Immunol* 11, 1014 (2020).

309. Zwieten, R. van, Wever, R., Hamers, M. N., Weening, R. S. & Roos, D. Extracellular proton release by stimulated neutrophils. *J Clin Invest* 68, 310–313 (1981).

310. Gatenby, R. A. & Gillies, R. J. Why do cancers have high aerobic glycolysis? *Nat Rev Cancer* 4, 891–899 (2004).

311. Corbet, C. & Feron, O. Tumour acidosis: from the passenger to the driver's seat. *Nat Rev Cancer* 17, 577–593 (2017).

312. Ward, T. T. & Steigbigel, R. T. Acidosis of synovial fluid correlates with synovial fluid leukocytosis. *Am J Medicine* 64, 933–936 (1978).

313. Farr, M., Garvey, K., Bold, A. M., Kendall, M. J. & Bacon, P. A. Significance of the hydrogen ion concentration in synovial fluid in rheumatoid arthritis. *Clin Exp Rheumatol* 3, 99–104 (1985).

314. Rauschner, M., Riemann, A., Reime, S. & Thews, O. Oxygen Transport to Tissue XLII. *Adv Exp Med Biol* 1269, 157–161 (2021).

315. Bosticardo, M. *et al.* Biased activation of human T lymphocytes due to low extracellular pH is antagonized by B7/CD28 costimulation. *Eur. J. Immunol.* 31, 2829–2838 (2001).

316. Martínez, D. *et al.* Extracellular Acidosis Induces Neutrophil Activation by a Mechanism Dependent on Activation of Phosphatidylinositol 3-Kinase/Akt and ERK Pathways. *J Immunol* 176, 1163–1171 (2006).

317. Martínez, D. *et al.* Extracellular Acidosis Triggers the Maturation of Human Dendritic Cells and the Production of IL-12. *J Immunol* 179, 1950–1959 (2007).

318. HEMING, T. A. *et al.* Post-transcriptional effects of extracellular pH on tumour necrosis factor-α production in RAW 246.7 and J774 A.1 cells. *Clin Sci* 100, 259–266 (2001).

319. Jancic, C. C. *et al.* Low extracellular pH stimulates the production of IL-1β by human monocytes. *Cytokine* 57, 258–268 (2012).

320. Díaz, F. E. *et al.* Extracellular Acidosis and mTOR Inhibition Drive the Differentiation of Human Monocyte-Derived Dendritic Cells. *Cell Reports* 31, 107613 (2020).

321. Rajamäki, K. *et al.* Extracellular Acidosis Is a Novel Danger Signal Alerting Innate Immunity via the NLRP3 Inflammasome. *J Biol Chem* 288, 13410–13419 (2013).

322. Fischer, B., Müller, B., Fischer, K.-G., Baur, N. & Kreutz, W. Acidic pH Inhibits Non-MHC-Restricted Killer Cell Functions. *Clin Immunol* 96, 252–263 (2000).

323. Louis, C. *et al.* NK cell–derived GM-CSF potentiates inflammatory arthritis and is negatively regulated by CIS. *J Exp Med* 217, e20191421 (2020).

324. Calcinotto, A. *et al.* Modulation of Microenvironment Acidity Reverses Anergy in Human and Murine Tumor-Infiltrating T Lymphocytes. *Cancer Res* 72, 2746–2756 (2012).

325. Pilon-Thomas, S. *et al.* Neutralization of Tumor Acidity Improves Antitumor Responses to Immunotherapy. *Cancer Res* 76, 1381–1390 (2016).

326. Davern, M. *et al.* Acidosis significantly alters immune checkpoint expression profiles of T cells from oesophageal adenocarcinoma patients. *Cancer Immunol Immunother* 1–17 (2022) doi:10.1007/s00262-022-03228-y.

327. Mendler, A. *et al.* MAIT cell activation in adolescents is impacted by bile acid concentrations and body weight. *Clin Exp Immunol* 200, 199–213 (2020).

328. Xu, Y., Hunt, N. H. & Bao, S. The role of granulocyte macrophage-colony-stimulating factor in acute intestinal inflammation. *Cell Res* 18, 1220–1229 (2008).

329. McGonagle, D. G., McInnes, I. B., Kirkham, B. W., Sherlock, J. & Moots, R. The role of IL-17A in axial spondyloarthritis and psoriatic arthritis: recent advances and controversies. *Ann Rheum Dis* 78, 1167 (2019).

330. Jr, W. O. *et al.* A protective function for interleukin 17A in T cell–mediated intestinal inflammation. *Nat Immunol* 10, 603–609 (2009).

331. Leng, T. *et al.* TCR and Inflammatory Signals Tune Human MAIT Cells to Exert Specific Tissue Repair and Effector Functions. *Cell Reports* 28, 3077-3091.e5 (2019).

332. Lamichhane, R. *et al.* TCR- or Cytokine-Activated CD8+ Mucosal-Associated Invariant T Cells Are Rapid Polyfunctional Effectors That Can Coordinate Immune Responses. *Cell Reports* 28, 3061-3076.e5 (2019).

333. Schaerli, P. *et al.* Cxc Chemokine Receptor 5 Expression Defines Follicular Homing T Cells with B Cell Helper Function. *J Exp Medicine* 192, 1553–1562 (2000).

334. Jadidi-Niaragh, F. & Mirshafiey, A. Th17 Cell, the New Player of Neuroinflammatory Process in Multiple Sclerosis. *Scand J Immunol* 74, 1–13 (2011).

335. Fruman, D. A. *et al.* The PI3K Pathway in Human Disease. *Cell* 170, 605–635 (2017).

336. White, A. D. *et al.* Gq/11-dependent regulation of endosomal cAMP generation by parathyroid hormone class B GPCR. *Proc National Acad Sci* 117, 7455–7460 (2020).

337. Pillai, S. *et al.* Lipogenesis mediated by OGR1 regulates metabolic adaptation to acid stress in cancer cells via autophagy. *Cell Reports* 39, 110796 (2022).

338. Liu, Y. *et al.* Cold stress-induced brain injury regulates TRPV1 channels and the PI3K/AKT signaling pathway. *Brain Res* 1670, 201–207 (2017).

339. Masoumi, F. *et al.* Malat1 long noncoding RNA regulates inflammation and leukocyte differentiation in experimental autoimmune encephalomyelitis. *J Neuroimmunol* 328, 50–59 (2019).

340. Smit, M. J. *et al.* CXCR3-mediated chemotaxis of human T cells is regulated by a Gi- and phospholipase C–dependent pathway and not via activation of MEK/p44/p42 MAPK nor Akt/PI-3 kinase. *Blood* 102, 1959–1965 (2003).

341. Raker, V. K., Becker, C. & Steinbrink, K. The cAMP Pathway as Therapeutic Target in Autoimmune and Inflammatory Diseases. *Front Immunol* 7, 123 (2016).

342. Song, G. *et al.* Global immune characterization of HBV/HCV-related hepatocellular carcinoma identifies macrophage and T-cell subsets associated with disease progression. *Cell Discov* 6, 90 (2020).

343. Wang, S. *et al.* Acidic extracellular pH induces autophagy to promote anoikis resistance of hepatocellular carcinoma cells via downregulation of miR-3663-3p. *J Cancer* 12, 3418–3426 (2021).

344. Juang, Y.-T. *et al.* Systemic lupus erythematosus serum IgG increases CREM binding to the IL-2 promoter and suppresses IL-2 production through CaMKIV. *J Clin Invest* 115, 996–1005 (2005).

345. Bodor, J. *et al.* Suppression of T-cell responsiveness by inducible cAMP early repressor (ICER). *J Leukocyte Biol* 69, 1053–1059 (2001).

346. Robert, C. A decade of immune-checkpoint inhibitors in cancer therapy. *Nat Commun* 11, 3801 (2020).

347. Lindner, K. *et al.* Proton pump inhibitors (PPIs) impact on tumour cell survival, metastatic potential and chemotherapy resistance, and affect expression of resistance-relevant miRNAs in esophageal cancer. *J Exp Clin Canc Res* 33, 73 (2014).

348. Li, S. L., Liou, L. B., Fang, J. T. & Tsai, W. P. Symptomatic renal tubular acidosis (RTA) in patients with systemic lupus erythematosus: an analysis of six cases with new association of type 4 RTA. *Rheumatology* 44, 1176–1180 (2005).

349. Jung, S. W. *et al.* Renal Tubular Acidosis in Patients with Primary Sjögren's Syndrome. *Electrolytes Blood Press* 15, 17–22 (2017).

350. Gobelet, C. & Gerster, J. C. Synovial fluid lactate levels in septic and non-septic arthritides. *Ann Rheum Dis* 43, 742 (1984).

351. Goldie, I. & Nachemson, A. Synovial pH in Rheumatoid Knee-Joints I. The Effect of Synovectomy. *Acta Orthop Scand* 40, 634–641 (2009).

352. Swietach, P. What is pH regulation, and why do cancer cells need it? *Cancer Metast Rev* 38, 5–15 (2019).

353. Muntyanu, A. *et al.* Differential gene and protein expression of chemokines and cytokines in synovial fluid of patients with arthritis. *Arthritis Res Ther* 18, 296 (2016).

354. Wu, H. *et al.* T-cells produce acidic niches in lymph nodes to suppress their own effector functions. *Nat Commun* 11, 4113 (2020).

355. Tang, F. *et al.* mRNA-Seq whole-transcriptome analysis of a single cell. *Nat Methods* 6, 377–382 (2009).

356. Stephenson, E. *et al.* Single-cell multi-omics analysis of the immune response in COVID-19. *Nat Med* 27, 904–916 (2021).

357. Hao, Y. *et al.* Integrated analysis of multimodal single-cell data. *Cell* 184, 3573-3587.e29 (2021).

358. Liu, Y. *et al.* ADAM12 is a costimulatory molecule that determines Th1 cell fate and mediates tissue inflammation. *Cell Mol Immunol* 18, 1904–1919 (2021).

359. Vorkas, C. K. *et al.* Single-Cell Transcriptional Profiling Reveals Signatures of Helper, Effector, and Regulatory MAIT Cells during Homeostasis and Activation. *J Immunol* 208, ji2100522 (2022).

360. Altshuler, D., Daly, M. J. & Lander, E. S. Genetic Mapping in Human Disease. *Science* 322, 881–888 (2008).

361. Uhlén, M. *et al.* Tissue-based map of the human proteome. *Science* 347, 1260419 (2015).

362. Schmiedel, B. J. *et al.* Impact of Genetic Polymorphisms on Human Immune Cell Gene Expression. *Cell* 175, 1701-1715.e16 (2018).

363. MAHADEVAN, M. S. *et al.* Isolation of a Novel G Protein-Coupled Receptor (GPR4) Localized to Chromosome 19q13.3. *Genomics* 30, 84–88 (1995).

364. Wang, T. *et al.* GPR68 Is a Neuroprotective Proton Receptor in Brain Ischemia. *Stroke* 51, 3690–3700 (2020).

365. Liu, Y., Beyer, A. & Aebersold, R. On the Dependency of Cellular Protein Levels on mRNA Abundance. *Cell* 165, 535–550 (2016).

366. Dana, H. *et al.* Molecular Mechanisms and Biological Functions of siRNA. *Int J Biomed Sci Ijbs* 13, 48–57 (2017).

367. Hsu, P. D., Lander, E. S. & Zhang, F. Development and Applications of CRISPR-Cas9 for Genome Engineering. *Cell* 157, 1262–1278 (2014).

368. Tcymbarevich, I. *et al.* Lack of the pH-sensing Receptor TDAG8 [GPR65] in Macrophages Plays a Detrimental Role in Murine Models of Inflammatory Bowel Disease. *J Crohn's Colitis* 13, 245–258 (2018).

369. Goldsmith, Z. G. & Dhanasekaran, D. N. G Protein regulation of MAPK networks. *Oncogene* 26, 3122–3142 (2007).

370. Maeyashiki, C. *et al.* Activation of pH-Sensing Receptor OGR1 (GPR68) Induces ER Stress Via the IRE1α/JNK Pathway in an Intestinal Epithelial Cell Model. *Sci Rep-uk* 10, 1438 (2020).

371. Vallière, C. de *et al.* G Protein-coupled pH-sensing Receptor OGR1 Is a Regulator of Intestinal Inflammation. *Inflamm Bowel Dis* 21, 1269–1281 (2015).

372. Mathieson, T. *et al.* Systematic analysis of protein turnover in primary cells. *Nat Commun* 9, 689 (2018).

373. Friese, M. A. *et al.* Acid-sensing ion channel-1 contributes to axonal degeneration in autoimmune inflammation of the central nervous system. *Nat Med* 13, 1483–1489 (2007).

374. Fergusson, J. R., Fleming, V. M. & Klenerman, P. CD161-Expressing Human T Cells. *Front Immunol* 2, 36 (2011).

375. Renner, K. *et al.* Restricting Glycolysis Preserves T Cell Effector Functions and Augments Checkpoint Therapy. *Cell Reports* 29, 135-150.e9 (2019).

376. Onozawa, Y. *et al.* Activation of T cell death-associated gene 8 regulates the cytokine production of T cells and macrophages in vitro. *Eur J Pharmacol* 683, 325–331 (2012).

377. Ciofani, M. *et al.* A Validated Regulatory Network for Th17 Cell Specification. *Cell* 151, 289–303 (2012).